This is to certify that the
dissertation entitled

ELECTROCATALYTIC HYDROGENATION OF α-FUNCTIONALIZED CARBOXYLIC ACIDS

presented by

Tulika Sanjeev Dalavoy

has been accepted towards fulfillment
of the requirements for the

Ph.D. degree in Chemistry

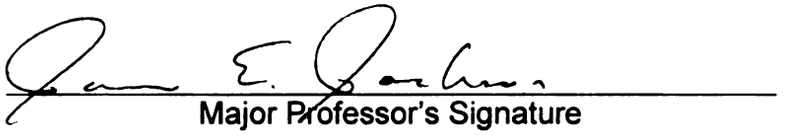

Major Professor's Signature

25 August 2006

Date

ELECTROCATALYTIC HYDROGENATION OF α-FUNCTIONALIZED CARBOXYLIC ACIDS

By

Tulika Sanjeev Dalavoy

A DISSERTATION

Submitted to
Michigan State University
in partial fulfillment of the requirements
for the degree of

DOCTOR OF PHILOSOPHY

Department of Chemistry

2006

ABSTRACT

ELECTROCATALYTIC HYDROGENATION OF α-FUNCTIONALIZED CARBOXYLIC ACIDS

By

Tulika Sanjeev Dalavoy

The goal of our research is to develop an alternative, greener, safer and milder process for the metal catalyzed hydrogenation of biomass-derived carboxylic acids to value-added products. Direct catalytic reduction of biomass-derived carboxylic acids avoids the additional esterification step, apart from other advantages such as easier product recovery and 100% atom economy. Ru/C catalyzed hydrogenation of lactic acid to propylene glycol requires high temperature and pressure (150°C, 1200 psi H_2).

Electrocatalytic hydrogenation (ECH) offers an alternative approach to traditional chemical catalysis. In this case the hydrogen is produced by electrolytic decomposition of water and the reaction occurs between hydrogen and the target molecule, both adsorbed on the electrode surface. This eliminates the kinetic barrier to the dissolution of the poorly soluble hydrogen gas in aqueous medium, mass transport of hydrogen and the splitting of hydrogen molecules into hydrogen atoms, and enables us to perform heterogeneous catalytic hydrogenations at ambient temperature and pressure. Advantages of this process include conservation of energy, possibility of stereoretention at low temperature and increased safety due to elimination of high pressure and hydrogen storage requirements. It also enables us to study catalytic surface mechanisms with *in-situ* spectroscopic techniques, such as ATR-IR and Raman. Electrocatalytic hydrogenation has previously been carried out on various substrates such as phenol, esters and

diketones, using electrodes, such as Raney Ni, Pt and Raney Co. However, to the best of our knowledge, this is the first study of the ECH of carboxylic acids. In this study, the ECH of various α-functionalized carboxylic acids has been attempted and optimized. Initial studies using the model compound, benzoyl formic acid showed that the ECH reaction is dependent more on the availability of surface sites, rather than the rate of mass transport, which is consistent with the results obtained with the catalytic hydrogenation of lactic acid. ECH of lactic acid using electrodeposited Ru on carbon felt, though giving a poor yield of product, enabled the determination of kinetic parameters, such as order of reaction, fractional surface coverages of lactic acid and hydrogen, rate constants, adsorption constants and activation energy using the Langmuir-Hinshelwood model. ECH of lactic acid using 5%Ru/C agglomerated in Reticulated Vitreous Carbon (RVC) resulted in much higher conversion. The effect of various parameters such as temperature, ECH current and nature of electrolyte on the yields and distribution of products was studied. The unexpected finding from this work is that lactaldehyde (2-hydroxypropanal), a proposed intermediate in the path of LA hydrogenation, is the major product instead of the expected propylene glycol, with small quantities of propylene glycol obtained only with 5%Ru/C/RVC. This thermodynamically unusual result reflects the relative surface adsorption and aqueous hydration properties of the starting materials and the two products. For the purpose of comparison, similar studies were carried using Ru deposited on non-carbon supports. *In-situ* ATR-IR spectroscopy has been used to probe the mode of binding of the substrate on the electrode surface, the effect of electrolyte anions and the mechanism by which the α-position functional group facilitates the hydrogenation of carboxylic acids.

ACKNOWLEDGEMENTS

I am grateful to all the people who have helped me during my graduate career. First of all I would like to thank my advisor, Dr. Jackson for his constant support and encouragement during the course of the project and for inspiring me to take up new challenges and try to solve them. Through frequent interactions with him, I have learnt to think critically and look at problems from various angles. I would also like to thank our collaborator, Prof. Dennis Miller from the Department of Chemical Engineering and Materials Science for his inputs. Our collaboration with the chemical engineering group has given me the unique opportunity to gain insights, develop critical thinking, work among diverse professionals and communicate effectively across disciplines. I am grateful to our collaborator, Dr. Swain for providing me the labspace and instrumentation to carry out my experiments and for sharing his expertise in electrochemistry. The occasional discussions with him on various aspects of the project has played an important role in expanding my knowledge. A special thanks to my committee members at Michigan State University, Dr. Bruening, Dr. Baker and Dr. Pinnavaia for reading my thesis and providing helpful suggestions.

I would like to acknowledge Prof. Jacek Lipkowski and his group from the University of Guelph for their help with the ATR-FTIR experiments. I am also grateful to Prof. Carol Kowzeniewski (Texas Tech Univ.) and Prof. Hugues Menard (Univ. of Sherbrooke) for their generous help and advice.

I would also like to thank the Jackson and Miller group members for their help and support and the Swain group members for helping me with the electrochemical techniques and instrumentation. I gratefully acknowledge the National Science

Foundation for financial support and the Department of Chemistry at Michigan State University for the teaching and research assistantships. Last, but not the least, I would like to thank my husband, parents, in-laws and friends for their support.

TABLE OF CONTENTS

LIST OF TABLES

LIST OF FIGURES

CHAPTER 1

INTRODUCTION

1.1 Importance of lactic acid and biomass based raw materials

Due to the increasing scarcity of petroleum and petroleum products, there is a great need to find alternative sources of raw materials for commodity chemicals. One such alternative source is biomass. Biomass-based organic acids such as lactic acid can be easily obtained by the fermentation of corn-derived glucose. Lactic acid can then be converted to propylene glycol (1,2-propanediol) by heterogeneous catalytic hydrogenation using metals or metal oxides (figure 1.1). Propylene glycol, an important commodity chemical, used at a rate of a billion kilograms per year in the U.S. is important in chemical and food industries[a]. It is also used as a coolant in automobiles and as a medium in formulations of cosmetics[a]. Currently, propylene glycol is commercially produced by the hydration of propylene oxide (2-methyl oxirane), which is obtained by the oxidation of propene, a petroleum based raw material.

Heterogeneous catalytic hydrogenation has the advantage of being an atom economical process, comprising of the addition of a molecule of hydrogen across a double or triple bond. Although a large number of processes are known for the heterogeneous catalytic hydrogenation of olefins, aldehydes and ketones, there are relative fewer examples of heterogeneous catalytic hydrogenation of carboxylate compounds.

[a] Information from http://en.wikipedia.org/wiki/Propylene_glycol

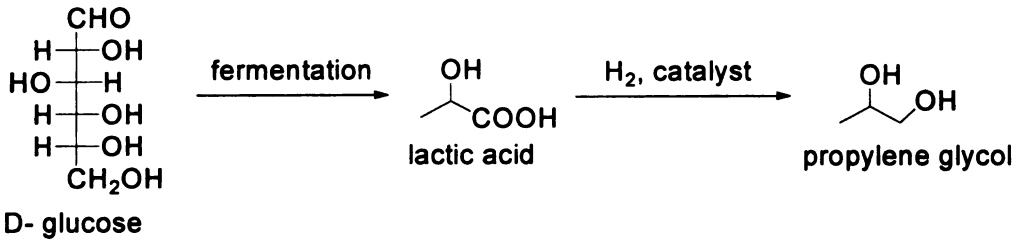

Figure 1.1: Conversion of biomass to propylene glycol

1.2 Advantages of heterogeneous catalytic hydrogenation

Carboxylic acid hydrogenations have been carried out using metal hydride reagents like $LiAlH_4$ and $NaBH_4$ and hydrogen in the presence of organometallic catalysts. But these methods suffer from several disadvantages. Metal hydrides are highly toxic and expensive and some of them are pyrophoric. They may bring about racemization of the stereogenic sites in the alcohol products. They are also difficult to use industrially or on a large scale because of the problems involved in separating the catalyst and the reductant's inorganic byproducts from the target compounds and the problems of waste disposal. Heterogeneous catalytic hydrogenations, on the other hand, do not involve any problems in the separation of the product from the catalyst. Such catalysts are also easier to handle compared to homogeneous catalysts and can be regenerated and reused. However, they may suffer from low selectivities due to the high temperature and pressure conditions involved, though this definitely can be overcome in some cases by the optimization of conditions and use of better catalysts.

1.3 Previous work on catalytic hydrogenation of esters and carboxylic acids

In the 1930's, Adkins and coworkers reported the heterogeneous catalytic hydrogenation of esters such as ethyl lactate, ethyl β-phenyl propanoate, diethyl sebacate, etc. over

$Cu/Ba/CrO_2$ at 250°C at 2800-4300 psi with yields in the range of 90-98%,[1a] hydrogenation of ethyl mandelate and ethyl phenyl acetate over Raney Ni and Cu chromite at 200°C and 1400-2400 psi with yields over 90%[1b] and the stereoretentive hydrogenation of optically active esters such as menthyl phenyl butyrates over Cu/CrO_2 at 200-250°C with yields ranging from 17 to 73%.[2]

Preparation of ethylene glycol from glycolic acid esters was reported by Um and coworkers[3] using oxide catalysts such as CuO, ZnO, CoO, etc. at 300-40,000 psi in alcohol solvent. Roesky and coworkers[4] prepared phenyl ethanols with 95% selectivity (ratio of the % yield of the desired product to the % conversion) and 65% conversion by the catalytic hydrogenation of phenylacetate esters at 200°C and 1305 psi over a CuO/ZrO_2 catalyst. Similarly cyclohexylmethanol was prepared by the gas phase hydrogenation of cyclohexyl carboxylic acid or the ethyl ester in the presence of oxides of Group IV A or IV B elements (eg. ZrO_2) at 250-400°C and 360-870 psi. Recently, Luo and coworkers[5] used $Ru\text{-}B/\gamma\text{-}Al_2O_3$, containing small amounts of Sn for the hydrogenation of ethyl lactate to 1,2-propanediol in n-heptane at 150°C and 800 psi with 91.5% selectivity at 90.7% conversion after 10 h. In this case, the hydrogenation to 1,2-propanediol was found to proceed directly from the ester and not through the lactic acid intermediate. Enantioselective hydrogenation of ethylpyruvate was reported by Schurch and coworkers[6] using 1-(9-anthracenyl)-2-(1-pyrrolidinyl)-ethanol modified Pt. The enantioselective hydrogenation of α-keto esters over cinchona modified Pt was discovered by Orito et al.[7] About 90-92% enantioselectivity was achieved using this catalyst.

The earliest examples of aqueous phase heterogeneous catalytic hydrogenation of carboxylate compounds were in 1948 by Adkins and coworkers[8] who carried out the hydrogenation of α-substituted esters like ethyl 2-amino propanoate, ethyl α-(N-piperidyl) acetate and ethyl lactate to the corresponding primary alcohols, 2 amino propanol, β (N-piperidyl) ethanol and propylene glycol respectively. The catalyst used was Raney Ni at 100°C and a pressure of 5000 psi. The products were obtained in a yield of 80% in all cases (figure 1.2). By using high catalyst loading, esters of alpha substituted acids were hydrogenated to the corresponding alcohols at a low temperature of 50°C with retention of configuration.

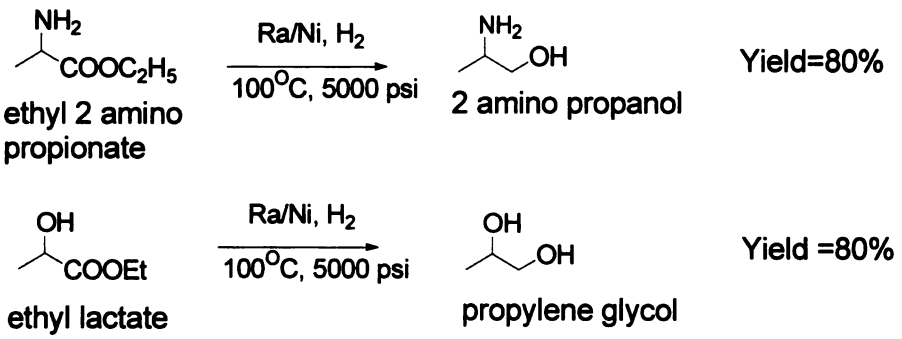

Figure 1.2: Catalytic hydrogenation of α-substituted esters to alcohols in water

Even though hydrogenation of esters is relatively easier than that of carboxylic acids, it is important to develop processes for the hydrogenation of carboxylic acids to the corresponding alcohols because carboxylic acids are more directly available from biomass processing and the direct hydrogenation of carboxylic acids eliminates the intermediate esterification step for the production of alcohols and therefore, is of high value in renewables-based chemicals production. The first aqueous phase hydrogenation

of free carboxylic acids was carried out in 1955 by Carnahan and coworkers.[9] Several carboxylic acids like acetic acid and α hydroxy acetic acid were hydrogenated to ethanol and ethylene glycol respectively in the presence of the ruthenium based catalysts and reaction conditions shown in figure 1.3.

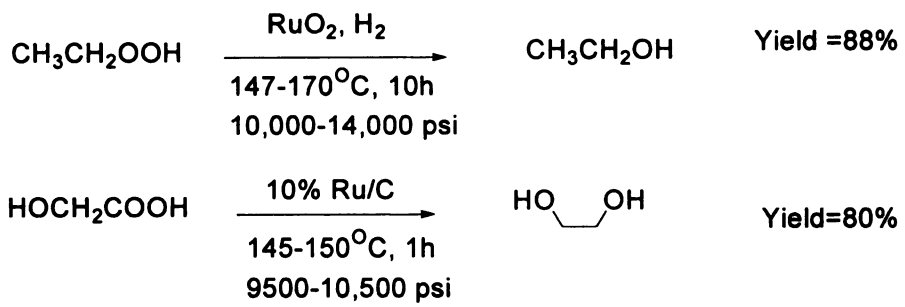

Figure 1.3: Catalytic hydrogenation of carboxylic acids to alcohols in water

Broadbent et al.[10] carried out the first catalytic hydrogenation studies of lactic acid using an unsupported Re black catalyst at 150°C and 3791 psi for 8 h, giving propylene glycol with an yield of 84%.

Mendes and coworkers[11] studied the hydrogenation of oleic acid to stearyl alcohol in tetradecane over TiO_2 and Al_2O_3 supported Ru catalysts. Hydrogenation over supported bimetallic Ru-Sn catalyst was found to selectively reduce the carboxylic acid group, leading to the formation of unsaturated alcohols. Toba and coworkers[12] reported the hydrogenation of dicarboxylic acids and saturated fatty acids to the corresponding diols and alcohols respectively using Ru-Sn-Al_2O_3 catalysts. In case of fatty acids the conversion and yield increased with increase in the carbon chain length. Rachmady and coworkers[13] studied the vapor phase hydrogenation of acetic acid over Pt supported on various oxides at 150-300°C, 100-700 Torr hydrogen and 50-70 Torr acetic acid. The product selectivity was found to be strongly dependent on the nature of the oxide support,

with the various being ethanol, ethyl acetate, acetaldehyde, methane, CO and CO_2. The TiO_2 support showed the highest activity.

1.4 Ru/C catalyzed hydrogenation of lactic acid

Recently, an efficient aqueous phase hydrogenation of lactic acid to propylene glycol, catalyzed by 5% Ru/C has been developed. This reaction shows a higher reaction rate and better selectivity to propylene glycol under milder conditions compared to the ones used earlier, offering real potential for industrial application.[14] The reaction is shown in figure 1.4. The aqueous environment in this case is favourable for the reaction and has the advantage of being non-hazardous and a good solvent for biomass-derived carboxylic acids such as lactic acid. Ru based catalysts were found to show good intrinsic hydrogenation activity for carbonyl compounds in earlier studies[9,11,12] and Ru has been found to be a highly efficient catalyst for hydrogenation especially in aqueous solution. Carbon is a good support for the catalyst due to its inertness in aqueous medium.

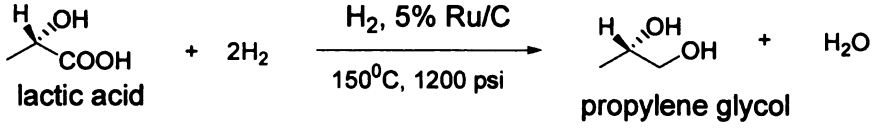

Figure 1.4: Aqueous phase hydrogenation of lactic acid to propylene glycol

Control experiments were carried out to prove that no propylene glycol was formed in the absence of either catalyst or hydrogen. Several catalysts were tested for efficiency of hydrogenation of lactic acid. It was found that the ruthenium on carbon catalyst is the most active catalyst. Almost 95-98% conversion and more than 90% ee was achieved

after 5 hours at 150°C and 1200 psi pressure. These conditions are mild compared to those used earlier for the hydrogenation of lactate esters.

The reaction both with respect to the rate of conversion and selectivity to propylene glycol are favoured by high pressure, but at temperatures above 170°C, there are more secondary reactions leading to the formation of gaseous and liquid by-products such as ethanol, propanol and hydrocarbons like ethane, propane, etc.

1.4.1 Mechanistic studies

The conversion of lactic acid to propylene glycol was found to occur 3-5 times faster than the conversion of propanoic acid to 1- propanol.[15] However, the mechanism by which the –OH group at the α position activates the hydrogenation is unclear. It may be due to the electron withdrawing effect of the –OH group which enhances the neighbouring carbonyl group's preference for sp^3 hybridization. This explanation is supported by the observation that protonated amino acids[16] and 2- chloro propanoic acid are also more reactive towards hydrogenation, and that the charged ammonium group in the case of protonated amino acids is more activating than the hydroxyl group in lactic acid. Stabilization of intermediates on the catalyst surface by intramolecular hydrogen bonding must play an important role.

As shown in figure 1.5, the measured heats of reaction for the hydrogenation of propanoic acid and lactic acid are almost the same.[14] Therefore, it was concluded that kinetic factors may play an important role in the reaction.

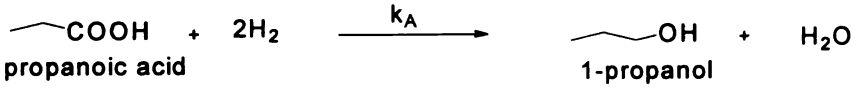

propanoic acid

1-propanol

ΔH= -10.49 kcal/mol

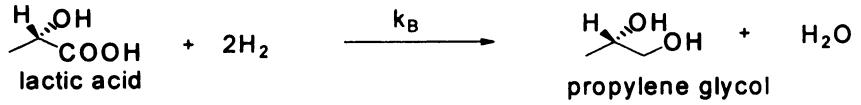

lactic acid

propylene glycol

ΔH= -11.00 kcal/mol

Figure 1.5: Comparison of the catalytic hydrogenation of substituted and unsubstituted carboxylic acids

In earlier studies, mechanisms for the hydrogenolysis of esters to alcohols were proposed. In the gas phase hydrogenolysis of methyl formate on Cu/SiO_2, it was suggested by Sorum and Onsager[17] that there is a formation of a hemiacetal intermediate followed by dissociation to formaldehyde and methanol. The aldehyde is then rapidly hydrogenated to methanol as shown in figure 1.6. This mechanism was confirmed by Monti et al.[18] by *in situ* infrared spectroscopy and labeling studies.

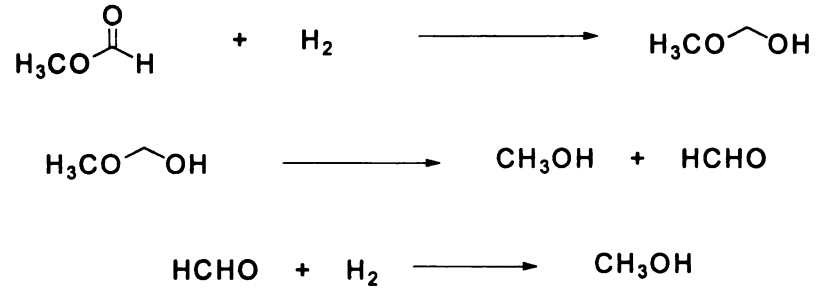

Figure 1.6: Mechanism of gas phase ester hydrogenation proposed by Sorum and Onsager[17]

In the case of Cu/SiO_2 catalyzed acetate hydrogenolysis, it was proved by Kohler et al.[19] using FTIR that the acetate is adsorbed dissociatively on the catalyst surface as shown in figure 1.7 where S indicates a catalytic site on the surface.

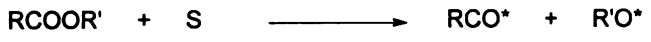

Figure 1.7: Mechanism of acetate hydrogenolysis described by Kohler et al.[19]

On carrying out isotopic labeling studies it was found that the alkoxy fragment, R'O* reacts quickly to form R'OH, while the acyl group, RCO* is adsorbed longer. The hydrogenation of the acyl fragment is believed to be the rate determining step, which can be hydrogenated to either the desired alcohol or to the aldehyde which is then hydrogenated to the alcohol.

In the hydrogenation of acetic acid on Cu/SiO_2, studied by Dumesic and coworkers,[20] adsorption of aliphatic carboxylic acids and esters was proposed to occur by the cleavage of the C-O bond of the carboxylate group, giving rise to acyl species, RCO*. The existence of this species on Cu/SiO_2 surface was supported by FTIR studies and was further confirmed by the high initial heats of adsorption observed in microcalorimetric studies of methyl acetate, ethyl acetate and acetaldehyde adsorption on Cu/SiO_2 at 300K as well as the observed production of gaseous species upon ester adsorption at higher temperatures. The surface bound acetyl is therefore a relatively stable species and does not immediately hydrogenate to the aldehyde and alcohol. DFT calculations[20] suggest that the activation energy required for dissociative adsorption increase in the order ethyl acetate < methyl acetate < acetic acid. This is due to differences in the C-O bond adjacent

to the carbonyl group, whose strength increases from ethyl acetate to acetic acid, due to the ability of the R group to donate electron density to the alkoxy oxygen atom. On the basis of DFT calculations, Neurock and coworkers[21] proposed a model like those above for acetic acid hydrogenation on Pd(111), which involves dissociation of acetic acid via C-OH bond breaking to form surface acetyl and hydroxyl species, and is followed by either addition of H to the α-carbon atom forming acetaldehyde and subsequent hydrogenation to ethanol or the decomposition of the acetyl species to form CO and methyl species via C-C bond scission. According to the calculations, the addition of H to the oxygen end of the acetyl species to form hydroxyl ethylidene is an endothermic reaction and is less likely to occur. It was also found that the initial adsorption of acetic acid prefers the η1 mode through the carbonyl oxygen, which is more favorable than the di-σ mode involving two oxygen atoms.

In the Ru-B/γ-Al_2O_3 catalyzed hydrogenation of ethyl lactate to 1,2-propanediol, it was observed by Luo and coworkers[22] that the addition of small quantities of Sn significantly increased the selectivity and conversion to the diol. The most active catalyst was the one containing a Sn/Ru ratio of 7%. It was proposed that the effect of Sn is based on the formation of an oxidized Sn surface (Sn^{2+}) in interaction with metallic Ru, in which Sn plays the role of activating and polarizing the carbonyl group, whereas the electron rich Ru site activates hydrogen. The activated hydrogen on each Ru site then attacks the positively charged C atom of the carbonyl group, forming an acetal of Sn, which is then converted to aldehyde, followed by rapid hydrogenation to the alcohol as shown in figure 1.8. A similar mechanism was proposed for the hydrogenation of fatty acid esters by

Deshpande et al.[23] and Pouilloux et al.[24] and for the hydrogenation of oleic acid over Ru-Sn catalysts by Mendes et al.[11]

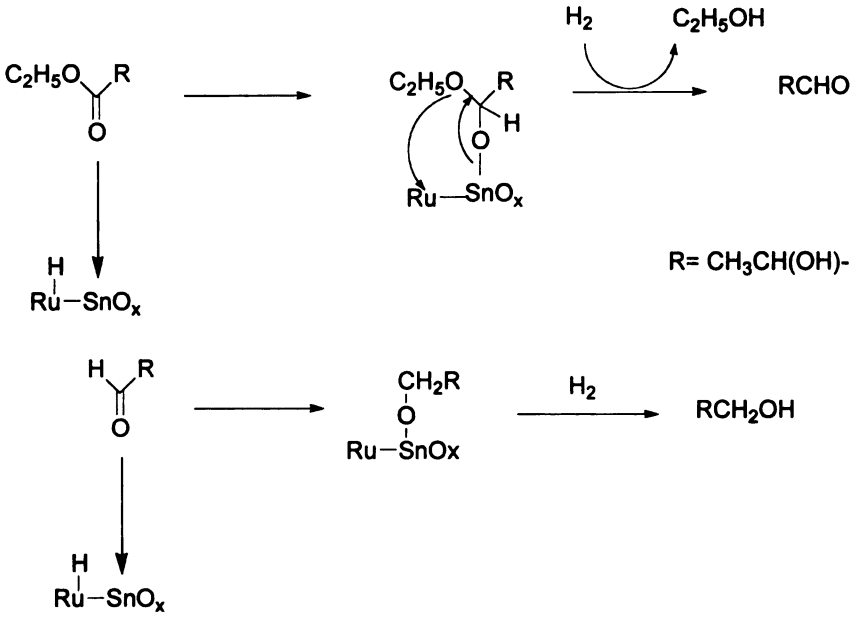

Figure 1.8: Mechanism of Ru catalyzed ethyl lactate hydrogenation involving promotion by Sn (Luo and coworkers[22])

Mechanistic studies were carried out on the hydrogenation of lactic acid using isotopic labeling, NMR analysis and chiral GC-MS by Jackson and coworkers.[25] The heterogeneous catalytic hydrogenation of lactic acid leads primarily to the formation of 1,2 propylene glycol with retention of stereochemistry at C2. There are several possible ways in which the hydrogenation might occur as shown in figure 1.9. One involves only the carboxylic carbon, C1 which leads to the formation of 1,2 propylene glycol via 1,1,2 propanetriol (lactaldehyde hydrate) and lactaldehyde with retention of configuration at C2. If this path is followed, then the reaction carried out using D_2 in D_2O should lead to

deuterium incorporation only at C1, leading to dideuterated propylene glycol. On the other hand, if fast tautomerization of the lactic acid to the enol form takes place followed by C=C hydrogenation and then the dehydration of the geminal diol, intermediate formation of pyruvaldehyde, and hydrogenation of the C=O bond leading to propylene glycol, C2 will also be involved in the mechanism of hydrogenation. In such a case hydrogenation in the presence of D_2/D_2O would lead to deuterium incorporation at both C1 and C2 of propylene glycol and a loss of stereochemistry as shown in scheme 2. However, the tautomerization of lactic acid shown in Route B is less likely to occur as it has a very high activation energy. Instead, based on standard pK_a data, the tautomerization of lactaldehyde shown in Route C appears more likely and chemical scrambling would lead to the same result with respect to D incorporation and stereoselectivity of the reaction.

In a key control experiment, propylene glycol was exposed to hydrogenation conditions in the presence of D_2/D_2O and the deuterium incorporation in the product was followed by ^{13}C NMR. The ^{13}C NMR spectra collected at different times after the beginning of the reaction showed D incorporation at both C1 and C2 of the product. The H/D exchange was much faster at C1 than at C2, giving almost complete incorporation at C1 well before significant exchange at C2. No H/D exchange was detected at C3[25].

The retention of stereochemistry and the slow exchange of D onto C2 even in propylene glycol suggest that the first proposed mechanism (path A) shown in figure 1.9 dominates over the alternative competing paths for lactic acid hydrogenation. Therefore, direct hydrogenation occurs at the carboxylic carbon, C1 only. The others (path B and C) involve tautomerization to enol forms followed by hydrogenation of the C=C double

bonds or equilibrated C=O bonds. All these alternative paths however reflect stereochemical scrambling at C2.

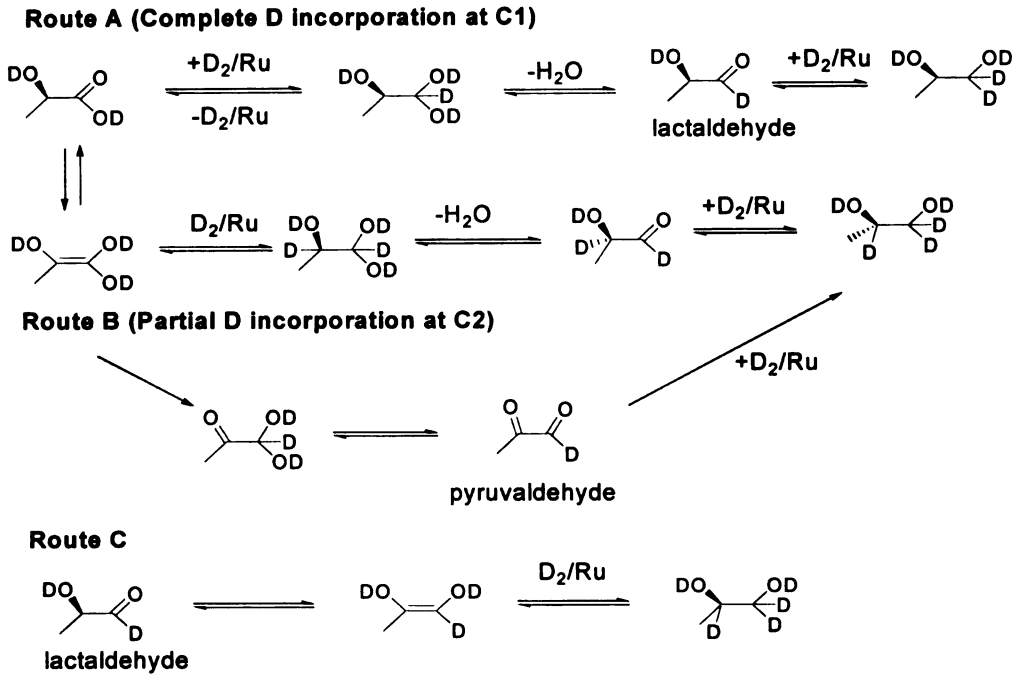

Figure 1.9: Proposed mechanism of lactic acid hydrogenation from deuterium labeling studies (Jackson and coworkers)[24]

1.4.2 Kinetic studies

In kinetic studies of the Ru/C catalyzed hydrogenation of lactic acid to propylene glycol,[15] the system was treated as a three-phase reaction involving H_2 gas, an aqueous solution of lactic acid and product propylene glycol in the liquid phase and the Ru/C catalyst in the solid phase. The reaction involves four types of mass transfer processes, namely hydrogen mass transfer from the gas to the liquid phase, lactic acid and hydrogen mass transfer from the liquid to the solid catalyst phase, diffusion of hydrogen and lactic

acid within the porous catalyst and the conversion of lactic acid to propylene glycol via a series of surface chemical reactions. In hydrogen solubility studies, the solubility of hydrogen in water was found to increase with increase in pressure, but the solubility of hydrogen in lactic acid solution was found to be 10% lower than that in water. Mass transfer analysis revealed very minor effects of liquid-solid and gas-liquid mass transfer rates and of the hydrogen partial pressure on the rate of hydrogenation. From initial rate analysis, the apparent activation energy of the process was calculated to be 94 kJ/mol. A Langmuir-Hinshelwood model was proposed for lactic acid hydrogenation in which molecular hydrogen and lactic acid adsorb on the catalyst surface, followed by reaction to form propylene glycol and desorption of propylene glycol from the surface, as shown in figure 1.10. The rate limiting step is irreversible.

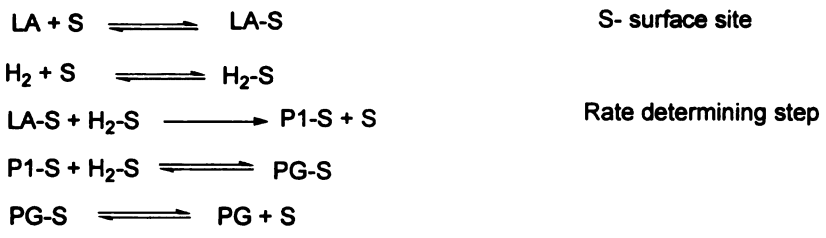

Figure 1.10: Langmuir-Hinshelwood mechanism for lactic acid hydrogenation

In accordance with the assumptions of the Langmuir-Hinshelwood model, the adsorption of water is neglected, the total catalyst site density is considered constant and all sites are assumed to be equivalent. The final rate expression in terms of kmol/kg of catalyst/s is given as follows.

$$-R \text{ (kmol/kg of cat/s)} = \frac{KC_{LA}P_{H2}}{(1 + K_{H2}P_{H2} + K_{LA}C_{LA})^2}$$

where K is the rate constant, C_{LA} is the lactic acid concentration, P_{H2} is the hydrogen partial pressure and K_{H2} and K_{LA} are the adsorption constants of lactic acid and hydrogen on Ru. The term for propylene glycol was not included in the denominator because the presence of propylene glycol was found to have negligible effect on the rate of lactic acid hydrogenation. The heats of adsorption of lactic acid and hydrogen were determined to be 47 and 79 kJ/mol respectively.

A Langmuir-Hinshelwood model was also proposed by Luo and coworkers[5] for Ru/Sn catalyzed ethyl lactate hydrogenation and by Rachmady and coworkers[13] for the hydrogenation of acetic acid over Pt/TiO_2. The apparent reaction order was found to be 0.4-0.6 with respect to H_2 and 0.2-0.4 with respect to acetic acid. Unlike the lactic acid hydrogenation, this model incorporates dissociated hydrogen and acetic acid adsorption on one type of site and only molecular acetic acid adsorption at another type of site on the oxide surface and only the latter species was considered catalytically significant for ethanol, acetaldehyde and ethane formation. Only Pt supported on TiO_2 and η-Al_2O_3 yielded ethanol and acetaldehyde as products whereas Pt/SiO_2 caused decarbonylation, leading to CH_4 and CO and Pt/Fe_2O_3 yielded acetone as the major product, indicating that catalyst activity and product selectivity are controlled by the adsorption behavior of acetic acid on the various oxide surfaces and the availability of activated atomic hydrogen on Pt.

1.4.3 Studies on other α substituted carboxylic acids

In order to study the trends in the reactivity of various acids to hydrogenation and to gain a better understanding of the mechanism, a number of α substituted carboxylic acids were

subjected to hydrogenation[26] and the rates and percentage conversion in each case was measured. The compounds can be listed in the order of increasing reactivity as follows. Propanoic acid < 2- methoxy propanoic acid < methoxy acetic acid < glycolic acid < lactic acid < ethyl lactate.

2-chloro propanoic acid and 2-acetoxy propanoic acid were converted to propanoic acid and lactic acid respectively under the hydrogenation conditions (150°C, 1200 psi H_2). Based on these studies, it was concluded that hydrogen bonding may have a significant effect on the rate of hydrogenation and selectivity of the product. This is proved by the higher reactivity of the α-hydroxy substituted lactic and glycolic acid relative to their CH_3-capped analogs. The lower reactivity of 2-methoxy propanoic acid, even in the presence of a higher catalyst to substrate ratio may be because hydrogen bonding with the carboxyl group is no longer possible when the –OH of lactic acid is replaced by $–OCH_3$. The much higher reactivity of methoxy acetic acid compared to that of methoxy propanoic acid indicates that steric factors may also affect the reactivity. However, the fact that isobutyric acid reacted much faster than propanoic acid indicates that the mechanism is more dependent on the exact mode of binding of the substrate to the catalyst surface which is believed to vary considerably with the structure of the substrate. However many of these results were somewhat qualitative in nature and no definite conclusions could be drawn from them.

The aqueous phase hydrogenation of alanine to alaninol over 5% Ru/C catalyst was studied by Jere and coworkers.[16] A selectivity of 95% to L-alaninol and ee of 99% was achieved at 150°C and 1000 psi in 4 h in the presence of 0.29 M H_3PO_4 (required to convert the zwitterionic form of the amino acid to the completely protonated form). In

more recent studies,[27] the replacement of the amine hydrogens with $-CH_3$ groups was found to significantly decrease the rate of hydrogenation to the corresponding alcohol, just as had been found in the OH/OCH_3 systems.

1.5 Introduction to electrocatalytic hydrogenation

The use of electrochemical methods to produce organic compounds could provide an alternative approach to the traditional chemical synthesis methods. Substantial work has been done in the past few years on electrocatalytic hydrogenation (ECH) or electrohydrogenation of various substrates like phenol, esters, α- and β-diketones, conjugated enones, etc. on electrodes such as Raney Ni, Pt, Raney Co, etc.

The electrocatalytic hydrogenation is thought to occur in two consecutive steps. The first step involves the electrolytic decomposition of the solvent, usually water, with the formation of hydrogen atoms adsorbed on the electrode. The second step involves hydrogen atom migration on the electrode surface to react with the organic substrate also adsorbed on the electrode surface to give the final reduction product. Therefore, ECH has a lot in common with heterogeneous catalytic hydrogenation, but it offers an advantage in bypassing the kinetic barrier to the dissolution of the poorly soluble hydrogen gas (especially in aqueous medium), the mass transport of hydrogen and the splitting of hydrogen molecules to hydrogen atoms. This obviates use of high pressure conditions to get the hydrogen into the aqueous phase and provides a method of carrying out heterogeneous catalytic hydrogenation under milder conditions. In most of the cases, the mechanism on the catalyst surface and the mode of binding of the substrate to the catalyst

surface in electrohydrogenation was found to be similar to that of heterogeneous catalytic hydrogenation carried out under high temperature and pressure conditions[28-30].

The various steps involved in ECH can be represented as in figure 1.11.

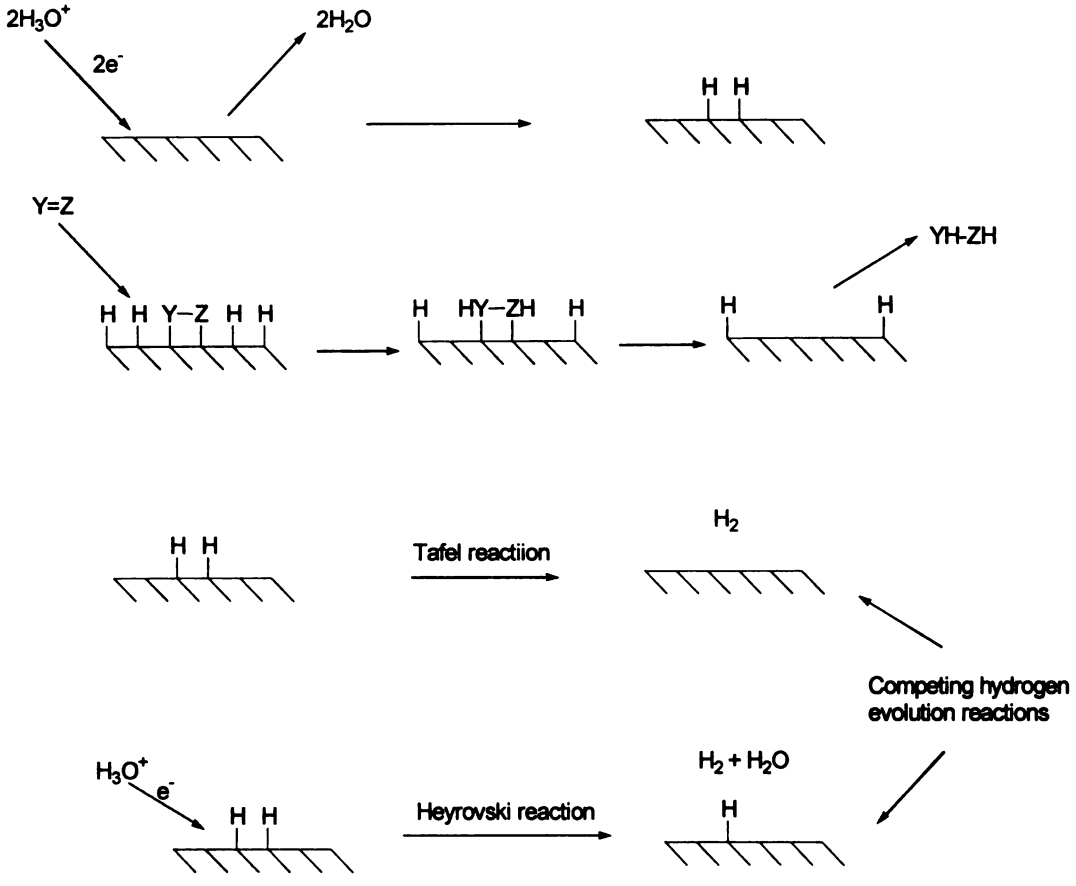

Figure 1.11: General scheme of electrocatalytic hydrogenation and hydrogen evolution

From the above steps it can be seen that for a given electrode at a given potential, both electrohydrogenation and hydrogen evolution can occur simultaneously and there is always competition between the two processes. Once the electrode surface is saturated with hydrogen atoms, some of them desorb and evolve as hydrogen gas. However the

relative amounts of hydrogenation and hydrogen evolution depend on several factors like the electrode material, morphology, applied potential, substrate concentration, reaction medium, pH and temperature. Since ECH occurs as a result of the reaction between the adsorbed substrate and adsorbed hydrogen and not with hydrogen gas, the process will be more efficient if the various parameters are optimized to a point where the electroreduction of protons to hydrogen atoms can occur, but where hydrogen evolution is minimized.

Though ECH has been carried out successfully on carbonyl compounds like diketones and enones, to the best of our knowledge, no such studies have been reported on carboxylic acids. This technique might be a greener, milder and more efficient alternative to the batch process developed earlier both with respect to industrial production and mechanistic studies.

Beyond the milder conditions, ECH might offer additional advantages; in some cases, the adsorption of poisons and the consequent fouling of the catalyst surface is prevented by the cathodic polarization of the electrode. In comparison to hydrogenation by electroreduction followed by protonation, ECH requires less energy because the formation of chemisorbed hydrogen by the electrolysis of water on a low hydrogen overvoltage cathode requires a less negative potential compared to the electroreduction of most organic functional groups. In some cases, ECH has also been found to be more selective compared to chemical catalytic hydrogenation due to the milder conditions involved. For example, Lessard and coworkers[28] achieved the ECH of 2-cyclohexen-1-one to cyclohexanone with high selectivity using electrodeposited Ni and Cu electrodes (about 100% selectivity at 94% conversion). In some cases the stereoselectivity of the

reaction can be controlled by controlling the potential. For example, in the ECH of m-xylene on platinized platinum electrodes in 0.5M H_2SO_4, Quiroz and coworkers[29] found that the stereoisomeric ratio of the products, cis and trans 1,3-dimethyl cyclohexane was strongly dependent on the potential. The cis/trans ratio was 7.9:92.1 at 0.24V (vs RHE) and decreased at more negative potentials.This was explained by the change in orientation of the adsorbed m-xylene from edgewise to parallel orientation as the concentration of H atoms and water molecules on the electrode surface increased at more negative potentials.

Many ECH reactions have been carried out successfully at room temperature and have produced reasonably good yields of desired products and high enantioselectivity. The conditions need to be optimized to obtain the maximum rate of hydrogenation and to minimize the rate of the competing hydrogen evolution reaction (HER) by the Heyrovsky and Tafel reactions. The current efficiency is a measure of the competition between hydrogenation and HER which depends on a number of factors such as substrate, electrode, electrolyte, pH and temperature. Most ECH reactions reported in the literature were found to be most efficient at low currents and moderate temperature and high currents and temperatures were found to increase the rate of HER.

Mahdavi and coworkers[30] studied the ECH of conjugated enones using nickel boride, fractal nickel and Raney nickel electrodes in aqueous methanol. In this case ECH was found to be more selective than catalytic hydrogenation. They showed that in the ECH of cyclohex-2-ene-1-one, the selectivity was quite low with the more active Raney Ni electrodes, but at nickel boride electrodes, the selectivity of the C=C hydrogenation and the hydrogenation efficiency can be increased to 100% at 95-100% conversion by

decreasing the current density and increasing the substrate concentration. Fractal nickel electrodes were found to give higher selectivity than nickel boride electrodes under certain conditions and were found to be useful for the selective ECH of C=C of a number of conjugated enones such as alkyl substituted cyclohexenones.

Grimshaw and coworkers[31] reported ECH of 4-phenylbuten-2-ones to 4-phenyl-butan-2-ones at Ni black cathode in aqueous ethanol containing H_2SO_4. The maximum current efficiency of 63-68% was obtained using high substrate concentrations.

Senda and coworkers[32] studied the ECH of 4-t-butyl cyclohexanone to the corresponding alcohol using Raney Ni, Raney Co and Pt/C powder electrodes. A high conversion of ketone to alcohol was observed on the Raney catalysts when the pKa of the proton source employed was around 5. The conversion over Pt/C was low (15%), but increased with increasing current density.

Navaro and coworkers[33] studied the ECH of diethyl fumarate to diethyl succinate in an undivided cell using electrodes such as Fe, Pt, Ni, Pb, Al, Cu, Zn and carbon felt. The conditions were optimized with respect to current density, supporting electrolyte, pH and co-solvent. The best results for hydrogenation were obtained using Fe electrode using a current density of 175 mA/dm^3 in H_2O/CH_3CN (4:1) at pH 5.5 with dimerization of the ester being the major competing reaction

Cheong and coworkers[34] studied the ECH of ketones and α and β diketones using Raney nickel, Raney cobalt or Devarda copper electrodes embedded in a nickel matrix in an aqueous medium. They achieved chemoselective reductions of only one carbonyl group of α-diketones and showed that the ECH of benzil gave either either benzoin or hydrobenzoin depending on the electrode used. Also the diastereoselectivity observed for

the diol formation in the ECH of α and β diketones was comparable to that obtained in catalytic hydrogenation. Using modified Raney nickel, the ECH of benzil produced hydrobenzoin with a threo:meso ratio of 7:93.

Romulus and coworkers[35] have shown that ECH of the heterocyclic aromatic ring can occur in competition with the electroreduction of carboxylic acids and esters of pyridine to the corresponding alcohols in a sulfuric acid medium using a lead cathode. ECH of the aromatic nucleus occurred mainly on non-reducible derivatives such as hemiacetal or hydrate. Hu and coworkers[36] carried out the ECH of 4-amino 5-nitrosodimethyl uracil to 4,5 diamino dimethyl uracil using a foamed nickel cathode. This reaction is an important step in the synthesis of caffeine and has the potential for replacing the currently used industrial method of Fe powder catalyzed hydrogenation which leads to poor hydrogenation efficiency and a high level of pollution due to the resulting Fe_3O_4 slurry. The foamed nickel was found to give better current efficiency compared to Raney nickel and other electrodes studied, due to its higher surface area and porosity and its reticulated three dimensional structure. Conversions of over 98% and current efficiencies of 95-100% were obtained at the optimum conditions i.e. pH 3-4, a current density of 84-168Am^{-2} and a temperature of 20-30°C.

Polcaro and coworkers[37] studied the ECH of benzaldehyde and acetophenone in acidic and alkaline ethanol/water mixture using Pd supported on carbon felt due to its high surface area and good fluid permeability. In this case the total current efficiency and the yields of the products were found to be greatly influenced by the method of preparation and the morphology of the electrode.

Thomalla and coworkers have carried out the ECH of phenol,[38] alkyl substituted phenols,[39] carvone and limonene[40] using Raney nickel electrodes in the presence of non-micelle forming cationic surfactants. The presence of a surfactant was found to increase the efficiency of ECH by increasing the substrate solubility and by the formation of an adsorbed hydrophobic surfactant layer on the electrode surface, thus increasing the efficiency of adsorption of the hydrophobic substrates. These hydrogenation products are widely used in the perfume and fragrance industry.

Roessier and coworkers[41] studied the ECH of an aqueous suspension of indigo to water soluble leuco indigo in a divided flow cell using Raney nickel particles fixed in a porous bed of plated nickel. The reaction could be scaled upto 10g/L. The reaction rate was enhanced by high pH, the presence of an organic cosolvent such as methanol and ultrasonic waves, due to the increase in the active reaction surface as as result of decrease in particle diameter. Under optimum conditions of current density and temperature a conversion of 95% and a current efficiency of 12.7% was achieved. However, the current efficiency could be increased to 19.2% by doping the Ranay nickel electrodes with Pt particles. In this case, the low current efficiencies are mainly due to the poor contact between the suspended indigo particles and the electrode surface.

Raney nickel has been widely used over the years for ECH reactions due to its easy availability, low cost and high stability in a wide range of solvents and pH, and its efficiency for the hydrogenation of carbonyl groups. Recently, however, a number of noble metal catalysts such as Pt, Ru, Rh, etc. are being used for the ECH of specific functional groups. Since these catalysts are expensive, they can be more efficiently utilized if they are dispersed in a support such as alumina or carbon. Amouzegar and

coworkers[42] reported the ECH of phenol to cyclohexanol at 60°C using Pt/C electrodes where a current efficieny of 85% was achieved with a Pt loading of 2%, higher than that on platinized Pt, Pt on carbon rod or smooth Pt. The rate determining step was found to be the reaction between adsorbed species on the electrode surface. In many studies, polymers were used to support noble metal catalysts used for ECH, providing a high surface area electrode with good chemical and mechanical resistence. Recently Lofrano and coworkers[43] reported ECH of isosafrole (olefin) and benzaldehyde in good yields using Pt dispersed on poly (allyl ether p-benzeneammonium derivatives). The metal was deposited using ion exchange involving the metal salt, followed by electrochemical reduction to the metal. Pd deposited on poly-[N-(5-hydroxypentyl) pyrrole][44] and poly-[N-(5-carboxyhexyl) pyrrole][45] film coated on carbon material was used for the ECH of acetylene and other organic compounds such as cyclohexenone and methyl-α-oxobenzeneacetate by Takano and coworkers. Other examples of ECH using noble metal catalysts dispersed on high surface area supports will be discussed in subsequent chapters.

Finally, several examples demonstrate the preparative and commercial applications of ECH. Navarro and coworkers[46] recently reported the selective ECH of several organic compounds such as cyclohexene, cyclohexenone, benzaldehyde, acetophenone, styrene, 1,3-cyclohexadiene, citral, linalool and geraniol using H_2O/MeOH, NH_4OAc, or NH_4Cl (0.2M) as the supporting electrolyte in an undivided cell using Ni deposited on Fe. They were the first to report the use of a sacrificial Ni anode which enabled deposition of fresh Ni on the cathode and avoided catalyst poisoning. A current density gradient was used to reduce electrolysis time and obtain good current efficiency. ECH of vat dyes such as

indigo was reported by Roessler and coworkers[47] as an alternative method to reduce vat dyes using electrodes comprised of a thin grid coated with a layer of Ni in which fine particles of Raney Ni are dispersed. ECH is convenient and environmentally beneficial in this case because it reduces the use of chemicals by avoiding the use of a chemical reducing agent such as sodium dithionite, which releases vast quantities of excess dithionite and its oxidation products, sulfite, sulfate, thiosulfate and toxic sulfide into the environment which are difficult to regenerate. Raney Ni was more active compared to Pt and Pd electrode, but showed a lower current efficiency. Raju and coworkers[48] reported the synthesis of non-steroidal anti-inflammatory drugs such as ibuprofen using ECH.

1.6 Motivation for research

The goal of this project is to develop an alternative method for the electrocatalytic hydrogenation of lactic acid and other α-functionalized carboxylic acids. The electrocatalytic method is milder, more convenient and environmentally friendly compared to the chemical catalytic or batch hydrogenation process currently in use. The generation of hydrogen on the catalyst surface eliminates the need for an external source of hydrogen gas, making the process much safer. The high pressure requirement which arises from the poor solubility of hydrogen gas in water is also eliminated because the hydrogen is generated where it is needed i.e. at the catalyst surface. Thus, the kinetic barrier for the dissolution of hydrogen gas and splitting into H atoms is eliminated and this enables the use of lower hydrogenation temperatures as well, compared to the batch process. Milder and environmentally friendlier conditions are certainly desirable if a process is to be used on a preparative scale in the laboratory or industry, especially for

the production of value added chemicals from easily available starting materials. Though this thesis describes the development of an electrocatalytic hydrogenation process, specifically for lactic acid and certain other α-functionalized carboxylic acids, our long term goal is to extend the process to other carboxylic acids as well.

The strategies and techniques used for electrocatalytic hydrogenation are ones that are reported in literature and have been used for the ECH of other compounds such as phenols, olefins, aromatic compounds, enones, ketones, etc. To the best of our knowledge however, no studies of ECH of carboxylic acids have been reported in literature. Carboxylic acids being some of the raw materials most readily available from biomass, it is important and interesting to explore their behavior under electrocatalytic conditions. A successful and practical reduction would enable the effective and controllable conversions of carboxylic acids into value added products. The work may also help to uncover the reaction mechanisms *in situ* during catalytic hydrogenation. From the previous work described, it is clear that though a few mechanistic paths have been probed for the Ru/C catalyzed hydrogenation of lactic acid using indirect deuterium labeling methods, there have been no studies to date of the nature of surface-bound intermediates involved and the exact catalyst surface mechanism. Recent studies[27] have shown that water is required for the Ru/C catalyzed hydrogenation and the use of organic solvents such as ethanol or THF either in the pure form or in aqueous mixtures significantly reduces the conversion efficiency of lactic acid. This suggests a unique mechanism involving the reaction of adsorbed water molecules on the catalyst surface, which significantly differs from hydrogenation mechanisms in the vapor phase or in other solvents. Electrocatalytic hydrogenation would make the process more amenable to in

situ spectroscopic studies. The reaction on the electrode surface can be better controlled by applying a suitable potential in the hydrogen adsorption/evolution and the electrochemical process can be easily coupled with surface spectroscopic techniques such as Surface Enhanced Raman Spectroscopy (SERS) and Attenuated Total Reflection Infrared (ATR-IR) spectroscopy to study the surface reaction. Part of this work involves exploring the feasibility of such spectroelectrochemical studies of lactic acid hydrogenation.

1.7 Outline of dissertation

This dissertation describes studies on the electrocatalytic hydrogenation of α-functionalized carboxylic acids. The study is based on the process optimized for the catalytic hydrogenation of aqueous lactic acid to propylene glycol using 5% Ru/C catalyst, 150°C and 1200 psi H_2 gas at a substrate concentration of 10-15g/100mL. It was observed from earlier studies that the hydrogenation of carboxylic acids having certain functional groups at the α position is much faster than the corresponding unsubstituted carboxylic acids. Chapter 2 describes some initial studies of electrocatalytic hydrogenation with a model α-functionalized carboxylic acid, benzoyl formic acid at low concentration (10 ppm) using boron doped diamond (BDD) electrodes modified with Pt and Pt/Ru. This compound was chosen in order to facilitate the detection and quantification of the reactant using HPLC-UV at low concentrations. A potential in the hydrogen evolution region for Pt was applied using chronoamperometry and a plot of current vs. time was obtained. The effect of varying the conditions such as analyte

concentration, step potential, pH and temperature on the yields of the various electrohydrogenation products was studied.

For the ECH to be useful at a preparative and commercial scale, the process needs to be carried out at much higher concentrations of carboxylic acid. Chapter 3 describes the ECH of lactic acid in mM concentrations in a bulk electrolysis cell using constant current electrolysis and Ru deposited on carbon felt as a cathode. The effects of variation in temperature, current, nature of electrolyte and lactic acid concentration are discussed followed by the calculation of kinetic parameters. In this case, the only product of the ECH of lactic acid is lactaldehyde and not propylene glycol. Since the conversion was very low, other strategies were developed to improve the conversion of lactic acid. Chapter 4 describes the ECH of lactic acid using 5% Ru/C powder catalyst entrapped in the pores of Reticulated Vitreous Carbon (RVC), a macroporous material with a high hydrogen overpotential. This method was developed by Menard and coworkers, and was used to study the hydrogenation of phenol to cyclohexanol. This method allows the use of the same powder catalysts that effect chemical hydrogenation and therefore, retains the essential features of the catalytic process. The effect of variations in temperature, current and nature of electrolyte on lactic acid conversion are reported. In this case, the major ECH product is lactaldehyde, but small quantities of propylene glycol (<10%) are also obtained. Also included is a discussion about studies on the adsorption of electrolyte anions on electrode surfaces reported in the literature and the possible reasons for the effects of electrolyte anions on the efficiency of lactic acid conversion. Chapter 5 describes the ECH of lactic acid using a similar strategy to that used in chapter 4, but using non-carbon supports for Ru. In this case, lactaldehyde is the major ECH product

along with small quantities of acrylic acid formed in some cases, but no propylene glycol formation was observed, indicating the importance of the precise structure of the catalyst in determining the nature of products.

Chapter 6 describes *in situ* Attenuated Total Reflection-Infrared (ATR-IR) spectroscopic studies of the ECH of lactic acid. The advantage of the ATR mode over other modes of FTIR spectroscopy is that it is highly selective to species very close to the electrode surface and minimizes interference from bulk species. The ECH of lactic acid in various electrolytes was followed in real-time and the IR spectra were recorded at regular intervals. We will see that the infrared spectra provide valuable information on the mode of adsorption of lactic acid and effect of electrolyte anions, thus proving the feasibility of using vibrational spectroscopic techniques to study the mechanistic details of the hydrogenation reaction. Finally chapter 7 presents the conclusions of the study and some directions for future research.

CHAPTER 2

ELECTROCATALYTIC HYDROGENATION OF A MODEL α-FUNCTIONALIZED CARBOXYLIC ACID, BENZOYL FORMIC ACID

2.1 Introduction

This chapter deals with studies on the ECH of a model α-functionalized carboxylic acid, benzoyl formic acid (BFA) using boron doped diamond (BDD) electrodes modified with Pt and Pt/Ru. The goal of this study was to determine the feasibility of carrying out ECH of carboxylic acids. It is important to carry out experiments at low concentration of analyte and to look at the extent of reaction and distribution of products before moving on to bulk electrolysis. Diamond as a material is known for its unique mechanical, thermal, optical and electrical properties and is currently being investigated as an electrode material by many groups.

Swain and coworkers[49,50] have developed boron doped diamond electrodes containing Pt particles for use in various types of electrocatalysis. These newly developed conductive sp^3 carbon electrodes are superb materials for various electrochemical applications. They are made by microwave assisted chemical vapor deposition (CVD) in a CH_4/H_2 gas mixture in a reactor, and have unique properties like high conductivity, chemical inertness, thermal conductivity, corrosion resistence and electrochemical stability. The high atomic density and the strong sp^3 bonding within the lattice inhibit morphological and microstructural damage due to oxidation by anodic polarization and chemical reagents as the oxidation is confined only to the surface. These properties enable diamond to withstand current densities on the order of 1A cm^{-2} for days, in both acidic and alkaline media without significant structural degradation that would result in

dislodging or instability of the deposited metal particles. Incorporation of metal adlayers like Pt, Pb, Hg, etc. into the surface of the boron doped diamond support by electrochemical deposition allows higher current densities and temperatures to be used for electrocatalysis without any effect on the structural characteristics of the electrodes. Pt can also be codeposited with Ru nanoparticles[51] to form a bimetallic catalytic surface for electrocatalysis.

These specially designed electrodes should be ideal for carrying out electrocatalytic hydrogenation of carboxylic acids and their derivatives, especially α-functionalized carboxylic acids. This would enable us to develop a method for the electrosynthesis of the reduction products using milder conditions compared to the batch process. It also opens up the possibility of using spectroscopic techniques coupled with electrochemistry to investigate the mechanism of the reaction on the catalytic surface and the nature of the adsorbed layer. This approach is much more feasible than a direct *in situ* spectroscopic study of the heterogeneous catalytic surface under the high temperature and pressure conditions of chemical hydrogenation, which could suffer from hurdles such as the instability of the Internal Reflection Element (IRE) in the harsh conditions.

The Pt/BDD composite electrodes used here were prepared by galvanostatic electrodeposition[50] from a solution containing 1mM K_2PtCl_6 in 0.1M $HClO_4$ using a current density of 0.1 mA/cm^2 for 400 s. The Pt//Ru/BDD composite electrodes were prepared by galvanostatic electrodeposition using a similar method, from a solution containing 1 mM K_2PtCl_6 and 1 mM $RuCl_3$. in 0.1 M $HClO_4$. The metal coated film was then placed back in the reactor and boron-doped diamond was deposited for an additional 3 h. During this step, the diamond film grows around the base of the particles, anchoring

them and stabilizing them within the diamond microstructure. The secondary diamond film thickness is less than 1μm. After preparation, the electrodes were cleaned by cycling the potential between -400 and 1500 mV (vs. Ag/AgCl) 100 times at 50 mV/s in order to oxidize non-diamond carbon impurities such as adsorbed carbon and hydrocarbons (formed during CVD) from the surface. The nominal Pt particle size is 30-500 nm and the distribution density is 10^9 cm^{-2}. The secondary diamond growth reduces the total active Pt exposed by about 30-40%.

The main goal of this project is to explore the possibility of applying electrocatalytic hydrogenation effectively to aqueous free carboxylic acids as an alternative to high pressure hydrogenation and to determine the nature of adsorbed species on the catalyst surface in the electrocatalytic hydrogenation of α-functionalized carboxylic acids like benzoyl formic acid and lactic acid. These two compounds are good model compounds for aromatic and aliphatic alpha functionalized carboxylic acids respectively and may show differences in behaviour due to different modes of adsorption on the catalyst surface. Since the alpha carbonyl group is easier to reduce, it is first converted to the alcohol which then facilitates the hydrogenation of the carboxylic acid group. In case of BFA, the expected intermediate is mandelic acid, the direct analogue of lactic acid, so the subsequent reduction is presumably similar except for extra features introduced by the presence of the phenyl group.

An analog of pyruvic acid, BFA, was chosen as the analyte in order to facilitate the analysis of the reactant to determine the conversion under various conditions. The analysis of BFA was performed using HPLC-UV at 210 nm. as BFA has a much higher extinction co-efficient for u.v. absorption than do pyruvic or lactic acids, which could not

be detected by HPLC with u.v. or refractive index detection in the range of concentrations used. Also there are four possible products that can be obtained by the hydrogenation of BFA and it is interesting to study their distribution under various ECH conditions. BFA has three reducible groups with the ease of reduction decreasing in the order, -COOH > $-C_6H_5$ > -C=O. For the purpose of comparison, mandelic acid, the aromatic analog of lactic acid, was also subjected to ECH under similar conditions and the results were compared to those of the ECH of BFA.

2.2 Experimental

2.2.1 Electrochemical cell

The ECH of BFA was carried out in a three necked glass cell of volume about 20 mL as shown in figure 2.1. The auxiliary electrode was graphite and the reference electrode was Ag/AgCl (E^0 vs. SCE= -47mV). The working electrode was connected to the external circuit through a Cu current collecting plate. The exposed surface area of the working electrode was determined by the o-ring between the cell and the electrode and was about 0.2 cm^2. The applied potential was controlled using a potentiostat, model CY2000 (Cypress Systems). All potentials reported are in reference to Ag/AgCl reference electrode.

The experiments with the Pt rotating disc electrodes were carried out in a three-necked cell of total volume about 40 mL (figure 2.2) containing an anodic and a cathodic compartment separated by a glass frit. The auxiliary and reference electrodes were similar to the ones used in the other experiments. The working electrode was a Pt rotating

disc electrode (A=0.07cm^2). The rotation speed was controlled by a rotation controller (Metrohm 628-10).

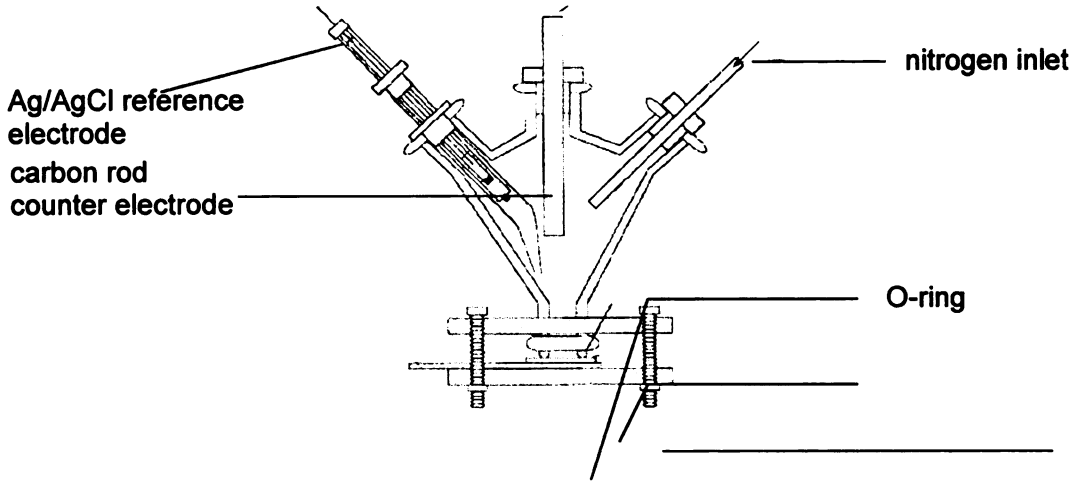

Figure 2.1: Schematic diagram of electrochemical cell (adapted from Granger, M.C.; Witek, M.; Xu, J.; Wang, J.; Hupert, M.; Hanks, A.; Koppang, M.D.; Butler, J.E.; Lucazeau, G.; Mermoux, M.; Strojek, J.W.; Swain, G.M. *Anal. Chem.*, **2000**, *72*, 3793-3804)

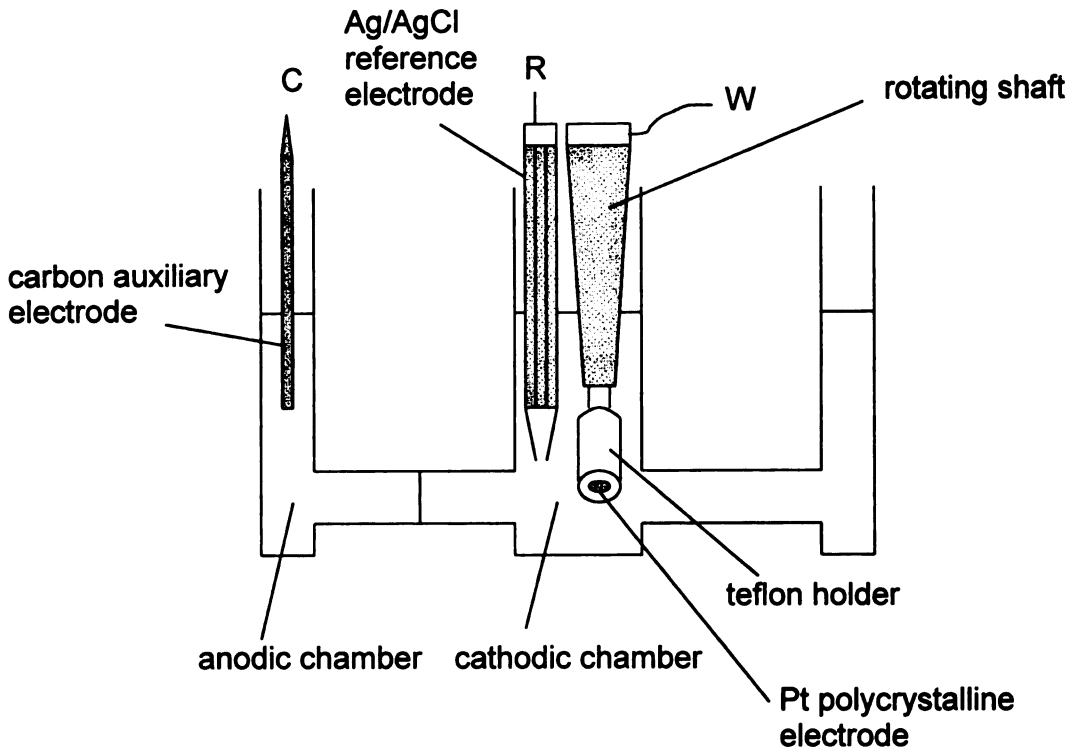

Figure 2.2: Schematic diagram of the electrochemical cell used with the rotating disc electrode (RDE) (R-reference, W-working, C-counter)

2.2.2 Electrode preparation

The Pt polycrystalline electrode was polished successively with a slurry of 1.0 μm, 0.8 μm and 0.05 μm alumina in water before use. After each step of the polishing process, the electrode was sonicated in ultrapure water for 10 min. to remove residual alumina from the surface followed by rinsing with water. The electrode was also polished with a slurry of the 0.05 μm alumina in water before every run.

The Pt/BDD and Pt/Ru/BDD electrodes were cleaned by immersing in distilled isopropyl alcohol in the cell for 20 min. The electrode was then rinsed with water and dried in a

stream of nitrogen, followed by cycling the potential between -200 mV and 1200 mV in 0.1M $HClO_4$ until the features of a clean Pt surface were clearly visible. The electrode was again rinsed with water and dried in nitrogen.

2.2.3 ECH method

The cell was filled with the solution of BFA of required concentration in 0.01 M H_2SO_4. The solution was degassed with nitrogen gas for 10 min. to remove dissolved oxygen. The potential was stepped from 400 mV to the required potential in the cathodic region and the current-time curve was recorded for 2 h at constant potential. After every experiment, the solution was removed from the cell and analysed by HPLC-UV and GC-FID.

For the experiments with the Pt rotating disc electrode, the procedure was the same, except that the anodic chamber was filled with 0.01M H_2SO_4, and the cathodic chamber was filled with 6.67 mM BFA in 0.01 M H_2SO_4.

2.2.4 Analysis of products

The standard compounds, benzoyl formic acid (99%), mandelic acid (99%) and hexahydromandelic acid (98%) were purchased from Aldrich. Cyclohexyl ethylene glycol was synthesized using the procedure described below.

2.2.4.1 Benzoyl formic acid (BFA), mandelic acid (MA) and 1-phenyl 1,2-ethanediol (PED)

Reaction mixtures were analyzed by HPLC with uv detection at λ=210 nm, using a Biorad HPX87H ion exchange column at 65°C, a Spectra-Physics pump model SP8810 and Hitachi uv detector model L-4000H. The mobile phase used was 5 mM H_2SO_4, run isocratically at a flow rate of 0.6 mL/min.

Solutions of BFA, MA and PED in 5 mM H_2SO_4 in the concentration range 2-10 mg/L were used to obtain calibration curves (figure 2.4). A standard HPLC chromatogram containing benzoyl formic acid, mandelic acid and phenyl ethylene glycol, each at 10 mg/L is shown in figure 2.3.

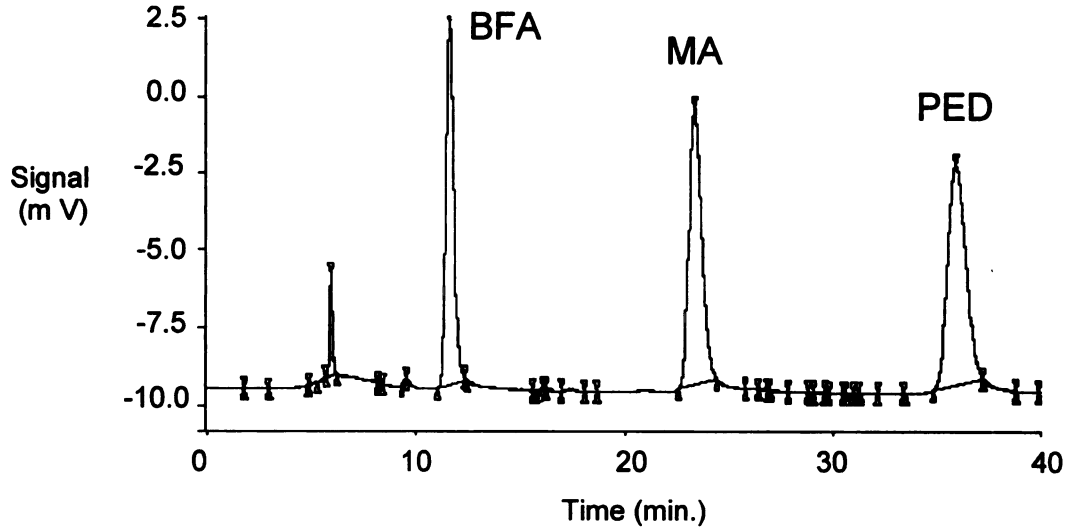

Figure 2.3: HPLC-UV chromatogram standard showing peaks for BFA, MA and PED (concentration=1.33 X 10^{-5}M)

The response factors were calculated using the following expression.

$$\text{Response factor} = \frac{\text{Molar concentration of analyte}}{\text{Peak area counts}}$$

$$= \frac{1}{\text{slope of the calibration curve}}$$

The concentrations of the unknown samples were calculated by multiplying the peak area counts of the respective sample with the response factors.

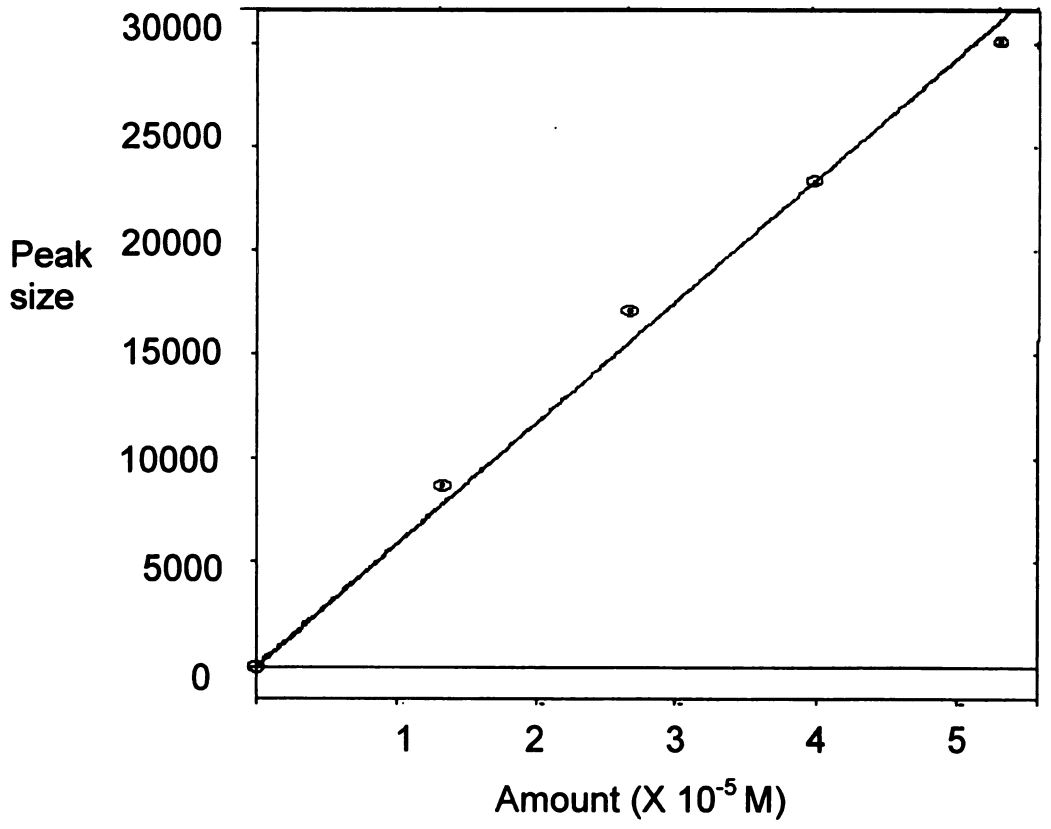

Figure 2.4a: Calibration curve for BFA (R^2=0.9951)

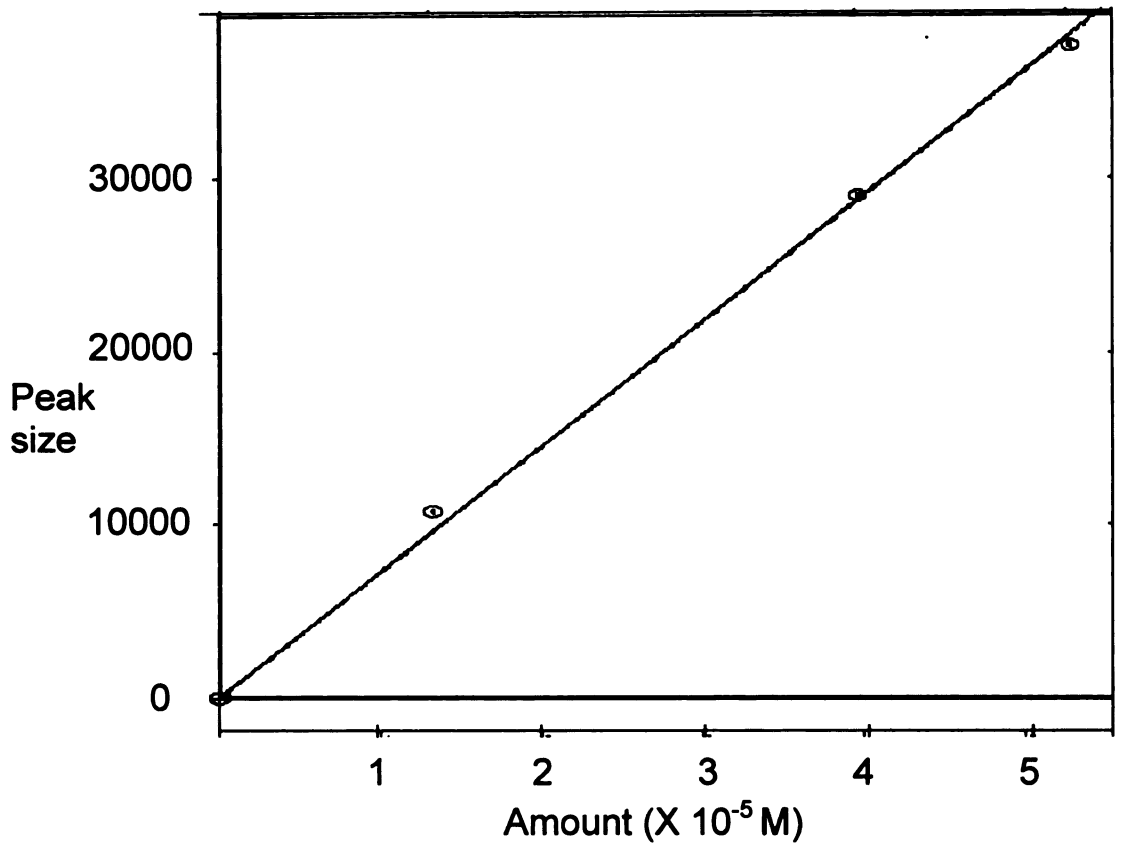

Figure 2.4b: Calibration curve for MA (R^2=0.9986)

2.2.4.2 Synthesis of cyclohexyl ethylene glycol (CEG)

CEG used as a standard for analysis was synthesized by the 5% Ru/C catalyzed hydrogenation of phenyl ethylene glycol in a Parr reactor (scheme 2.1). The 5% Ru/C catalyst was reduced overnight in the reactor in the presence of H_2 (300 psi) at 150°C. 100 mL of an aqueous solution containing 1.0 wt% of phenyl ethylene glycol was charged into the reactor and reduced at 150°C and 1200 psi H_2 for 7 h with constant stirring at 1100 rpm. After the reaction, the reactor was cooled to room temperature and the excess H_2 was vented out of the reactor. The reaction mixture was transferred to a 250mL beaker and allowed to stand overnight. The product precipitated due to poor

solubility in water and was collected by filtration and dried in air (for characterization, see appendix).

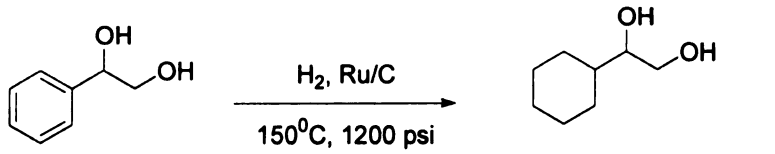

phenyl ethylene glycol — cyclohexyl ethylene glycol

Scheme 2.1: Batch synthesis of CEG

2.2.4.3 Hexahydromandelic acid (HMA) and cyclohexyl ethylene glycol (CEG)

HMA and CEG were detected and quantified using derivatization, followed by GC-FID since these compounds do not absorb in the u.v. region.

For the derivatization, 2 mL of the sample was treated with 0.2 mL of 0.1 M $Ba(NO_3)_2$ to precipitate the sulfate ions from the electrolyte. The solution was then evaporated to dryness in a vacuum centrifuge. 0.5 mL of bis trimethylsilyl trifluoro acetamide (BSTFA) containing 1% trimethyl chloro silane (TMCS) (Supelco) was added to the sample, mixed thoroughly, the mixture is transferred to a vial and allowed to stand for 1h at room temperature.

The analysis was performed using a Perkin Elmer model 8500 gas chromatograph equipped with a flame ionization detector, using a SPB-35 column (30m, 25mm ID).

2 μL of the mixture was injected into the GC with the injector temperature at 300°C. The column temperature was held at 50°C for 5 min., ramped to 250°C at 15°C/min. and held at 250°C for 15 min. The detector was maintained at a temperature of 330°C and the total runtime of each sample was 33.3 min.

Solutions of CEG and HMA in 5 mM H_2SO_4 in the concentration range 2-10 mg/L were used to obtain calibration curves. A standard GC chromatogram containing the trimethyl silyl (TMS) derivatives of CEG and HMA (10 mg/L) is shown in figure 2.5a. The blank chromatogram is shown in figure 2.5b. The peaks at 13.5 and 14.0 min. are present in the blank as well and are therefore assigned to species present in the derivatizing reagent. The presence of two peaks for each derivative is probably due to the incomplete derivatization, leading to the formation of both the monosilylated and disilylated derivatives. For the quantification, only the disilylated derivatives were considered. The TMCS peak (ret. time 8.59 min., not shown) was used as the reference peak. The calibration curves for CEG and HMA are shown in figures 2.6. The concentration of HMA and CEG in the unknown samples were determined by dividing the peak area ratio by the response factors.

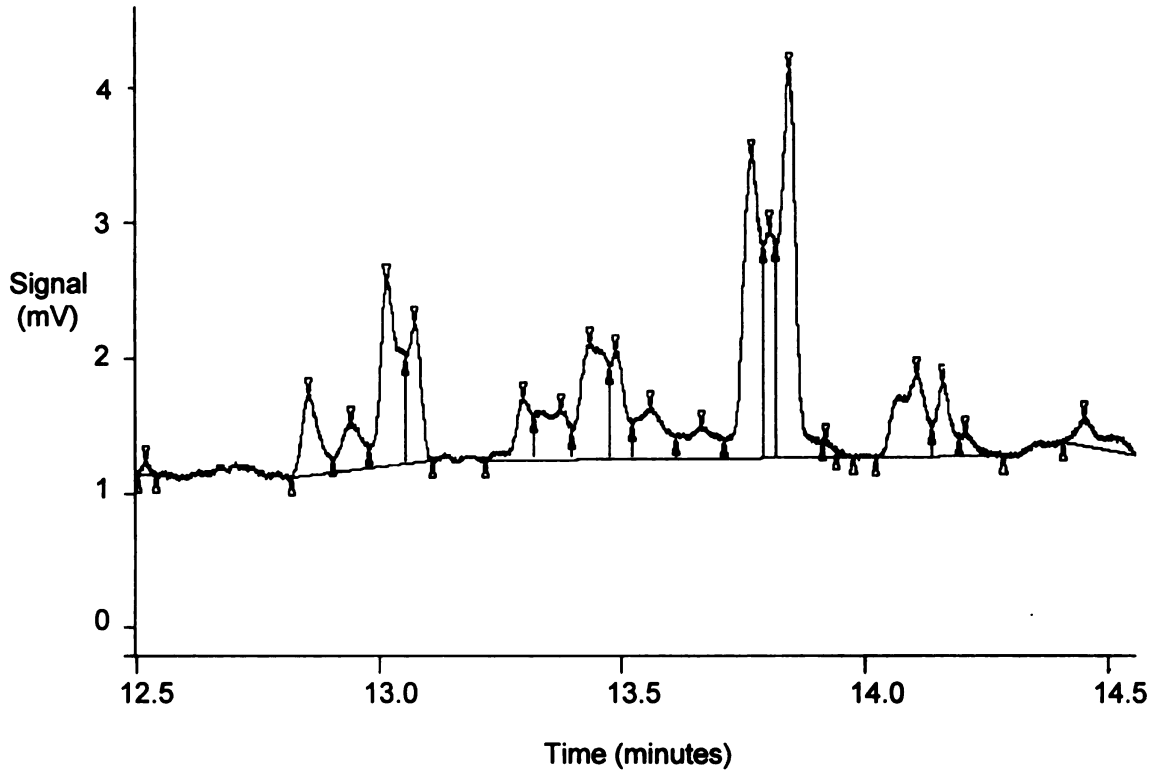

Figure 2.5a: GC-FID chromatogram standard showing peaks for the TMS derivatives of CEG and HMA (concentration= 2.0 mg/L)

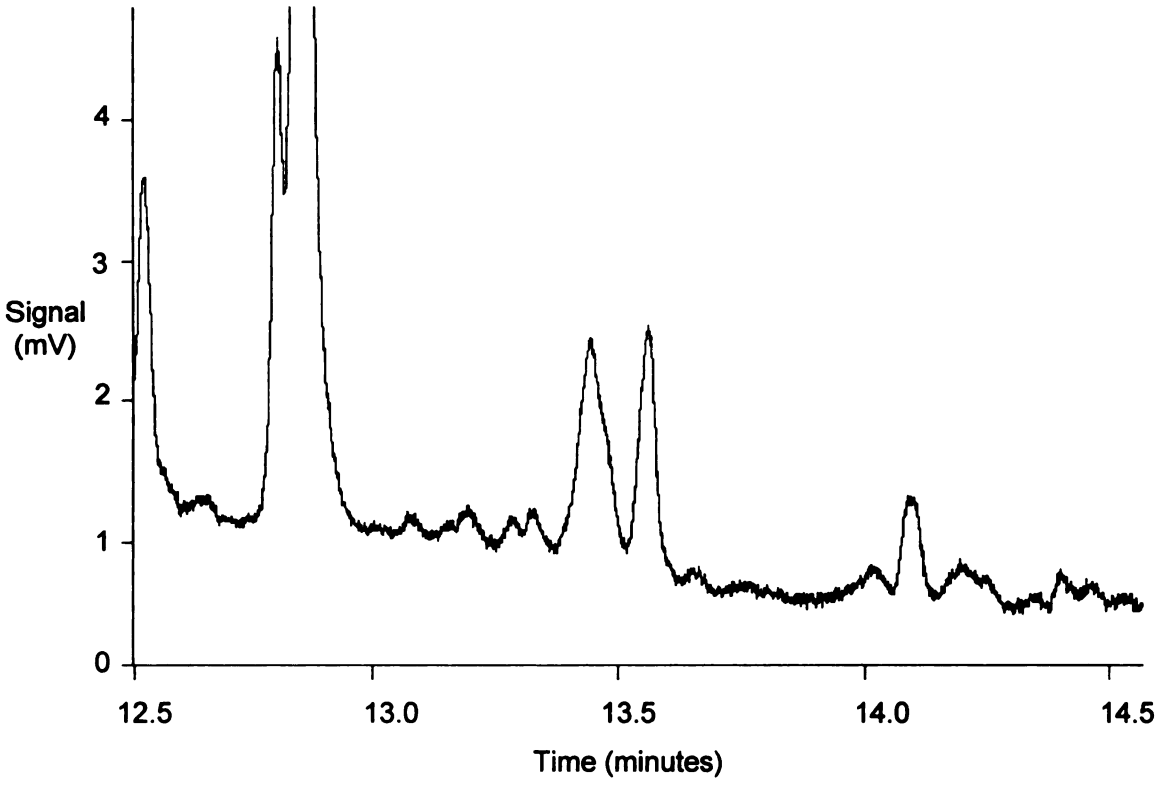

Figure 2.5b: GC-FID chromatogram standard showing peaks from the blank reagent (BSTFA + TMCS) run under similar conditions

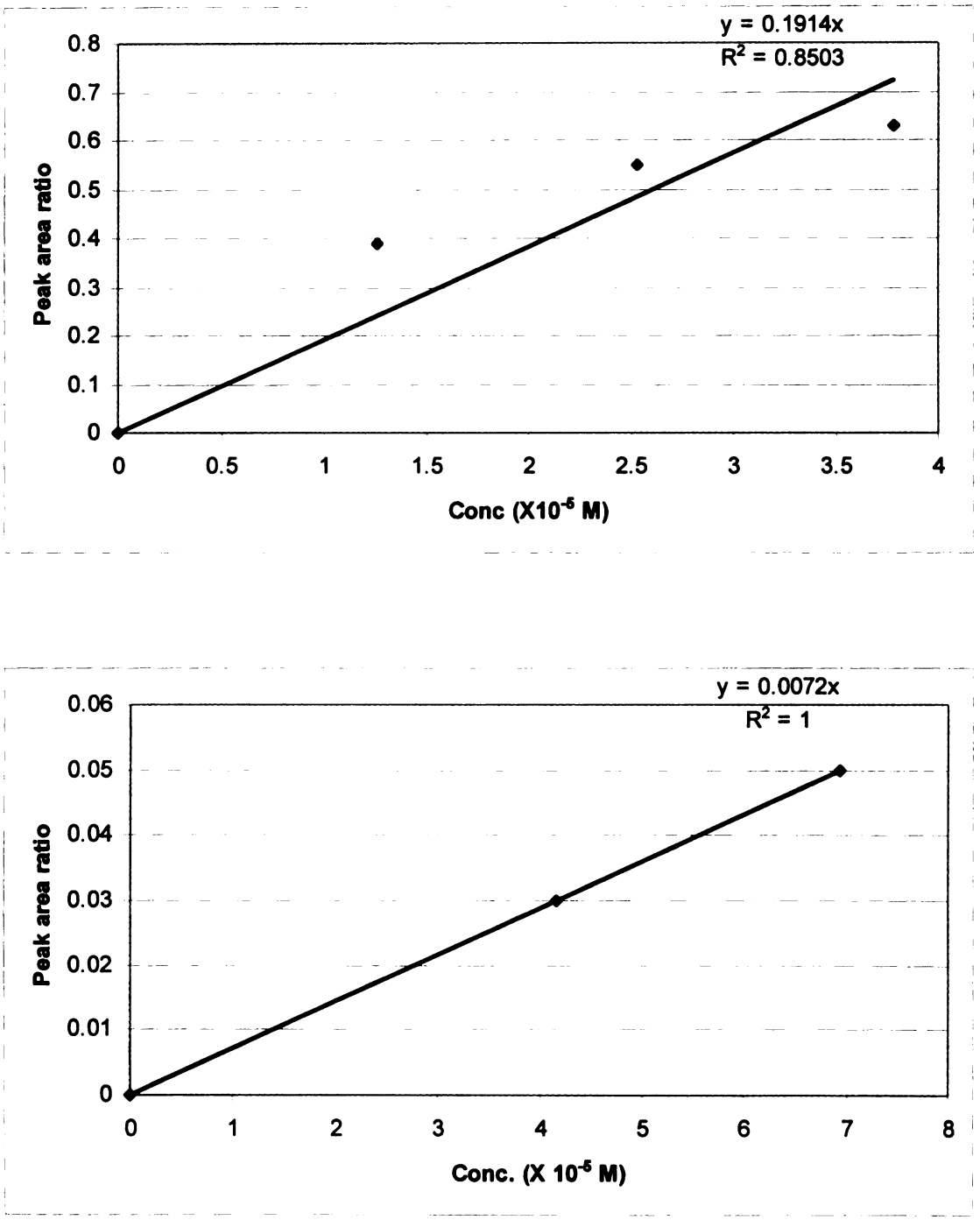

Figure 2.6: Calibration curves for HMA (top) and CEG (bottom)

2.3 Results and Discussion

2.3.1 Cyclic voltammetry of benzoyl formic acid

Shown in figure 2.7 is the cyclic voltammogram of 6.67 X 10^{-5} M (10 ppm) BFA in 0.01 M H_2SO_4 on Pt polycrystalline working electrode at a scan rate of 10 mV/s. The figure shows scans 1, 2, 5 and 10 out of 10 scans in the range -600 to 1200 mV. After the first scan, there is a significant increase in the anodic oxidation current due to oxidation of other carbonaceous impurities, forming a cleaner surface and providing more sites for the adsorption of BFA. This indicates that BFA is not oxidized easily even at higher potential. The CV indicates an irreversible and strong adsorption of BFA on the Pt surface, involving partial charge transfer from the π-orbital in the aromatic ring to the Pt d-orbital. This explains the appearance of a broad oxidation peak and the absence of sharp and distinct oxidation and reduction peaks.

Cyclic voltammograms were also obtained in 0.01 M H_2SO_4 on Pt polycrystalline electrode by scanning the potential in the range -200 to 400 mV at 50 mV/s in the presence and absence of BFA (70 μM). The results are shown in figure 2.8. There are no features due to BFA in the potential range used, indicating that BFA does not undergo oxidation or reduction by direct electron transfer in this potential range. However, the peak areas of the hydrogen adsorption and desorption peaks at 200 mV are lower in the presence of BFA, indicating that part of the surface is covered by BFA which decreases the surface area available for hydrogen adsorption.

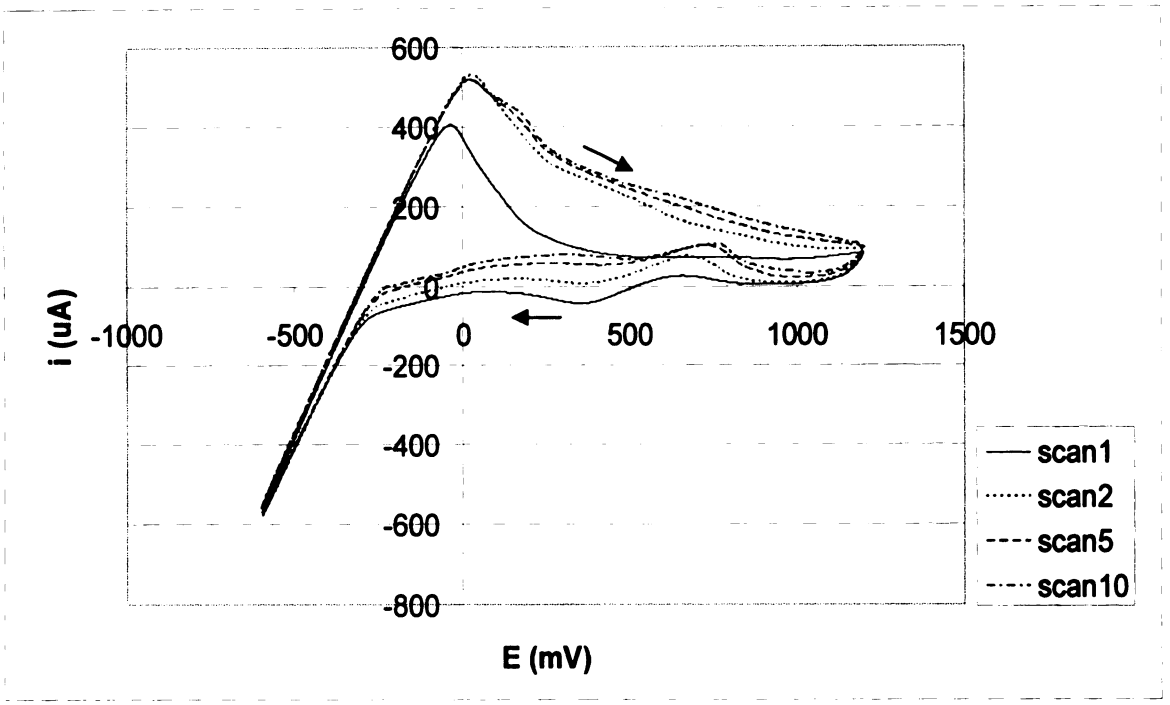

Figure 2.7: Cyclic voltammogram of 6.67 X 10^{-5} M (10 ppm) BFA in 0.01M H_2SO_4 on a Pt polycrystalline working electrode at a scan rate of 10 mV/s. Arrows indicate direction of scan.

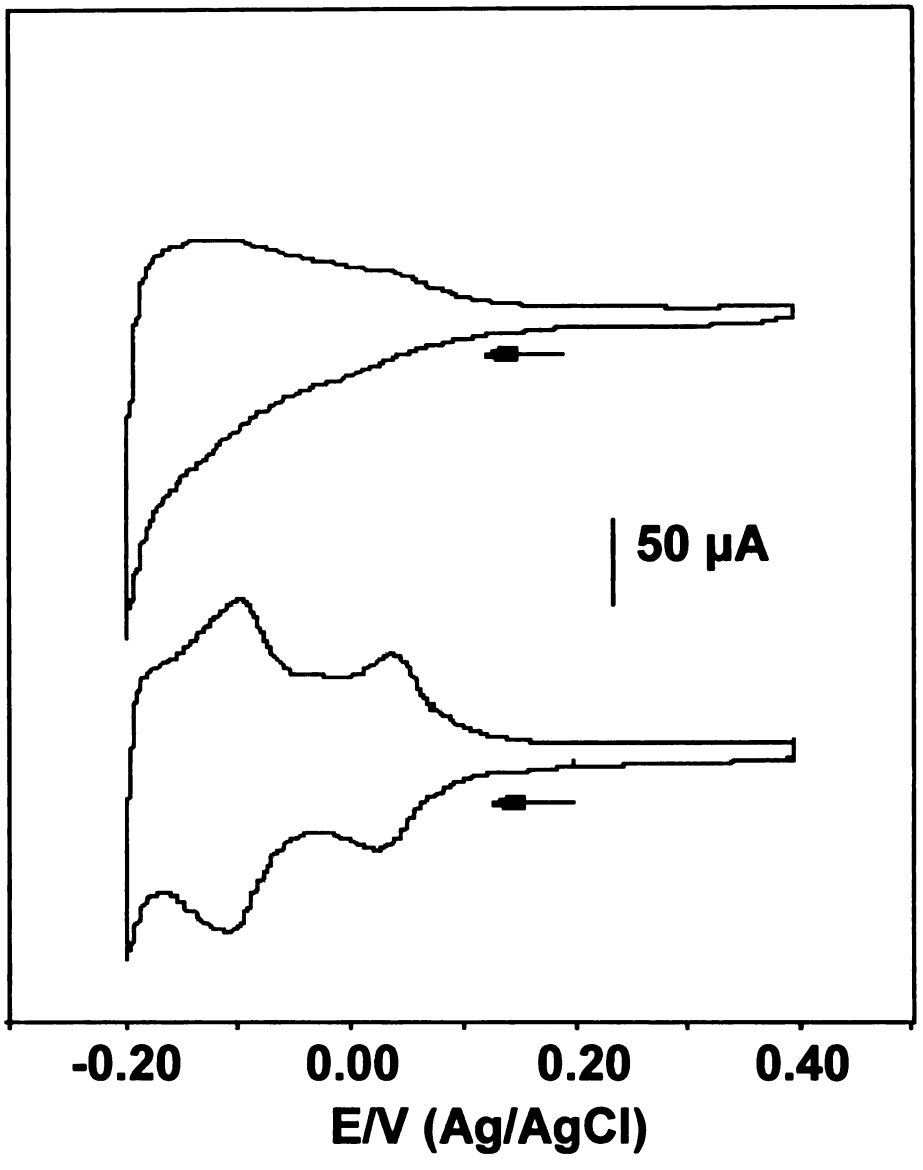

Figure 2.8: Cyclic voltammograms of Pt in 0.1 M H_2SO_4 in the presence (top) and absence (bottom) of BFA (70 µM) at a scan rate of 50 mV/s (data obtained by Prof. Carol Korzeniewski at Department of Chemistry, Texas Tech University)

2.3.2 Determination of active metal surface area

The active metal surface areas of the two working electrodes, namely Pt/BDD and Pt/Ru/BDD were determined from the hydrogen desorption charge, obtained from the area under the hydrogen desorption peaks at 200 mV. The hydrogen desorption charges were calculated by integration to determine the area under the peaks followed by subtraction of the area under the baseline due to double layer charging. The calculated areas are reported in table 2.1. Figure 2.9 shows the cyclic voltammograms of the Pt polycrystalline, Pt/BDD and Pt/Ru/BDD in 0.1 M $HClO_4$ in the potential range, -200 to 1200 mV, scanned at 100 mV/s, in comparison with Pt polycrystalline electrode. It can be seen that both the composite electrodes show features similar to Pt, but have active surface areas much lower than Pt polycrystalline electrode.

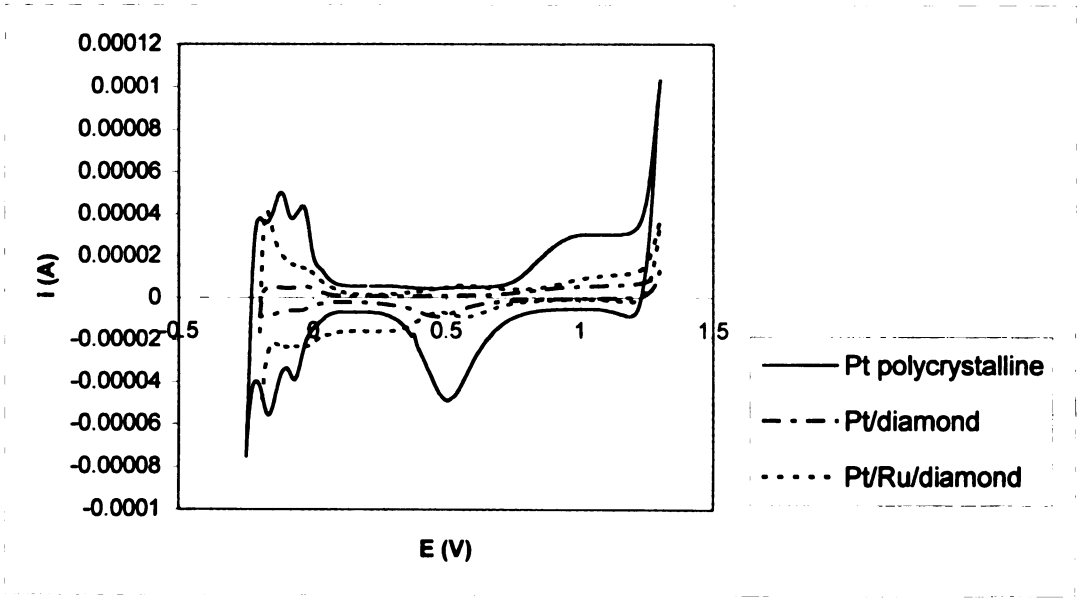

Figure 2.9: Cyclic voltammograms of Pt polycrystalline, Pt/BDD, and Pt/Ru/BDD in 0.1 M $HClO_4$ at 100 mV/s.

Electrode	Actual Pt surface areas (cm^2)
Pt polycrystalline	0.77
Pt/BDD	0.13
Pt/Ru/BDD	0.21

Table 2.1: Active Pt surface areas for the Pt electrode and composite electrodes calculated from the area under the hydrogen desorption peaks in figure 2.9

2.3.3 Current-time transients

The i-t curve for one of the experiments on Pt/Ru/BDD is shown in figure 2.10 (Initial potential (E_1)= 0.4 V, Final potential (E_2)= -0.4 V). The i-t curve for the run without the substrate and the theoretical curve as predicted by the Cottrell equation are also plotted. The current response in chronoamperometry is proportional to the flux or the rate of diffusion of the electroactive material (H_3O^+ in this case) to the electrode surface. As time progresses, there is an increase in the length of the diffusion layer leading to a decrease in the concentration gradient of the electroactive species between the electrode surface and the bulk solution. This leads to a decrease in the flux of the electroactive species to the electrode surface, and a decrease in current. In figure 2.10, it can be seen that the theoretical curve shows a much sharper decay in current compared to the experimental curve, thus indicating that the reaction is not completely diffusion controlled, but may be controlled by convection or the availability of surface sites. The total charge passed (obtained by integrating the area under the curve) is slightly lower in the presence of the substrate, indicating that some of the surface sites may be occupied by

the substrate molecules even at the more negative hydrogen evolution region, thus reducing the total surface area for hydrogen adsorption.

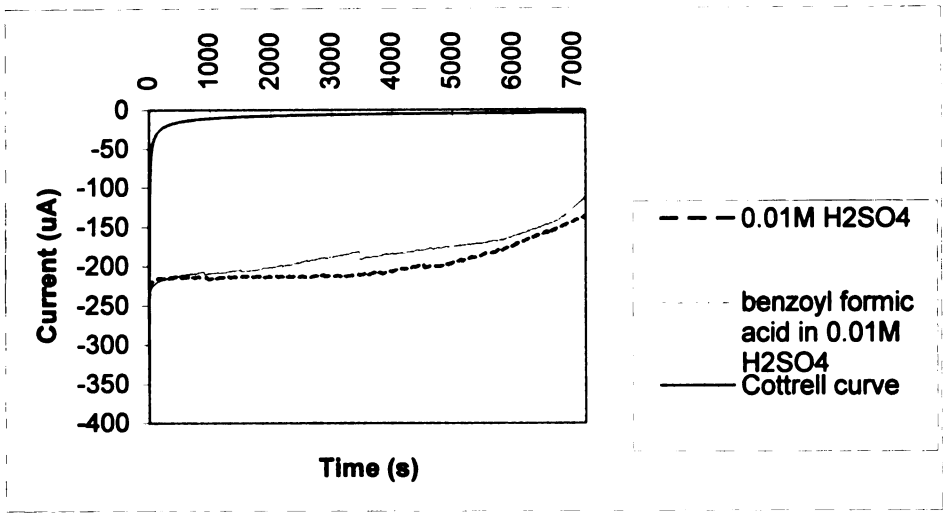

Figure 2.10: Current-time response of an ECH experiment with Pt/Ru/BDD in 0.01 M H_2SO_4 (E_1=400 mV, E_2=-400 mV)

2.3.4 ECH of BFA on Pt polycrystalline electrode

The reaction for the ECH of BFA and the various possible products are shown in scheme 2.2. BFA had three different functional groups with different ease of reduction. MA is formed by the reduction of the α-keto group. HMA is formed by the reduction of the α-keto group and the aromatic ring. PED is formed by the reduction of the α-keto group and carboxylic acid group, and CEG is formed by complete reduction of all the three functional groups. Therefore the optimum conditions for ECH were considered as the ones giving maximum yield of CEG. In all the experiments, there was no PED detected in any of the mixtures at the end of the ECH experiment and HMA was formed in

negligible amounts. However, though the total conversion of BFA was low (<25%), the yields of MA and CEG vary with conditions.

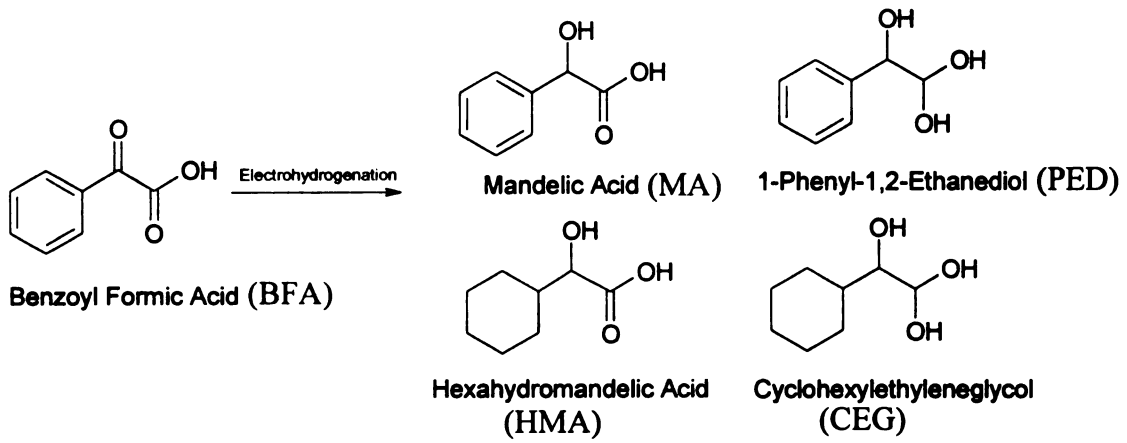

Scheme 2.2: ECH of benzoyl formic acid (possible products)

The next few sections describe the effect of ECH conditions and nature of electrode material on the yields of MA and CEG. Several parameters such as analyte concentration, step potential, pH and temperature were varied and the final concentration of the products, determined by HPLC-UV and GC-FID, were plotted as a function of the parameter.

The conditions used for the ECH experiments are summarized below.

- Method: Chronoamperometry
- Analyte: Benzoyl formic acid (6.67 X 10^{-5} M)
- Cell volume: 20 ml.
- Working electrode: Polycrystalline Pt (0.2 cm^2), Pt/BDD ot Pt/Ru/BDD
- Reference electrode: Ag/AgCl (E^0= -47 mV vs. SCE)
- Auxilliary electrode: Graphite

- Electrolyte: 0.01 M H_2SO_4
- Time: 2 h

2.3.5 Determination of optimum analyte concentration

Chronoamperometry was carried out using different concentrations of BFA in the range 1 to 100 ppm in 0.01 M H_2SO_4 at E_2= -425 mV. The final concentrations of the products and the percentage yields after 2 h are shown in figure 2.11.

From the results, we see that the yield of MA is maximum at an initial BFA concentration of 6.67 μM or 1 ppm and the yield of the desired product, CEG is maximum at 10 ppm or 6.67 X 10^{-5} M (10 ppm) analyte concentration. No significant quantities of HMA and PED were detected in the product mixtures. It should be noted that while the final concentration of CEG was maximum at a starting BFA concentration of 25 ppm, the percentage yield at this concentration was lower than at 10 ppm. Beyond this limit, there is a decrease in both turnover and yield. The decrease in the yields of products at higher substrate concentration is probably due to the saturation of the electrode surface with substrate molecules which compete with H atoms for surface sites. All further experiments were carried out using 6.67 X 10^{-5} M BFA. In the case of Pt/BDD and Pt/Ru/BDD, the active metal surface areas are much lower compared to polycrystalline Pt and so we would expect the surface to be saturated at much lower concentrations than that in polycrystalline Pt.

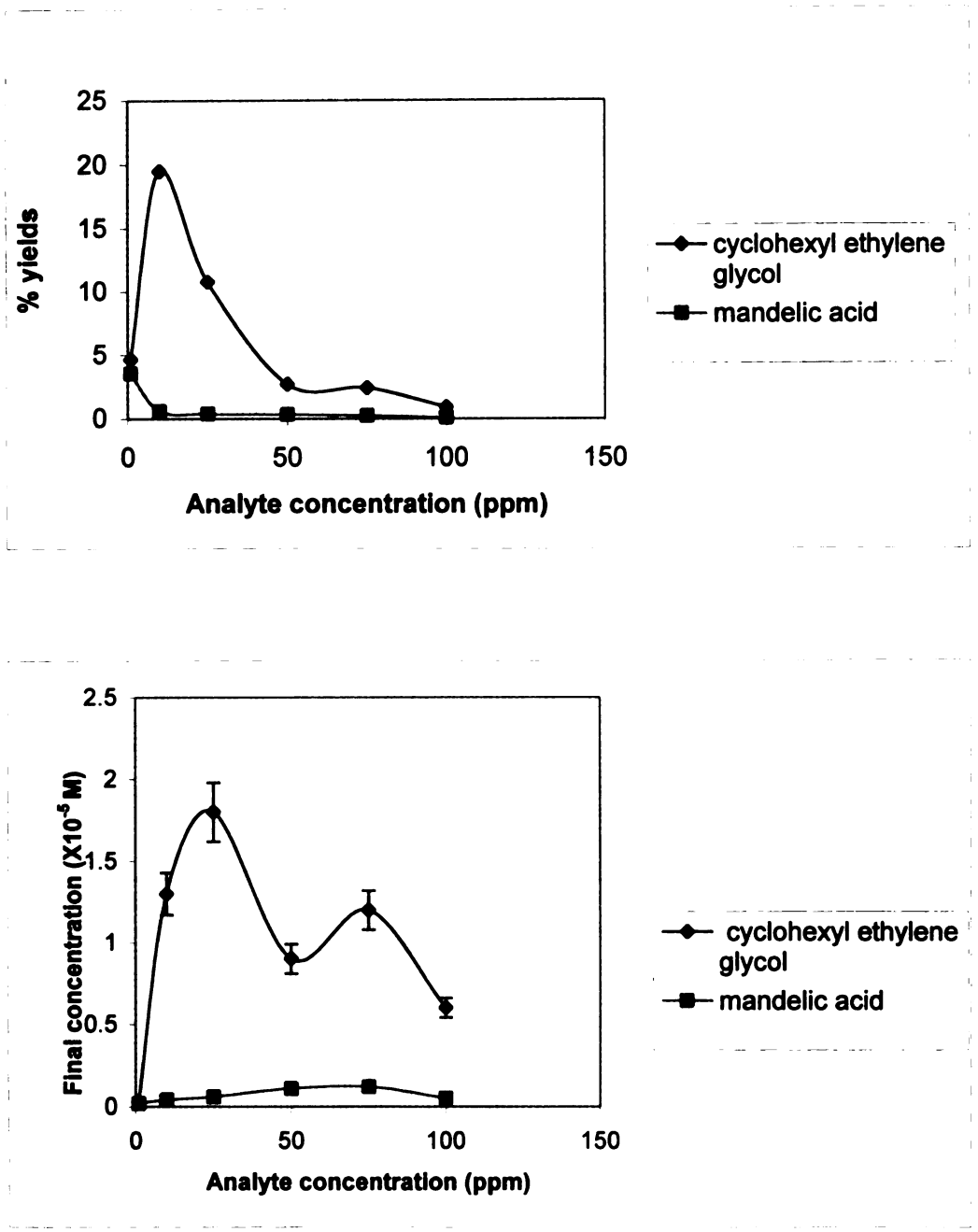

Figure 2.11: Conversion of BFA as a function of initial analyte concentration during ECH on polycrystalline Pt electrode (electrolyte: 0.01 M H_2SO_4, temperature= 25°C, E_1= 400 mV, E_2= -425 mV, time=2 h). Error bars indicate uncertainty in the analysis of products (±10%) using GC-FID

2.3.6 Effect of step potential on ECH

Electrohydrogenation of benzoyl formic acid was carried out at various step potentials ranging from –200 mV to –600 mV in 0.01 M H_2SO_4 for 2 h. The results are shown in figure 2.12. Moving towards more negative potentials, the yield of products increases and then decreases due to competition from the hydrogen evolution reaction at more negative potentials, which leads to lesser availability of adsorbed H atoms for hydrogenation of BFA. Maximum yield of the desired product (CEG) was obtained at –425 mV, at which point there is an optimum balance between surface hydrogen concentration and rate of hydrogen evolution. Conversions are indicated in terms of final concentrations of products.

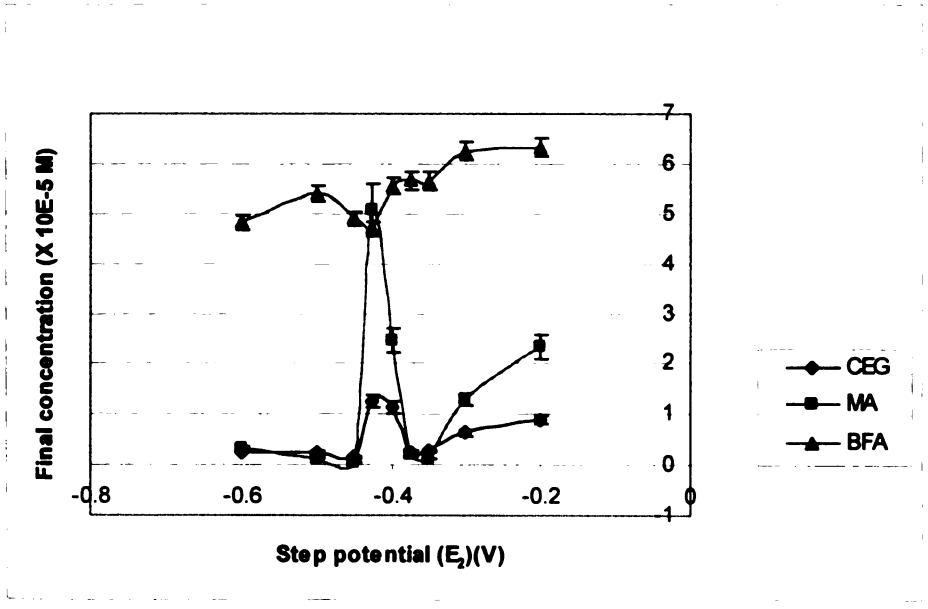

Figure 2.12: Conversion of BFA as a function of final step potential (E_2) during ECH on polycrystalline Pt electrode (electrolyte: 0.01M H_2SO_4, initial [BFA]= 6.67 X 10^{-5} M, temperature= 25°C, time = 2 h)

2.3.7 ECH of BFA using boron-doped diamond (BDD) composite electrodes

2.3.7.1 Effect of step potential

Study of electrohydrogenation of BFA at various step potentials ranging from –200 mV to –600 mV indicates that the trends in the ECH turnovers and yields as a function of potential are similar to that using a polycrystalline Pt electrode. The results are shown in figure 2.13 for Pt/BDD and Pt/Ru/BDD. In the case of Pt/BDD, the yields are decreased by a factor of 3 relative to polycrystalline Pt, which is roughly proportional to the decrease in active Pt surface area. This suggests that Pt/BDD has insufficient surface sites available for the adsorption of analyte, since Pt is known to favor hydrogen adsorption and evolution. However, in the case of Pt/Ru/BDD, there is a significant increase in the yield of the hydrogenated product at the optimum potential. This indicates that the Ru electrocatalyst plays a role in enhancing the rate of hydrogenation of BFA in comparison to hydrogen evolution.

The maximum yield of CEG is obtained at -425 mV and -375 mV for Pt/BDD and Pt/Ru/BDD respectively. Thus, in all cases, the optimum cathode potential for ECH appears to be between -375 and -425 mV. The maximum yield at the optimum potentials for Pt/BDD and Pt/Ru/BDD are 6.0% and 25.3% respectively. The yield of CEG on Pt/Ru/BDD is slightly higher than that obtained on the Pt polycrystalline electrode, even though the active metal surface area on the Pt/Ru/BDD electrode was much lower than that on the Pt polycrystalline electrode. Yield of mandelic acid is much lower at this point compared to that on polycrystalline Pt.

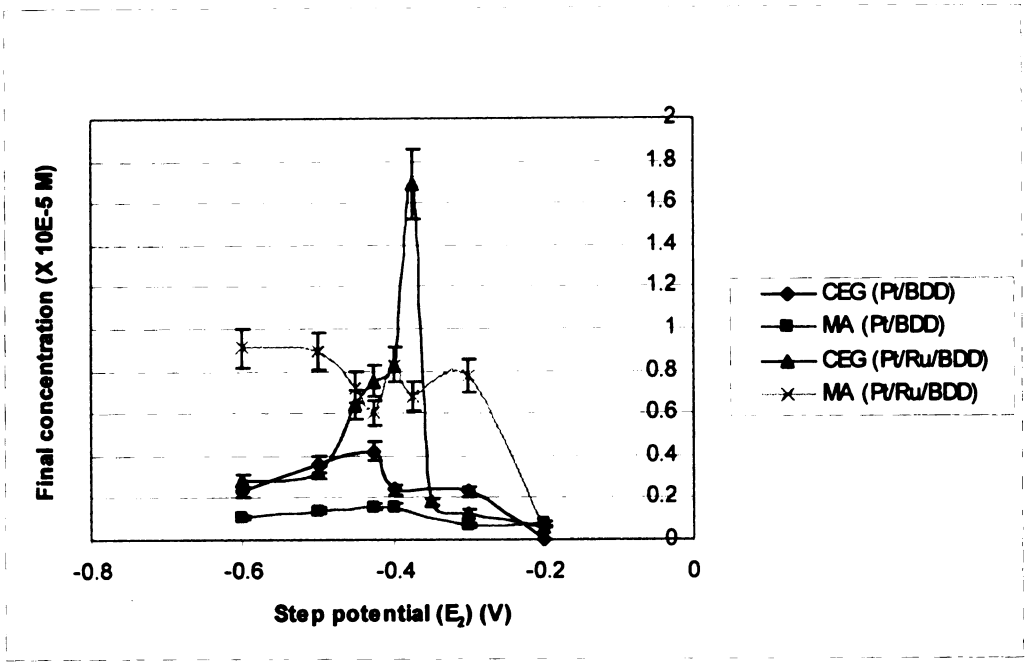

Figure 2.13: Conversion of BFA as a function of final step potential (E_2) during ECH on Pt and Pt/Ru composite electrodes (electrolyte: 0.01 M H_2SO_4, initial [BFA]= 6.67 X 10^{-5} M, temperature= 25°C, time = 2 h)

The possible reason for the enhanced hydrogenation activity of the Ru electrocatalyst may be explained by the fact that Ru is less active than Pt with respect to hydrogen adsorption and evolution[52] due to differences in the electronic properties of the two metals. Therefore, Ru provides sites for adsorption of the analyte adjacent to the adsorbed H atoms on Pt, thus increasing the rate of hydrogenation, since the rate of hydrogenation is dependent on the surface concentration of both the organic acid and hydrogen. This is depicted in figure 2.14.

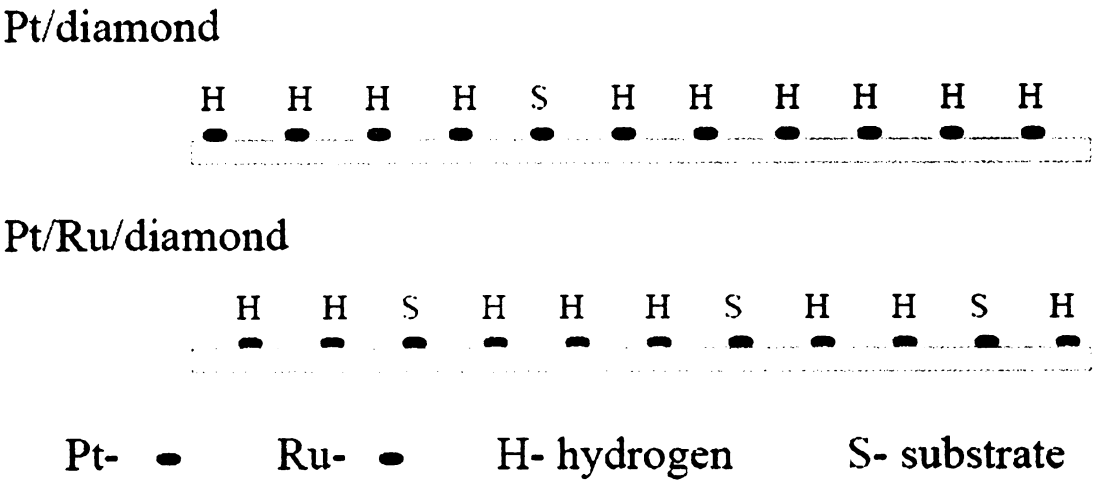

Figure 2.14: Comparison between adsorption patterns on Pt/BDD and Pt/Ru/BDD electrodes

2.3.7.2 Effect of pH

ECH of BFA was studied at pH values in the range of 2-12 at -400 mV. The pH of the solution was varied using calculated amounts NaOH and KH_2PO_4. The results are shown in figure 2.15. A study of product concentrations as a function of pH indicates that in case of both Pt/BDD and Pt/Ru/BDD, the yield of CED decreases steadily as the pH increases, indicating difficulty in hydrogenating the carboxylate group formed in basic medium. The pKa of BFA is ~3, therefore at pH>3, the –COOH group is partially dissociated. The optimum pH on both the electrodes was 2. The yield of CEG decreases sharply at higher pH due to the formation of the carboxylate anion, which has a higher affinity for the polar solvent rather than for the electrode surface. Also carboxylates resist hydrogenation because the pKa values of the product alcohols are about 10 units higher than those of the carboxylic acids, which corresponds to a difference in ΔG of about 15 kcal/mol. The

reason for the huge increase in the formation of mandelic acid at pH 7 is not yet understood.

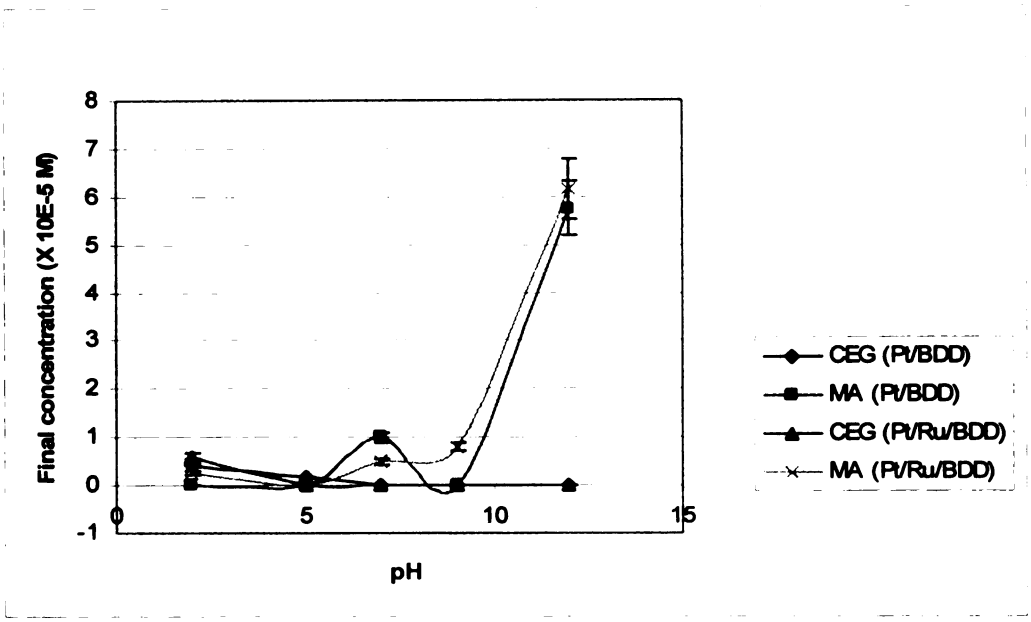

Figure 2.15: Conversion of BFA as a function of pH during ECH on Pt and Pt/Ru composite electrodes (electrolyte: 0.01 M H_2SO_4, E_2= -400 mV, initial [BFA]= 6.67 X 10^{-5} M, temperature= 25°C, time = 2 h)

2.3.7.3 Effect of temperature

ECH of BFA was carried out at various temperatures from 25 to 90°C at -400 mV. The results show completely different behavior between the two electrodes, as shown in figure 2.16. In case of Pt/BDD, the yield of CEG decreases slightly at 50 and 70°C probably due to the higher rate of desorption of reactants from the electrode surface decreasing the efficiency of ECH. There is a slight increase in the yields at 90°C, which could be due to the increase in the rate of ECH overcoming the effect of faster desorption

of reactants. In case of Pt/Ru/BDD, even though the product yields are much higher than on Pt/BDD at room temperature, the yields sharply decrease at higher temperature. This may be attributed to either faster desorption of reactants or the leaching of Ru from the electrode surface at higher temperature.

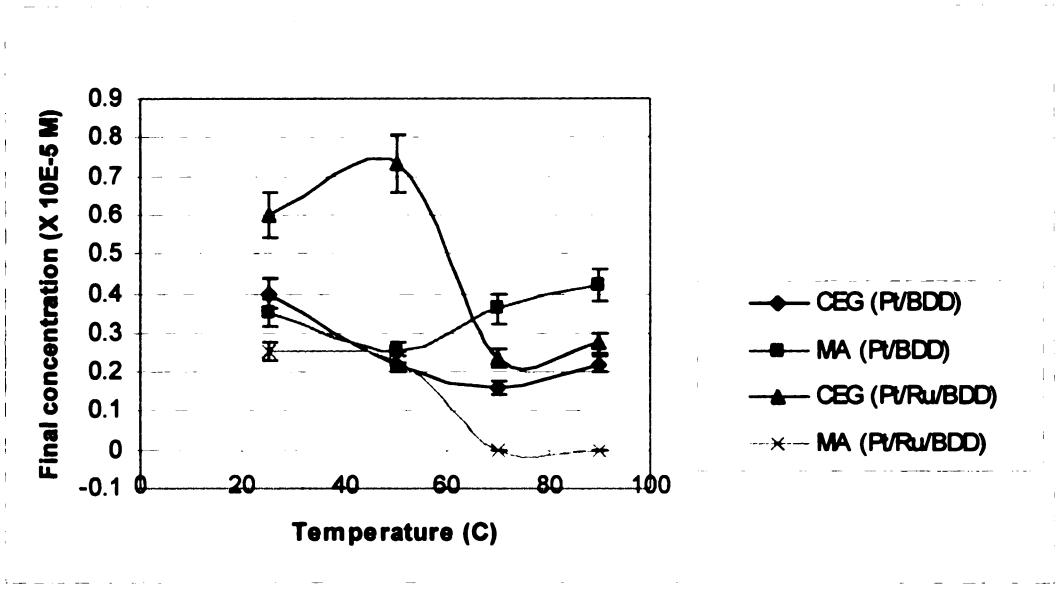

Figure 2.16: Conversion of BFA as a function of temperature during ECH on Pt and Pt/Ru composite electrodes (electrolyte: 0.01 M H_2SO_4, initial [BFA]= 6.67 X 10^{-5} M, E_2= -400 mV, time = 2 h)

2.3.8 ECH of MA

For the purpose of comparison, the ECH was carried out using MA (6.58 X 10^{-5} M) as the analyte. Chronoamperometry was carried out at various step potentials. The results are shown in figure 2.17 for polycrystalline Pt, Pt/BDD and Pt/Ru/BDD. In this case, unlike BFA, there is an increase in the yield of CEG at more negative potentials with the highest

yield at -600 mV. Pt/Ru/BDD was much more active compared to the others due to the enhancement of hydrogenation rate by Ru.

MA is expected to be the intermediate in the hydrogenation of BFA to HMA or CEG, since the hydrogenation of the keto group is much more facile than that of the other two functional groups. If this is the case, then one would expect the hydrogenation of MA to follow the same trend with applied potential as BFA i.e. exhibit maximum conversion at an intermediate potential, followed by a decrease in conversion at more negative potentials.

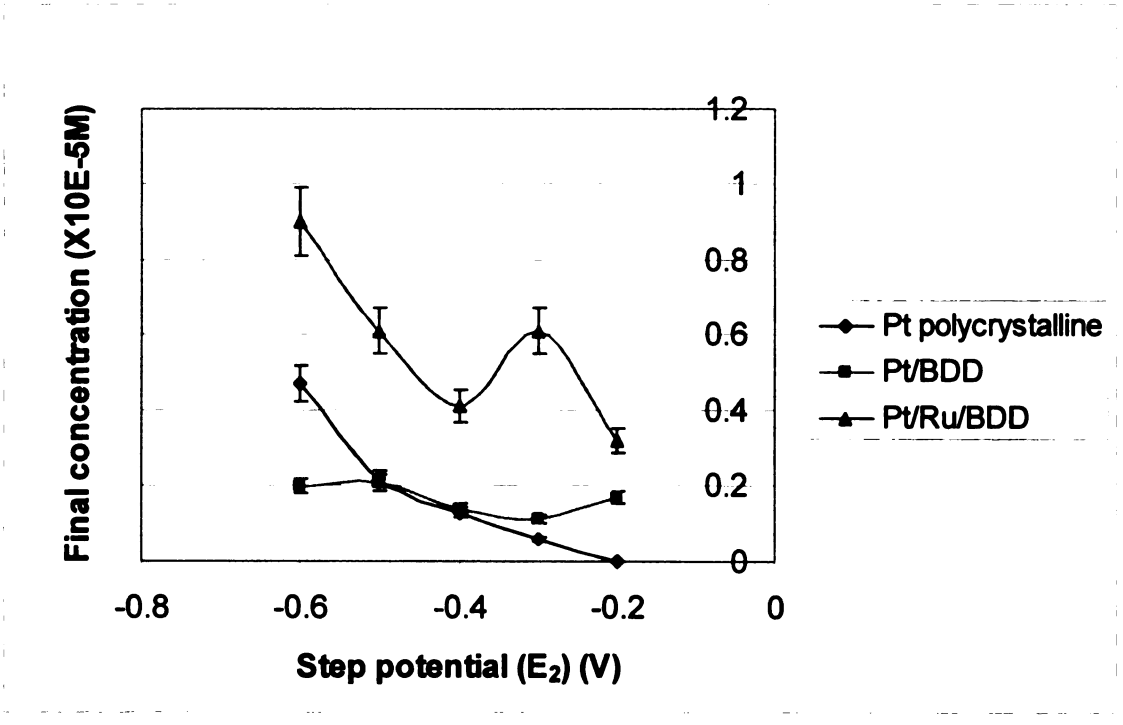

Figure 2.17: Conversion of MA as a function of step potential (E_2) during ECH on polycrystalline Pt and composite electrodes (electrolyte: 0.01 M H_2SO_4, initial [MA]= 6.58 X 10^{-5} M, temperature = 25°C, time = 2 h). Graph shows yields of CEG.

The difference in the behavior of BFA and MA with increasing step potential indicates that there is a difference in the efficiency of adsorption of the two acids on the electrode surface. BFA is much more strongly adsorbed at all potentials due to its planar structure and extended conjugation and the hydrogenation to CEG occurs very fast before the intermediate MA desorbs from the surface. This is supported by the low yields of MA as compared to CEG in all of the experiments with BFA. Therefore the hydrogenation of BFA is only limited by the concentration of adsorbed H adjacent to adsorbed BFA. On the other hand, hydrogenation of MA is probably limited by the concentrations of both adsorbed MA and H.

2.3.9 Effect of mass transport

In order to study the effect of mass transport on the ECH of BFA (6.67×10^{-5} M), experiments were carried using a Pt rotating disc electrode at various rotation speeds. In each experiment, the potential was stepped to -400 mV and the ECH was carried out for 2 h in 0.01 M H_2SO_4. The results are shown in figure 2.18.

At all rotation rates, the yields of the products are similar and within the range of experimental error. No MA was detected in any of the mixtures. Increasing the stirring rate did not enhance the rate of ECH. From these results, it is clear that mass transport does not significantly influence the ECH reaction.

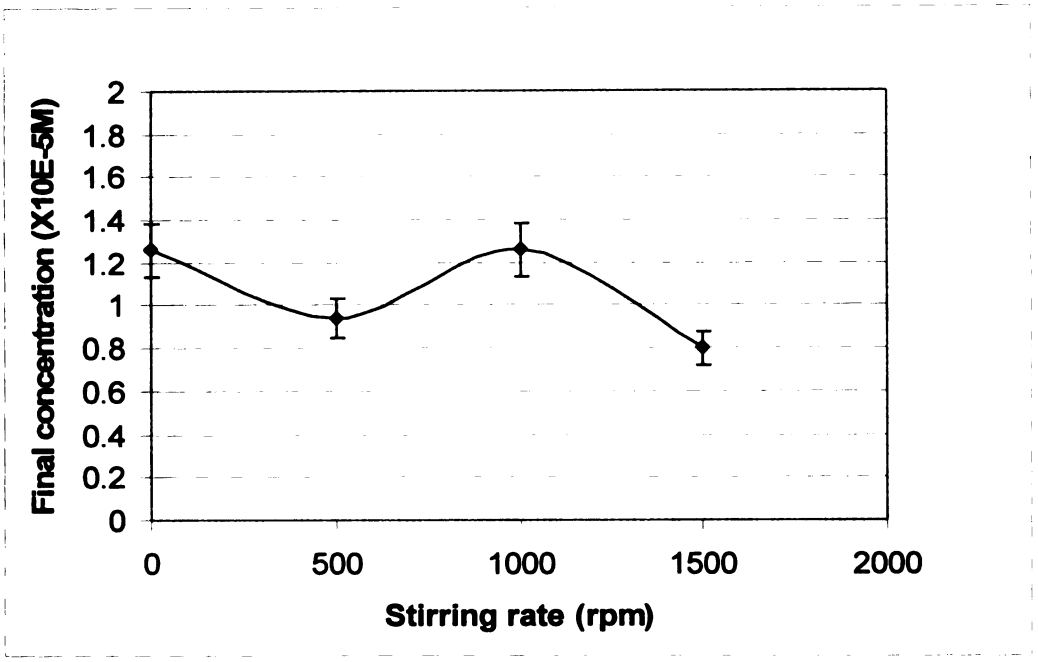

Figure 2.18: Conversion of BFA as a function of rotation rate during ECH on a polycrystalline Pt rotating disc electrode (electrolyte: 0.01 M H_2SO_4, initial [BFA]= 6.67 X 10^{-5} M, E_2=-400 mV, temperature = 25°C, time = 2 h). Graph shows yields of CEG.

2.4 Conclusions

In this study, a model α-functionalized carboxylic acid, namely benzoyl formic acid, an analog of pyruvic acid, was subjected to ECH under various conditions. This study was carried out to achieve proof of principal of electrocatalytic hydrogenation of carboxylic acids and also to determine the effect of various conditions on the ECH of a compound having multiple reducible groups. The technique used was chronoamperometry, in which the potential was stepped from a value at which there is no hydrogen generation on Pt to various potentials in the hydrogen evolution region, and the distribution of ECH products was determined under various conditions of step potential, pH and temperature. Maximum yield of the desired product, CEG was obtained at a potential close to -400 mV

on both Pt/BDD and Pt/Ru/BDD electrodes. However, the Ru containing electrode showed a significant enhancement in the final yield of CEG, probably due to the Ru atoms providing surface sites for the adsorption of BFA. The ECH was favored at more acidic pH, at which the –COOH group is undissociated, and also by higher temperature. However, an anomalous temperature effect on ECH was obtained on the Pt/Ru/BDD probably due to the leaching of Ru from the diamond surface at higher temperature. ECH of BFA using a Pt rotating disc electrode at various speeds of rotation showed that the yields of the products did not vary significantly with the rotation rate. These results indicate that the rate of the ECH reaction is influenced more by the availability of surface sites for the adsorption and reaction, and the surface concentration of reactants rather than the rates of mass transport, consistent with the findings in the batch hydrogenation of lactic acid.

CHAPTER 3

ELECTROCATALYTIC HYDROGENATION OF LACTIC ACID USING RUTHENIUM ON CARBON FELT ELECTRODE

3.1 Introduction

For the electrocatalytic hydrogenation to be useful on a preparative and commercial scale, the process needs to be optimized at much higher substrate concentrations, compared to those used for ECH of BFA, and different cell and electrode designs are required for this purpose. Several approaches have been used in the past for bulk scale electrocatalytic hydrogenation of organic substrates, some of which are described in chapter 1. Raney Ni in various forms has been used for the hydrogenation of carbonyl compounds, but when expensive noble metals such as Ru and Pt are required, it would not be cost effective to use pure metal electrodes. The best approach in this case would be to deposit the metal in a highly dispersed form on a high surface area support using electrodeposition from a salt solution of the metal. The deposition can also be done by physical vapor deposition or sputtering, but electrodeposition is known to result in particles of more uniform size and distribution. In many cases, noble metals deposited on high surface area materials have resulted in better electrochemical efficiencies for ECH, when compared to smooth metal electrodes. The reasons for this may be the higher surface area as well as the unique properties of highly dispersed metal micro or nanoparticles.

Polcaro and coworkers[37,53] studied the ECH of benzaldehyde and acetophenone in acidic and alkaline ethanol/water mixtures using Pd supported on carbon felt, a support chosen for its high specific surface area and good fluid permeability. In the case of

benzaldehyde, two parallel reactions were found to occur, leading to two different products, benzyl alcohol and toluene, These products were believed to form from the adsorption of benzaldehyde at two different types of sites and therefore, the product distribution was greatly influenced by the method of electrode preparation and the resulting morphology and distribution of active sites. The acidity of the supporting electrolyte also influenced the product distribution with acetophenone and benzaldehyde forming phenylethanol and benzyl alcohol respectively as the only products in alkaline medium, whereas ethyl benzene and toluene were also obtained in acidic medium. Comparison between two different electrocatalysts, Pt and Pd, deposited on carbon felt under identical conditions revealed that the same hydrocarbon/alcohol ratio (15%) in HCl medium was obtained in both the cases, but the product ratio was different when the electrodeposition time was increased. The current efficiency, influenced by the relative rates of hydrogenation and hydrogen evolution, also varied with the nature of the metal and the supporting electrolyte.

Iwakura and coworkers[54,55] studied the ECH of 4-methyl styrene to 4-ethyl toluene using a Pd sheet electrode modified by Pd black, Pt and Au. The deposition was performed chemically by using active hydrogen passing through the Pd sheet electrode as the reducing agent. A current efficiency of 100% was obtained using Pd deposited on Pd sheet, which was 40 times higher than that obtained using bare Pd sheet electrode, indicating that hydrogenation occurs on the three dimensionally expanded surface of the Pd black deposits. Similar enhancements in efficiency were obtained using Pt and Au deposits as well, with the current efficiencies being 95% and 70% respectively, though

these deposits showed lower rates of permeation of active hydrogen with increases in metal loading.

Savadogo and coworkers[56] studied the ECH of phenol to cyclohexanol using Pt deposited on Vulcan carbon. The current efficiency and product selectivity were found to depend on the electrode material, but not on the electrochemically active surface area or metal particle size. Pt/C showed the highest electrocatalytic activity, whereas Ru/C showed the highest selectivity. A Pt-Co/C based alloy electrode showed the highest activity and selectivity for cyclohexanol production among the alloy electrodes studied. Further, the current efficiency did not change significantly for Pt loadings of 2-30%, but there was a decrease in activity when 60% Pt was used.

In an earlier study, Savadago and coworkers[57] reported ECH of phenol with current efficiency as high as 85% using only 2% Pt deposited on graphite particles. Again, this high efficiency was assumed to be due to the high surface area of dispersed metal particles. The ECH was inhibited in the presence of quaternary ammonium salts due to the blocking of active sites by the quaternary ammonium ions. The rate of ECH increased with increase in temperature and was influenced by the Teflon (used as a binder) content of the electrode, which was believed to affect the phenol concentration on the electrode surface. Baturova and coworkers[58] studied the ECH of acetophenone over Pd deposited on carbon fiber in 1 N NaOH at 20°C. Phenyl carbinol was the only product obtained with a yield of 50% and a current efficiency of 50-80%. In this case, only Pd deposited at a potential close to the equilibrium potential for Pd reduction was electrocatalytically active because this deposition occurs through the specific adsorption of Pd. Pd deposited at more negative potential showed no activity.

In the present study, carbon felt was chosen as the support for deposition of Ru, due to its high specific surface area, good fluid permeability, more rapid dynamic adsorption characteristics (mass transfer rates) and lower resistance to the flow of liquids and gases compared to other carbon supports.

3.2 Experimental

3.2.1 Set up of electrochemical cell and ECH method

Electrohydrogenation studies were carried out on 75 mL volumes of several electrolytes containing 11.1 mM lactic acid (Aldrich). The glass electrochemical cell employed (figure 3.1) is a two compartment cell with the anode and the cathode compartments separated by a glass frit in order to prevent the diffusion of gaseous products. The reference electrode was Ag/AgCl (E^0= -0.35 V vs. SCE). The counter electrode was Pt wire. The Carbon felt (CF) working electrode (dimensions 4.0 X 3.0 X 0.25 cm) was connected to the external circuit via a copper wire, positioned to minimize surface area exposed to solution; electrochemistry on the copper surface could thus be assumed to be negligible. A voltmeter was connected between the reference and working electrode to measure the potential of the working electrode. Controlled current was applied using a model 273 potentiostat/galvanostat from Princeton Applied Research. The temperature of the system was controlled using a heating tape wrapped around the cell and connected to a temperature controller from Omega. The solution was stirred using a magnetic stirrer. Samples were withdrawn for analysis immediately after the cell was switched on and at intervals during the electrohydrogenation.

The electrolytes were prepared by the dilution of the concentrated acids, namely 98% sulfuric acid (CCI), 36.5% hydrochloric acid (CCI), and 70% perchloric acid (Spectrum) with HPLC grade water. S-Lactic acid and propylene glycol were purchased from Aldrich and were used without further purification.

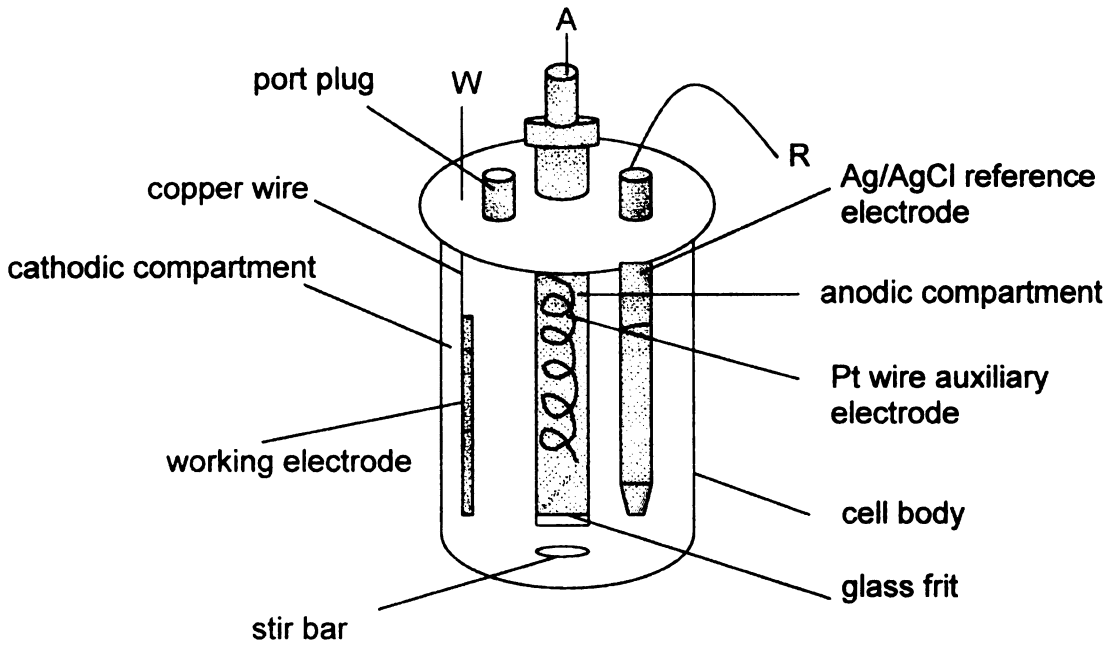

Figure 3.1: Schematic diagram of the electrochemical cell used for ECH (W-Working, A-Auxiliary, R-Reference)

3.2.2 Electrode preparation

The Ru/carbon felt electrode (4.0 X 3.0 X 0.318 cm) was prepared by electrodeposition of Ru from 5 mM $RuCl_3.xH_2O$. A constant current of 10 mA for 90 min was used for the electrodeposition, and the potential was maintained between 0 and -0.2 V to ensure complete reduction of Ru^{3+} to the metallic state. After deposition the electrode was

thoroughly rinsed with ultrapure water and then with the electrolyte to ensure complete removal of traces of $RuCl_3$.

3.2.3 Characterization of the electrode surface

The electrode surface was characterized using a JSM-6400 V scanning electron microscope (JEOL, Ltd., Tokyo, Japan). Micrographs were recorded using secondary electron mode generated with an accelerating voltage of 20 kV. The presence of Ru was verified by energy dispersive X-ray (EDX) analysis (Noran Instruments, Inc., Middletown, WI) connected to the JSM-6400 V. SEM images were obtained using the AnalySIS software (Software Imaging System Corp., Lakewood, CO).

3.2.4 Analysis of the products of ECH

(a) Lactic acid and propylene glycol

Reaction mixtures were analyzed by HPLC with refractive index detection, using a Biorad HPX87H ion exchange column at 65°C. The mobile phase used was 5 mM H_2SO_4, run isocratically at a flow rate of 0.6 mL/min.

Solutions of lactic acid and propylene glycol in 5 mM H_2SO_4 in the concentration range 0.2-1.0 g/100 mL were used to obtain a calibration curve. A standard HPLC chromatogram containing lactic acid and propylene glycol (0.1 g/mL) is shown in Figure 3.2. The calibration curves for lactic acid and propylene glycol are shown in Figure 3.3 and 3.4. The response factor was calculated using the following expression.

$$\text{Response factor} = \frac{\text{Concentration of analyte (wt\%)}}{\text{Peak area counts}}$$

$$= \frac{1}{\text{slope of the calibration curve}}$$

The concentrations of the unknown samples were calculated by multiplying the peak area counts of the respective sample with the response factors.

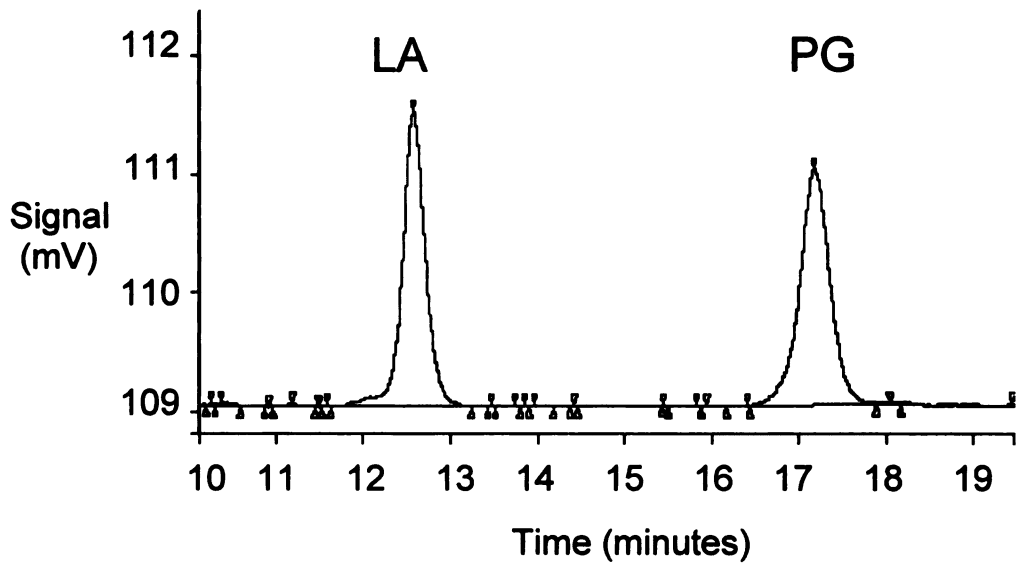

Figure 3.2: HPLC chromatogram (standard 0.1 wt %) showing peaks for lactic acid (LA) (retention time = 13.4 min.) and propylene glycol (PG) (retention time= 17.4 min.)

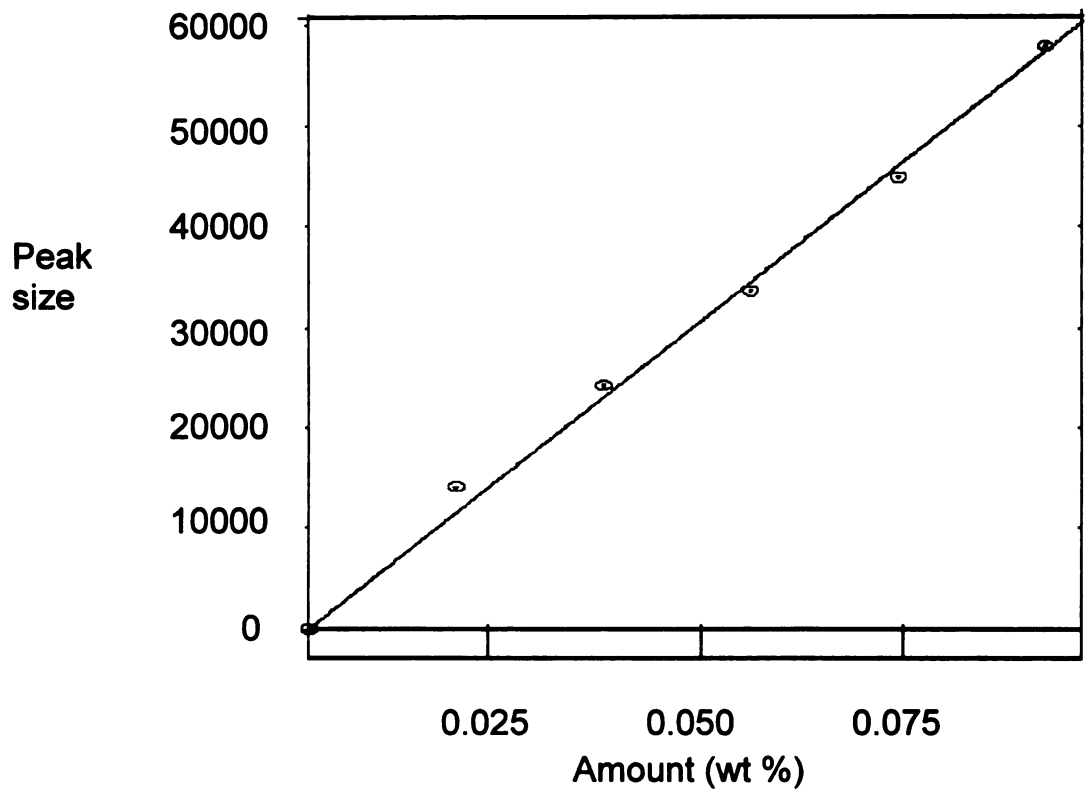

Figure 3.3: Calibration curve for lactic acid (R^2= 0.9966)

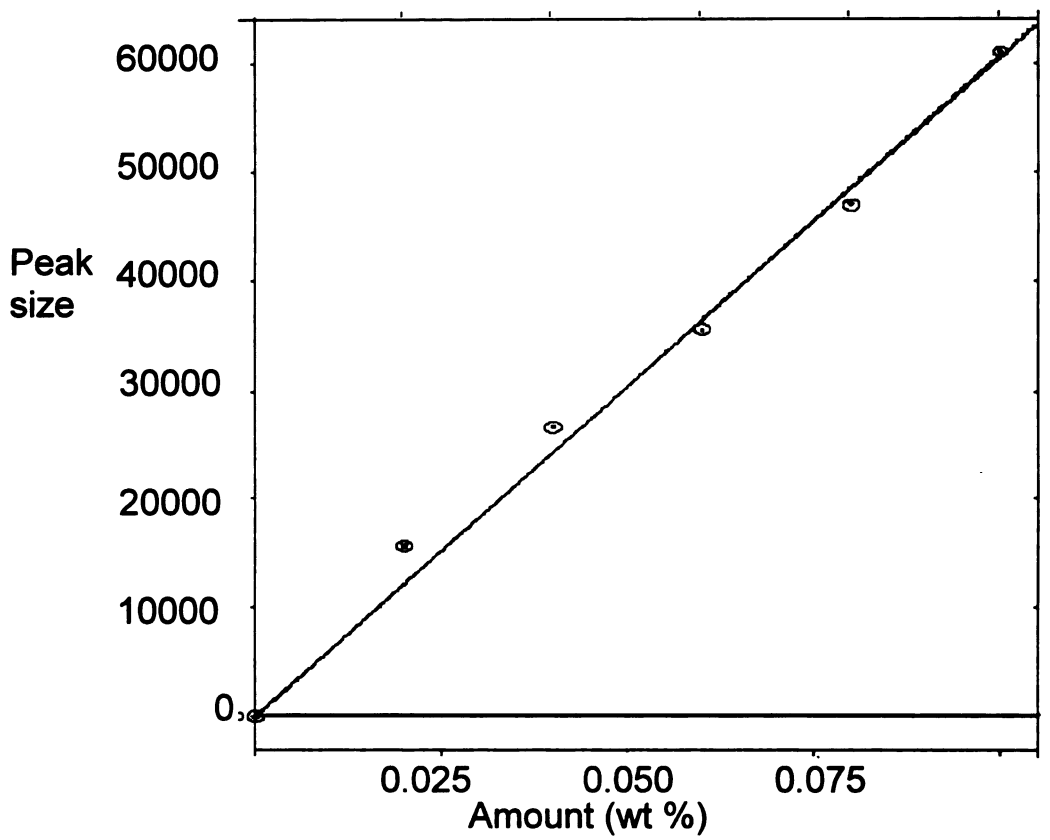

Figure 3.4: Calibration curve for propylene glycol (R^2= 0.9937)

(b) Synthesis of lactaldehyde

Method 1

Lactaldehyde to be used as a standard for analysis was synthesized by the oxidation of propylene glycol with pyridinium chlorochromate (PCC), using the procedure described by George.[59] A 50 mL round bottomed flask was charged with 3.23 g of PCC and 20 mL of CH_2Cl_2 and fitted with a reflux condenser. Propylene glycol in 10 mL CH_2Cl_2 was added slowly through the condenser with swirling to the suspended PCC. The reaction mixture turned brown black and CH_2Cl_2 began to boil gently. After 1.5 h, 10 mL of anhydrous diethyl ether was added, and the supernatant liquid was decanted from the

gummy black residue. The residue was washed twice with ether and the combined CH_2Cl_2-ether solution was filtered through a Buchner funnel. The solvent was removed by rotary evaporation. The product was extracted from the residue with 10 mL of D_2O. The reaction scheme is shown in Scheme 3.1.

Method 2

The sample of lactaldehyde prepared using method 1 was used as a standard for HPLC analysis of the ECH reaction mixtures. However, the NMR of the sample (see Appendix) indicates the presence of pyruvic aldehyde, propylene glycol and pyridine in the sample in addition to the desired lactaldehyde. An alternative method[60] was used to obtain lactaldehyde in a pure form. Pyruvic aldehyde dimethyl acetal (2g) in 10 mL CH_3OH was placed in a 50 mL round bottomed flask and stirred in an ice bath for 30 min. to allow the temperature of the mixture to reach 0°C. $NaBH_4$ (0.64g) was added to the reaction mixture, and the mixture was stirred for 20 h at room temperature after which the mixture was neutralized with 10 mL of 0.1 M HCl, separated by vacuum filtration to remove the solids and concentrated in a rotary evaporator. The residue was purified by vacuum distillation. The fraction distilling at 68-70°C was collected. The NMR (see appendix) of this compound clearly indicates the presence of pure lactaldehyde dimethyl acetal. The purified product was then hydrolyzed in 0.05 M H_2SO_4 for 2 h to form lactaldehyde. The final product was characterized by ^1H and ^{13}C NMR and ESI-MS. The scheme for the reaction is shown in Scheme 3.1.

This sample of lactaldehyde was used as a qualitative standard for NMR and ESI-MS, but could not be used as a HPLC standard due to the presence of an intense peak overlapping

with the lactaldehyde peak which made the peak integration and quantification difficult. Since the NMR and ESI-MS indicated the presence of lactaldehyde as the only organic component of this sample, the impurity peak was assumed to be due to the presence of an inorganic anion such as borate, which did not appear in the ESI-MS due to its low volatility. No further attempt was made to remove this impurity or to characterize it.

Method 1

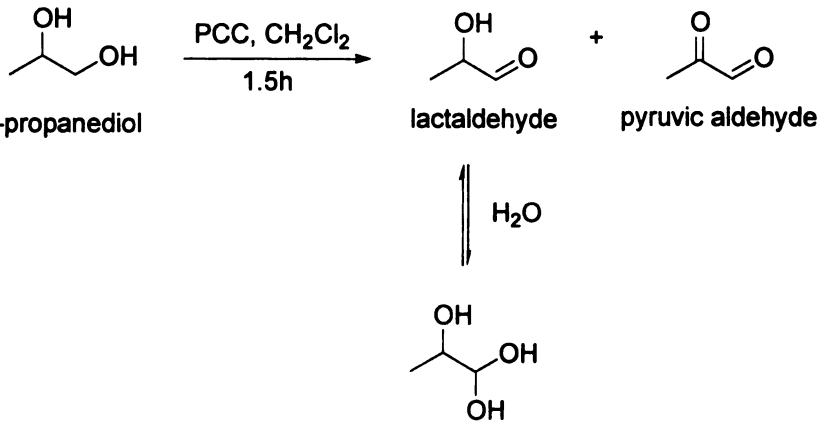

Method 2

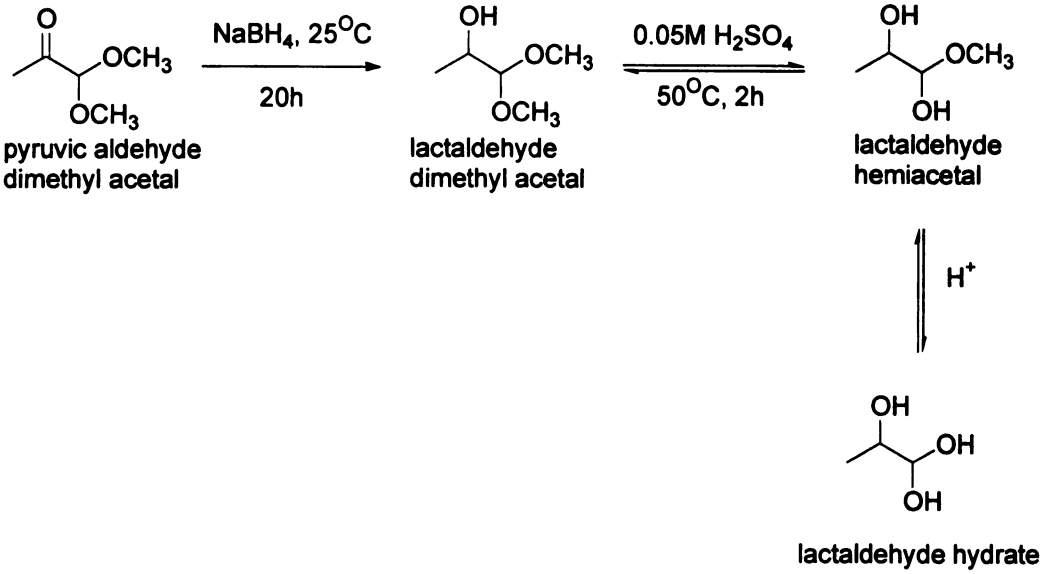

Scheme 3.1: Synthesis of lactaldehyde

(c) Quantification of lactaldehyde

Due to the difficulty involved in obtaining a 100% pure sample of lactaldehyde and the fact that chemically synthesized lactaldehyde showed a relatively broad peak in the HPLC probably due to the presence of lactaldehyde in more than one form in solution (such as acetol, hydrate, dimers, etc.) the quantification of lactaldehyde posed a major problem. Therefore, instead of using a calibration curve, all the quantification was carried out using a single standard. Even though this method is less accurate, it gives us a good estimate of the relative yields of lactaldehyde in the unknown samples. From the ^{1}H NMR of the D_2O extract of lactaldehyde (see appendix) prepared using method 1, the approximate concentration of lactaldehyde was estimated to be 0.14 g/100mL by comparison of the relative intensities of the C2-H peaks of lactaldehyde and propylene glycol (whose concentration was determined from HPLC). The HPLC chromatogram of the sample using conditions similar to those used for the analysis of lactic acid and propylene glycol (described in section 3.2.4 a) is shown in Figure 3.5. Since the lactaldehyde could not be isolated from the D_2O extract, the broadening of the peak may be a result of the reversible interaction of lactaldehyde with the other components in solution such as reagents, byproducts, etc. which causes it to exist in more than one form. The dip in the baseline is caused by the presence of D_2O. The peak area of the lactaldehyde peak is 50161 units. Using this data, the response factor for lactaldehyde was calculated. The concentration of lactaldehyde in the unknown samples were determined by multiplying the peak area counts with the response factor.

The response factors for lactic acid, lactaldehyde and propylene glycol are shown in table 3.1.

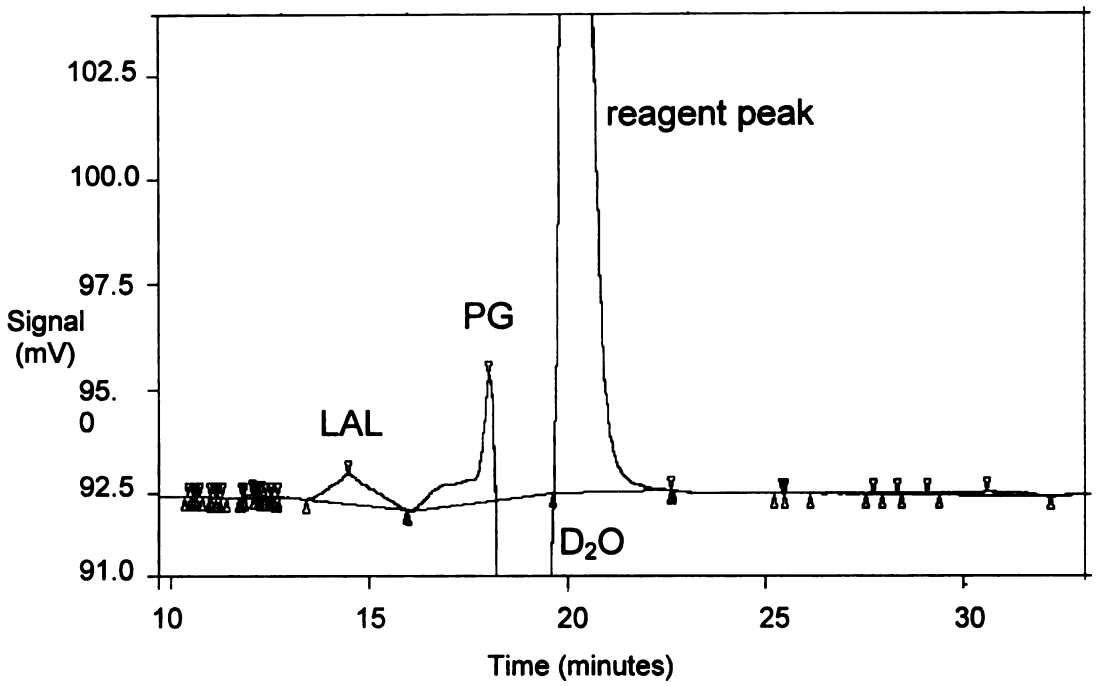

Figure 3.5: HPLC chromatogram of the D_2O extract from the synthesis of lactaldehyde using Method 1. The mixture contains the product lactaldehyde (LAL) (retention time= 14.7 min.) and reactant, propylene glycol (PG)

Analyte	**Response factor (X 10^{-6} wt%)**
Lactic acid	1.74
Lactaldehyde	2.59
Propylene glycol	1.64

Table 3.1: Response factors of analytes used for quantifying unknown samples from ECH

3.3 Results and Discussion

3.3.1 Electrodeposition of Ru on carbon felt

The electrodeposition of Ru on carbon felt was carried out from 5 mM $RuCl_3.xH_2O$ in 0.01M H_2SO_4 using a constant current of 10 mA for 90 min. Figure 3.6B shows the carbon felt surface after 10 s of Ru electrodeposition from 5 mM $RuCl_3$ in 0.01M H_2SO_4 at 10 mA current. The SEM clearly shows the formation of hemispherical metal particles serving as nuclei for further growth.

The Ru content of the surface was determined using EDS, and the average value of three different regions was found to be 22.4 wt. % and 3.8 atom % after 90 min of deposition. This is higher than the calculated value (from the Faradaic current) of 11.4% because only the parts of the carbon felt that were rich in particles were used for the EDS analysis, as shown in figure 3.7.

From the lower magnification SEM micrograph in figure 3.7, it is clear that most of the deposition takes place on the fibers at the surface, whereas fibers that are deeper inside have fewer or no metal particles on them. This may be due to the hydrophobic nature of carbon felt, which may prevent the penetration of electrolyte deeper into the felt material, introducing a mass transport limitation on the rate of deposition.

Figure 3.8 shows the scanning electron micrographs of the surface of a carbon felt fiber at 1, 5, 30 and 90 minutes of electrodeposition time. From the SEM's, it is observed that Ru particles grow on the carbon felt surface in the form of clusters with particle sizes in the range of 1-5 μm. The deposited metal does not appear as distinct particles, but overlap with each other. After 1 min of deposition, significant particle growth is observed. The SEM's display the surface of a single fiber of carbon felt where a substantial amount of

metal deposition has occurred, but a majority of the carbon felt fibers had no metal particles deposited on them. With increasing time, the number of felt fibers deposited with metal particles increases and some of them contain larger and more irregular clusters. This indicates that nucleation and growth of particles occurs simultaneously in the case of Ru deposition on carbon felt.

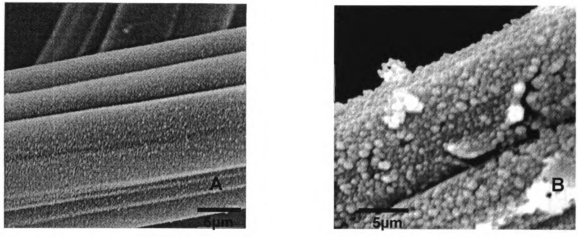

Figure 3.6: (A) SEM of bare carbon felt; (B) SEM of carbon felt after 10 s of Ru electrodeposition from 5 mM $RuCl_3.xH_2O$ in 0.01 M H_2SO_4 (i= 10 mA)

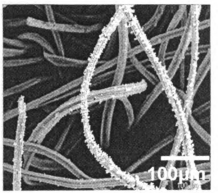

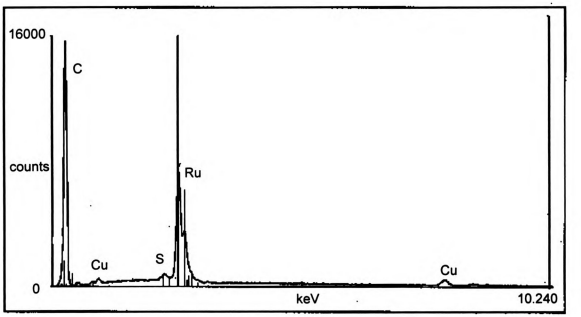

Figure 3.7: Low magnification image of Ru/carbon felt deposited from 5 mM $RuCl_3.xH_2O$ in 0.01 M H_2SO_4 (i= 10 mA) with a deposition time of 90 min (top). This is the magnification used for the quantitative analysis with EDS

Energy dispersive spectrum (EDS) of Ru/carbon felt showing the X-ray signal for the Ru L line (bottom)

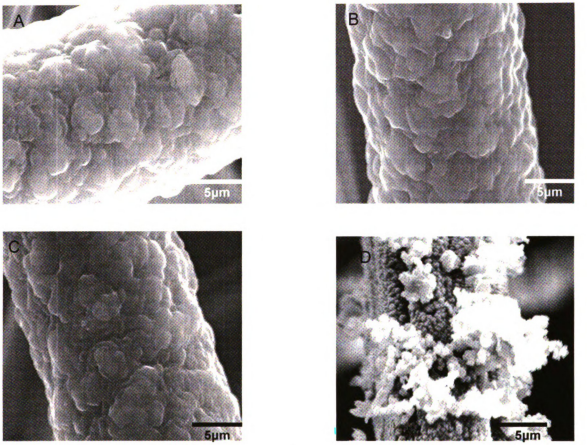

Figure 3.8: SEM images of Ru/carbon felt after electrodeposition of Ru from 5 mM $RuCl_3.xH_2O$ in 0.01 M H_2SO_4 (i= 10 mA) for (A) 1 min; (B) 5 min; (C) 30 min; (D) 90 min.

In the electrodeposition of Pd on carbon felt carried out by Polcaro and coworkers[37] from a solution of 1 mM $PdCl_2$/0.1 M H_2SO_4, it was observed that a constant current deposition under kinetic control produces smaller and more uniformly distributed nuclei resulting in more uniform sized hemispherical particles with no cluster formation. However, when the deposition was carried out using constant potential conditions under diffusion control with the same amount of Pd, the crystal growth occurred prevalently on the nuclei that were more exposed to the solution, resulting in center overlap and cluster formation. By comparison with this model, the Ru deposition on carbon felt can be assumed to be occurring under diffusion limited conditions under the conditions employed. This might be expected, since the working electrode potential during the electrodeposition was maintained in the negative potential region which is well below the potential for the onset of hydrogen adsorption.

In an earlier study on the electrodeposition of Pd on carbon felt from $PdCl_2$ in 0.1 M HCl carried out by Polcaro and coworkers,[53] the number density of the Pd nuclei was found to increase at more negative potentials and as the deposition time increased, the centers of the nuclei on the outer fibers grew and partially overlapped, but there was no increase in the size of the nuclei on the inner fibers. From cyclic voltammetric studies of Pd electrodeposition, it was also found that at more negative potentials, the current efficiency for Pd deposition decreased due to the competition with hydrogen adsorption and hydrogen gas evolution catalyzed by the deposited metal.

The cyclic voltammogram (CV) of the carbon felt electrode (3.0 X 2.0 X 0.318 cm) obtained in 0.01 M H_2SO_4 containing 5 mM $RuCl_3.xH_2O$ is shown in figure 3.9 at three different scan rates in the potential range, 0.6 to -0.4 V. The current during the cathodic

scan consists of components due to both Ru^{3+} electroreduction and hydrogen adsorption and evolution on the deposited Ru. The voltammograms were recorded in a stirred solution and resemble more closely those of a system which is not limited by semi-infinite linear diffusion. Therefore the redox processes are not diffusion limited and should be governed by the steady state kinetics of electron transfer. A current crossover is observed indicating a modification of the electrode surface due to Ru deposition. The current in the negative potential region observed during the cathodic scan is due to the combined processes of Ru^{3+} reduction and hydrogen adsorption and evolution on the deposited Ru. The current in the positive potential region during the anodic scan is due to the desorption and oxidation of adsorbed hydrogen on Ru. The current maximum due to Ru^{3+} reduction/H adsorption shifts to more negative potential and currents on the reverse (anodic) scan larger than on the forward one are observed with increase in scan rate. This behavior indicates that the electrodeposition of Ru is controlled by the formation of growth centers or nuclei which are thermodynamically stable. The simultaneous reduction of H_3O^+ is catalyzed by the metal deposits formed on the carbon felt. In the absence of Ru^{3+}, very low currents are observed in the same potential range. However, unlike Pd electrodeposition, there are no features due to co-deposition of hydrogen with the metal, resulting in hydrogen diffusing into the metal lattice as observed in the Polcaro case, indicating that hydrogen is not incorporated in the metal lattice of Ru during electrodeposition.

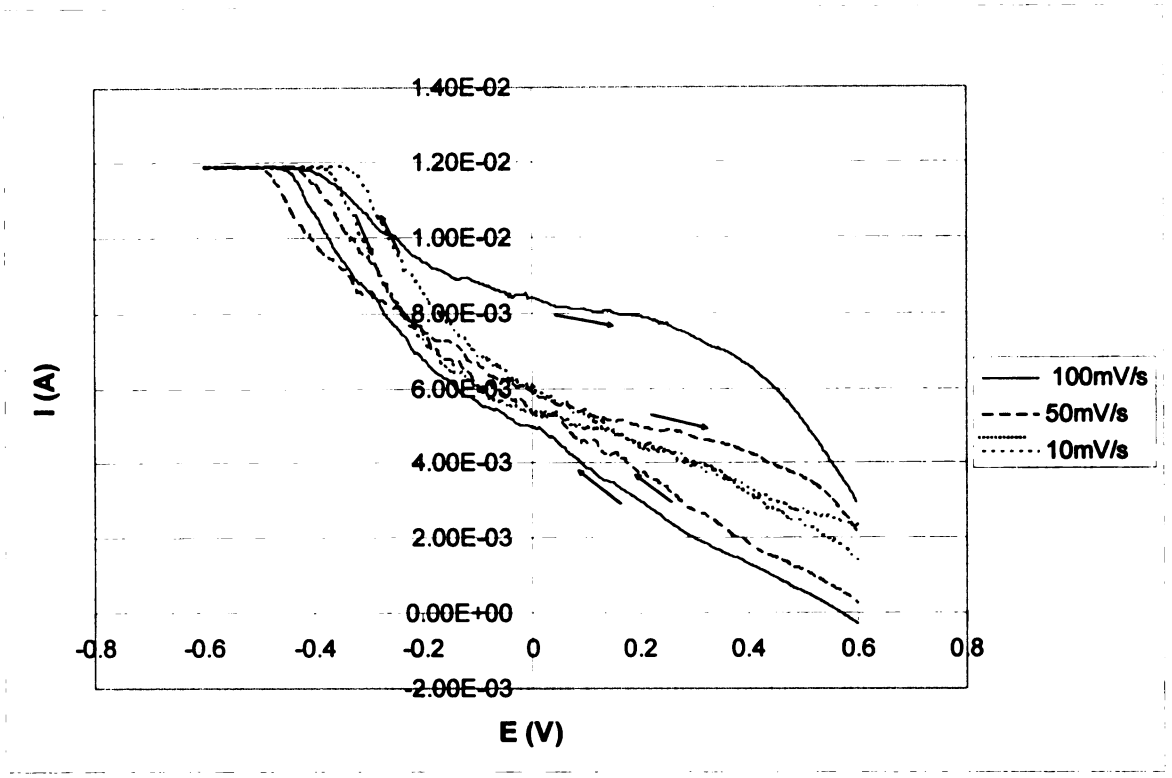

Figure 3.9: Cyclic voltammetry (I-E curve) of carbon felt in 5 mM $RuCl_3.xH_2O$ in 0.01 M H_2SO_4 at three different scan rates. Arrows indicate the direction of scan

The current transients following the application of various values of constant potentials are shown in figure 3.10. The measurements were performed in 5 mM $RuCl_3$ in 0.01 M H_2SO_4 by applying the required potential, E, and recording the amperometric i-t curve. The applied potentials were sufficiently cathodic to induce nucleation and growth of Ru on carbon felt. The current increases immediately after the application of the potential and decreases at very short times as the electrode double layer fully charges (figure 3.11). The current then increases as a result of the formation of stable nuclei and growth of the metal deposits. As the individual diffusion zones of the growing crystallites coalesce, the current passes through a maximum and then decays as a function of $t^{-1/2}$ according to the Cottrell equation.

Similar behaviour was observed for the electrodeposition of Pd on carbon felt by Polcaro and coworkers[53] and for the electrodeposition of Cu on boron-doped diamond by Wang and coworkers.[61] With an increase in the applied overpotential, there is a decrease in the time at which the current maximum occurs, indicating that at more negative potentials, the nucleation and growth is much faster and gets to the diffusion limited regime much faster. Therefore at higher overpotentials, the time period required for the coalescence of the diffusion zones of the individual nuclei decreases, implying an increase in the number density of growth centers. At E = -300 mV and lower, the nucleation step occurs within the first 200 ms as shown in figure 3.11. The maximum current, on the other hand, remains almost constant at different applied potentials. These results support the idea that under the given operating conditions, the nucleation and growth of Ru is occurring under diffusion controlled conditions.

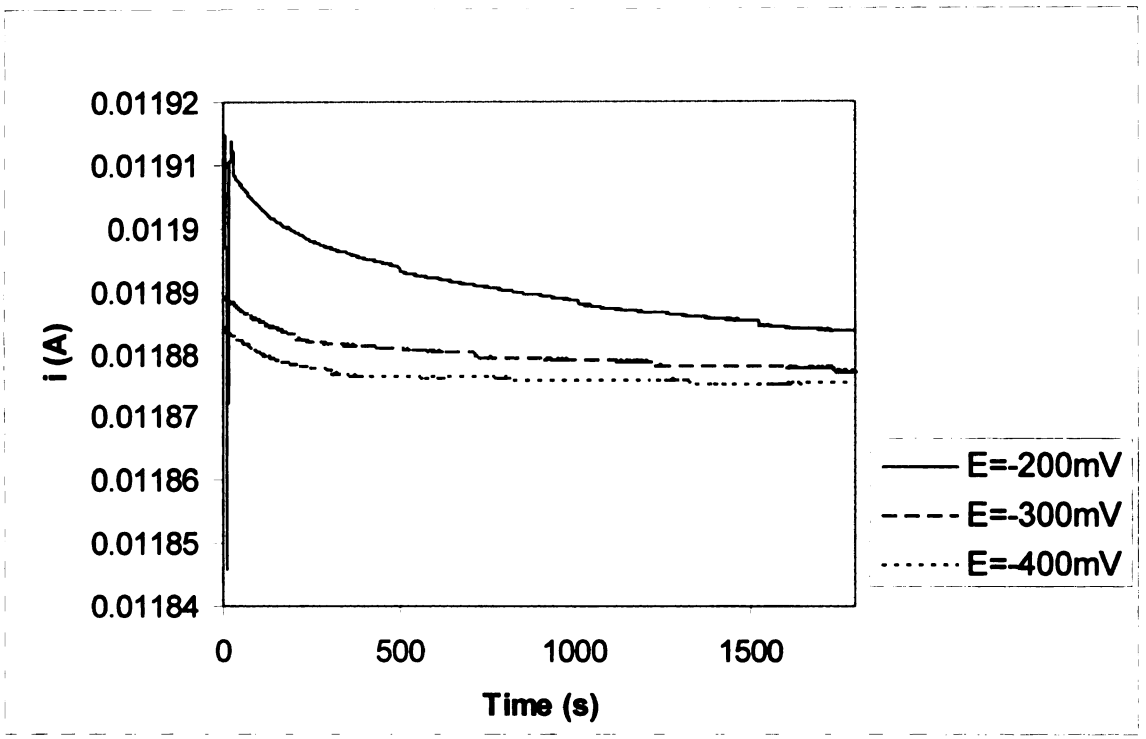

Figure 3.10: Amperometric i-t curve of carbon felt in 5 mM $RuCl_3.xH_2O$ in 0.01 M H_2SO_4 at three different applied potentials.

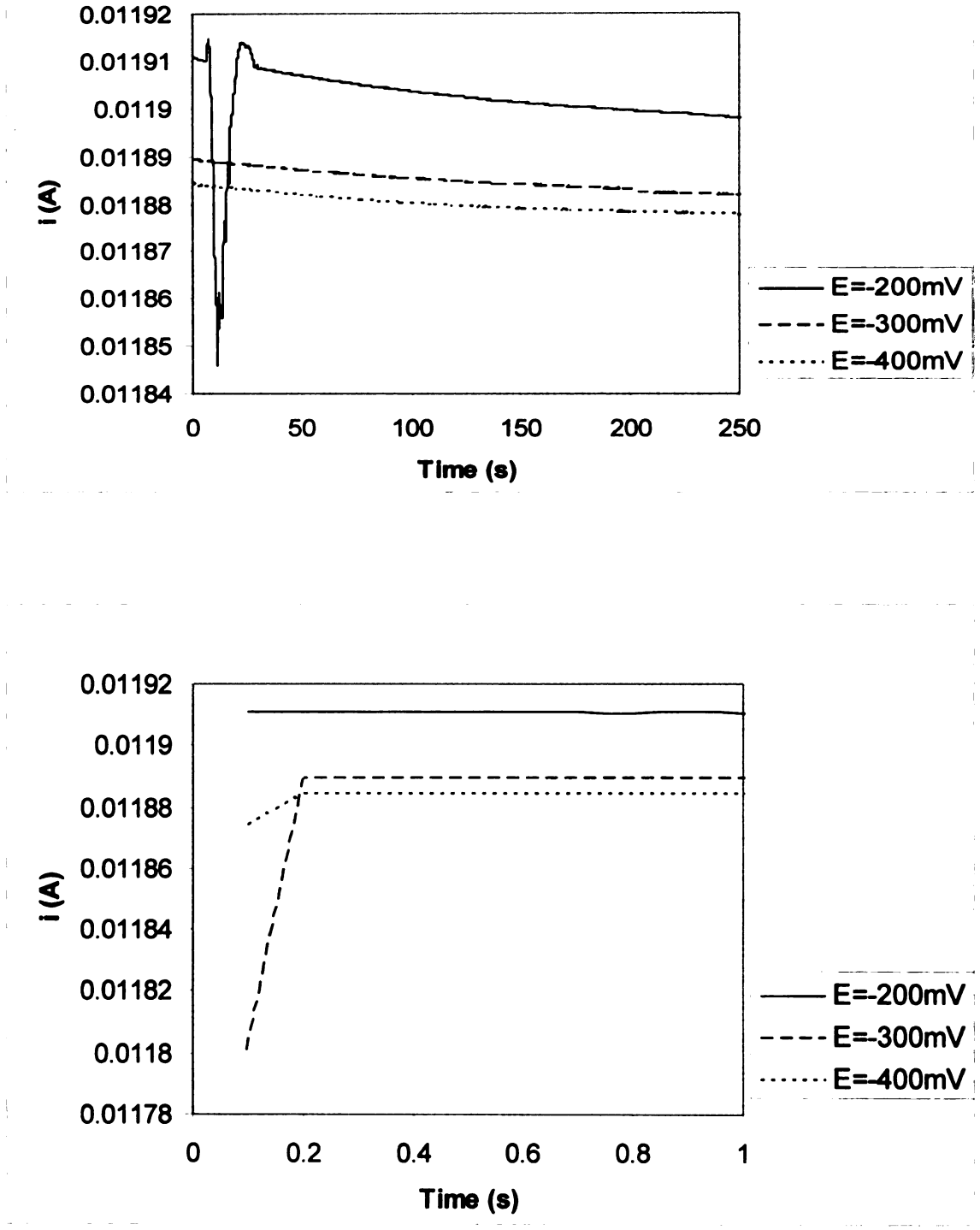

Figure 3.11: Amperometric i-t curve of carbon felt in 5 mM $RuCl_3.xH_2O$ in 0.01 M H_2SO_4 at three different applied potentials; expansions of the shorter time regions showing rapid current increase due to nucleation

3.3.2 Factors governing lactic acid conversion

The optimized conditions for the electrodeposition of Ru is shown in table 3.2. These were the conditions used for electrode preparation in all the experiments. A series of experiments was carried out using the Ru/carbon felt electrodes in order to determine the effect of various experimental conditions on lactic acid conversion. The only product of the ECH of lactic acid using Ru/carbon felt is lactaldehyde. There was no conversion to propylene glycol under any condition. A control experiment was carried out using lactic acid (11.1 mM in 0.01 M H_2SO_4) on bare carbon felt for 21 h at 100 mA current. There was negligible conversion of lactic acid, indicated that lactic acid is not hydrogenated on bare carbon felt and the Ru electrocatalyst is required for ECH.

Electrolyte	0.01 M H_2SO_4
Ru^{3+} concentration	5 mM
Current	10 mA
Time	30-90 min.

Table 3.2: Summary of Ru electrodeposition conditions

3.3.2.1 Ru deposition time

ECH of lactic acid was carried out using two different electrodes on which the Ru electrodeposition was carried out for 30 and 90 min. The ECH was carried out using 11.1 mM lactic acid in 0.01 M H_2SO_4 for 21 h at 70°C and 100 mA current. The results are shown in Table 3.3. The yield of lactaldehyde is higher on the electrode obtained from 90

min electrodeposition. From the characterization of Ru electrodeposition on carbon felt in the previous section, it can be inferred that the amount of Ru metal on the electrode surface is directly related to the electrodeposition time. Therefore, the higher yield of lactaldehyde in the electrode prepared using a 90 min electrodeposition time can be attributed to the greater amount of Ru electrocatalyst on the electrode surface. The results also indicate that the ECH of lactic acid requires the presence of Ru and that carbon felt alone cannot catalyze the ECH reaction. Therefore, a 90 min. electrodeposition time was used for the preparation of subsequent Ru/carbon felt electrodes.

An increase in the yield of product with increase in the metal electrodeposition time was also observed by Polcaro and coworkers[37] in the ECH of acetophenone using Pd/carbon felt electrodes.

Ru deposition time (min)	**LA (mM)**	**LA (% remaining**	**LAL (mM)**	**LAL (% yield)**
Initial	14.4	-	-	-
30	13.3	91.7	0.54	4.7
90	10.0	77.3	2.57	18.8

Table 3.3: ECH of lactic acid using Ru/carbon felt prepared using two Ru electrodeposition times (11.1 mM lactic acid in 0.01 M H_2SO_4 for 21 h at 70°C, i= 100 mA). The error in the HPLC is estimated to be ±3%. The standard deviation of the yield of lactaldehyde at 11.1 mM initial concentration of lactic acid is ±5.2%

3.3.2.2 Temperature

Lactic acid (11.1 mM in 0.01 M H_2SO_4) was subjected to ECH at 25, 50 and 70°C for 21 h. A constant current of 40 mA was used in order to prevent the heating of the system due to resistence at high currents. The results are shown in Table 3.4. There is an increase in the yield of lactaldehyde with increase in temperature. At higher temperatures, there is an increase in the the rates of both ECH and hydrogen evolution by the Tafel reaction. In this case, the increase in the rate of hydrogenation appears to exceed the increase in the rate of hydrogen evolution. There is negligible conversion of lactic acid at room temperature.

The relative rates of hydrogenation and hydrogen evolution depend on the strength of the bond to be hydrogenated and on various factors that influence the adsorption phenomena and the activity of chemisorbed hydrogen.[38] A similar increase in the conversion and current efficiency with increase in temperature was observed by Hu and coworkers in the ECH of 4-amino 5-nitroso dimethyl uracil on a foamed nickel cathode in $(NH_4)_2SO_4$ due to greater increase in the rate of hydrogenation compared to hydrogen evolution[36]. An increase in the rate of ECH of lignin models such as guaicol[62] and 4-phenoxy phenol[63] to phenol and cyclohexanol with increase in temperature at given current was observed by Menard and coworkers using Raney Ni powder and 5% Pd/C in Reticulated Vitreous Carbon (RVC) and 1 M NaOH as the electrolyte. Roessler and coworkers[41] observed an increase in conversion with increase in temperature up to 60-80°C in the ECH of vat dyes such as indigo in 1M NaOH, but there was a significant drop in current efficiency and conversion beyond this temperature. These findings were interpreted in terms of the competition between hydrogen incorporation into the substrate and decreasing surface

concentration due to H_2 desorption. Bryan and coworkers[31] observed an increase in the ECH rate and current efficiency with increase in temperature in the ECH of 4-phenylbutene-2-one to 4-phenylbutan-2-one with no change in product selectivity on Ni cathode in ethanol containing H_2SO_4. Amouzegar and coworkers[56] observed an increase in the ECH of phenol to cyclohexanol with increase in temperature on dispersed Pt electrode in 0.05 M H_2SO_4. In all these cases, the reported trends were believed to be due to greater increase in the rate of hydrogenation compared to hydrogen evolution.

Temperature (°C)	**LA (mM)**	**LA (% remaining)**	**LAL (mM)**	**LAL (% yield)**
Initial	10.0	100	-	-
25	9.3	88.6	0.17	1.7
50	9.1	87.1	1.01	7.7
70	7.8	77.3	1.89	14.5

Table 3.4: ECH of lactic acid using Ru/carbon felt at various temperatures (11.1 mM lactic acid in 0.01 M H_2SO_4 for 21 h, i= 40 mA). The error in the HPLC is estimated to be ±3%. The standard deviation of the yield of lactaldehyde at 11.1 mM initial concentration of lactic acid is ±5.2%.

3.3.2.3 ECH current

Lactic acid (11.1 mM in 0.01 M H_2SO_4) was subjected to ECH at various currents in the range of 10-100 mA at 70°C for 21 h. . Though the rate of ECH was maximal at 90°C, the 70°C temperature was chosen in order to prevent excessive evaporation of water from the

system during the long run times. The results are shown in Table 3.5. The yield of lactaldehyde was found to increase with increase in the ECH current. These results suggest that the rate of hydrogenation is dependent on the concentration of hydrogen atoms on the catalyst surface at a given time, which increases with increasing current. Thus, in spite of the increased rate of hydrogen evolution, the rate of product formation is also higher at higher currents. The surface concentration of hydrogen may be directly related to the current because it is the surface H atoms that form gaseous H_2 either by the Tafel or Heyrovski mechanism.

Current (mA)	**LA (mM)**	**LA (% remaining)**	**LAL (mM)**	**LAL (% yield)**
Initial	13.9	100	-	-
10	13.3	95.4	0	0
20	13.0	93.6	0.17	1.2
40	12.9	92.6	0.22	1.6
60	12.5	90.6	0.84	6.0
80	10.4	75.1	1.11	8.0
100	10.8	77.3	1.89	14.5

Table 3.5: ECH of lactic acid using Ru/carbon felt at various currents (11.1 mM lactic acid in 0.01 M H_2SO_4 for 21 h at 70°C). The error in the HPLC is estimated to be ±3%. The standard deviation of the yield of lactaldehyde at 11.1 mM initial concentration of lactic acid is ±5.2%.

The conversion of lactic acid to lactaldehyde after 21 hours at low current (10 mA) is close to zero, suggesting a requirement for adsorbed molecular hydrogen (or at least closely spaced atoms) on the surface rather than isolated hydrogen atoms. This mechanism was proposed earlier from kinetic studies of lactic acid hydrogenation[15]. Thus, the low surface concentration of hydrogen and the low surface area of active catalyst, along with mild temperatures, may explain why ECH of LA is slow compared to classical high pressure hydrogenation.

3.3.2.4 Nature of electrolyte

ECH of lactic acid (11.1 mM) was carried out in three different electrolytes at 0.01 M electrolyte concentration at 70°C for 21 h. The electrolytes studied were H_2SO_4, $HClO_4$ and HCl. The results are shown in Figure 3.12 and 3.13. Similar experiments were carried out using 0.1 M concentrations of the same electrolytes, but the conversions were found to be insignificant, probably due to competitive adsorption of electrolyte anions on the electrode surface preventing adsorption and reaction of lactic acid, which is present in much lower concentration. From the results, it can be seen that there is considerable variation in the rates of formation of lactaldehyde in various electrolytes due to differences in the nature of the electrolyte anions and surface modification of the catalyst by these anions. In general, the relative rate of formation of LAL was found to be higher in $HClO_4$ and HCl and lowest in the presence of H_2SO_4. A more detailed discussion of anion effects on electrodes is included in Chapter 4.

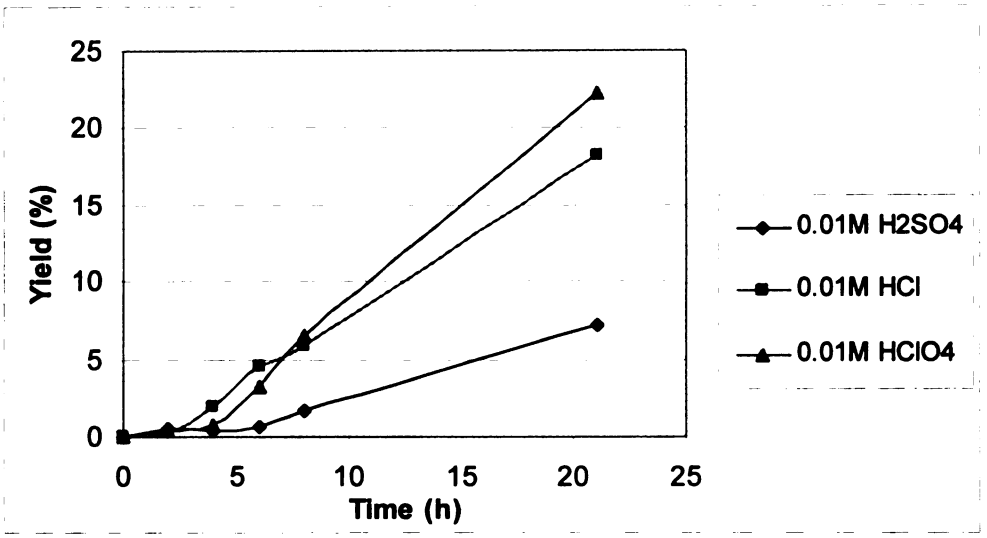

Figure 3.12: Yield of lactaldehyde as a function of time in various electrolytes (11.1 mM lactic acid in 0.01 M electrolyte concentration at 70°C for 21 h, i=100 mA)

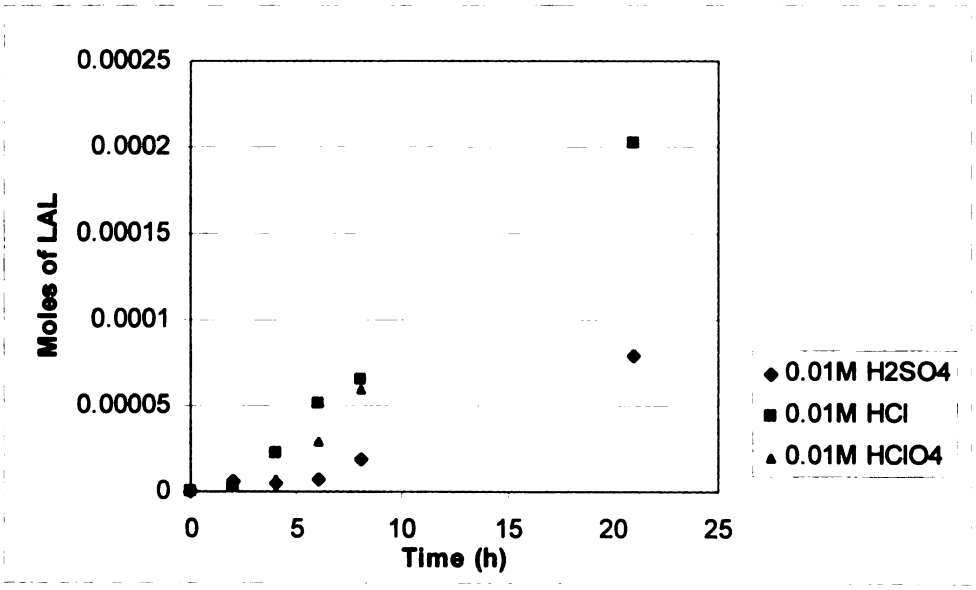

Figure 3.13: Moles of lactaldehyde as a function of time in various electrolytes (11.1 mM lactic acid in 0.01 M electrolyte at 70°C for 21 h, i=100 mA)

3.3.2.5 Initial lactic acid concentration

ECH of lactic acid was carried out at three different lactic acid concentrations, 11.1 mM, 55.5 mM and 0.11 M in 0.01 M HCl at 70°C for 21 h. A constant current of 100 mA was used. The results are shown in Figure 3.14. The final yields of lactaldehyde are shown in Table 3.6. There is an increase in the moles of lactaldehyde formed with an increase in the initial lactic acid concentration, though the % yield decreases with increase in the initial substrate concentration.

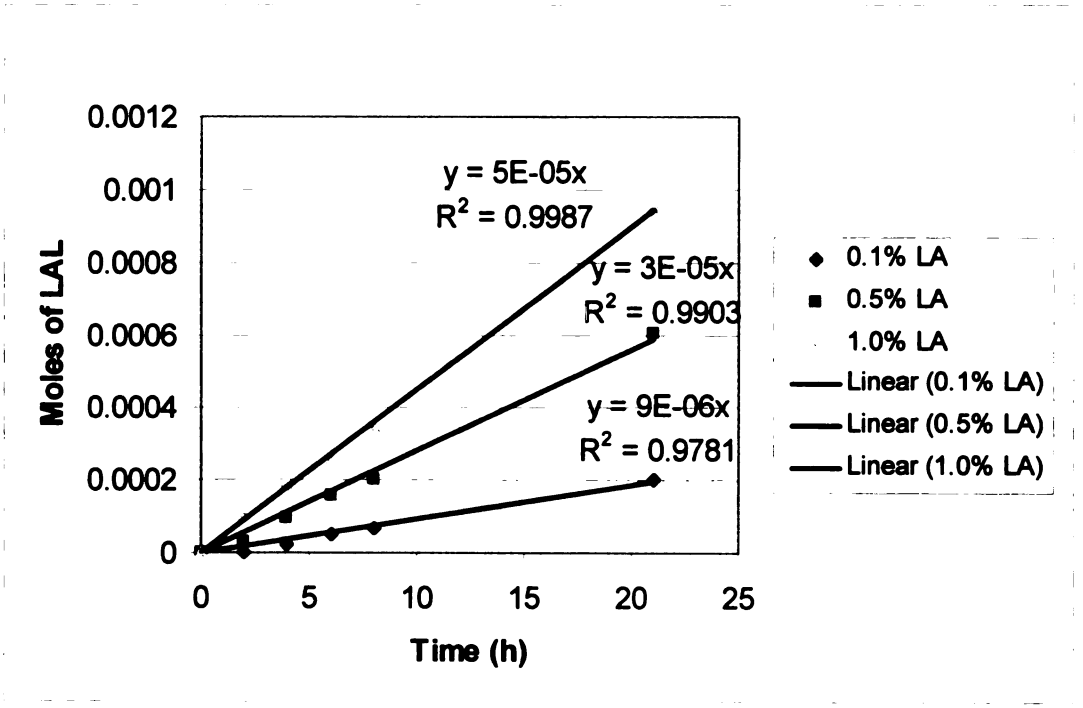

Figure 3.14: Moles of lactaldehyde formed as a function of time at various initial lactic acid concentrations (lactic acid in 0.01M HCl at 70°C for 21 h, i=100 mA)

LA initial concentration (wt. %)	LA initial molar concentration (M)	LAL (wt.%)	LAL (% yield)
0.10	0.011	0.02	25.0
0.49	0.054	0.06	15.0
1.00	0.111	0.09	11.5

Table 3.6: Final yields of lactaldehyde after ECH of lactic acid at various initial concentrations (Electrolyte: 0.01 M HCl, T=70°C, time = 21 h, i=100 mA)

3.3.3 Determination of the order of reaction

For the purpose of calculating the order of the reaction, the data for the ECH of lactic acid in 0.01 M HCl at 70°C were used. The order of the reaction was determined with respect to both lactic acid and hydrogen. The order of reaction with respect to lactic acid was determined from the log-log plot of the turnover frequencies (TOF) at various initial lactic acid concentrations in the range of 0.1 to 1 wt.% (11.1 mM to 0.11 M). The order of reaction with respect to hydrogen was determined from the log-log plot of the TOFs at various currents. Variation of the current, in this case is considered to be equivalent to variation of H_2 partial pressure in the batch hydrogenation because the surface hydrogen concentration is directly proportional to the current and the H_2 partial pressure, respectively, in the two cases.

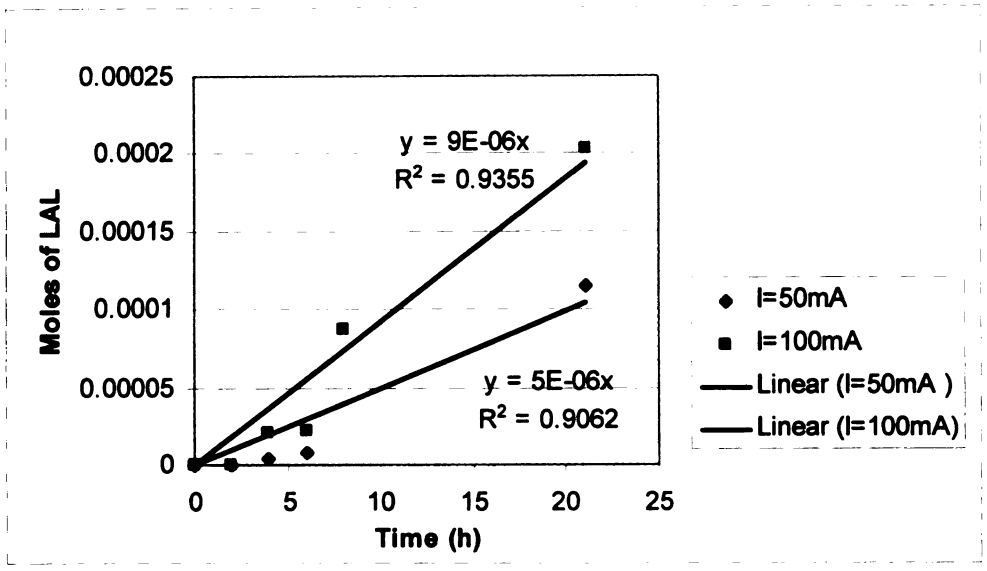

Figure 3.15: Moles of lactaldehyde formed as a function of time at various ECH currents (11.1 mM lactic acid in 0.01 M HCl at 70°C for 21 h)

A plot of the number of moles of lactaldehyde formed versus time at various currents is shown in Figure 3.15. The turnover frequencies (TOF) were obtained from the slopes of the plot. The plots of TOF versus initial lactic acid concentration and TOF versus moles of H atoms produced per hour are shown in figures 3.16 and 3.17 respectively. From the slopes of the log-log plots of TOF versus concentration, the order of reaction with respect to lactic acid and hydrogen were found to be 0.86 and 0.84 respectively.

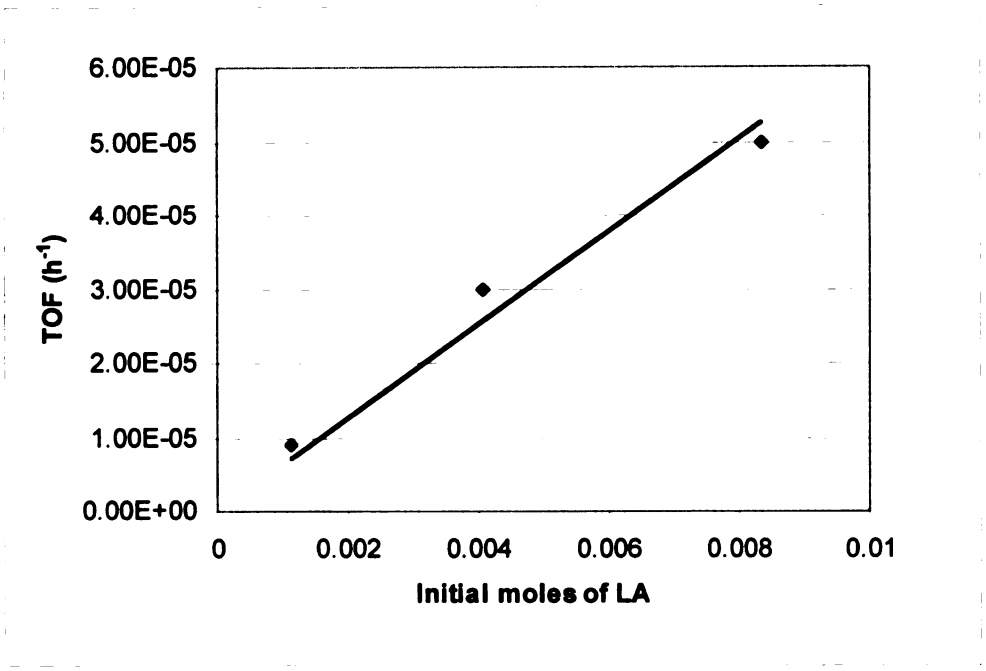

Figure 3.16: TOF for lactaldehyde formation as a function of initial moles of lactic acid in 0.01 M HCl at 70°C after 21 h, i=100 mA

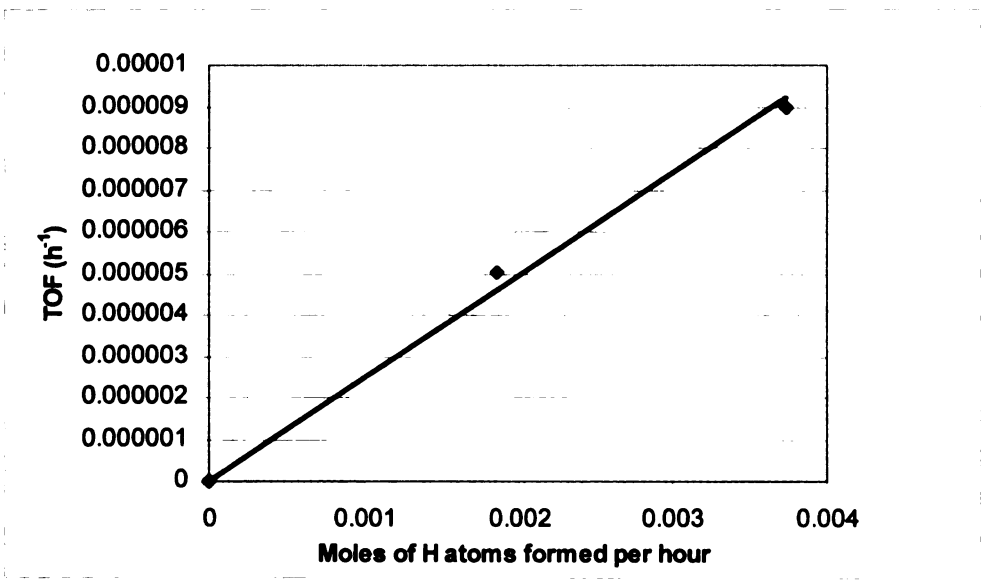

Figure 3.17: TOF for lactaldehyde formation as a function of moles of H atoms formed per hour (assumed to be directly proportional to current) (11.1 mM lactic acid in 0.01 M HCl at 70°C after 21 h)

In case of both lactic acid and hydrogen, a positive reaction order indicates that increase in the surface coverage of either reactant is definitely beneficial in terms of TOF for lactaldehyde formation by ECH. However, a fractional order of reaction indicates that the surface coverage reaches a saturation value on the electrode surface, corresponding to almost complete coverage at a certain concentration. This indicates strong adsorption of lactic acid and hydrogen on the electrode surface.

3.3.4 Hydrogen evolution on Ru

Giles and coworkers[64] studied the hydrogen evolution reaction (HER) using Ru on carbon electrodes. Using plots of the potential dependence of HER of various electrodes, it was determined that HER on Ru is shifted in the cathodic direction compared to HER on Pt/C prepared under similar conditions. The Tafel slope at a constant $[Ru^{3+}]$ and $[H^+]$ was given by the following expression.

$$\delta \log \frac{i_{H2}}{\delta E} = \frac{1}{[RT/(1+\alpha)F]}$$

where α is the symmetry factor of the plot of ΔG versus the reaction co-ordinate. Considering $\alpha = 0.5$, the Tafel slope was calculated to be 40 mV. Based on these results, the following mechanism (scheme 3.2) was proposed for HER on Ru deposited on carbon.

$$H^+ + e \rightleftharpoons H.$$

$$H^+ + H. + e \longrightarrow H_2$$

Scheme 3.2: Proposed mechanism for hydrogen evolution on Ru

The formation of H. is considered as the transition state of the reaction and the stability of this transition state determines the rate of HER and hence, the current.

Tafel curves of Ru deposited on vitreous carbon obtained by Breiter and coworkers[65] at various stages in the deposition revealed that the rate of HER at constant potential depends on the size of the electrocatalyst centers. Since HER was delayed until relatively large centers were formed, the rate detemining step was assumed to be the surface diffusion of hydrogen from one type of site to the other and the hydrogen coverage of both types of sites was assumed to be negligible. Such a rate determining process was also suggested by Grenness and coworkers[66] in an earlier study. However due to simultaneous occurrence of other phenomena such as anion adsorption on the electrode surface, it is not possible to determine the surface hydrogen coverage by voltammetric current-potential curves. Examination of Tafel curves and exchange current densities using smooth Ru in H_2SO_4 revealed that the rate determining step for HER on Ru at low polarization is the Tafel reaction and convective diffusion of H_2 whereas at high polarization, the rate determining step becomes the Volmer-Heyrovski reaction.

3.3.5 Determination of the rate constant of lactic acid electrohydrogenation

The rate expression for the ECH reaction can be described as follows.[38,39]

$$R = k\theta_{LA}{}^{a}\theta_{H}{}^{b} \qquad (1)$$

where k is the apparent rate constant, θ_{LA} and θ_H are the fraction of surface sites occupied by lactic acid and hydrogen respectively, and a and b are the order of the reaction with respect to lactic acid and hydrogen, respectively. k is a function of the concentration of the solution and the electrode surface area.

Substituting the values of a and b determined in section 3.3.3, the rate expression can be written as follows.

$$R = k\theta_{LA}^{0.86}\theta_H^{0.84} \quad (2)$$

The fractional coverage by the organic substrate and hydrogen were assumed to be independent of each other in previous studies of ECH kinetics[37] due to the difference in the nature of the species involved. Also due to the low overpotential, the electrochemical formation of adsorbed H (Volmer reaction) was considered at quasi-equilibrium state. Mass transfer effects are assumed to be insignificant since in the ECH of the model compound, benzoyl formic acid, the rate of ECH was found to be dependent on the availability of surface sites and not on the rate of mass transfer. Mass transfer effects were also found to be negligible in the batch hydrogenation of lactic acid since the rate of hydrogenation was independent of the stirring speed[15]. A Langmuir-Hinshelwood rate equation, similar to that described by Zhang[15] was used to describe the kinetics of the ECH of lactic acid.

The rate of desorption of adsorbed H or the rate of formation of molecular H_2 by the Tafel reaction, which is a parallel reaction to ECH can be expressed as follows[37].

$$R_H = k_H\theta_H^2 \quad (3)$$

where k_H is the rate constant for hydrogen evolution.

According the Langmuir adsorption isotherm, the fractional catalyst coverage by lactic acid can be expressed as follows.

$$\theta_{LA} = \frac{K_{LA}C_{LA}}{1 + K_{LA}C_{LA}} \quad (4)$$

where K_{LA} is the adsorption constant of lactic acid on Ru and C_{LA} is the concentration of lactic acid in solution.

The fractional catalyst coverage by hydrogen can be expressed as follows.

$$\theta_H = \frac{K_H[H^+]\exp(-\eta F/RT)}{1 + K_H[H^+]\exp(-\eta F/RT)} \quad (5)$$

where K_H represents the adsorption constant for hydrogen on Ru, η is the overpotential during the ECH, F is Faraday's constant, R is the universal gas constant and T is the absolute temperature. η is given by the equation,

$\eta = E - E^0$

where E is the potential of the working electrode and E^0 is the equilibrium potential of the proton reduction reaction written as

$2H^+ + 2e^- \rightleftharpoons H_2$ $\qquad E^0 = -0.197$ V vs. Ag/AgCl

E^0 is dependent on the pH of the solution. The actual equilibrium potential, $E^{0'}$ at the solution pH can be calculated using Nernst equation.

$$E^{0'} = E^0 + \frac{0.059}{n} \log \frac{a_{H+}^2}{a_{H2}} \quad (6)$$

The activity of gaseous H_2 can be assumed to be unity. At $a_{H+}=1$, $E^0=E^{0'}$. In 0.01 M HCl, $E^{0'}$ is calculated as -0.433 V. The applied overpotential, η was calculated to be -0.767 V. For calculating the temperature dependent adsorption constants, K_{LA} and K_H, the following expression was used.[15]

$$K_i = K_{0i} \exp \frac{\Delta H_i}{RT} \quad (7)$$

Where, K_i is the adsorption equilibrium constant of a particular species at the given temperature, K_{0i} is the adsorption constant at 0 K, T is the absolute temperature and ΔH_i is the heat of adsorption. The adsorption constants, K_{0LA} and K_{0H2} were determined to be 4.45×10^{-7} and 2.13×10^{-13} respectively, considering ΔH_{LA}= 47 kJ mol^{-1} and ΔH_{H2}= 79 kJ mol^{-1}, K_{LA} (403 K)= 0.55 and K_{H2} (403 K)= 3.7×10^{-3} [15] and assuming hydrogenation via adsorption of molecular hydrogen on the surface, as inferred from the increase in the hydrogenation yield with increase in current. K_{LA} and K_H at 323 K and 343 K were then calculated using equation 7.

The values of the exponential terms in equation 5 at 323 and 343K are 1.19×10^{10} and 4.28×10^{8} respectively. Therefore, $K_H[H^+]\exp(-\eta F/RT) >> 1$, which gives a value for the fractional coverage of hydrogen close to unity. The rate of hydrogenation in this case is determined only by the temperature and lactic acid coverage. However, at a lower current of 50mA, the fractional hydrogen coverage decreases significantly (table 3.7) to 0.39 at 343 K which leads to a decrease in the rate of hydrogenation.

In order to calculate the apparent activation energy of the reaction, the rate constant of the reaction was calculated at two different temperatures, 323 K and 353 K. The plot of the number of moles of lactaldehyde formed as a function of time at 323 K is shown in figure 3.18. The TOF is determined from the slope of the plot to be 4×10^{-6} h^{-1}.

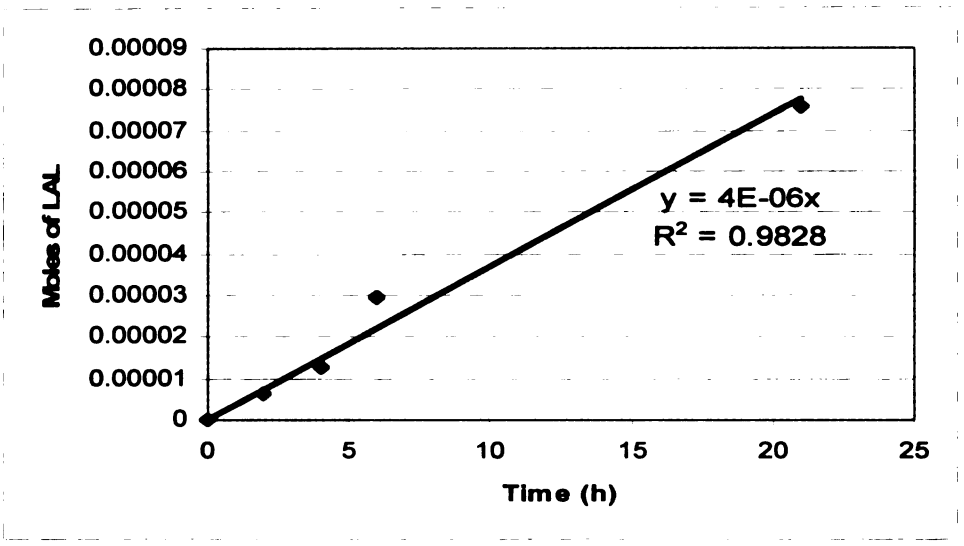

Figure 3.18: Moles of lactaldehyde formed as a function of time at 50°C (323 K) (11.1 mM lactic acid in 0.01 M HCl, i=100 mA)

The values of the TOF's, adsorption constants, fractional coverages and rate constants at the two different temperatures, 323 K and 343 K are shown in Table 3.7. According to Arrhenius equation,

$$\ln k = \ln A - \frac{E_a}{R}\,\frac{1}{T} \qquad (8)$$

where k is the rate constant, T is the absolute temperature, R is the universal gas constant, Ea is the activation energy, A is the frequency factor.

Therefore, a plot of ln k versus 1/T is obtained with slope = $-E_a/R$ and intercept = ln A.

Temperature	323 K	343 K
TOF (h^{-1})	4×10^{-6}	9×10^{-6}
K_{LA}	17.75	6.40
K_H	1.27	0.23
θ_{LA}	0.16	0.06
θ_H	1	1
θ_H (i= 50mA)	0.84	0.39
k (h^{-1})	1.93×10^{-5}	1.01×10^{-4}

Table 3.7: Kinetic parameters for the ECH of lactic acid at two different temperatures

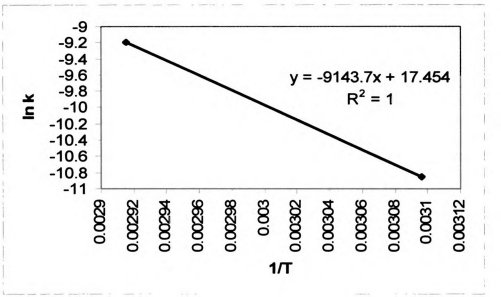

Figure 3.19: Arrhenius plot for the ECH of lactic acid

From the plot in figure 3.19, the activation energy, E_a and the frequency factor, A were determined to be 76.0 kJ mol^{-1} and 3.8 X 10^7 h^{-1} respectively. It should be noted that the values of rate constant and activation energy are apparent values, as a major part of the hydrogen adsorbed on the electrode surface is used up in HER. Since the rate of hydrogen evolution was not considered in the calculations of the kinetic parameters, values of rate constants higher than the actual values and that of activation energy lower than the actual value are obtained. The apparent activation energy determined in this case is approximately half the value of 138 $kJmol^{-1}$, determined from the analysis of the batch hydrogenation of lactic acid.[15]

3.4 Conclusions

ECH of lactic acid was carried out using carbon felt modified with Ru. Carbon felt was chosen as the support due to its high fluid permeability, specific surface area, more rapid dynamic adsorption characteristics (mass transfer rates) and lower resistance to the flow of liquids and gases. The electrodeposition of Ru was carried out at constant current under diffusion limited conditions which resulted in formation of micrometer sized Ru particles as well as larger clusters mainly on the carbon felt fibers closer to the surface. The only product of ECH of lactic acid under these conditions is lactaldehyde, and the yields are low (<20%). The yield of the product was found to increase with increase in the Ru electrodeposition time, temperature and current. Studies on the ECH of lactic acid in various electrolytes showed higher rates in HCl and $HClO_4$, compared to that in H_2SO_4 at 0.01 M concentration. However, when the electrolyte concentration was increased to 0.1 M, there was a significant inhibition of the ECH of lactic acid. The turnover

frequency with respect to lactaldehyde formation increased with increasing initial lactic acid concentration.

TOF values at various initial lactic acid concentrations and various currents were used to determine the order of the reaction. The order of the surface reaction was found to be 0.86 with respect to lactic acid and 0.84 with respect to hydrogen. The kinetics of the surface reaction was described using the Langmuir Hinshelwood kinetic model, the adsorption constants and fractional surface coverages of lactic acid and hydrogen and the apparent rate constants of the reaction were calculated at 323 and 343 K. Using these data the activation energy and frequency factor of the reaction were determined to be 76.0 kJ mol^{-1} and 3.8 X 10^{7} h^{-1} respectively. Comparison of the values for θ_H at i= 50 mA and 100 mA at constant temperature shows that the fractional surface coverage was almost unity at 100 mA and decreased to 0.39 at 50 mA, which may be one of the reasons for the lower rate of hydrogenation at lower current.

CHAPTER 4

BULK ELECTROCATALYTIC HYDROGENATION OF LACTIC ACID USING RETICULATED VITREOUS CARBON AGGLOMERATED WITH RUTHENIUM ON CARBON

4.1 Introduction

In chapter 3, ECH of lactic acid was achieved using Ru dispersed on a high surface area carbon felt support. However, the yield was low and the major product was lactaldehyde. In order to improve the yields, an alternative strategy was used for ECH in which 5% Ru/C was agglomerated in a cathode made of a macroporous material, namely a Reticulated Vitreous Carbon (RVC), by simply stirring the catalyst under cathodic polarization. This chapter describes a series of ECH studies carried out with lactic acid using RVC working electrode suffused with the same 5% Ru/C powder catalyst as was used in the chemical reduction. Previous work using this type of electrode was reported by Menard and coworkers.[68-71] Trapped in the pores of the RVC, the catalyst particles are in electrical contact with the electrode. The same powder catalyst was used previously in our studies of the chemical catalytic hydrogenation. The RVC has a high overpotential for hydrogen evolution and is a relatively inert material that does not participate in electrohydrogenation and hydrogen evolution. It is also electrochemically stable and its three dimensional network of large pores provides electrically conductive host sites to support composite powder catalyst particles. The electrolyte penetrates the RVC by forced convection and the suspended catalyst particles are trapped inside the pores. These catalyst particles are in electrical contact with the RVC electrode and show electrocatalytic activity.

The method provides an attractive way to electrochemically explore the reducing ability of new supported metal powder catalysts, such as those used in chemical catalytic hydrogenation, without changing their chemical or physical characteristics. Thus, the physical form of the catalyst, and presumably the essential components of the catalytic process can be retained, allowing maximum comparability between the electrochemical and the chemical processes.

The rate of ECH depends on several parameters such as the catalyst particle size and current density. The electrochemical cell design is also important in this case because the catalyst agglomeration process is governed by the fluid dynamics. In these reactions, the organic compound is usually thought to be adsorbed on the support, the H atoms are adsorbed on the metals, and the hydrogenation takes place at the adlineation point between the metal and the support particles.[71] The efficiency of hydrogenation therefore depends on the nature and adsorbing power of the support. The rate of the ECH process also depends on the nature of the metal and the heat of adsorption of H on the metal. Since the rate of ECH is determined by the surface concentration of both reactants, i.e. organic substrate and hydrogen, supports such as carbon and alumina which are strong adsorbers of organic molecules show high efficiency. The rate determining step is the hydrogen transfer from the metal surface to the unsaturated molecule.

The electrocatalytic hydrogenation of lignin models[68] to useful organic molecules and the ECH of 4-phenoxy phenol to phenol[69] showed the successful use of Pd/alumina, Pd/C and Rh/alumina catalysts. The cleavage of the strong diphenyl ether bond is much more difficult compared to the glycosidic bonds of lignin and thermal cracking and catalytic hydrogenation give very low conversion rates. ECH provided higher efficiencies of 50-

60%. The cleavage of the diphenyl ether bond is very promising for the conversion of biomass to useful organic molecules, as these types of bonds are found in Kraft lignin produced by the paper and pulp industry. ECH of the pyrrole ring in pyrrole and its carboxylic acid and ester derivatives was also studied using Pd/alumina, Pt/alumina and Rh/alumina catalysts by Menard and coworkers.[70] It was shown that the hydrogenation is specific to the pyrrole ring of the alkyl pyrrole 2-carboxylate and does not modify the ester function of the molecule. The ECH of the alkyl pyrrole carboxylates was found to be more efficient with a Rh/alumina catalyst in 0.1 M NaCl at pH 1.2, whereas pyrrole and pyrrole-2-carboxylate gave better results in phosphate solution at pH 7. The ECH process could be used to hydrogenate the pyrrole ring in a complex natural product, ryanodine, but there was no diastereoselection in the formation of the reduced compound due to the easy access of hydrogen to both sides of the pyrrole ring. The ECH was faster with the Rh/C catalyst compared to Rh/alumina, but there was stronger adsorption of the hydrogenated product on Rh/C, leading to lower recovery.

The ECH of phenol to cyclohexanol using RVC electrodes was studied in the presence of various catalysts, namely Pd/Al_2O_3, $Pd/BaCO_3$ and $Pd/BaSO_4$.[67] Pd/Al_2O_3 was found to be the most efficient catalyst due to the stronger adsorbing power of alumina. The ECH of cyclohexanone to cyclohexanol was carried out using various metals supported on carbon and alumina.[71] In this case also, the ECH was found to be largely dependent on the nature of both the metal and the support. The ECH efficiency is higher on carbon support compared to alumina due to the greater adsorbing power of carbon and for both types of matrices, the best performance was observed with Rh. In this study, the cell was designed so as to allow the catalyst particles to flow through the RVC electrode. The

electrode seemed to work like a fluidized bed and could be compared to a "current pulse electrochemical reaction". This allowed the catalyst to be in open circuit condition when it is circulating in the cell and in an applied current state when it is flowing through the electrode. H atoms are produced only when the catalyst is in the applied current state. When the catalyst is in the open circuit mode, the adsorbed atomic hydrogen favors the hydrogenation of organic molecules rather than hydrogen evolution, leading to a higher ECH efficiency compared to a constant current method because the Tafel reaction cannot proceed.

4.2 Experimental

S-Lactic acid and propylene glycol were purchased from Aldrich and were used without further purification. 5% Ru/C was purchased from PMC Catalysts.

4.2.1 Electrochemical cell setup

Electrohydrogenation studies of lactic acid in several aqueous electrolyte solutions were carried out in the glass electrochemical cell described in chapter 3. It is a two compartment cell with the anode and the cathode compartments separated by a glass frit in order to prevent the diffusion of gaseous products. The reference electrode is Ag/AgCl (E^0= -0.35 V vs. SCE). The counter electrode is Pt wire. The Reticulated Vitreous Carbon (RVC) working electrode (dimensions 4.0 X 3.0 X 0.5 cm); pore size 100 pores per inch (ppi) is connected to the external circuit via a copper wire, positioned to minimize the surface area of Cu exposed to solution; electrochemistry on the copper surface can thus be assumed to be negligible. A voltmeter is connected between the reference and working

electrode to measure the potential of the working electrode. Controlled current was applied using a model 273 potentiostat/galvanostat from Princeton Applied Research. The temperature of the system was controlled using a heating tape wrapped around the cell and connected to a temperature controller from Omega. Samples were withdrawn for analysis immediately after the cell was switched on and at intervals during the electrohydrogenation.

The electrolytes were prepared by the dilution of the concentrated acids, namely 98% sulfuric acid (CCI), 36.5% hydrochloric acid (CCI), and 70% perchloric acid (Spectrum) with HPLC grade water. S-Lactic acid and propylene glycol were purchased from Aldrich and were used without further purification.

4.2.2 Electrocatalytic hydrogenation

Before each experiment, 1.0 g (dry weight) of 5% Ru/C was added to the electrolyte solution and the solution was stirred for 2 hours under cathodic polarization (I= 20-40 mA) in order to ensure proper agglomeration of the catalyst in the pores of the RVC. The potential of the working electrode during this process was in the range of -100 to -400 mV (vs. Ag/AgCl) depending on the electrolyte and the temperature of the cell. The stirring rate was kept low in order to prevent the agglomerated catalyst from being washed off the pores. The RVC surfaces before and after agglomeration were examined by Scanning Electron Microscopy (SEM) as shown in figure 4.1. Elemental composition as measured via Energy Dispersive Spectral (EDS) analysis showed the average surface Ru content to be about 5.5±0.1 %. After the agglomeration, 1 mL of lactic acid solution in the respective electrolyte was added so that the final concentration of lactic acid in

solution was 0.1 wt.% or 11.1 mM, and the total volume of the solution was 75 mL. Samples were withdrawn for analysis immediately after addition of lactic acid and at intervals during the electrohydrogenation.

4.2.3 Characterization of the electrode surface

The electrode surface was characterized using a JSM-6400 V scanning electron microscope (JEOL, Ltd., Tokyo, Japan). Micrographs were recorded using secondary electron mode generated with an accelerating voltage of 20 kV. The presence of Ru was verified by energy dispersive X-ray (EDX) analysis (Noran Instruments, Inc., Middletown, WI) connected to the JSM-6400 V. SEM images were obtained using the AnalySIS software (Software Imaging System Corp., Lakewood, CO).

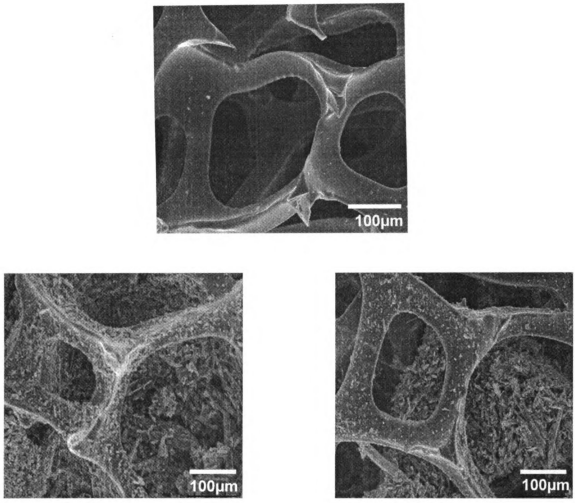

Figure 4.1: SEM images of an RVC working electrode (100 ppi): bare RVC electrode (top); two regions of the RVC electrode after entrapment of Ru/C via agglomeration for 2 h at 20 mA under cathodic polarization (bottom).

4.2.4 Analysis of products

Reaction mixtures were filtered using Millipore syringe filters (0.25 μm) in order to remove the catalyst before analysis of the reaction products by HPLC with refractive index detection, using a Biorad HPX87H ion exchange column at 65°C. The mobile phase used was 5 mM H_2SO_4, run isocratically at a flow rate of 0.6 mL/min.

The method used for the analysis and quantification of reactant, lactic acid and products, lactaldehyde and propylene glycol is similar to the one described in chapter 3.

4.3 Results and Discussion

ECH of lactic acid yields lactaldehyde and/or propylene glycol under all conditions studied. The efficiency of electrocatalytic hydrogenation of lactic acid was found to be highly dependent on the nature of the cell and the stability and dynamics of the system. The reductive catalyst agglomeration process before substrate addition was used to ensure that all Ru in contact with the RVC was in the metallic state and saturated with hydrogen. This step is equivalent to catalyst reduction in traditional batch hydrogenation.

A control experiment carried out at 90°C using RVC with no catalyst in 10 mM H_2SO_4 showed no LA conversion, indicating that the RVC alone is not capable of hydrogenation. Another control with Ru/C catalyst and gaseous hydrogen (1 atm) run at 90°C in the absence of the RVC similarly showed no reaction, indicating that Ru needs to be in electrical contact for the hydrogenation of lactic acid to occur at the mild conditions of this study. To maximize its current efficiency, the ECH should be carried out under

conditions that minimize the competing hydrogen evolution by the Tafel or Heyrovski processes.

As an additional control experiment, lactaldehyde, synthesized chemically using the procedure described by Nambiar and coworkers[60] was subjected to electrohydrogenation in 10 mM $HClO_4$ at 70°C and 100 mA current. There was negligible conversion of lactaldehyde to propylene glycol. Lactaldehyde produced *in situ* from pyruvaldehyde dimethyl acetal and from pyruvaldehyde was also not hydrogenated to propylene glycol.

4.3.1 Factors governing lactic acid conversion

4.3.1.1 Temperature

Electrohydrogenation experiments with 11.1 mM lactic acid in 0.01 M H_2SO_4 were carried out at 25, 50, 70, and 90°C for 9 h using a constant current of 40 mA. The yields of the products, namely lactaldehyde and propylene glycol, were found to increase at higher temperatures as shown in table 4.1, indicating an increase in current efficiency with temperature. At higher temperatures, there is an increase in the the rates of both ECH and hydrogen evolution by the Tafel reaction. In this case, the increase in the rate of hydrogenation appears to exceed the increase in the rate of hydrogen evolution. There is no conversion of lactic acid at room temperature. The relative rates of hydrogenation and hydrogen evolution are thought to depend on the strength of the bond to be hydrogenated and on various factors that influence the adsorption phenomena and the activity of chemisorbed hydrogen[38]. These trends are similar to those observed with Ru/carbon felt in chapter 3.

Temperature (°C)	LA remaining (%)	LAL (%)	PG (%)	Material balance (%)
25	71.8	1.2	1.6	74.6
50	63.0	3.3	3.5	69.8
70	66.3	4.2	5.1	75.6
90	67.0	5.7	9.8	82.5

Table 4.1: Yields of products of ECH of lactic acid at various temperatures (11.1 mM lactic acid in 0.01 M H_2SO_4 after 9 h; i= 40 mA). The error in the HPLC-determined concentrations is estimated to be ±3%.

4.3.1.2 ECH Current

Electrohydrogenation of 11.1 mM lactic acid in 0.01 M H_2SO_4 for 9 hours at 90°C at different currents indicated that with increasing current, the yield of propylene glycol increases and that of lactaldehyde decreases slightly, as shown in figure 4.2. These results suggest that the rate of hydrogenation is dependent on the concentration of hydrogen atoms on the catalyst surface at a given time, which increases with increasing current. Thus, in spite of the increased rate of hydrogen evolution, the rate of propylene glycol formation is also higher at higher currents. In the ECH of benzaldehyde and acetophenone studied by Polcaro and coworkers[37] using Pd/carbon felt electrodes, the surface hydrogen atom concentration was assumed to increase with an increase in the current. The conversion of lactic acid to propylene glycol at low current (10 mA) is close to zero and rises with increasing current in spite of the attendant increased rate of hydrogen evolution. Assuming the sequential mechanism of scheme 4.1, the aldehyde reduction step appears to require adsorbed molecular hydrogen (or at least closely spaced atoms) on the surface rather than isolated hydrogen atoms.

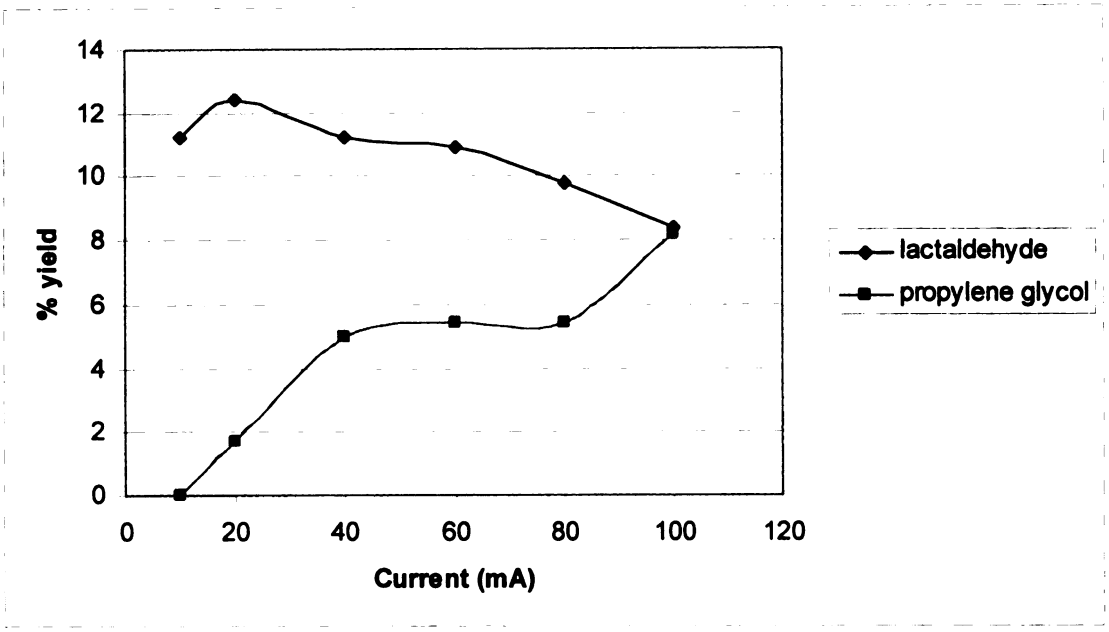

Figure 4.2: Yield of lactic acid reduction products after electrohydrogenation (11.1 mM lactic acid in 0.01 M H_2SO_4 for 9 h at 90 °C). Only lactaldehyde and propylene glycol were detected. The error in the HPLC is estimated to be ±3%.

In the ECH of cyclohexenone using nickel boride electrode, Mahdavi and coworkers[30] observed an increase in the conversion rate with a decrease in current density due to a greater increase in the rate of hydrogen evolution compared to hydrogenation. However, there was a decrease in the further hydrogenation of cyclohexanone to cyclohexanol. This was explained by the fact that the more negative potential at higher current densities would cause the chemisorbed hydrogen to be more active leading to faster hydrogenation of cyclohexanone molecules generated at the electrode surface by cyclohexenone hydrogenation. At lower current densities, the hydrogenation of cyclohexanone would become slow enough to allow its diffusion to the bulk solution before being hydrogenated. Cyclohexanone is expected to be more weakly adsorbed on the electrode

surface compared to the conjugated enone, cyclohexenone. In the ECH of phenanthrenes on Raney Ni electrode studied by Robin and coworkers,[72] an increase in the extent of ECH (yield of octahydrophenanthrene) was observed with an increase in current up to a certain value beyond which there was a decrease in yield. On the other hand, Senda and coworkers[32] reported an increase in the ECH of 4-t-butyl cyclohexanone to alcohol with decrease in current.

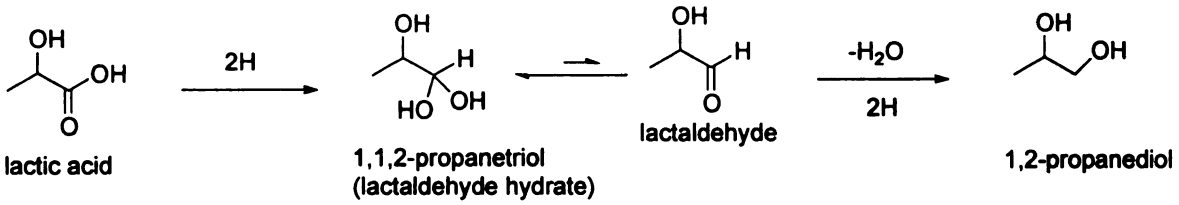

Scheme 4.1: Sequence of reactions in lactic acid hydrogenation

The case of lactic acid hydrogenation is similar to the Mahdavi results above, but more complex due to the intermediate dehydration step involved before lactaldehyde can be further hydrogenated to propylene glycol. With increasing currents, yields of lactaldehyde and propylene glycol decrease and increase, respectively. The simplest interpretation for this observation is that lactic acid conversion to propylene glycol occurs via two sequential hydrogen additions with lactaldehyde hydrate and lactaldehyde as discrete intermediates. At low current, displacement of the relatively weakly bound lactaldehyde hydrate (1,1,2-propanetriol) by lactic acid is faster than its dehydration and capture by surface hydrogens. At higher currents lactaldehyde (also relatively weakly bound) would be more quickly converted to propylene glycol due to the availability of

more surface hydrogen atoms. But the nearly complete absence of propylene glycol at low currents suggests another factor: base-promoted acceleration of lactaldehyde formation at the surface via dehydration of lactaldehyde hydrate in the diffusion layer. Like other carbonyl hydrates, lactaldehyde hydrate's equilibration with the free carbonyl form is accelerated at pH values both above and below neutral. At higher currents, solution protons are more quickly adsorbed and reduced, so the pH at the cathode surface is also higher. Not only are more hydrogen atoms available for reaction but also the concentration of free LAL in proximity to the surface is enhanced, increasing PG formation.

An alternative to the sequential interpretation involves independent paths: parallel reactions might form LAL and PG simultaneously from LA adsorbed on two different types of catalytic sites. In the ECH of benzaldehyde and acetophenone by Polcaro and coworkers,[37] the aldehydes were converted to two different products, the corresponding alcohol and hydrocarbon, and the formation of the two types of products were assumed to involve parallel reactions of the aldehyde adsorbed on different catalytic sites. Adsorption of aldehyde on low coordination sites such as steps and kinks was assumed to lead to the formation of hydrocarbon whereas the alcohol was thought to form by adsorption on high co-ordination sites. Moreover, the ratio of the two types of products was found to depend on the particle size, morphology and the method of preparation of the catalyst due to differences in the relative number of structural features such as edges and terraces, resulting in different ratios of the two catalytic sites. Lacking information on the reactivity of multiple catalyst morphologies, the two-site interpretation of the lactaldehyde and propylene glycol production cannot be ruled out. However, the

sequential scheme is simple, consistent with all observations, and represents a satisfactory working model for this reaction.

The increase in the rate of formation of propylene glycol at higher current may also be attributed to higher electrode surface energy at more negative potential, resulting in higher mobility of H atoms, similar to the phenomenon observed by Mahdavi and coworkers[30] in the ECH of cyclohexenone. The trend observed here also points to the involvement of overpotential deposited hydrogen (OPD-H), rather than underpotential deposited hydrogen (UPD-H) in the ECH of lactic acid. UPD-H atoms are strongly bound to the electrode surface and are believed to be formed on Ru at around 0.0 V, whereas the weakly bound OPD-H atoms are formed at more negative potentials and may co-exist with UPD-H. These weakly bound H atoms were found to be involved in the hydrogen evolution reaction and in the ECH of the olefinic double bond in substrates such as maleic acid.[73]

4.3.1.3 Nature of electrolyte

Electrohydrogenation of 11.1 mM lactic acid was carried out in different electrolytes at 70°C and 100 mA current. Electrolytes studied were H_2SO_4, $HClO_4$ and HCl, at concentrations of 0.01 M and 0.1 M. Though the rate of ECH was maximal at 90°C, the 70°C temperature was chosen in order to prevent excessive evaporation of water from the system during the long run times. The experiments with 0.01 M electrolyte could be carried out only for 21 hours because of the increase in resistance of the system due to depletion of protons. The results are shown in figure 4.3.

From the results, it can be seen that there is considerable variation in the rates of formation of lactaldehyde and propylene glycol in different electrolytes due to the difference in the nature of the electrolyte anions and surface modification of the catalyst by these anions. The final yields of the products are listed in table 4.2. The low material balances may be due to the adsorption of the products in the carbon support of the catalyst and the formation of volatile or polymerized products; volatiles such as methane have been observed under severe conditions in the chemical hydrogenation of carboxylic acids with 5% Ru/C.

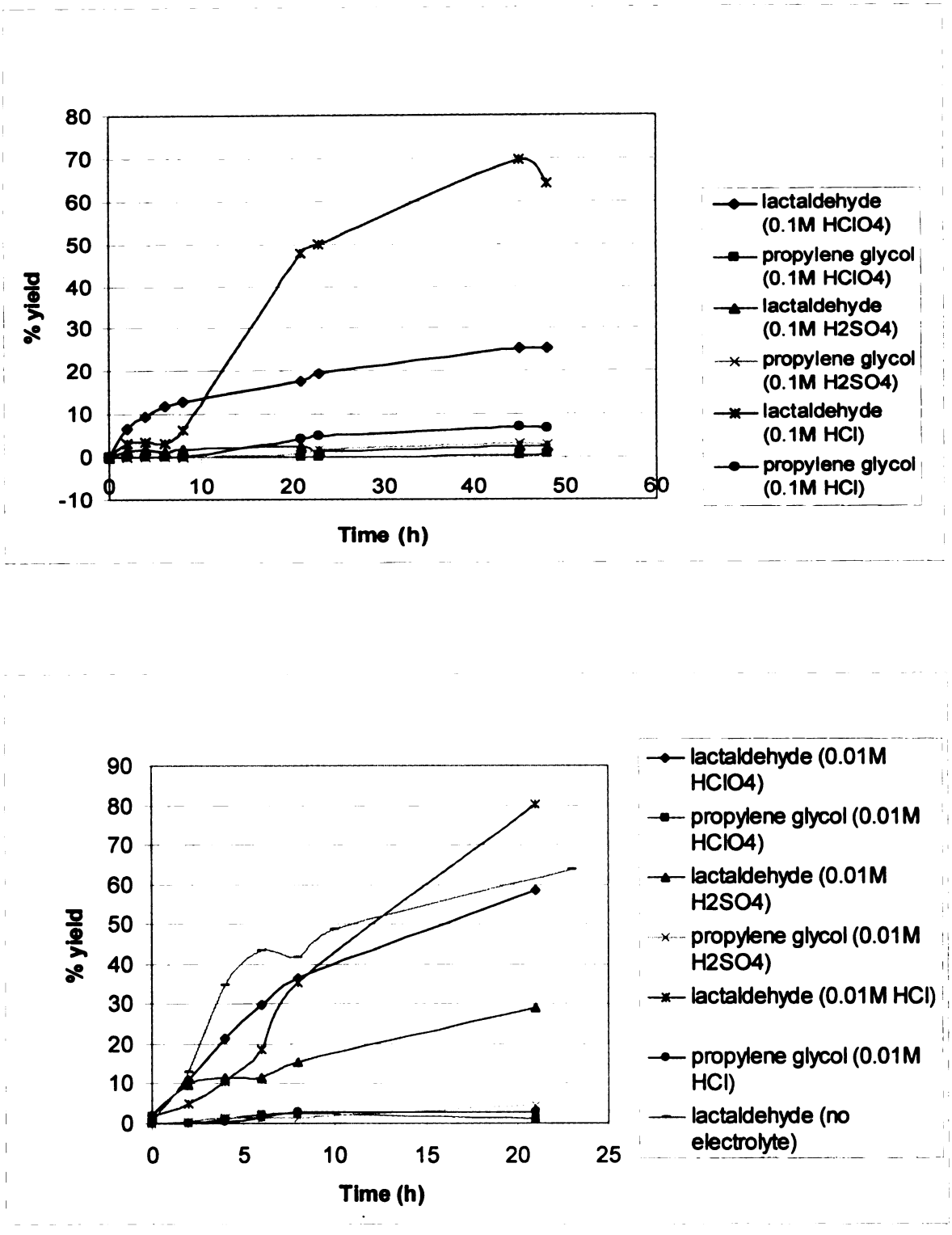

Figure 4.3: Comparison of rates of ECH of lactic acid (11.1 mM) with 5% Ru/C/RVC in various electrolytes at a concentration of 0.1 M (top) and 0.01 M (bottom) (T= 70°C, i= 100 mA). The error in HPLC is estimated to be ±3%.

Electrolyte	Lactic acid (% remaining)	Lactaldehyde	1,2-propanediol	Material balance	Current efficiency
	Time = 48h				
0.1M H_2SO_4	91.8	2.6	2.7	97.1	7.48×10^{-7}
0.1M HCl	8.9	64.0	6.6	79.5	7.17×10^{-6}
0.1M $HClO_4$	54.5	25.4	0.7	80.6	2.48×10^{-6}
	Time = 21h				
0.01M H_2SO_4	37.4	29.1	4.5	71.0	8.09×10^{-6}
0.01M HCl	9.4	80.3	2.9	92.6	1.83×10^{-5}
0.01M $HClO_4$	0.2	58.6	1.1	59.9	1.29×10^{-5}

Table 4.2: Final yields (%) of products after lactic acid (11.1 mM) electrohydrogenation in various electrolytes (T= 70°C, i= 100 mA)

The overall current efficiency, η_F, for ECH may be calculated using the following equation.[74]

$$n_F = \frac{\sum \frac{(n_i - n_i^0)}{z_i}}{\frac{1}{F} \sum_{t_0}^{t} I.dt}$$

where n_i and n_i^0 represent the moles of product formed at the cathode at times t and t_0 respectively, z_i is the number of electrons involved in the electrode reaction, and F is the

Faraday constant. The calculated current efficiencies in each electrolyte, calculated was over the period of time between t_0=0 h and t = 21 or 48 h are listed in table 4.2. Only conversion to lactaldehyde and propylene glycol were considered in the calculations. It can be seen that the current efficiencies are very low due to the long electrolysis time and high current involved. The highest current efficiency of 1.83 X 10^{-5} was obtained in 0.01 M HCl.

In general, in case of both 0.1 M and 0.01 M electrolyte concentrations, the relative rate of formation of lactaldehyde was found to decrease in the order, $HCl>HClO_4>H_2SO_4$. Formation of propylene glycol was generally slow, maximal in 0.1 M HCl and almost negligible in 0.1 M $HClO_4$ due to an inhibitory effect of the ClO_4^- anion. In the case of ECH of lactic acid in 0.01 M and 0.1M HCl, it was found that the rate of conversion of lactic acid to lactaldehyde and propylene glycol was low initially and increased after a period of time. Apparently, as the electrohydrogenation proceeds, Cl_2 evolution at the anode decreases the Cl^- concentration in solution, leading to the desorption of Cl from the cathode surface and leaving more sites for the adsorption of lactic acid, hydrogen or other active species. It is also possible that partial surface coverage by adsorbed Cl is beneficial for the ECH reaction due to the electronegative Cl atoms modifying the electronic state of the Ru atoms and enhancing adsorption of reactants. In order to test this hypothesis, an experiment was conducted in which ECH of lactic acid was carried out in the absence of an electrolyte. Since lactic acid is ionizable to some degree, it was expected to function as the electrolyte. However, the resistence of the solution was very high and the ECH current was reduced to half the value, i.e.50 mA. Theoretically, even at this current the quantity of H atoms produced should be large enough to completely hydrogenate all the

lactic acid present in solution. As expected there was no propylene glycol formed in this case due to the low concentration of protons in solution, leading to a low surface coverage of H (figure 4.3). This is consistent with the requirement for a high surface coverage of H for propylene glycol formation. Also there was no induction period like that observed in HCl, supporting the idea that the initial low rate of ECH is due to Cl adsorption. The rate of ECH during the later stages of the reaction was not as high as that observed with HCl. From this it was concluded that the anomalous behavior observed with HCl may be a result of the combination of two effects, namely, the partial desorption of Cl during the later stages of ECH and the electronic enhancement effect of Cl partially covering the Ru electrode surface.

Earlier attempts at ECH of lactic acid using Ru/carbon felt and 10% Ru/Pt mesh electrodes in 10 mM H_2SO_4 under similar conditions produced only lactaldehyde; formation of propylene glycol was seen only when the electrohydrogenation was carried out using 5% Ru/C catalyst agglomerated in the RVC working electrode. Evidently, the hydrogenation of lactic acid to propylene glycol depends on specific characteristics of the Ru/C catalyst such as the nature and distribution of pores and of the Ru nanoparticles in these pores.

4.3.2 Anion adsorption on electrode surfaces

The adsorption of anions on electrode surfaces and their effects on hydrogen adsorption on metal surfaces have been extensively studied. The relative strengths of adsorption of the anions were found by Horanyi to decrease in the order $Cl^- > HSO_4^- > ClO_4^-$ on Pt electrode.[75] In studies of chemical catalytic hydrogenation of lactic acid, Cl^- was found to

inhibit hydrogenation, whereas an opposite effect is observed in ECH. This discrepancy reflects the fundamental difference in the initial step of the two processes. In catalytic hydrogenation, the first step in the process is the dissociation of the H_2 molecule into atoms, which is equivalent to the electrocatalytic oxidation of H_2. In the case of ECH, the initial step involves the cathodic reduction of protons in solution. Adsorption of anions was found to inhibit the hydrogen oxidation process on Pt, but not the electroreduction step.[73] Therefore, the effect of anions depends on the source of H atoms, i.e. molecular H_2 or protons. This difference was attributed to the involvement of overpotential deposited OPD H atoms in ECH and not underpotential deposited UPD H atoms, which are the ones whose adsorption is influenced by anion adsorption. OPD hydrogen atoms are weakly bound on the cathode surface and have a certain degree of mobility, thus enabling them to reach the active sites. However, in the case of ECH of lactic acid on Ru, the adsorption of anions seems to be strong and accompanied by some amount of charge transfer since they are not easily desorbed even in the hydrogen evolution region. The increase in ECH activity at more negative potentials may also be attributed to the increase in the mobility of OPD H atoms and a change in the electronic properties of the metal surface due to cathodic polarization.[73] In several studies, the adsorption of Cl^- on the electrode surface was found to shift the metal oxide formation peak in the cyclic voltammogram to more positive potentials and the hydrogen adsorption peak to more negative potentials.[76] Therefore, Cl^- adsorption was found to inhibit the formation of metal oxides such as RuOH, resulting in increased hydrogen adsorption. Some Cl^- adsorption was assumed to occur even at more negative potentials of hydrogen evolution. The enhancement effect of HCl towards ECH of lactic acid observed in our

studies may thus be attributed to the inhibition of Ru oxide formation. The adsorption of Cl^- does inhibit lactic acid conversion initially, but the effect is overcome at longer times by the desorption of Cl^- resulting from anodic oxidation of Cl^- and reduced solution concentration.

Using FTIR spectroscopy, HSO_4^- and ClO_4^- were found to adsorb on metals through three of the O atoms in a C_{3v} configuration.[77-79] Even though ClO_4^- is considered to be weakly adsorbed on electrode surfaces in many cases, Colom and coworkers[80] observed electroreduction of ClO_4^- to Cl^- on Ru electrodes as shown in scheme 4.2. The extent of reduction was found to be dependent on the concentration of ClO_4^-, hydrogen adsorption and temperature. The perchlorate reduction process requires the presence of adsorbed hydrogen and is enhanced at higher temperatures. Therefore, despite the similar modes of adsorption of perchlorate and sulfate, the enhancement of lactaldehyde formation with perchlorate may to some extent be attributed to its decomposition to Cl^- on the surface followed by the desorption and anodic oxidation of Cl^-. Cl_2 evolution at the anode was observed when $HClO_4$ was used as the electrolyte.

$$(ClO_4^-)_{ad} + 8H_{ad} \longrightarrow Cl^- + 4H_2O$$

Scheme 4.2: Electrocatalytic reduction of perchlorate to chloride on Ru proposed by Colom[80]

However, it is interesting to note that there is significant concentration dependent inhibition of lactaldehyde and propylene glycol formation with 0.01 M and 0.1 M H_2SO_4

and $HClO_4$. Comparison of rates of product formation between the different electrolytes reveals that SO_4^{2-} has a significant detrimental effect towards lactaldehyde formation whereas perchlorate significantly inhibits propylene glycol formation only at high concentration. These results indicate a general adsorption of Cl^- on all types of active sites, whereas perchlorate and sulfate show preferential adsorption on specific active sites. On the basis of *in situ* FTIR studies, Marinkovic and coworkers[81] have reported that bisulfate ions adsorb strongly on Ru(0001) surface due to the right geometry provided by the hexagonal symmetry at potentials about 300 mV more negative than for adsorption on Pt, whereas its adsorption on polycrystalline Ru is inhibited by surface oxide formation. The potential at which anion adsorption on a metal surface occurs is determined by its work function.[82] A more detailed picture of the effect of anion adsorption on lactic acid conversion can be obtained using *in situ* spectroscopic studies with Ru single crystal electrodes in order to determine the exact mode of adsorption and the nature of surface sites occupied by each type of anion.

4.3.3 Study of anion hydrogen adsorption on Ru using cyclic voltammetry

Shown in figures 4.4a and b are the cyclic voltammograms of a polycrystalline Ru electrode (0.2 cm^2) in the three electrolytes at 0.01 M concentration in the absence and presence of lactic acid (11.1 mM) recorded at a scan rate of 10 mV/s. In all cases, the cathodic hydrogen adsorption and anodic hydrogen oxidation/desorption peaks can be observed. In figure 4.4a, in the case of $HClO_4$ and HCl, the H adsorption peaks overlap with the hydrogen evolution current. Also, in the presence of lactic acid, the oxygen evolution occurs at much lower potentials. However, in the case of H_2SO_4, in the absence

and presence of lactic acid, there is significant hysteresis, which can be attributed to the differences in the properties of the surface caused by anion adsorption on Ru.[83] The peak currents are also much lower in the case of H_2SO_4. Unlike $HClO_4$ and HCl, there is a delay in the onset of hydrogen desorption in H_2SO_4, indicating the formation of a stable adlayer of H which is resistant to oxidation. All these results are consistent with adsorption of sulfate on Ru at the H adsorption/desorption potential. There is no cathodic peak after the hydrogen desorption peak during the oxidation sweep in 0.01 M $HClO_4$, indicating that perchlorate reduction to chloride, which is known to be a slow and irreversible process at room temperature[80] does not occur at this scan rate and at this concentration.

In the presence of lactic acid (figure 4.4b), the hydrogen adsorption peak currents decrease in the case of H_2SO_4 and $HClO_4$ due to partial blocking of surface sites by lactic acid adsorption, but remain constant in the case of HCl. This indicates that in HCl, in spite of lactic acid adsorption, the surface coverage of adsorbed hydrogen remains constant due to an enhancement of hydrogen adsorption by adsorbed Cl. Using radiotracer analysis, Horanyi and coworkers[84] reported strong adsorption of Cl on Ru in the hydrogen adsorption/evolution region at negative potentials even with high surface coverage of H and stated the possibility of Cl^- ions influencing the adsorption of H and O on Ru. They also showed much stronger adsorption of Cl^- ions compared to ClO_4^- and SO_4^{2-}. Though the cyclic voltammograms yield some information about the extent of anion adsorption in the hydrogen adsorption region, they don't reveal much about anion adsorption/desorption in the more negative hydrogen evolution region, where ECH

actually occurs. ATR-SEIRAS studies of the ECH of lactic acid, described in chapter 6 give more detailed information about the effect of anion adsorption on ECH.

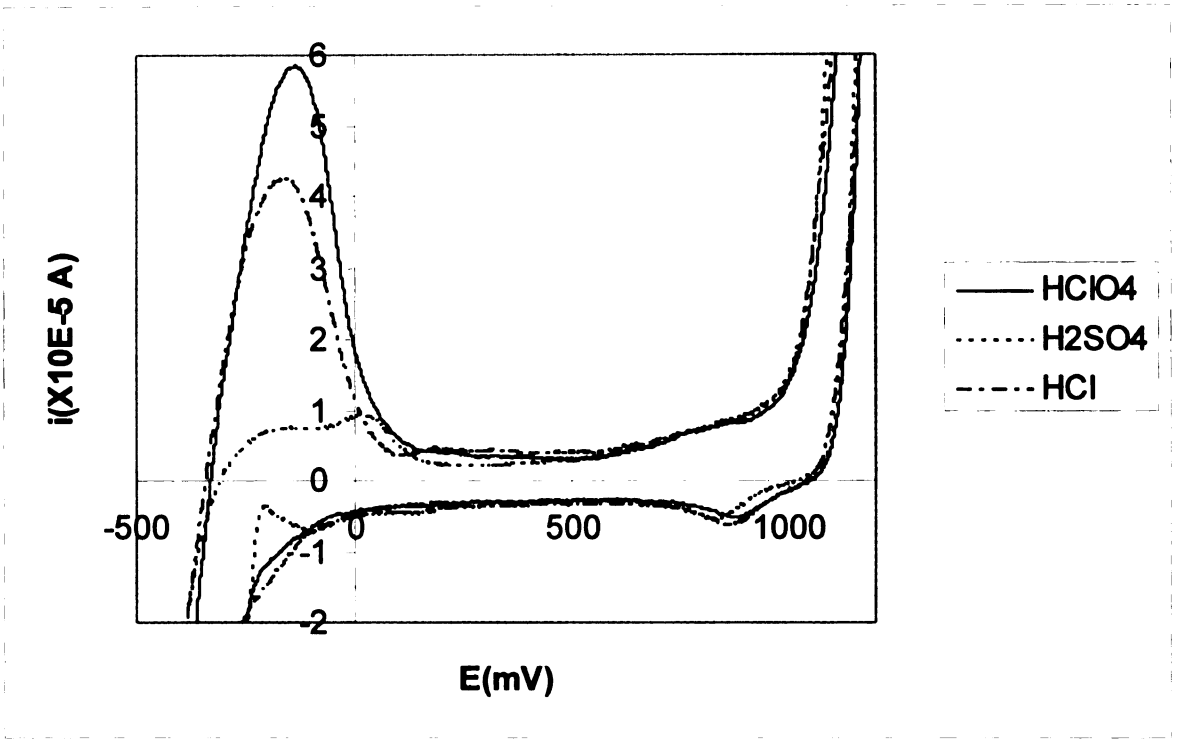

Figure 4.4a: Cyclic voltammogram of a Ru polycrystalline electrode in various electrolytes (0.01 M) (A= 0.2 cm^2, υ= 10 mV/s)

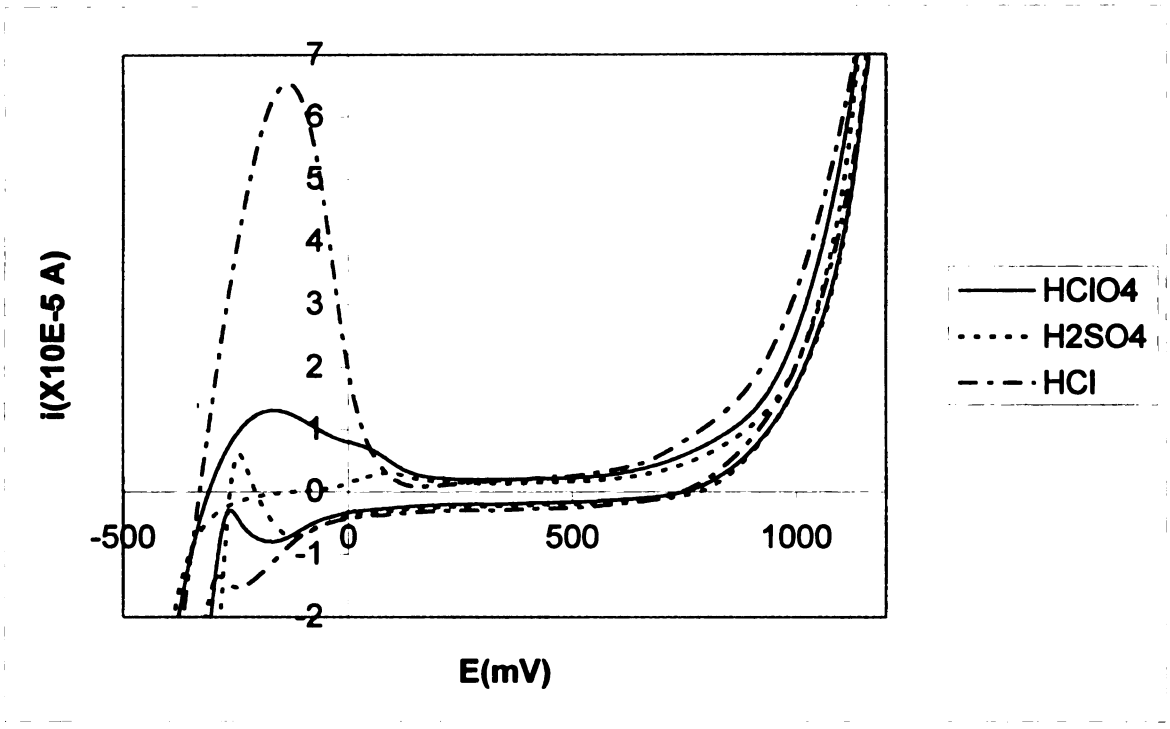

Figure 4.4b: Cyclic voltammogram of a Ru polycrystalline electrode in various electrolytes (0.01 M) in the presence of lactic acid (0.01 M) (A= 0.2 cm^2, υ= 10 mV/s)

4.3.4 Hydrogen adsorption on metal surfaces

The activity of the metal in catalytic hydrogenation is thought to depend on the heat of adsorption of H_2 on the metal and the dissociation energy of the adsorbed molecular hydrogen to atomic hydrogen.[71] It also depends on the relative rates of hydrogen evolution and hydrogenation. The supporting matrix can also modify the adsorption energy of atomic hydrogen on the metal through the effect of the empty d orbital of the matrix. These orbitals can increase or decrease the strength of the M-H bond and change the activity of the catalyst. Since ECH occurs at the adlineation point, a higher concentration of the organic molecule at the adlineation point, which can be achieved by using a stronger adsorbing support, increases the rate of the reaction. The selectivity of the metals and their supports towards the hydrogenation of specific functional groups such as ketones, aldehydes, carboxylic acids, aromatic rings, nitro groups, etc. has been extensively studied, but there is no physical theory to explain the selectivity on the basis of molecular hydrogen energy of adsorption, organic molecule adsorption energy or π-bond energy. Though Ru is known to be one of the least active metals for hydrogen evolution and is thus expected to be efficient for hydrogenation, Menard and coworkers in the study of the ECH of cyclohexanone[71] found Ru to be less efficient for hydrogenation compared to Rh and Pt, thus indicating that hydrogen transfer from the metal to adsorbed organic molecules is the rate limiting step and an increase in the organic molecule concentration at the catalyst-solution interface should increase the rate of hydrogenation. This was proved by the improvement of the ECH rate on using a more strongly adsorbing carbon support instead of alumina.

Electrocatalysis in the hydrogen evolution region is affected by the states and binding energies of chemisorbed H. The kinetics of HER at any electrode are characterized by specific values of exchange current density, i_0 and fractional hydrogen coverage (θ_H in the steady state of HER). The exchange current density is given by the following equation.[85]

$$i_0 = kC_A (1-\theta_H) \exp(\alpha \Delta G_H^0/RT) \exp(-\alpha F\eta/RT)$$

where k is a constant, C_A is the concentration of protons in solution, ΔG_H^0 is the standard Gibbs free energy of chemisorption of H, α is the activation barrier symmetry factor, F is the Faraday constant and η is the overpotential.

The exchange current density is determined by the work function of the metal, which in turn is correlated with the MH chemisorption energy. The MH chemisorption energy is derived from the Eley-Pauling relation shown below.[86]

$$D_{HM} = (D_{MM} + D_{HH})/2 + (\chi_M - \chi_H)^2$$

where D represents the respective diatomic bond dissociation energies in kcal mol^{-1} and χ the electronegativities of M and H. The $(\chi_M - \chi_H)^2$ is an important factor relating log i_0 to the properties of the metal, since the repulsion between M-H dipoles leads to a coverage dependent work function that determines the polarity of the M-H bond.

Gerisher[87] showed that when log i_0 values were plotted versus the standard Gibbs energy of chemisorption of H, ΔG_H^0 for a series of metals, a volcano curve was obtained with the active noble metals lying around the vertex and the other metals lying on either side of the maximum, as shown in figure 4.5. The maximum corresponds to $\Delta G_H^0 = 0$ and weak or strong H chemisorption corresponds to positive and negative values of ΔG_H^0

respectively. The maximum in the volcano curve results from the enhancing effect of an increase in the free energy of chemisorption, ΔG_H^0 and the retarding effect of an increase in the surface coverage, θ_H as ΔG_H^0 increases. Though not shown in the figure, Ru might be expected to appear near the maximum of the volcano curve, similar to the other Pt group metals.

The appearance of Pt group metals at the top of the volcano curve is not consistent with the fact that these metals have high negative values of free energies of H chemisorption. It was proposed by Conway[88] that the relevant ΔG_H^0 for Pt group metals is not the ΔG_H^0 for adsorption of H on the bare metal, but the lower ΔG_H^0 for the OPD H, which is the adsorbed intermediate in HER and is deposited among the UPD H atoms, which in turn are deposited on the metal surface, thus proving the involvement of OPD H atoms in HER and hydrogenation at the potential of HER.

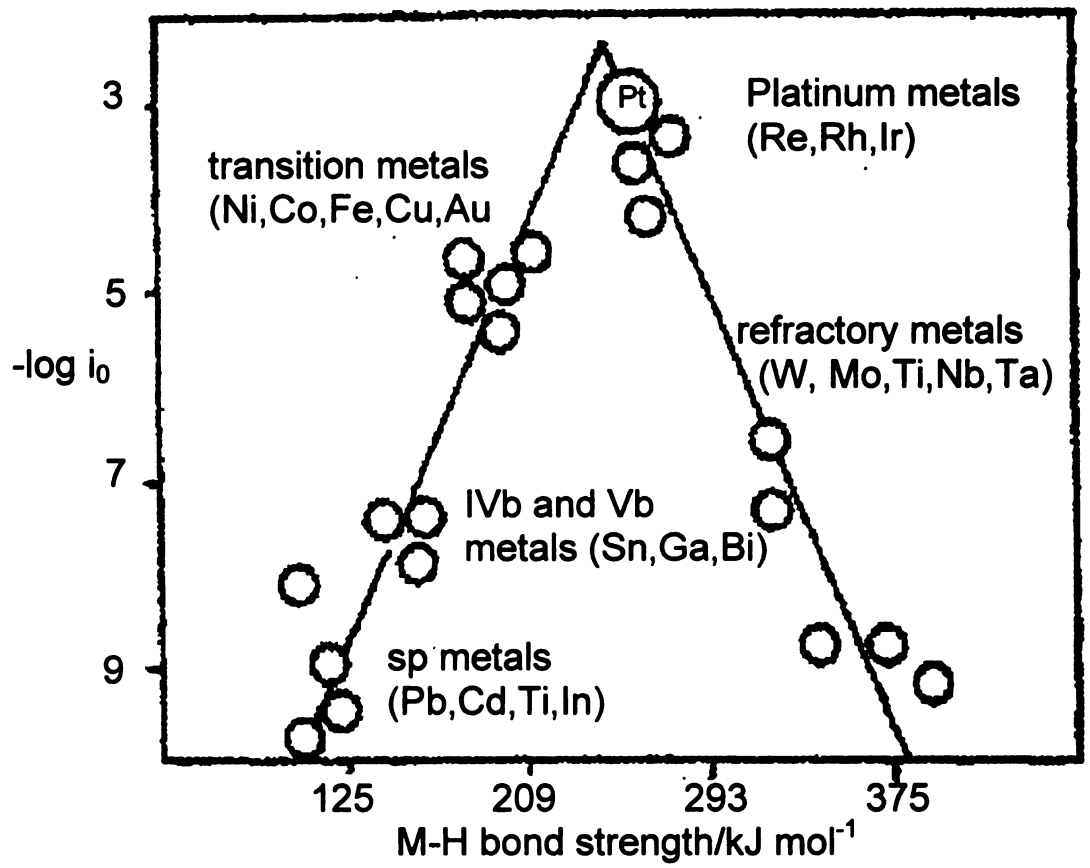

Figure 4.5: Volcano curve for electrocatalysis in the hydrogen evolution region (HER) in terms of log i_0 plotted as a function of heat of adsorption of H (from ref. 86)

4.3.5 ECH of other α-functionalized carboxylic acids

To further confirm the unexpected formation of lactaldehyde via ECH of lactic acid, glycolic (2-hydroxyacetic) acid, the C2 analogue of lactic acid, was subjected to electrohydrogenation in 10 mM $HClO_4$ at 70°C and 100 mA current for 21 h. The products of electrohydrogenation were analyzed by HPLC-RI, ESI-MS and ^{1}H NMR (see Appendix). Almost complete conversion of glycolic acid to glycolic aldehyde was observed (scheme 4.3). Similarly, glyceric acid was converted to glyceraldehyde. Both of these products are well known and their identification and quantification is

straightforward. The amino acid, alanine which is an analog of lactic acid with an α–NH_2 group in place of –OH was also converted to the corresponding aldehyde.

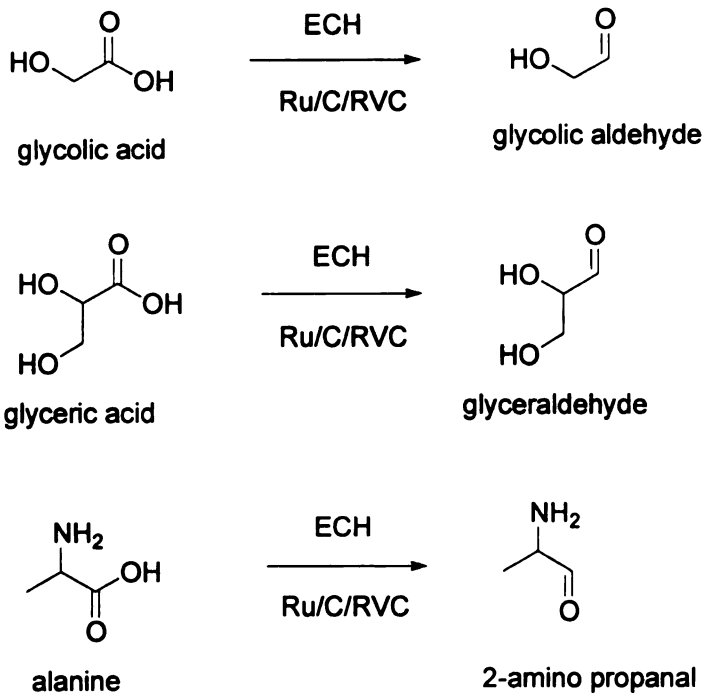

Scheme 4.3: ECH of lactic acid analogs using 5% Ru/C agglomerated in RVC (T= 70°C, i= 100 mA, electrolyte: 0.01 M HCl). Complete conversion of the reactants was obtained, but actual yields of the aldehydes were not determined.

4.3.6 Reason for lactaldehyde formation

The unexpected finding that lactaldehyde (2-hydroxypropanal), a proposed intermediate in the path of lactic acid hydrogenation, is the major product instead of the expected propylene glycol, which only appears as a minor part of the product mixture is a thermodynamically unusual result which reflects the relative surface adsorption and aqueous hydration properties of the starting materials and the two products.

Why does electrohydrogenation of lactic acid stop at lactaldehyde, rather than progressing on to 1,2-propanediol as in the chemical reduction? The most likely reason is that the lactic acid reduction leads directly to the hydrated form of lactaldehyde. Like other α-hydroxy aldehydes, lactaldehyde strongly favors the hydrated form (scheme 4.1). Under the relatively low temperature and acidic conditions, the dehydration required to enable further hydrogenation to the diol would be slow, thus leading to the formation of small quantities of propylene glycol. This notion is also supported by the fact that when mandelic acid, an aromatic analog of lactic acid was subject to ECH under similar conditions (scheme 4.3), the completely hydrogenated product, namely cyclohexyl ethylene glycol was formed to an extent of approximately 50%, which is much higher than the lactic acid to propylene glycol conversion (scheme 4.4). The intermediate, cyclohexyl glycolic aldehyde, which was also present in the product mixture is expected to be less hydrated than lactaldehyde due to the higher electron donating effect of the cyclohexyl substituent.

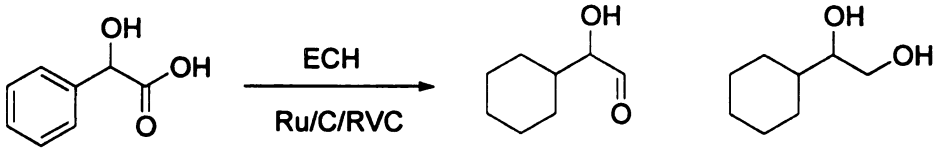

Scheme 4.4: ECH of mandelic acid

A similar selectivity to the corresponding aldehyde was observed by Yokoyama and coworkers[89] in the vapor phase hydrogenation of benzoic acid using a Cr/ZrO_2 catalyst. In

this case, the carboxylic acid interacts strongly with the catalyst surface, displacing the weakly bound aldehyde as soon as it is formed, preventing successive hydrogenation to the alcohol and resulting in high aldehyde selectivity (96% at 98% conversion in the Yokoyama case). Studies of lactic acid, propylene glycol and glycerol binding on Ru surfaces,[90] show preferential lactic acid binding by at least 2 orders of magnitude. In terms of chemical functionality, the hydrated lactaldehyde (1,1,2-propanetriol) is much more like propylene glycol and glycerol than lactic acid, and its expected affinity for the surface should be similarly weak. Thus, like Yokoyama, we interpret the lactaldehyde preference as evidence for the desorption rate exceeding the dehydration/hydrogenation rate at these low temperatures.

It is also interesting to note that although no lactaldehyde formation was observed in the Ru/C catalyzed aqueous phase chemical hydrogenation of lactic acid, Dumesic and coworkers[91] did observe lactaldehyde formation in the vapor phase hydrogenation of lactic acid using a 10% Cu/SiO_2 catalyst. The formation of the aldehyde was found to be dependent on the equilibrium between the aldehyde and diol at a given hydrogen partial pressure. The highest yield of lactaldehyde (22.2%) was obtained at a hydrogen partial pressure of 0.10 MPa at 473 K, and the yield was found to decrease with decreasing temperature and increasing hydrogen partial pressure. Acetaldehyde formation by the vapor phase hydrogenation of acetic acid over silica-supported copper catalyst was also described by Dumesic and coworkers in an earlier report.[92] In these cases, the formation of aldehyde was attributed to the hydrogenation of intermediate surface acyl species. Falorni and coworkers[93] reported the Pd/C catalyzed hydrogenation of substituted amino acids to aldehydes at atmospheric pressure in ethanol. The conversion involved the

preparation of an ester with 2-chloro-4,6-dimethoxyl [1,3,5] triazine followed by hydrogenation. Reduction of the aldehyde to the alcohol was reported only at higher pressures and longer reaction times. However, as with the mandelide studies, alcohol was formed as the major product when aromatic carboxylic acids were used. These studies reflect a dependence of the relative rates of product formation on the surface hydrogen concentration, reaction conditions and the mode of adsorption of the substrate.

4.4 Conclusions

Electrocatalytic hydrogenation of lactic acid has been accomplished using 5% Ru/C agglomerated in Reticulated Vitreous Carbon (RVC) under mild conditions of temperature and pressure as compared to chemical catalytic hydrogenation. The major product of electrocatalytic hydrogenation is lactaldehyde with small quantities of 1,2-propanediol. This unexpected process can provide a clean, convenient and efficient method to prepare lactaldehyde, a compound that is not commercially available and that is difficult to obtain in pure form.

In the previous preparative and mechanistic studies[25] of the Ru/C catalyzed hydrogenation of lactic acid to 1,2-propanediol, lactaldehyde was proposed as an intermediate, but was never detected. Using electrohydrogenation, lactaldehyde is the primary lactic acid conversion product, supporting its proposed intermediacy en route to 1,2-propanediol. Though this project was begun as a way to carry out lactic acid to propylene glycol reduction under mild conditions, the discovery of a pathway that directly reduces aqueous carboxylic acid to aldehyde and then stops is substantially more interesting, in terms of both fundamental chemistry and practical process. The conversion

of amino acids to amino aldehydes, achieved in the case of alanine is an important application, as amino aldehydes are used as chiral building blocks in the synthesis of more complex molecules used in pharmaceuticals.

The fact that the product ratio of ECH depends on the electrolyte used is also intriguing and can be exploited in future applications to control the selectivity of the reaction towards specific products by using specific electrolytes or a combination of various electrolytes. Study of ECH of lactic acid under various conditions showed trends similar to those observed with Ru/carbon felt, i.e. increase in product yields with increase in temperature and ECH current. A significant enhancement of the ECH rate was observed in HCl electrolyte compared to that in H_2SO_4 and $HClO_4$, especially during the later stages of the reaction. The results suggest that this effect is due to the desorption of Cl from the electrode surface at longer times (as a result of Cl_2 evolution at the anode and decrease in the solution concentration of Cl^-) and also an electronic effect of Cl partially covering the Ru electrode surface, which facilitates adsorption of reactants.

Using cyclic voltammetric studies on Ru polycrystalline electrode in various electrolytes, it was found that sulfate is strongly adsorbed on the electrode surface at the potential of hydrogen adsorption/desorption. Furthermore, lactic acid adsorption suppresses hydrogen adsorption in H_2SO_4 and $HClO_4$, but not in HCl. Although these studies give us some insights into the effect of electrolyte anion adsorption on the ECH of lactic acid, the infrared spectroelectrochemical studies described in chapter 6 allowed us to study these effects in more detail.

CHAPTER 5

BULK ELECTROCATALYTIC HYDROGENATION OF LACTIC ACID USING RETICULATED VITREOUS CARBON AGGLOMERATED WITH RUTHENIUM ON NON-CARBON SUPPORTS

5.1 Introduction

In chapter 4, ECH of lactic acid was studied using RVC agglomerated with 5% Ru/C, the same catalyst that was used for the catalytic hydrogenation of lactic acid in the batch reactor. Using ECH, a greener and milder process was achieved for the hydrogenation of lactic acid with the products being lactaldehyde and small quantities of propylene glycol. It is intriguing that conversion of lactic acid to propylene glycol was achieved only with the 5% Ru/C powder catalyst. In earlier studies with electrodeposited Ru on carbon felt as the cathode, lactaldehyde was the only product and the rate of ECH was much slower. The reason for the better performance of the former method and the difference in product distribution is not yet clear. Due to the dynamic nature of the catalyst agglomeration process during the course of ECH, it is difficult to determine the exact quantity and surface area of active catalyst at given time. However, the particle size (<2 nm) of Ru in the 5% Ru/C catalyst is much smaller than that of the electrodeposited Ru on carbon felt, so the dispersion of Ru on the carbon support is much higher, thus implying much higher active surface area per gram of Ru in the commercial catalyst. Also nanometer sized metal particles are known to have properties vastly different from bulk metal. Furthermore, in the case of Ru/C catalyzed lactic acid hydrogenation, the role of carbon as a support is believed to be merely to provide a high surface area for dispersion of Ru, since the carbon support is highly porous with a BET surface area of ~600 m^2/g. Since

hydrogenation of lactic acid to propylene glycol was also achieved with Ru sponge in the batch process, it was concluded that carbon does not play a chemically active role in the catalytic reaction, though it is certainly capable of adsorbing considerable product and feed, complicating carbon balance analyses.

In order to explore in more detail the role of the support material, ECH of lactic acid was attempted with a similar RVC cathode, but using powder catalysts containing Ru dispersed on non-carbon supports. The two support materials chosen were SiO_2 and $BaSO_4$, both of which are relatively inert materials and are common catalyst supports for various metals. Alumina is known to have a high concentration of basic sites, resulting in a strong affinity for acids such as lactic acid and was therefore not used. The study used a commercial 5% Ru/SiO_2 catalyst and a 5% $Ru/BaSO_4$ (not commercially available) catalyst prepared in the lab by the wet impregnation method. Additionally, 5% Ru/SiO_2 catalyst was also prepared by the wet impregnation method and the activity of the catalyst prepared in-house was compared to that of the commercial catalyst.

Menard and coworkers in their study of the ECH of phenol[67] and cyclohexanone[71] to cyclohexanol found that the rate of ECH was dependent on the nature of the support and that a higher rate of ECH was obtained when a strongly adsorbing support such as carbon was used, as opposed to Al_2O_3 or $BaSO_4$. This was attributed to the support playing a major role in the adsorption of the organic substrate and the hydrogenation occurring at the adlineation point between the support and the hydrogen covered metal. The present study of the ECH of lactic acid using various supported Ru catalysts offers similar insight into the role of the support in lactic acid hydrogenation.

5.2 Experimental

5.2.1 Catalyst preparation

The support material,$BaSO_4$ and the Ru precursor, $RuCl_3.xH_2O$ were purchased from Aldrich and were used without further purification. SiO_2 was purchased from Silicycle (Quebec, Canada) and 5% Ru/SiO_2 obtained from Kaida Chemicals (Shaanxi, China). 5% Ru/SiO_2 and 5% $Ru/BaSO_4$ were also prepared using the wet impregnation method.[192]

To measure the incipient wetness, the support was first dried for 5 h at 100°C. Then HPLC grade water was added to 5 g of dried support until the appearance of liquid phase. The incipient wetness of the support is given by the maximum weight of water added just before the appearance of the liquid phase. The incipient wetness of SiO_2 and $BaSO_4$ were determined to be 1.56 g and 0.26 g of water per gram of catalyst, respectively.

For the preparation of 5% Ru/SiO_2, 0.513 g. of $RuCl_3.xH_2O$ was dissolved in 7.8 g of HPLC grade water and 5 g of SiO_2 was added to the solution. The mixture was stirred for 5 min to ensure uniform distribution of Ru and then dried in a rotary evaporator for 2 h at 80°C. The catalyst was dried at room temperature overnight and then transferred to the quartz tube reactor for reduction. The reactor was purged with argon for 2 h at room temperature. Hydrogen gas was then passed through the catalyst at 30 mL/min, and the temperature was ramped to 400°C at 2°C per minute. The reduction was carried out for 16 h and the catalyst was then cooled in a flow of argon.

For the preparation of 5% $Ru/BaSO_4$, 1.026 g of $RuCl_3.xH_2O$ was dissolved in minimum quantity of HPLC grade water, and 10 g of $BaSO_4$ was added to the solution. The rest of the procedure was similar to that for the preparation of 5% Ru/SiO_2 described above.

The SEM images of the catalysts are shown in figures 5.1, 5.2 and 5.4. The presence of Ru was confirmed by the presence of the Ru L- peak in the EDS (figures 5.3 and 5.5).

5.2.2 Electrochemical cell setup

Electrohydrogenation studies of lactic acid in several aqueous electrolyte solutions were carried out in the glass electrochemical cell described in chapter 3. It is a two compartment cell with the anode and the cathode compartments separated by a glass frit in order to prevent the diffusion of gaseous products. The reference electrode is Ag/AgCl (E^0= -0.35 V vs. SCE). The counter electrode is Pt wire. The Reticulated Vitreous Carbon (RVC) working electrode (dimensions 4.0 X 3.0 X 0.5 cm), with a pore size of 100 pores per inch (ppi) is connected to the external circuit via a copper wire, positioned to minimize the surface area of Cu exposed to solution; electrochemistry on the copper surface can thus be assumed to be negligible. A voltmeter is connected between the reference and working electrode to measure the potential of the working electrode. Controlled current was applied using a model 273 potentiostat/galvanostat from Princeton Applied Research. The temperature of the system was controlled using a heating tape wrapped around the cell and connected to a temperature controller from Omega. Samples were withdrawn for analysis immediately after the cell was switched on and at intervals during the electrohydrogenation.

The electrolytes were prepared by the dilution of the concentrated acids, namely 98% sulfuric acid (CCI), 36.5% hydrochloric acid (CCI), and 70% perchloric acid (Spectrum) with HPLC grade water. S-Lactic acid and propylene glycol were purchased from Aldrich and were used without further purification.

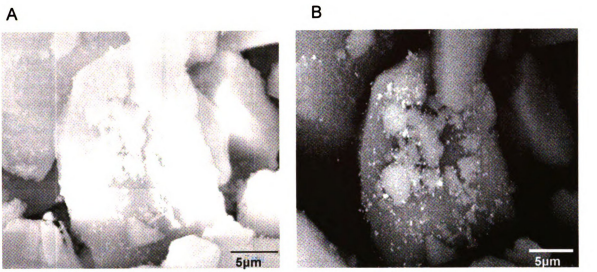

Figure 5.1: SEM images of 5% Ru/SiO_2 (commercial catalyst) (A) Secondary electron image (B) Backscattered electron image

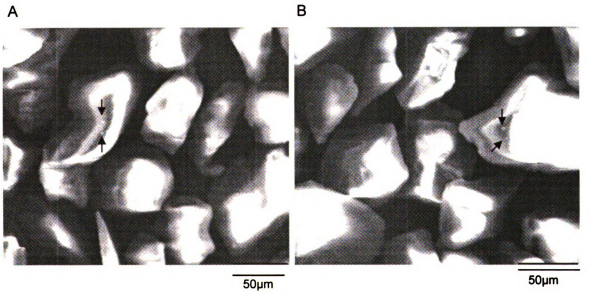

Figure 5.2: SEM images of 5% Ru/SiO_2 prepared by wet impregnation method. Arrows indicate Ru particles

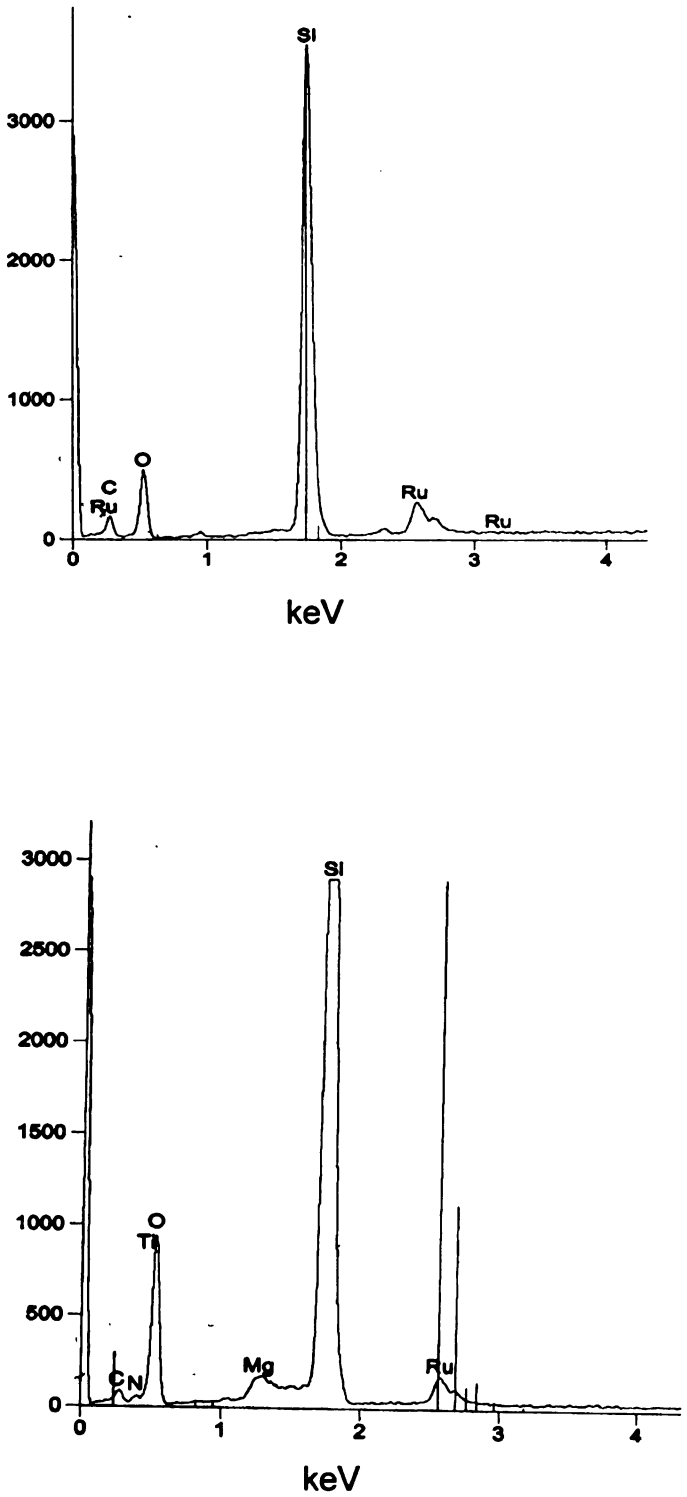

Figure 5.3: Energy Dispersive Spectra (EDS) of 5% Ru/SiO_2: commercial catalyst (top); in-house prepared catalyst (bottom)

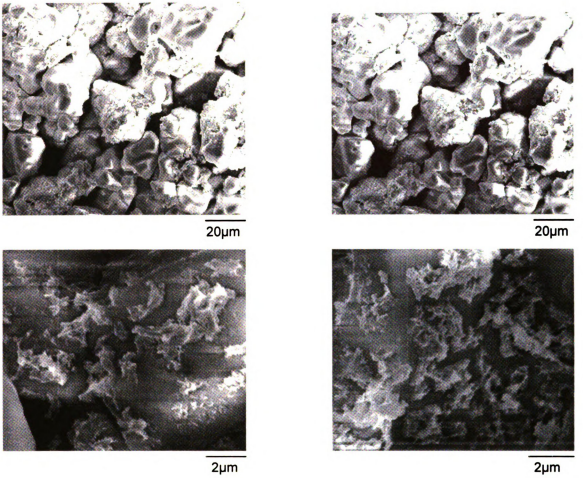

Figure 5.4: SEM images of 5% $Ru/BaSO_4$ prepared by wet impregnation method, showing both low magnification (top) and high magnification (bottom) images of two different regions.

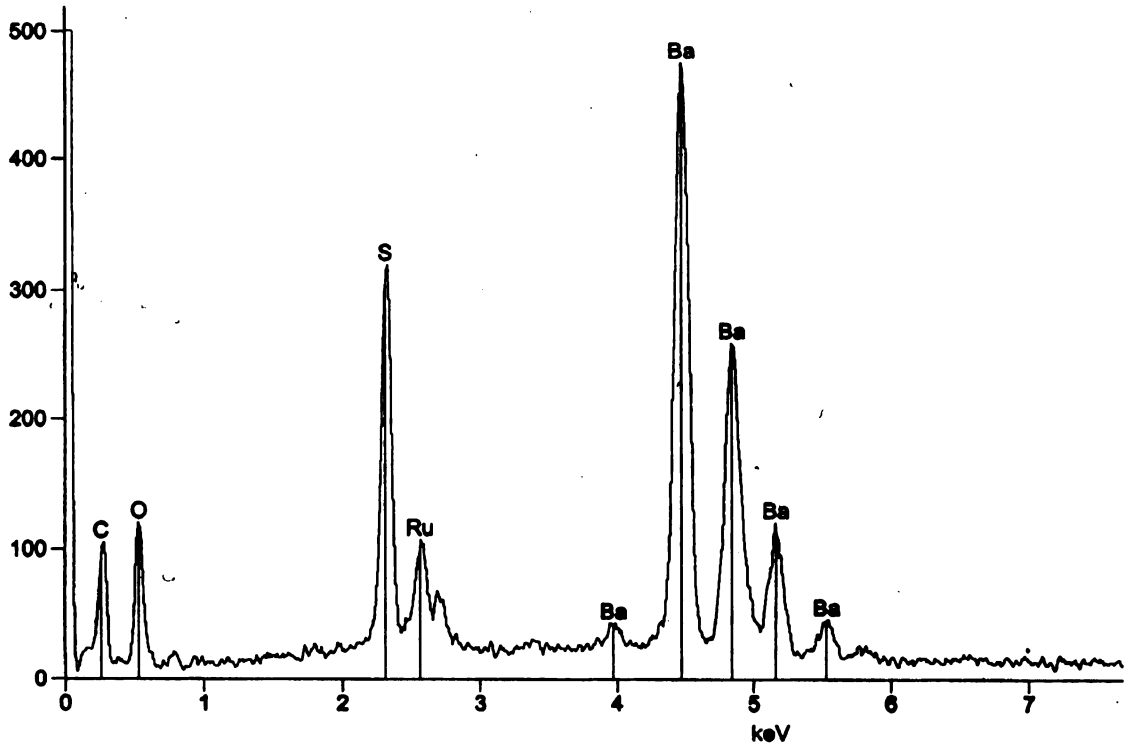

Figure 5.5: Energy Dispersive Spectra (EDS) of 5%Ru/$BaSO_4$

5.2.3 Electrocatalytic hydrogenation

Before each experiment, 1.0 g (dry weight) of the catalyst (5% Ru/SiO_2 or 5% Ru/$BaSO_4$) was added to the electrolyte solution, and the solution was stirred for 2 hours under cathodic polarization (I= 20-40 mA) in order to ensure proper agglomeration of the catalyst in the pores of the RVC. The potential of the working electrode during this process was in the range of -100 to -400 mV (vs. Ag/AgCl) depending on the electrolyte and the temperature of the cell. The stirring rate was kept low in order to prevent the agglomerated catalyst from being washed off the pores. After the agglomeration, 1 mL of lactic acid solution in the respective electrolyte was added so that the final concentration of lactic acid in solution was 0.1 wt.% or 11.1 mM, and the total volume of the solution

was 75 mL. Samples were withdrawn for analysis immediately after addition of lactic acid and at intervals during the electrohydrogenation.

5.2.4 Characterization of the electrode surface

The electrode surface was characterized using a JSM-6400 V scanning electron microscope (JEOL, Ltd., Tokyo, Japan). Micrographs were recorded using secondary electron mode generated with an accelerating voltage of 20 kV. The presence of Ru was verified by energy dispersive X-ray (EDX) analysis (Noran Instruments, Inc., Middletown, WI) connected to the JSM-6400 V. SEM images were obtained using the AnalySIS software (Software Imaging System Corp., Lakewood, CO).

5.2.5 Analysis of products

Reaction mixtures were filtered using Millipore syringe filters (0.25 μm) in order to remove the catalyst, and then analyzed by HPLC with refractive index detection, using a Biorad HPX87H ion exchange column at 65°C. The mobile phase used was 5 mM H_2SO_4, run isocratically at a flow rate of 0.6 mL./min.

The method used for the analysis and quantification of reactant, lactic acid and products, lactaldehyde and propylene glycol is similar to the one described in chapter 3.

5.3 Results and Discussion

5.3.1 Catalyst structure

Figure 5.1 shows the SEM images in the secondary electron (A) and backscattered electron mode (B) of the commercial 5% Ru/SiO_2 catalyst. In the backscattered electron

mode, the areas with higher atomic number elements appear brighter. The backscattered electron image is therefore an atomic number image rather than a topographical image. Here the Ru particles can be seen as bright spots, which correspond to the brighter areas in the secondary electron image.

The characteristics of the silica support used in the commercial catalyst and the in-house prepared catalyst are shown in table 5.1 (data provided by the manufacturer).

	Commercial 5%Ru/SiO_2	**In-house prepared 5% Ru/SiO_2**
Particle size (μm)	100	40-63
Pore diameter (Å)	100	60
Specific surface area (m^2/g)	300	500

Table 5.1: Comparison of the characteristics of the silica support in 5% Ru/SiO_2 catalyst

Figure 5.2 shows the SEM of the 5% Ru/SiO_2 catalyst prepared by the wet impregnation method. Some Ru particles can be seen as bright spots on the silica surface and are indicated by arrows.

Figure 5.4 shows the SEM of the 5%Ru/$BaSO_4$ catalyst prepared by the wet impregnation method. In this case, the morphology of the deposits is very different from that of Ru/SiO_2. The Ru appears to be deposited in the form of islands or patches, which are about an order of magnitude larger than the Ru particles on silica. The reason for this is that due to the low porosity and specific surface area of $BaSO_4$, all the Ru^{3+} from the precursor solution is deposited only on the outer surface of the support particles, and this

results in much higher concentration of Ru in a smaller area. This leads to aggregation of the particles and island formation. On the other hand, on the highly porous silica support, the same metal loading leads to the formation of more highly dispersed and smaller sized Ru particles.

5.3.2 Factors governing lactic acid conversion (5% Ru/SiO_2)

ECH of lactic acid (LA) yields lactaldehyde (LAL) and/or propylene glycol (PG) under all conditions studied. The reductive catalyst agglomeration process before substrate addition was used to ensure that all Ru in contact with the RVC was in the metallic state and saturated with hydrogen.

5.3.2.1 Temperature

Electrohydrogenation experiments with 11.1 mM lactic acid in 0.01 M HCl were carried out at 25, 50 and 70°C for 21 h using a constant current of 40 mA. Lactaldehyde was the only product detected at lower temperatures. At 70°C, a small amount of acrylic acid was detected. The formation of acrylic acid may be explained by the dehydration of part of the lactic acid on the acidic sites of the silica support at high temperature. The yields of the product, lactaldehyde obtained at various temperatures are shown in table 5.2.
The trend here is quite different from those observed with Ru/carbon felt and with 5% Ru/C/RVC. Since the material balances are low, it is clear that other volatile or polymerized products may be formed. Therefore, the actual current efficiencies at various temperatures cannot be compared, as other reactions such as dehydration, etc. are occurring apart from hydrogenation, especially at higher temperatures. Some amount of

the reactant and product may be adsorbed on silica. No attempt was made to desorb and quantify these materials. Unlike the case with Ru/carbon felt and 5% Ru/C/RVC, significant conversion occurs even at room temperature, but at 50°C, the conversion to lactaldehyde appears to be minimum. No specific conclusions can be drawn about the relative rates of hydrogenation and hydrogen evolution at various temperatures with the available data.

Temperature (°C)	**LA (% remaining)**	**LAL (% yield)**	**Material balance(%)**
25	29.3	28.8	58.1
50	59.1	1.5	60.6
70	34.4	21.8	56.2

Table 5.2: ECH of lactic acid using 5% Ru/SiO_2/RVC at various temperatures (11.1 mM lactic acid in 0.01 M HCl for 21 h, i= 40 mA). The error in the HPLC is estimated to be ±3%.

5.3.2.2 ECH Current

Electrohydrogenation of 11.1 mM lactic acid was carried out in 0.01 M HCl for 21 h at 70°C at various currents. The results are shown in table 5.3. The material balances are quite low suggesting the formation of other products and adsorption on silica. However, the highest conversion and yield of lactaldehyde was obtained at 100 mA.

Current (mA)	LA (% remaining)	LAL (% yield)	Material balance(%)
20	56.2	11.3	67.5
60	60.8	6.7	67.5
100	0.4	54.5	54.9

Table 5.3: ECH of lactic acid using 5% Ru/SiO_2/RVC at various currents (11.1 mM lactic acid in 0.01 M HCl for 21h at 70°C). The error in the HPLC is estimated to be ±3%.

5.3.2.3 Nature of electrolyte

ECH of 11.1 mM lactic acid was carried out using 5% Ru/SiO_2 agglomerated in RVC in various electrolytes at 0.01 M and 0.1 M concentrations. The results are shown in figure 5.6. In both cases, lactaldehyde is the major product formed and no propylene glycol formation was observed. Small amounts of acrylic acid were also formed (not shown in the figure) due to dehydration of lactic acid on the acidic sites of silica. In the case of both 0.01 M and 0.1 M electrolyte concentrations, the relative rate of formation of LAL was found to decrease in the order, $HCl > HClO_4 > H_2SO_4$. In H_2SO_4, there is negligible conversion of LA. In $HClO_4$, the rate of formation of lactaldehyde was somewhat slower than the corresponding rate with 5% Ru/C/RVC.

Similar to the previous case, the initial induction period in HCl, followed by a rate increase at longer times is also seen in this case.

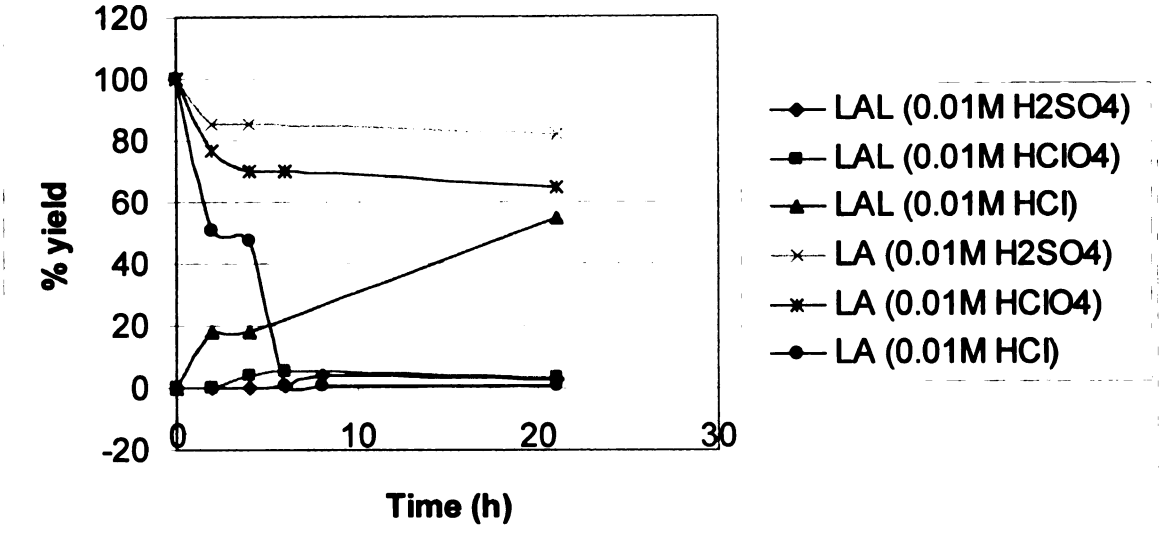

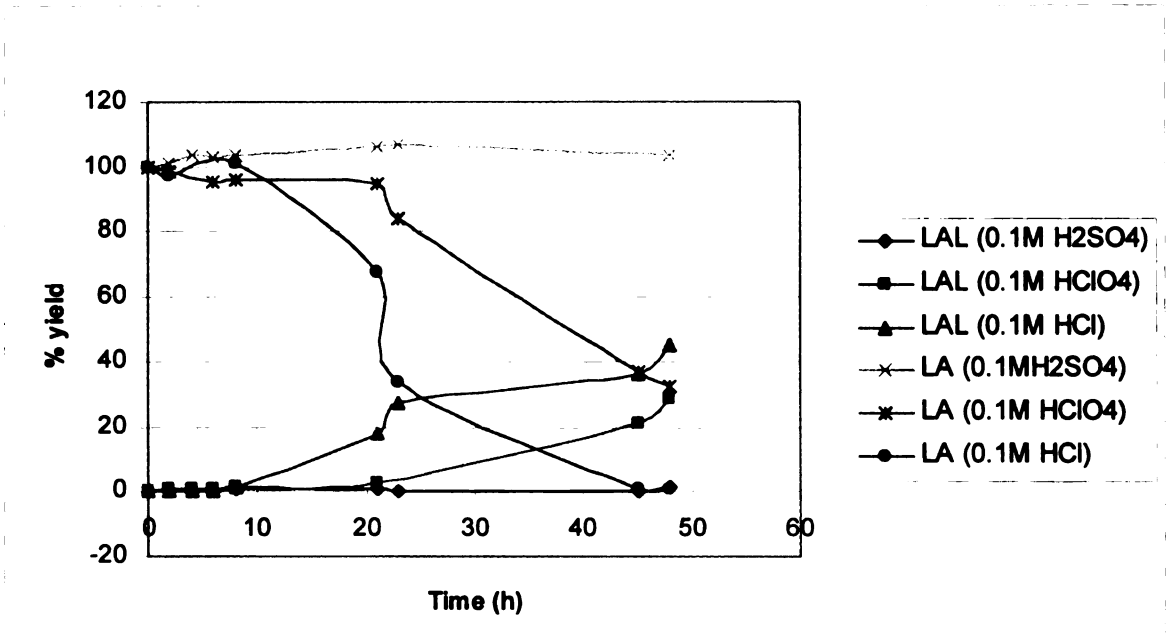

Figure 5.6: Comparison of rates of ECH of lactic acid (11.1 mM) with 5% $Ru/SiO_2/RVC$ in various electrolytes at a concentration of 0.01 M (top) and 0.1 M (bottom) (T= 70°C, i= 100 mA). The error in HPLC is estimated to be ±3%.

For the purpose of comparison, ECH of lactic acid was carried out in 0.01 M and 0.1 M HCl using 5% Ru/SiO_2, prepared in-house by the wet impregnation method. The results are shown in figure 5.7. Quite surprisingly, the results were significantly different from those obtained with the commercial catalyst. Lactaldehyde formation was much slower and in 0.1 M HCl, propylene glycol formation was observed at longer times (45 h) with the yield being similar to that obtained with 5% Ru/C/RVC. The slower rate of lactaldehyde formation may be attributed to the lower metal loading on the external silica surface, in case of the in-house prepared catalyst, as seen in the EDS. Some Ru particles may be distributed in the pores of the catalyst and are not accounted for in the EDS. From table 5.1, it can be seen that the silica support used for the in-house prepared catalyst has a smaller pore volume and higher specific surface area compared to the silica support in the commercial catalyst. It is possible that this allows higher dispersion of the deposited Ru nanoparticles, thus providing more surface area for hydrogen adsorption, which in turn favors the formation of propylene glycol.

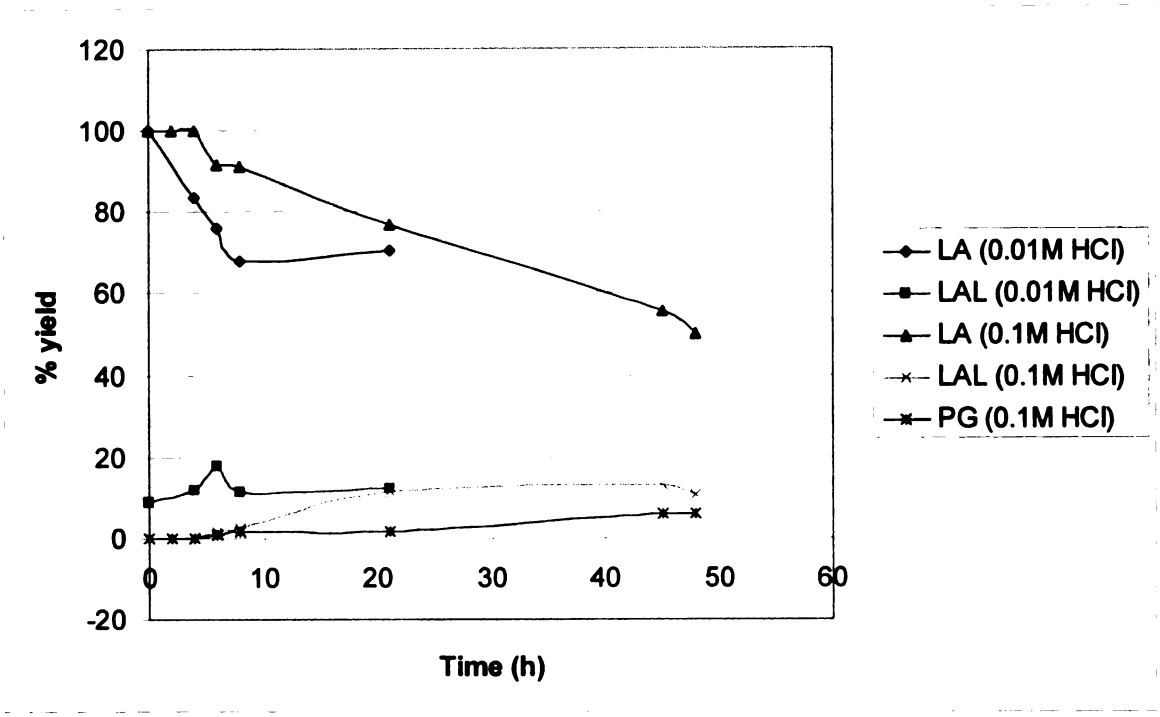

Figure 5.7: ECH of lactic acid (11.1 mM, T= 70°C, i= 100 mA) in HCl, with 5% Ru/SiO_2/RVC prepared in-house. The error in HPLC is estimated to be ±3%.

5.3.3 Factors governing lactic acid conversion (5% $Ru/BaSO_4$)

5.3.3.1 Temperature

Electrohydrogenation experiments with 11.1 mM lactic acid in 0.01 M H_2SO_4 were carried out at 25, 50 and 70°C for 21 h using a constant current of 40 mA. The results are shown in table 5.4. Lactaldehyde was the only product detected. The increase in the yield of lactaldehyde was not much when the temperature was raised from 25 to 50°C, but on increasing the temperature to 70°C, a much larger increase in yield was obtained. The data obtained in this case reflect a greater increase in the rate of hydrogenation compared to hydrogen evolution with increase in temperature.

Temperature (°C)	LA (% remaining)	LAL (% yield)	Material balance(%)
25	75.9	1.2	77.1
50	72.3	2.9	75.2
70	64.4	10.8	75.2

Table 5.4: ECH of lactic acid using 5% Ru/$BaSO_4$/RVC at various currents (11.1 mM lactic acid in 0.01 M H_2SO_4 for 21 h at 70°C). The error in the HPLC is estimated to be ±3%.

5.3.3.2 ECH Current

Electrohydrogenation of 11.1 mM lactic acid was carried out in 0.01 M H_2SO_4 for 21 h at 70°C at various currents. The results are shown in table 5.5. As expected, there is an increase in the yield of lactaldehyde with increase in the ECH current, similar to the trend observed with Ru/carbon felt and 5% Ru/C/RVC.

These results suggest that the rate of hydrogenation is dependent on the concentration of hydrogen atoms on the catalyst surface at a given time, which increases with increasing current. Thus, in spite of the increased rate of hydrogen evolution, the rate of lactaldehyde formation is also higher at higher currents.

Current (mA)	LA (% remaining)	LAL (% yield)	Material balance(%)
20	94.4	0.9	95.3
60	75.8	11.4	87.2
100	54.0	27.0	81.0

Table 5.5: ECH of lactic acid using 5% Ru/$BaSO_4$/RVC at various currents (11.1 mM lactic acid in 0.01 M H_2SO_4 for 21 h at 70°C). The error in the HPLC is estimated to be ±3%.

5.3.3.3 Nature of electrolyte

ECH of 11.1 mM lactic acid was carried out using 5% Ru/$BaSO_4$ agglomerated in RVC in various electrolytes at 0.01 M and 0.1 M concentrations. The results are shown in figure 5.8. In both cases, lactaldehyde is the major product formed and no propylene glycol formation was observed.

In this case, the results are quite different from the ones obtained with other systems. Similar rates of ECH were obtained in all the electrolytes at 0.01 M concentration. However, at 0.1 M electrolyte concentration, ECH was strongly inhibited in H_2SO_4 and $HClO_4$. In 0.1 M HCl, after an initial induction period, there is a significant increase in the rate and complete conversion of LA is obtained after 48 h.

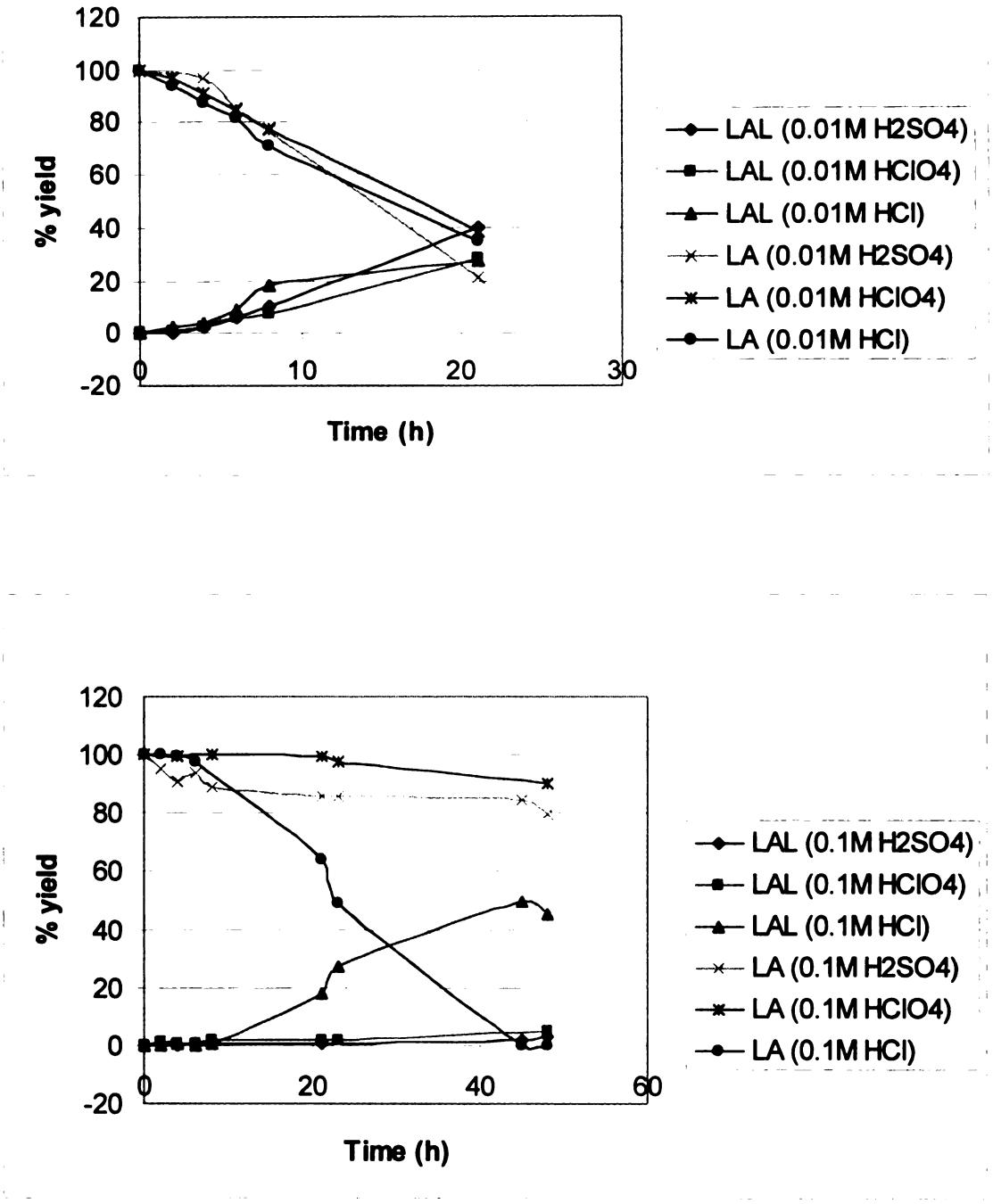

Figure 5.8: Comparison of rates of ECH of lactic acid (11.1 mM) with 5% $Ru/BaSO_4/RVC$ in various electrolytes at a concentration of 0.01 M (top) and 0.1 M (bottom) (T= 70°C, i= 100 mA). The error in HPLC is estimated to be ±3%.

These results indicate that the nature of the support plays an important role in determining the nature and distribution of products formed during ECH. It also supports the conclusion that propylene glycol formation depends on certain specific characteristics of the Ru/C catalyst such as the nature and distribution of pores and of the Ru nanoparticles in these pores and not just on the nature of the metal electrocatalyst. The supports used in this study differ both chemically and physically and therefore they differ in the relative amounts of organic substrates and electrolyte anions adsorbed on the surface. Silica has a porosity comparable to that of carbon, but barium sulfate has a very low porosity. This can be concluded from the far lower incipient wetness value of $BaSO_4$, compared to SiO_2, indicating lower uptake of water by $BaSO_4$. From the SEM images of these catalysts, it is clear that the Ru particles are deposited mostly on the surface of the support and are a few hundred nanometers in diameter. This is very different from the case of 5% Ru/C where many of the Ru particles are present inside the pores and are less than 10 nm in diameter.

From the results on 5% $Ru/BaSO_4$, it is clear that there is a limiting electrolyte concentration between 0.01 and 0.1 M at which most of the catalytic sites are blocked by the anions and there is significant inhibition of ECH. Once again the desorption of Cl^- ions at longer times, as a result of Cl_2 evolution at the anode and depletion of Cl^- in solution, results in an increase in the rate of ECH. However, at 0.01 M concentration, sulfate does not exert the inhibitory effect that is observed in the case of LAL formation on Ru/C and Ru/SiO_2. Therefore, support nature and porosity plays an important role in determining the nature and amount of surface area available for the adsorption of the various species, namely organic acid, hydrogen and anions.

5.4 Conclusions

ECH of lactic acid was carried out using RVC cathode agglomerated with 5% Ru/SiO_2 and 5% $Ru/BaSO_4$, in order to study the effect of support on the rate and product distribution of ECH. The results obtained in various electrolytes showed some general trends similar to 5% Ru/C/RVC, but a few differences were observed. Lactaldehyde was the only product in all cases except with 5% Ru/SiO_2 prepared in-house by wet impregnation, where in spite of the low rate of ECH, some propylene glycol formation was observed at longer times.

The rate of ECH was highest in HCl in all cases, whereas much stronger inhibition of ECH was observed with 5% Ru/SiO_2 in H_2SO_4 and $HClO_4$, compared to 5% Ru/C/RVC. However, with 5% $Ru/BaSO_4$, in 0.01 M electrolytes, the rate of ECH was similar in all three electrolytes, indicating a limiting electrolyte concentration between 0.01 and 0.1 M at which most of the catalytic sites are blocked by the anions. While the data reported here are not sufficient to exactly determine the role of the support and the extent of adsorption of various species (reactants, products, electrolyte anions, etc.) on the support, it does indicate a dependence of the ECH of lactic acid on the chemical nature and porosity of the support and the nature and distribution of Ru particles on the support.

CHAPTER 6

IN-SITU VIBRATIONAL SPECTROSCOPIC STUDIES OF ELECTROCATALYTIC HYDROGENATION OF LACTIC ACID

6.1 Introduction

To date no studies have been carried out to probe the nature of the adsorbed species on the surface of the Ru/C catalyst during lactic acid hydrogenation. Attenuated total reflection (ATR)-IR, coupled with ECH is one of the best ways to study the mechanism on the surface of the heterogeneous catalytic reaction described above.

Most of the surface analytical techniques are suited for ex situ analysis in which the solid surface to be studied has to be removed from the solution, washed and subjected to ultra high vacuum before analysis. Though such methods can provide some insight into the morphology and the nature and distribution of chemical species on the surface, they may completely change the surface characteristics of the solid. Examples of ex situ techniques are X-ray Photoelectron spectroscopy (XPS), ultra violet photoelectron spectroscpopy (UVPES), Scanning tunneling microscopy (STM), Atomic force microscopy (AFM), Fourier transform infra red transmission and emission spectroscopies and Diffuse reflectance Fourier transform infrared spectroscopy (DRIFT). Transmission spectroscopy generally involves dispersal of the sample in an infrared transparent medium like KBr, leading to difficulties due to absorption of water and undesired reactions with the infrared transparent medium.

A number of studies of aromatic compounds like benzene,[94] benzoquinone,[95-97] hydroquinone,[98-108] pyridine carboxylic acids,[109] hydroxy pyridines,[110] etc. coordinated to electrode surfaces have been carried out during the past two decades by Soriaga and

coworkers. They used ultra high vacuum (UHV) techniques such as Electron Energy loss spectroscopy (EELS) and Auger electron spectroscopy to determine the intensities of the vibrational modes, orientations and packing densities of the adsorbed molecules at various applied potentials in order to determine potential dependent changes in the structure of the adsorbed molecules. However in all these techniques, the electrode had to be transferred after the electrochemical reaction from the electrolyte solution to the UHV chamber for analysis of the interface. Shorter lived intermediates could therefore not be detected. Moreover, in many cases adsorbed species on surfaces behave differently in solution and in UHV.

Spectroelectrochemistry has been used for the past few decades to study electrochemical interfaces in situ to get information on molecular structure which can be difficult to obtain using other techniques. In situ IR-RAS (Infrared Reflection Absorption Spectroscopy)[111-134] and SNIFTIRS (Subtractively Normalized Interfacial Fourier Transform Infrared Spectroscopy)[135-139] studies have been reported for CO oxidation,[111-113] electrooxidation of formic acid,[114-118] methanol,[119-122] ethanol,[123-125,130] acetonitrile,[126] ethylene glycol,[127] acetaldehyde[128] and amines[129] and the orientation of interfacial water and electrolyte anions on electrode surfaces.[131-134] In SNIFTIRS, the solution background is removed by minimizing the spectral drift, which involves co-adding sets of interferograms acquired at a suitable pair of electrode materials and alternating the potential periodically.[140] But these techniques have inherent problems such as low sensitivity and the inability of simple background subtraction to correct for changes in the concentration of ionic species in the diffusion layer with change in potential. Therefore, they have limited applications in the study of adsorbed species because in spite of the thin

layer configuration used, the spectra contain artifacts and features from solution species. The higher surface sensitivity of ATR allows much higher signal to noise ratio by averaging only a few interferograms aquired in relatively shorter time, which is advantageous for real-time monitoring of surface reactions. However, in the external reflection mode, the working electrode has to be pressed against the prism in order to minimize the thickness of the electrolyte layer. This limits mass transport of chemical species to and from the electrode surface and also increases the resistance in the cell. Further, when used in the study of ECH which occurs in the hydrogen adsorption/evolution region, the evolved H_2 gas is trapped between the working electrode and the cell window and distorts the spectral and electrochemical measurements.

In situ Raman spectroscopy can be used for monitoring electrogenerated reactive intermediates and adsorbates on electrode surfaces as all molecules show some amount of Raman scattering at characteristic wavelengths. This is especially useful for carbon electrodes which do not support electromagnetic field enhancement that forms the basis of SERS (Surface Enhanced Raman Spectroscopy). With the advent of highly advanced spectrometers using sensitive detectors, Raman spectra of molecules can be obtained on carbon electrode interfaces without the surface enhancement. This technique has been used to follow molecular structural changes associated with electrochemical charge transfer and to study the structure and behaviour of monolayers on carbon surfaces in air, vacuum and electrolyte solutions.[141]

6.2 ATR-IR and the SEIRAS effect

ATR-IR (Attenuated total reflection- infrared) spectroscopy was developed by Harrick and Fahrenfort. In this technique, the sample is placed in contact with an internal reflection element (IRE) of high refractive index, either in the form of a thin film, liquid or powder. Infrared radiation is focused onto the edge of the IRE, reflected through the IRE and then directed to a suitable detector as shown in figure 6.1.[142] The material of the IRE should be chosen according to the refractive index of the sample to be studied. Although complete internal reflection occurs at the sample/IRE interface, the IR beam penetrates a short distance into the sample, in the form of an evanescent wave. This wave is perpendicular to the reflecting surface and its electric field amplitude decays exponentially with distance from the surface. The IR radiation can be absorbed by molecules close to the surface of the IRE, and an absorption spectrum characteristic of the sample in contact with the IRE can be obtained. The penetration depth, d_p of the wave is defined as the distance required for the amplitude of the electric field to fall to e^{-1} of its value at the surface. It is given by the following equation.

$$d_p = \frac{\lambda}{2\pi n_1[\sin^2\theta-(n_2/n_1)^2]^{1/2}} \qquad (1)$$

where n_1 and n_2 are the refractive indices of the IRE and sample respectively, λ is the wavelength of the IR beam and θ is the angle of incidence with respect to the surface normal.

The incident light passes through the higher refractive index IRE and is reflected at the surface of the sample. The propagating light passing through the IRE forms a stationary wave perpendicular to the reflecting surface. ATR can be carried out in single as well as

multiple reflection modes. The intensity of the propagating wave is attenuated with each reflection due to absorption by the sample. The energy loss in the reflected wave is termed as attenuated total reflectance. For N reflections, the total reflectance or the reflected power, R_N is expressed as follows.

$$R_N = (1-\alpha d_e)^N \qquad (2)$$

where d_e is the effective layer thickness and α is the absorption co-efficient of the layer. The reflection loss is proportional to the number of reflections.

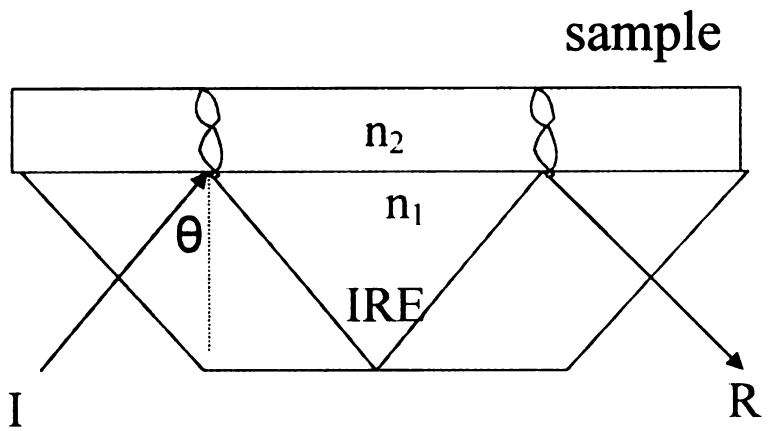

Figure 6.1: Schematic diagram of Attenuated Total Reflection (ATR) in the horizontal configuration showing the important parameters for spectral acquisition and calculation of penetration depth

Several examples exist in literature where ATR-IR has been used to study solid/liquid interfaces both in organic and aqueous solvents, and valuable information has been obtained not only about the nature of the bonds present on the surface, but also on the exact mode of binding and the orientation of the species. This has been made possible due to the development of Surface Enhanced Infrared Absorption Spectroscopy

(SEIRAS). This is based on the principle that there is an enhanced absorption of IR radiation on surfaces by certain types of bonds, which leads to an increase in the intensity of the bands in the IR spectrum. The signal enhancement is believed to arise due to an enhanced electric field within the metal film, caused by the excitation of surface plasmons associated with the metal and depends on the metal morphology, i.e size and shape of particles and interparticle distance. The enhancement is restricted to molecules very near the metal film, specifically adsorbed species, thus enabling the selective characterization of adsorbed species. The enhancement factors found in SEIRAS are usually in the range of 10-100, but in some cases can range up to 10^3.

The SEIRAS enhancement has been explained using both electromagnetic and chemical theories and is believed to be analogous to SERS (Surface Enhanced Raman Spectrometry).[140,143] Models described by Osawa[140] and Chew[144] have been used to calculate enhancement factors. The island film has been modeled as a set of rotating ellipsoids with the axis of rotation normal to the substrate surface, as shown in figure 6.2. The enhancement factor is found to be proportional to the background absorption by the metal, which in turn depends on the thickness of the metal film.[140,145]

The local electric field is normal to the local surfaces of the island. Therefore only molecular vibrations that give dipole changes normal to the surface can be excited, yielding the surface selection rule. This surface selection rule has been used in numerous studies to determine the orientation of adsorbed molecules because the enhancement factors and hence the intensities of the vibrational bands are proportional to $\cos^2\theta$, where θ is the angle of the oscillating dipole with the surface normal. Therefore, bands due to vibrations parallel to the surface will not be observed in the SEIRAS spectrum. For

example, in the ATR-FTIR studies of adsorption of anthraquinone 2-carboxylic acid (AQ-COOH)[140] on Ag electrode surfaces, compared with the transmission IR spectrum in KBr pellet of the Na salt of AQ-COOH, it was observed that the COO_{sym} mode and the b_{2u} modes of the aromatic ring are selectively enhanced, whereas the COO_{asym} and the b_{3u} modes are absent in the surface spectrum. On the basis of the surface selection rule, it was concluded that the molecule is oriented with the aromatic ring perpendicular to the surface. On the other hand, the reduced species, 9,10-dihydroxy anthracene-2-carboxylate, shows only two weak bands at 780 and 757 cm^{-1} due to the C-H out-of-plane bending modes, suggesting a flat orientation on the surface.

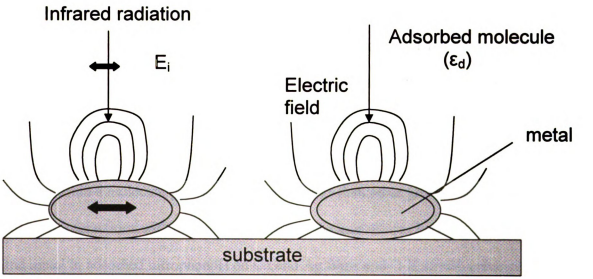

Figure 6.2: Electromagnetic enhancement effect of Surface enhanced infrared absorption spectroscopy (SEIRAS) showing the metal particles of the island film modeled as a set of rotating ellipsoids with the axis of rotation normal to the substrate surface (from ref. 140) (E_i is the electric field of the incident radiation).

The vibrations of the adsorbed molecules excited by the enhanced local field also polarize the metal island, resulting in the perturbation of the polarizability of the islands at the frequencies of molecular vibrations. The image dipole induced in the island by oscillating dipoles of adsorbed molecules may also contribute to the perturbations. This phenomenon also explains the appearance or enhancement in some cases of totally symmetric modes compared to antisymmetric modes in the surface spectra, for example, in the case of p-nitro benzoic acid (PNBA) adsorption on Ag.[145]

The chemical model of SEIRAS was proposed to explain the fact that chemisorbed molecules exhibit larger enhancement than physisorbed molecules.[140] One possible reason for this is that chemisorption aligns the surface molecules and preferentially oriented molecules give larger intensities than randomly oriented molecules for vibrations that give dipole changes normal to the surface. The increase of absorption co-efficient or dipole moment of molecules upon chemisorption also contributes to the enhancement. For example, the absorption co-efficient of CO increases by a factor of 4 by chemisorption on Ag.[146] Griffiths[147] suggested that vibrations of strongly polarizable groups within a molecule give larger enhancements than other groups due to donor-acceptor interactions with the metal surface, eg. the interactions between the nitro group and metal in adsorbed nitrophenols on Cu and Ag films and O-H stretch enhancement on metal bonding. However, the contribution of chemical effects is believed to be much smaller than that of the electromagnetic effects. The chemical enhancement effect in SEIRAS operates over a shorter range, usually one monolayer from the surface, compared to the electromagnetic enhancement effect, which operates over several monolayers, depending on the conditions. Devlin and Constani[148] suggested an

enhancement of IR absorption resulting from the coupling of vibrational modes with charge transfer between the metal and adsorbate, eg. the charge transfer enhancement observed for thiocyanate[149] and tetracyano ethylene anion radical.[150] The total enhancement is found to be roughly equal to the product of the enhancements due to each of the three contributions, namely electromagnetic effect, chemical effect and molecular orientation.

Hahn and coworkers[151] used SEIRAS to study the anodic oxidation of methane at noble metal electrodes (Pt, Pd, Au, Ru and Rh) in order to explore the possibility of using methane as a fuel in fuel cells. Using deuterated water solutions, adsorbed intermediates such as CO and CHO was detected with the final product being CO_2. A mechanism involving dissociative adsorption of CH_4, followed by reaction with adsorbed water or –OH was proposed.

The most remarkable application of SEIRAS is the study of methanol electrooxidation on Pt and Pt-Ru electrodes in order to determine the role of Ru in reducing anode poisoning by adsorbed CO. In 2001, Watanabe and coworkers[152] proposed a mechanism for methanol electrooxidation from results of ATR-SEIRAS. Adsorbed CO_L (linearly adsorbed), CO_B (bridged) and formate were identified as intermediates of methanol electrooxidation to CO_2 at intermediate potentials, and CO and COOH were detected at high potentials. In 2003, Osawa et al.[153] detected using SEIRAS the formate species, HCOO, giving rise to the COO vibration around 1300 cm^{-1}, which increased in intensity on Pt when CO was oxidized, leading to increased methanol oxidation current. Based on this finding, the dual path mechanism of methanol oxidation, involving both CO and non-CO paths was established. In 2004, Yajima et al.[154] in their study of methanol

electrooxidation on Pt, Pt/Ru and Ru, detected water molecules adsorbed on Ru sites giving rise to an O-H stretching vibration at 3610 cm^{-1} and assigned water molecules as the oxygen donor for CO oxidation, which resulted in removal of the poison from the electrode surface and led to enhanced methanol oxidation current. Recently Okada and coworkers[155] observed water molecules on the surface of Pt in 0.1 M $HClO_4$, with the O-H stretching frequency having two components at 3500 and 3000-3100 cm^{-1}. These characteristics changed by interaction with neighbouring adsorbed CO in the presence of methanol giving rise to a new O-H stretching band at 3658 cm^{-1}. In both cases, a linear quantitative relationship was observed, with an increase in the formate band intensity at 1330 cm^{-1} being correlated with a simultaneous decrease in the C-O and water band intensities. This served as a proof that the water molecules adsorbed along with methanol and co-existing with adsorbed CO intermediate are the species responsible for the oxidation of the catalytic poison.

Recently Adzic and coworkers[156] studied ethanol electrooxidation on a Pt film electrode using ATR-SEIRAS. By following the behavior of acetic acid, one of the products of ethanol oxidation, as a function of potential, it was found that acetate was strongly adsorbed even at high potentials, thus blocking Pt sites and inhibiting ethanol oxidation. The acetate was found to be derived mainly by direct oxidation of ethanol and partially from adsorbed acetaldehyde at low potentials. The main reaction intermediates are adsorbed acetaldehyde and acetyl, which formed adsorbed CO and acetic acid. The first and second layer adsorbates on Au electrodes with increase in potential were elucidated by Futamata[157] with respect to the peak frequency of the electrolyte ions such as sulfate and perochlorate. The constant peak frequency of the second layer ions were explained

by the fact that first layer adsorbates suppress the specific interaction of the second layer adsorbates with the Au surface. Watanabe and coworkers[158] used ATR-SEIRAS to study the oxidation of adsorbed CO on a Pt-Fe alloy, the surface of which was covered by Pt skin, and found that the linear CO had a much lower saturation coverage and higher mobility on the Pt skin compared to pure Pt due to increased d vacancy on the Pt skin and weakening of the Pt-C bond. An adsorbed HOOH species, which could not be observed on pure Pt, was observed on the alloy above 0.6 V in the electrolyte solution in the absence of CO. However, unlike the case with Pt/Ru, the Pt skin did not show high activity for direct CO oxidation and hence it was concluded that the CO tolerance is due to lower CO coverage and bond strength and not due to enhanced oxidation. Using ATR-SEIRAS, Osawa and coworkers[159,160] also elucidated the mechanism of galvanostatic formic acid electrooxidation on Pt and the cause of the observed potential oscillations. By following the band intensities of CO_L, formate and CO_B as a function of potential and by using ^{13}C labeled formic acid, adsorbed formate was identified as the intermediate of oxidation of formic acid to CO_2. In a different set of experiments,[161] the oxidation current was found to correlate well with the formate band intensity in the electrooxidation of formic acid on Pt, pointing to the involvement of formate as the intermediate and the oxidation of formate to CO_2 as the rate determining step.

Osawa and coworkers reported time-resolved ATR-SEIRAS studies of fumarate adsorption on a Au(111) surface in 0.1 M $HClO_4$ solution.[162] By correlating the appearance of the COO symmetric stretch and the disappearance of the C=O stretching bands with the change in potential, it was concluded that fumaric acid adsorbed on the electrode surface through one of its two COOH groups. The absence of the COO

asymmetric stretching band indicates that the carboxylate group is symmetrically bonded to the surface with a perpendicular orientation. Finally, surface enhanced IR with ATR configuration was also used to study hydrogen adsorption on Pt at potentials under which hydrogen gas evolution occurs.[163,164] The kinetics and mechanism of the HER were determined from the IR and electrochemical data, and it was determined that adsorbed H atoms giving a Pt-H vibration around 2100 cm^{-1} i.e. H_{OPD} and not H_{UPD}, are the reaction intermediates of HER. These studies demonstrate the monitoring of fast dynamics at electrochemical interfaces using the ATR-SEIRAS technique at the same timescale as that used in electrochemical measurements, but providing much more detailed information about kinetics, dynamics and structural details.

In the hydrogenation reaction, our aim is to look at the surface coordinated species without interference from other IR absorbing species like water which is present in large excess. ATR is a technique where the passage of the IR radiation through bulk water can be effectively avoided as the evanescent wave penetrates only small distances from the surface of the internal reflection element allowing the detection of mainly adsorbed species and species very close to the surface. This technique also provides high sensitivity, no mass transport limitations and no distortion from hydrogen gas evolution.

6.3 Experimental

6.3.1 ATR cell configuration

The spectroelectrochemical cell used in the present work is shown in figure 6.3. It consists of a hemispherical Si window, 25 mm in diameter, and a teflon holder, screwed onto a stainless steel base plate. The glass ATR cell (about 20mL in volume) was

mounted on the base plate and sealed with an o-ring to prevent leaks. The surface area of the IRE exposed to the solution was 3.14 cm^2. The cell consists of a water jacket through which water was circulated using a water circulator in order to maintain a constant temperature. The counter electrode was a Pt wire, which was attached to the cell and the Ag/AgCl reference electrode is connected through the salt bridge. The Si window coated with a thin film of Ru on Au was used as the working electrode. Electrical contact with the window was attained through a gold wire sealed to a teflon holder, which was mounted in a glass tube. The gold wire was sealed to the glass tube at the top and the entire assembly was screwed onto the cell. A constant potential was controlled using a PAR 173 potentiostat.

6.3.2 Preparation of Au thin film

The Si window was polished with 0.01 μm alumina powder for 10 min., rinsed with milli-Q water, sonicated with acetone for 40 min. and in water for 40 min. The window was then heated in piranha solution (1:1 H_2O_2 and H_2SO_4) at 80°C for 1 h in order to remove surface oxides, cooled and rinsed with water.

The chemical deposition of Au on the Si Internal Reflection Element (IRE) was carried out using the method described by Osawa and coworkers.[165] The total reflecting plane was immersed in 40% NH_4F solution for 3 min to terminate the Si surface with hydrogen. Deposition of Au was done at 60°C by adding a mixture of plating solution and 2% HF onto the hydrogen terminated Si surface. The composition of the plating solution was 0.015 M $NaAuCl_4.2H_2O$ + 0.15 M Na_2SO_3 + 0.05 M $Na_2S_2O_3.5H_2O$ + 0.05 M NH_4Cl.

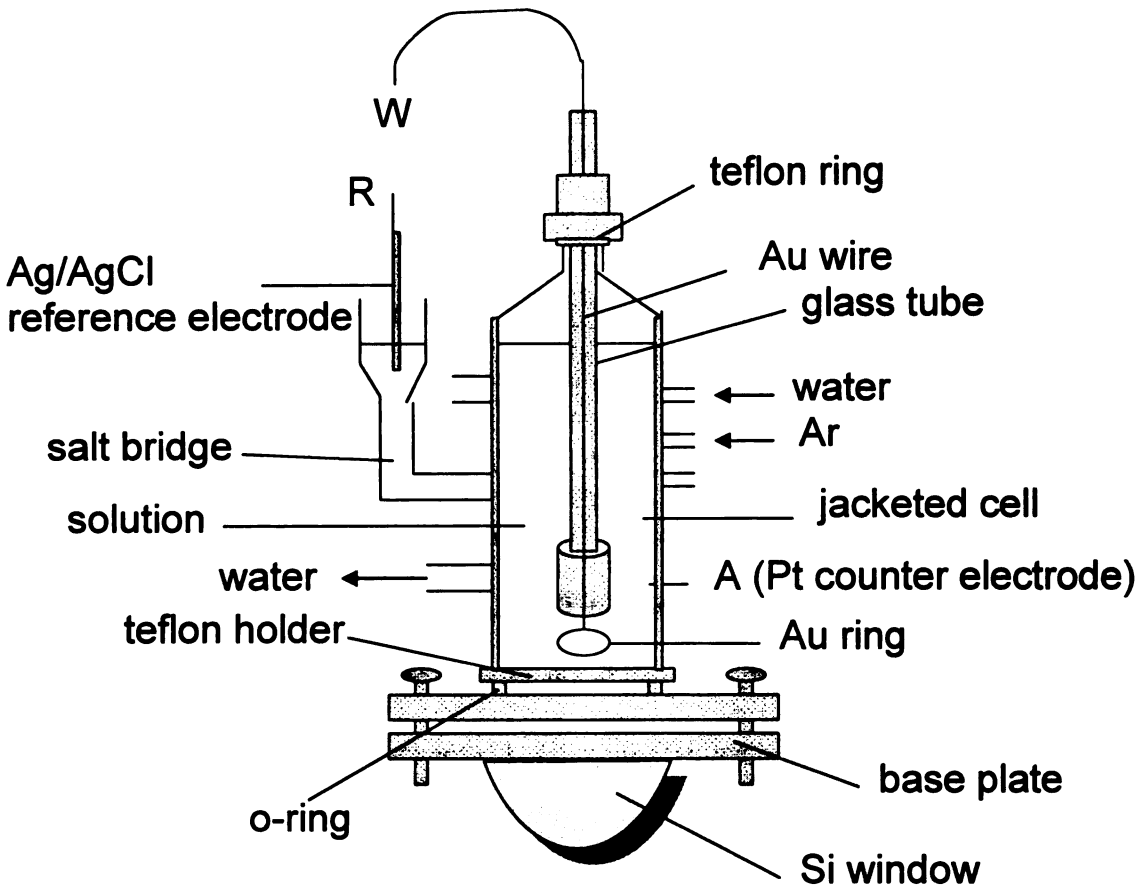

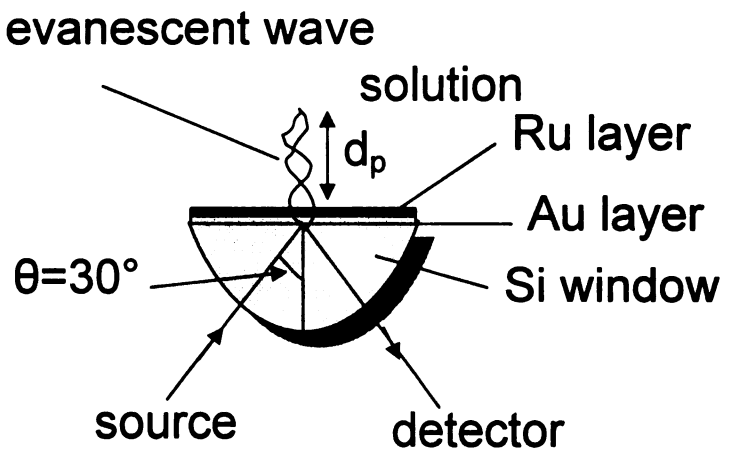

Figure 6.3: Schematic diagram of the cell used in the *in-situ* ATR-FTIR studies of the ECH of lactic acid

The thickness of the Au deposit can be controlled by varying the deposition time. The purpose of HF is to reduce the metal complex i.e. Au^{3+} to Au^0. The reaction for Au deposition is shown below.

$Si^0(s) + 6F^-(aq) \rightarrow SiF_6^{2-}(aq) + 4e^-$

$AuCl_4^-(aq) + 3e^- \rightarrow Au^0(s) + 4Cl^-(aq)$

6.3.3 Deposition of Ru

Once theAu film was formed, the window was rinsed with milli-Q water and then immersed in a solution of 1 mM $RuCl_3.xH_2O$ in order to deposit an adlayer of Ru^{3+} on the Au surface. Prior to the ECH experiments, the electroreduction of Ru^{3+} to Ru^0 was carried out in the spectroelectrochemical cell by applying a potential of 0.0 mV (vs. Ag/AgCl).

6.3.4 Experimental setup

After the cell was assembled, the water circulator was turned on. Once the temperature was stabilized at 30°C, about 19 mL of water was added to the cell and an IR spectrum was recorded. Then the required amount of electrolyte was added to the water so that the final electrolyte concentration was about 0.01 M. Argon gas was bubbled through the solution for about 30 min. in order to remove oxygen and other dissolved gases. A constant potential of 0.0 V (vs. Ag/AgCl) was applied for 10 min. to reduce the Ru^{3+} adlayer to metallic Ru. The working electrode was then polarized at -400 mV and an IR spectrum was recorded. Then the required amount of lactic acid solution was added so that the final concentration of lactic acid in the system was 0.01 M and this point marked

the beginning of ECH. The working electrode was maintained at a constant potential of -400 mV and IR spectra were recorded every 8 min. for 20 h.

FTIR spectra were taken with a Nicolet 20SX/C FTIR spectrometer, equipped with a liquid nitrogen cooled linearized narrow band MCT-B detector. The sample compartment was purged using CO_2 and H_2O free air from a Puregas Heatless Dryer. The IR source (Everglow) was focused at the electrode/electrolyte interface by passing it through the Si window. The incident angle was 30° from the surface normal, the beam diameter was 8 mm and the area of the IRE exposed to the solution was 3.14 cm^2. Each spectrum was acquired by integrating 1000 interferograms with a resolution of 4 cm^{-1}, to achieve the required sensitivity. The acquisition time was 8 min. per spectrum. The spectra were referenced against the spectrum of water or the spectrum of the electrolyte alone taken at the same potential under identical conditions. All spectra are shown in absorbance units, defined as $A= -\log (I/I_0)$, where I and I_0 are the intensities of the reflected radiation at the sample and reference solutions respectively.

6.4 Results and Discussion

6.4.1 Optimum concentration of lactic acid

For the IR spectra to be selective to species adsorbed on or close to the surface, the concentration of the lactic acid and electrolytes in solution should be optimum, so that interference from solution species can be minimized. In order to calculate the optimum concentration, the penetration depth, d_p of the IR beam needs to be determined from equation 1. Assuming $\theta= 30°$, $\lambda= 5.88$ μm (1700 cm^{-1}), $n_1= 3.4$ and $n_2= 1.33$, the penetration depth was calculated to be about 800 nm. Assuming the lactic acid molecular

diameter to be 0.5 nm and the molecular cross section to be 0.2 nm^2, the monolayer coverage of lactic acid was calculated to be 5 X 10^{14} molecules/cm^2 or 8.3 X 10^{-10} moles/cm^2. Considering the adsorbed lactic acid to be the only lactic acid present in the cylindrical volume enclosed by the penetration depth, the required solution concentration of lactic acid needs to be approximately 0.01 M. This would ensure that the IR spectra recorded are characteristic only of the adsorbed layer or species present in the electrical double layer.

6.4.2 IR spectra of electrolytes

The IR spectra of the three electrolytes at 0.01 M concentration, recorded at -400 mV are shown in figure 6.4. The IR spectrum of water taken under similar conditions (without the cathodic polarization) was used as reference. In all cases, the bands below 900 cm^{-1} cannot be clearly distinguished due to noise caused by absorption of IR radiation by Si in that region. Using cyclic voltammetry and ATR-SEIRAS studies of CO adsorption and a metal deposition technique similar to that used in this study, Osawa[193] demonstrated the the formation of metal overlayers that are almost pinhole free and having electrochemical and surface properties similar to those of the corresponding bulk metals with apparent surface enhancement factors relative to the smooth metal surfaces, in the range of 20-70. Therefore, the observed spectral features may be attributed to adsorbed species on Ru and adsorption on Au may be assumed to be negligible.

The spectrum of 0.01 M H_2SO_4 consists of bands at 1110 (not shown), 1617 and 3190 cm^{-1}. The 1110cm^{-1} peak is due to the S-O stretching vibration,[183,190] indicating the presence of adsorbed sulfate on the electrode surface. The 1617 and 3190 cm^{-1} peaks are

due to the H-O-H bending and O-H stretching vibrations of adsorbed water molecules. These bands indicate the presence of water molecules co-adsorbed with sulfate ions on the electrode surface. Isolated or non-hydrogen bonded water molecules show O-H stretching frequencies around 3600 cm^{-1}.[184] The shift in the O-H stretch frequency from this value is indicative of the extent of hydrogen bonding. The H-O-H bending frequency of water adsorbed on Ru(001) surface in UHV has been reported to be in the range of 1560-1520 cm^{-1}. [166,167] Therefore, a downward shift of the O-H stretch frequency to 3190 cm^{-1} and an upward shift of the δH-O-H mode to 1617 cm^{-1} is indicative of strongly hydrogen bonded water.[183] A similar phenomenon was observed by Osawa and coworkers in the study of interfacial water molecules on Au electrodes.[168,183] Since sulfate is an effective hydrogen bond acceptor, it is usually co-adsorbed with water molecules on the electrode surface. A δH-O-H frequency of 1617 cm^{-1} is also indicative of interaction of water with the metal surface via an oxygen lone pair orbital.[190] The frequency of this mode is higher in this case compared to that obtained under UHV due to the decrease in the strength of interaction with the metal in the presence of hydrogen bonding.

The spectrum of 0.01 M HCl consists of strong negative bands at 1647 and 3380 cm^{-1}. This indicates displacement of the adsorbed water molecules from the electrode due to chloride adsorption. The spectrum of 0.01 M $HClO_4$ also consists of negative bands at 1600 and 3350 cm^{-1} due to partial displacement of adsorbed water by ClO_4^- ions. These results are consistent with those of Osawa and coworkers,[168] who reported stronger adsorption of chloride anion, compared to perchlorate anion on a Au(111) surface. This was confirmed in their studies by a shift in the peak intensity versus potential profile to

the negative direction on adding 1 mM HCl to 0.5 M $HClO_4$ due to the displacement of perchlorate ions from the electrode surface by chloride ions. Since perchlorate and chloride ions are poor hydrogen bond acceptors, the co-adsorbed ion disrupts the hydrogen bonding between interfacial water molecules and either partially or completely displaces them.[169,170,188] It is believed that in the case of perchlorate ions, the observed IR bands are not due to water adsorbed directly on the electrode surface, but are due to the water molecules present in the hydration shell of the adsorbed perchlorate ions, associated with the anions through electrostatic interactions, thus resulting in non-hydrogen bonded or asymmetrically hydrogen bonded water molecules.[168,189] In our case, we only observe negative bands due to displacement of adsorbed water from the surface. No bands are observed due to non-hydrogen bonded or asymmetrically hydrogen-bonded water molecules. These observations serve as evidence that the IR spectra recorded are mainly due to adsorbed molecules and ions or species present very close to the electrode surface in the electrical double layer and are not due to solution species as in the latter case, the spectra would be dominated by strong water bands even in the presence of electrolytes.

The band at 1110 cm^{-1} due to the Cl-O stretch indicates the adsorption of ClO_4^- on the electrode surface in the C_{3v} or lower configuration, i.e. with only the Cl-O vibration perpendicular to the surface being IR active. There exists some evidence in literature showing that the perchlorate anion adsorbs on the Au(111) electrode surface via three O atoms on a threefold hollow site, due to the symmetry of arrangement of the surface atoms on the Au(111) surface. Sawatari and coworkers[77] studied perchlorate adsorption on Pt(111) surface using IR-RAS and concluded that perchlorate is adsorbed through one

or three O atoms with C_{3v} symmetry. The coordination mode of adsorbed perchlorate may be deduced from the vibrational spectra on the basis of group theory, though the process involves some amount of ambiguity. The free perchlorate ion has T_d symmetry, which makes it IR inactive because there is no change in the overall dipole moment of the ion on vibration of the Cl-O bonds. However, upon adsorption on a surface, the perchlorate anion assumes C_{3v} or C_{2v} or lower symmetry, depending on the orientation, adsorption site and the nature of the surface. Due to the reduction in symmetry, the triply degenerate Cl-O stretching mode splits into two for C_{3v} symmetry and three for C_{2v} or lower symmetry. According to the surface selection rule, in case of the C_{3v} and C_{2v} symmetries, only the mode which gives a dipole change normal to the surface is IR active. Therefore, the presence of a single band at 1110 cm^{-1}, assigned to the symmetric Cl-O stretching mode indicates a C_{2v} or C_{3v} symmetry for the adsorbed perchlorate. However, infrared spectra alone do not enable us to distinguish between the C_{2v} and C_{3v} modes. The Cl-O stretching frequency observed here is very close to that of the symmetric Cl-O stretching modes of perchlorate ions with monodentate or bidentate co-ordination with metal ions (1060-1030 cm^{-1})

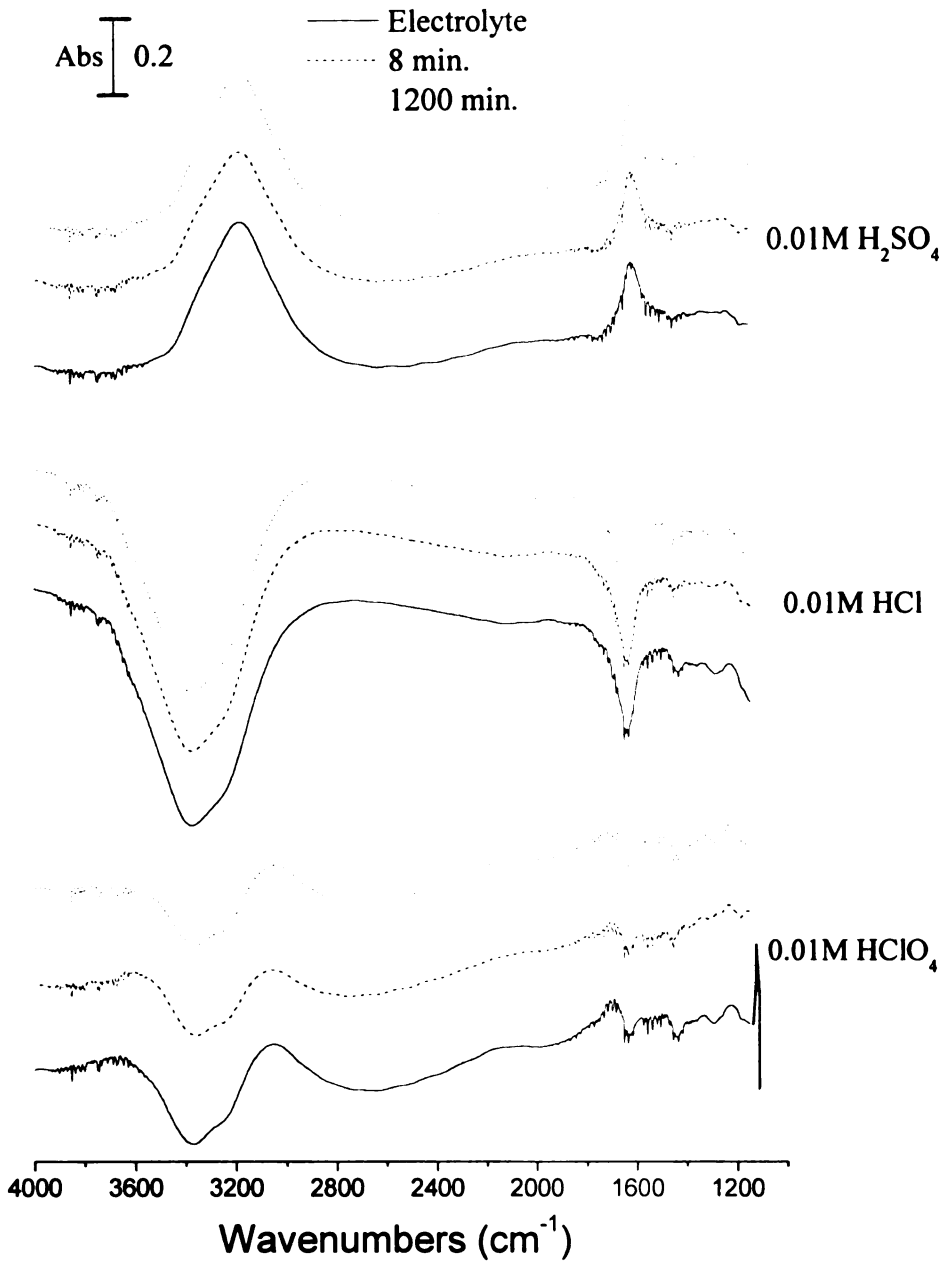

Figure 6.4: ATR-IR spectra of the electrolyte solutions, obtained using the spectrum of water as reference (T= 30°C, E= -400 mV) (solid lines) and ATR-IR spectra taken during the ECH of lactic acid with the water spectrum as the reference (T= 30°C, E= -400 mV) (dotted lines)

The mode of adsorption of water and electrolyte anions as a function of potential have been studied by a number of researchers using spectroscopy[168] and theoretical models.[171-179,187] It is believed that at potentials below the pzc (potential of zero charge) of the metal, water molecules are adsorbed on the surface via an oxygen lone pair and are oriented with the hydrogen atoms closer to the surface than the oxygen atom (mode A in figure 6.5). Around the pzc, the water molecules are oriented flat on the electrode surface and no bands are observed in the IR spectrum due to the surface selection rule (mode B). At potentials above the pzc, the hydrogen atoms of water are oriented towards the solution and are hydrogen bonded with the second water layer, forming an ice-like structure (mode C).[178] This ice-like structure is disrupted at more positive potential due to anion adsorption. The various possible modes of adsorption of water are shown in figure 6.5. By comparison with the IR spectra of adsorbed water at various potentials reported by Osawa,[168] the ice-like structure and parallel orientations may be ruled out. On the basis of similarity in band shapes and the cathodic polarization used, the spectra can be attributed to water molecules adsorbed on the Ru surface through the oxygen atom with the hydrogen atoms oriented towards the surface (mode A).[190,191]

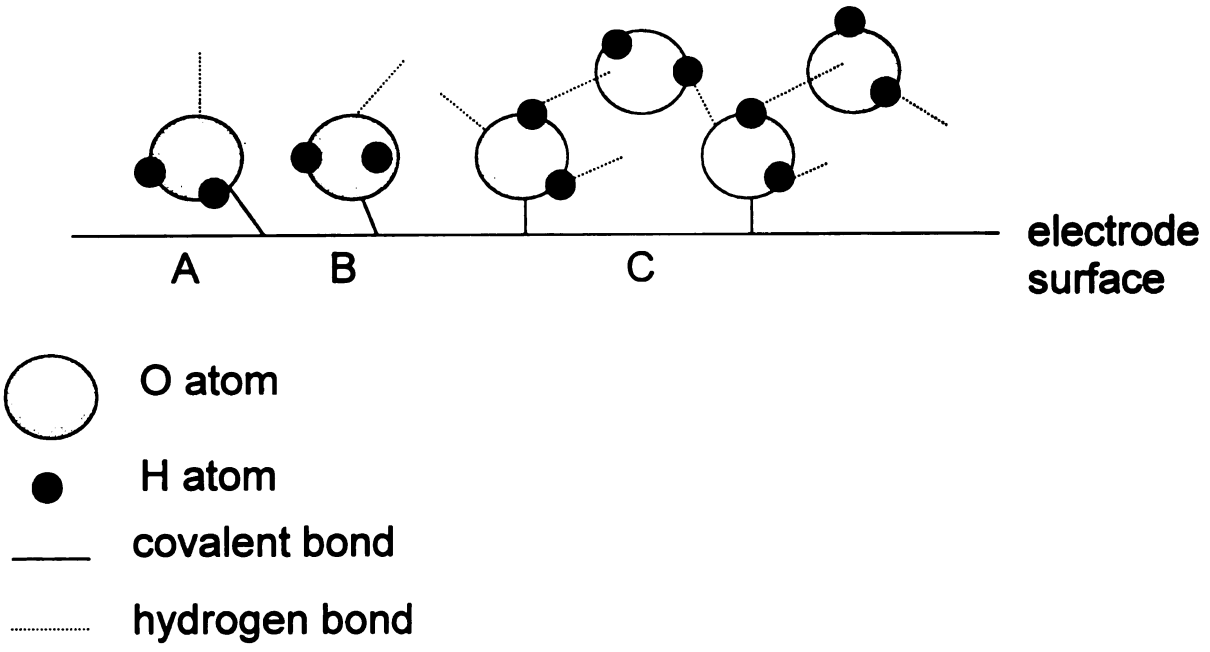

Figure 6.5: Schematic diagram showing different modes of adsorption of water molecules on the electrode surface at various potentials

6.4.3 In-situ FTIR study of the ECH of lactic acid

6.4.3.1 ECH of lactic acid in 0.01 M H_2SO_4

The infrared spectra of lactic acid solutions recorded at various times at 30°C and -400 mV are shown in figure 6.6. The spectrum below 1200 cm^{-1} is not shown due to strong absorption by Si in the range of 1150 to 1100 cm^{-1}.

In order to obtain useful information from infrared spectra, a suitable reference spectrum should be chosen. In many cases, particularly in *in situ* FTIR studies of methanol electrooxidation, the reference spectrum is the one taken at a high positive potential where most of the surface bound species (CH_3OH, CO and intermediates) are completely oxidized to gaseous CO_2. In case of ECH of lactic acid, the organic acid is known to adsorb strongly on the electrode surface and is very stable to oxidation. Therefore, the

reference spectrum cannot be taken in the presence of lactic acid, as this would not allow us to distinguish features from surface bound lactic acid and the changes over time. Therefore, all spectra were referenced against the spectra of the respective electrolyte solutions taken under identical conditions, unless otherwise mentioned.

The initial spectrum taken immediately after addition of lactic acid to the electrolyte shows bands at 3610, 1630, 1435, 1357 and 1283 cm^{-1} and a negative band at 3168 cm^{-1}. The weak band at 1712 cm^{-1} has been assigned to the doubly degenerate H-O-H bending mode of adsorbed H_3O^+ ions.[180-183,190] The O-H stretching bands of H_3O^+ are obscured by the O-H bands of water. Osawa and coworkers observed a similar peak in their study of interfacial water at various potentials.[168] On the basis of this 1712 cm^{-1} band and the absence of the band due to the symmetric H-O-H bending mode, a structure for adsorbed H_3O^+ was proposed in which the C_{3v} axis is nearly parallel to the surface, as shown in figure 6.7. Since at potentials below the pzc, water molecules are adsorbed with the oxygen lone pair directed towards the solution, the hydronium ion with this orientation is readily formed by addition of a proton to the oxygen lone pair without disturbing the orientation of the other two H atoms.

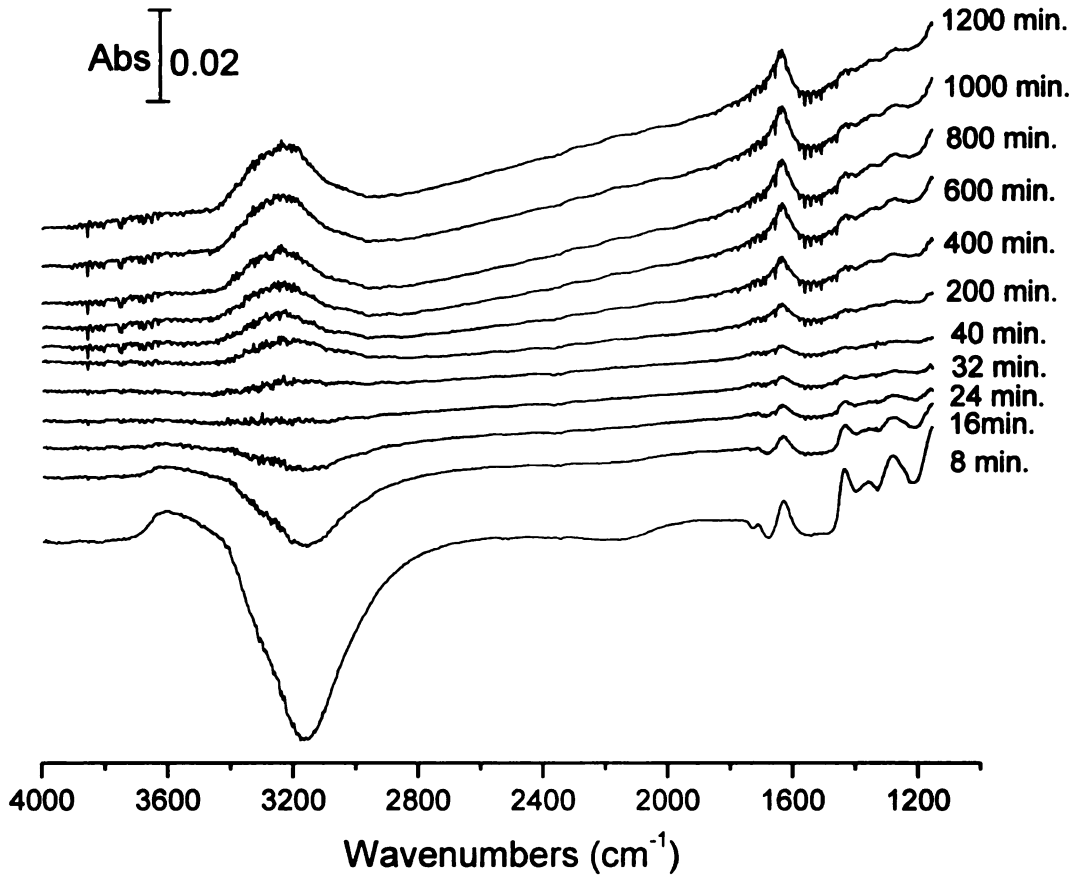

Figure 6.6: Real time ATR-IR spectra of the ECH of lactic acid in 0.01 M H_2SO_4 (T=30°C, E= -400 mV) using the spectrum of 0.01 M H_2SO_4 taken under identical conditions as the reference

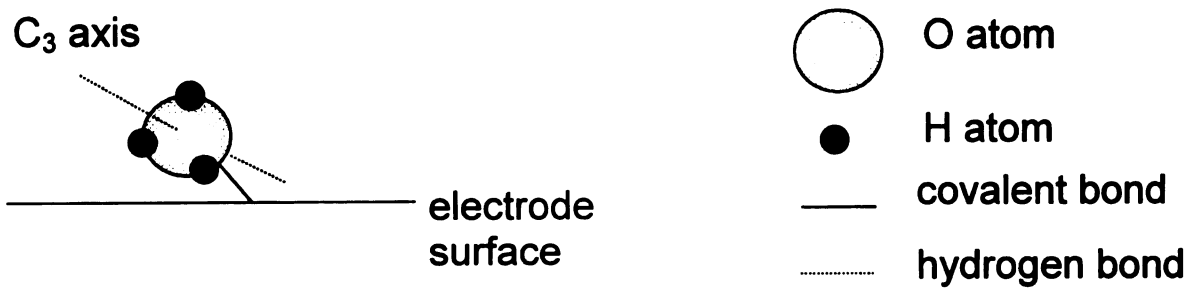

Figure 6.7: Schematic diagram showing the mode of adsorption of hydronium ion on the electrode surface

The 1283, 1357 and 1435 cm^{-1} bands are due to the alcoholic C-O stretch, O-H deformation and the carboxylate symmetric stretch respectively.[185] The spectra clearly show strong bands due to the COO symmetric stretch and the alcoholic C-O stretch, indicating that lactic acid is adsorbed on Ru in the chelating bidentate mode. Therefore, the α-hydroxy group is not involved in bonding to the metal catalyst. Shown in figure 6.8. are some possible modes of adsorption of lactic acid on the Ru surface. The monodentate and the dissociative adsorption modes may be ruled out as these modes would result in much stronger C=O stretching bands. The weak band observed around 1710 cm^{-1} may be attributed to the C=O stretch of solution phase lactic acid.

The spectra show strong symmetric stretching (1435 cm^{-1}) and weak asymmetric stretching bands. These observations can be explained by the surface selection rule and strongly support the chelating bidentate mode of adsorption and the fact that spectra show predominantly adsorbed lactic acid species, as SEIRAS is sensitive to surface species and less sensitive to solution species. The transition dipole of the symmetric COO vibration is parallel to the diagonal of the carboxylate group and when lactic acid is co-ordinated to the metal surface through the carboxylate group, has a strong component in the direction

normal to the surface as shown in figure 6.9, which explains the high intensity of this band. In contrast, the direction of the transition dipole of the COO asymmetric stretch is along the line joining the two oxygen atoms, which in the adsorbed molecule is parallel to the surface and hence this vibration is IR inactive. The O-H deformation mode also gives a weak band at 1357 cm^{-1} due to this bond being parallel to the surface when lactic acid is adsorbed in the chelating bidentate orientation.

The negative band at 3168 cm^{-1} indicates the displacement of strongly hydrogen bonded water molecules from the surface by lactic acid. However, the bands at 1630 and 3610 cm^{-1} are due to the H-O-H bending and O-H stretching vibrations of non-hydrogen bonded water molecules. Therefore, it can be concluded that the adsorption of lactic acid on the electrode surface is associated with the presence of relatively more isolated water molecules on the surface. The O-H stretching vibrations of lactic acid cannot be distinguished from those of water and this band is believed to overlap with the 3610 cm^{-1} peak from water. The close-packed monolayer of lactic acid adsorbed on Ru through the carboxylate groups is also expected to have –O-H groups, which are isolated from one-another and from water molecules in the vicinity, forming very few hydrogen bonds, thus giving the high frequency band around 3610 cm^{-1}.

As the reaction progresses, several changes are observed in the spectra. The peak at 3168 cm^{-1} due to the O-H stretching vibration of strongly hydrogen bonded water reappears and the peaks at 1435, 1357 and 1283 cm^{-1} from adsorbed lactic acid decrease in intensity. This indicates that as the reaction progresses, the Ru surface is poisoned and this results in the decrease in the adsorption of lactic acid. The poison may be associated with sulfate or S containing species derived from the sulfate ions of the electrolyte, as the

decrease in adsorption of lactic acid is associated with the appearance of strongly hydrogen bonded water near the electrode surface, which has been shown to be associated with the hydrophilic sulfate anions. This explains the lower rate of ECH of lactic acid in H_2SO_4 compared to HCl and $HClO_4$.

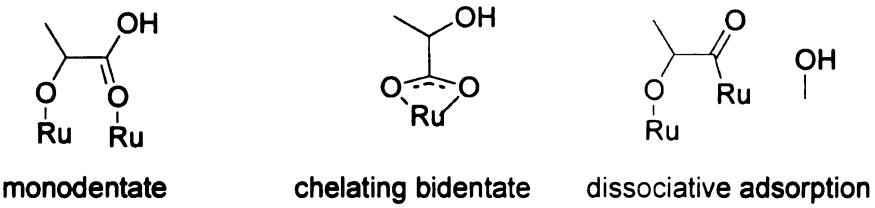

Figure 6.8: Possible modes of adsorption of lactic acid on a metal surface

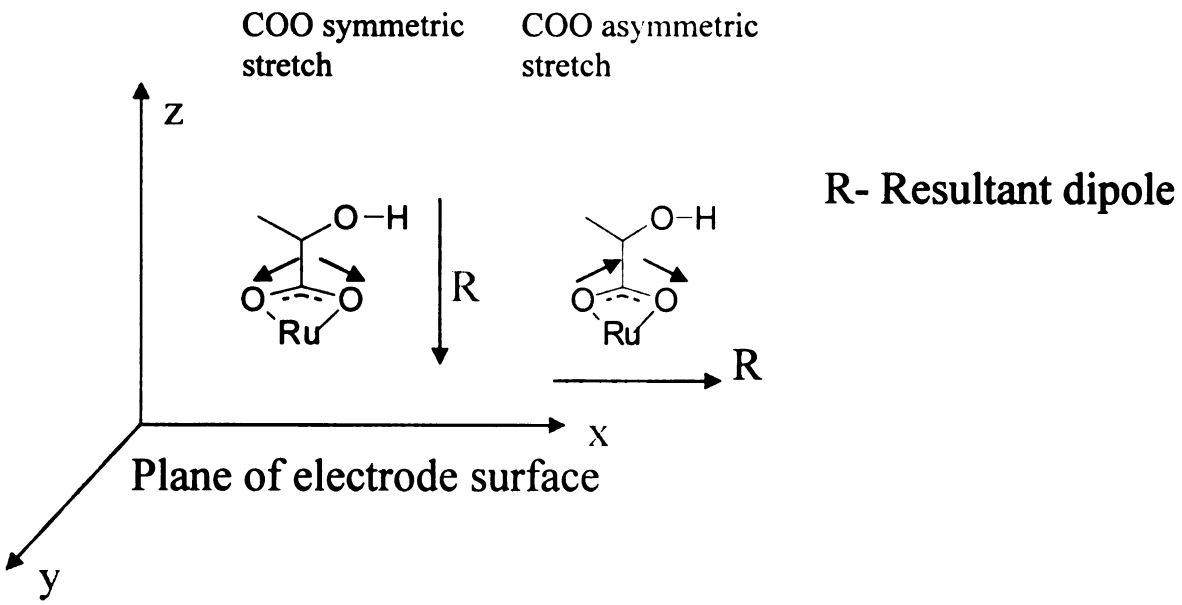

Figure 6.9: Symmetric and asymmetric stretching modes of the carboxylate group and their resultant transition dipoles

6.4.3.2 ECH of lactic acid in 0.01 M HCl

The infrared spectra of lactic acid recorded at various times at 30°C and -400 mV are shown in figure 6.10. The bands due to lactic acid are similar in position and intensity to those observed with H_2SO_4. The initial spectrum taken immediately after addition of lactic acid to the electrolyte shows bands at 1435, 1357 and 1283 cm^{-1}. The weak band at 1712 cm^{-1} has been assigned to the doubly degenerate H-O-H bending mode of adsorbed hydronium (H_3O^+) ions. The 1283, 1357 and 1435 cm^{-1} bands are due to the alcoholic C-O stretch, O-H deformation and the carboxylate symmetric stretch respectively. The presence of strong bands due to the COO symmetric stretch and the alcoholic C-O stretch and a weak band due to O-H deformation indicate that lactic acid is adsorbed on Ru in the chelating bidentate mode.

The O-H stretching bands from water and lactic acid and H-O-H bending bands from water appear at 3120 and 1595 cm^{-1} respectively. Therefore, the lactic acid may be associated with strongly hydrogen-bonded water. However, in this case there is no decrease in intensity with time of bands due to lactic acid. Therefore, the Ru surface is apparently not poisoned by electrolyte anions in this case.

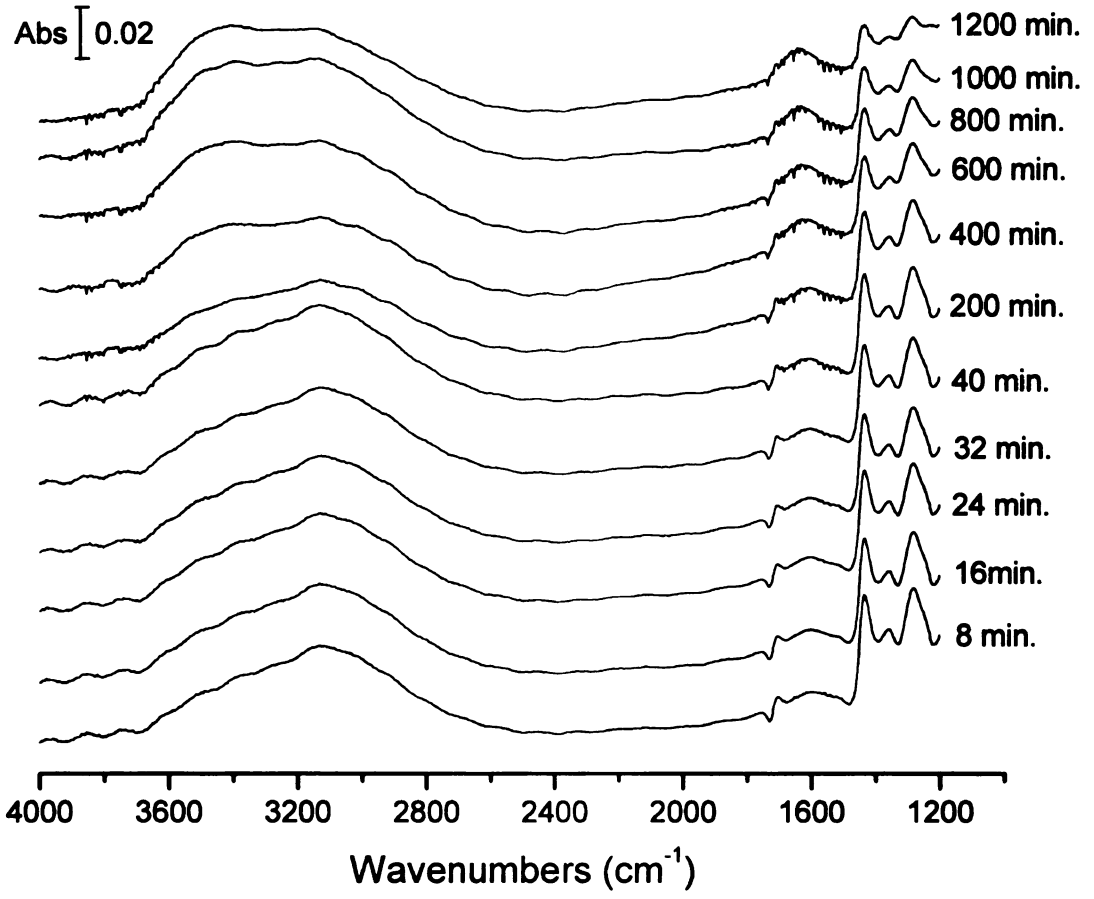

Figure 6.10: Real time ATR-IR spectra of the ECH of lactic acid in 0.01 M HCl (T=30°C, E= -400 mV) using the spectrum of 0.01 M HCl taken under identical conditions as the reference

Figure 6.4 shows IR spectra taken during the ECH of lactic acid using the water spectrum as the reference. Therefore, the spectra are characteristic of both lactic acid and electrolytes. It can be seen that the spectra are dominated by peaks associated with electrolytes, indicating strong adsorption of electrolyte even in the presence of lactic acid. However, in the case of 0.01 M HCl, a comparison of the relative intensities of the negative going water bands at the beginning and end of the reaction indicates a slight

decrease in the intensity of the bands probably associated with desorption of some amount of chloride from the surface, followed by re-adsorption of water molecules, as a result of a decrease in the solution concentration of chloride as Cl_2 is evolved at the anode.

It is also interesting to note the appearance of new bands at 3400 and 1647 cm^{-1} at around 200 min, associated with O-H stretching and H-O-H bending vibrations of water in figure 6.9. The appearance of these bands corresponds approximately to the increase in the rate of ECH of lactic acid after an initial slower phase, observed while using HCl as the electrolyte with 5% Ru/C agglomerated in RVC. This suggests that the partial desorption of chloride frees up sites allowing the adsorption of water molecules, which are required for ECH. From the frequencies of the water bands, they appear to be relatively isolated or poorly hydrogen bonded, which may be a result of association with the Ru surface and the hydrophobic nature of the co-adsorbed chloride. These observations are consistent with the conclusion that adsorbed water plays an important role in lactic acid hydrogenation, derived from the experiments indicating a decrease in the rate of hydrogenation of lactic acid in organic solvent/water mixtures[27]. From *ab initio* studies of the water layer on Pt(111) and Rh(111) surfaces, Vassilev and coworkers[186] discovered that water molecules adsorbed on a metal surface possess a small metal-like conductivity resulting from the mixing of local states of the oxygen atom with the electron bands of the metal substrate. The extent of mixing of the atomic states from oxygen and metal was found to depend on the orientation of the water molecules, the distance from the surface and the polarization of the surface. The analysis of the electronic states indicated an electron charge transfer from the water molecules towards the surface, resulting in a

reduction of the work function of the system. This phenomenon may be responsible for facilitating the electron transfer to protons or H_3O^+ to form H atoms, which are required for ECH. In the case of H_2SO_4 and HCl electrolytes, a weak feature due to H_3O^+ was observed in the IR spectra. However, the peak corresponding to the M-H bond, known to appear around 2100cm^{-1} [163,164] was not observed in any of the spectra, indicating that either the surface concentration of adsorbed H is too low to be detected by IR or it is a very short-lived species, with lifetime much shorter than the timescale of the scans. The cyclic voltammetry results described in chapter 4 indicate that adsorbed Cl on the electrode surface when HCl is used as the electrolyte is favorable for H adsorption. Therefore, the enhancement of the ECH rate in HCl is probably a result of the electronic effects of both adsorbed chloride and water. The specific sites occupied by the water molecules and the exact configuration required for involvement in the hydrogenation rate enhancement is not yet clear.

6.4.3.3 ECH of lactic acid in 0.01 M $HClO_4$

The infrared spectra of lactic acid recorded at various times at 30°C and -400 mV are shown in figure 6.11. The bands due to lactic acid are similar in position and intensity to those observed with H_2SO_4 and HCl. The initial spectrum taken immediately after addition of lactic acid to the electrolyte shows bands at 1435, 1340 and 1275 cm^{-1}. The 1275, 1340 and 1435 cm^{-1} bands can be assigned to the alcoholic C-O stretch, O-H deformation and the carboxylate symmetric stretch respectively. The presence of strong bands due to the COO symmetric stretch and the alcoholic C-O stretch and a weak band

due to O-H deformation indicate that lactic acid is adsorbed on Ru in the chelating bidentate mode.

The O-H stretching bands from water and lactic acid and H-O-H bending bands from water appear at 3400 and 1625 cm^{-1} respectively. There is a slight decrease in the intensity of the lactic acid bands with time at 1000 min., indicating poisoning of the surface by perchlorate or chloride, but the decrease in intensity is not as pronounced as in the case of H_2SO_4 and occurs at much longer time compared to the H_2SO_4 case.

Since in all the three electrolytes, lactic acid was found to adsorb on the Ru surface in the chelating bidentate mode without involving the α-hydroxy groups, it can be concluded that the α-hydroxy group does not facilitate the hydrogenation of lactic acid (and other α-hydroxy acids) by forming a more stable adsorbed intermediate or by influencing the initial adsorption of lactic acid, but it may indirectly increase the hydrogenation rate by facilitating the adsorption of water on the metal surface through the formation of hydrogen bonds. This might be expected from the fact that in the chelating bidentate mode, the lactic acid is adsorbed with the –O-H groups exposed to the solution.

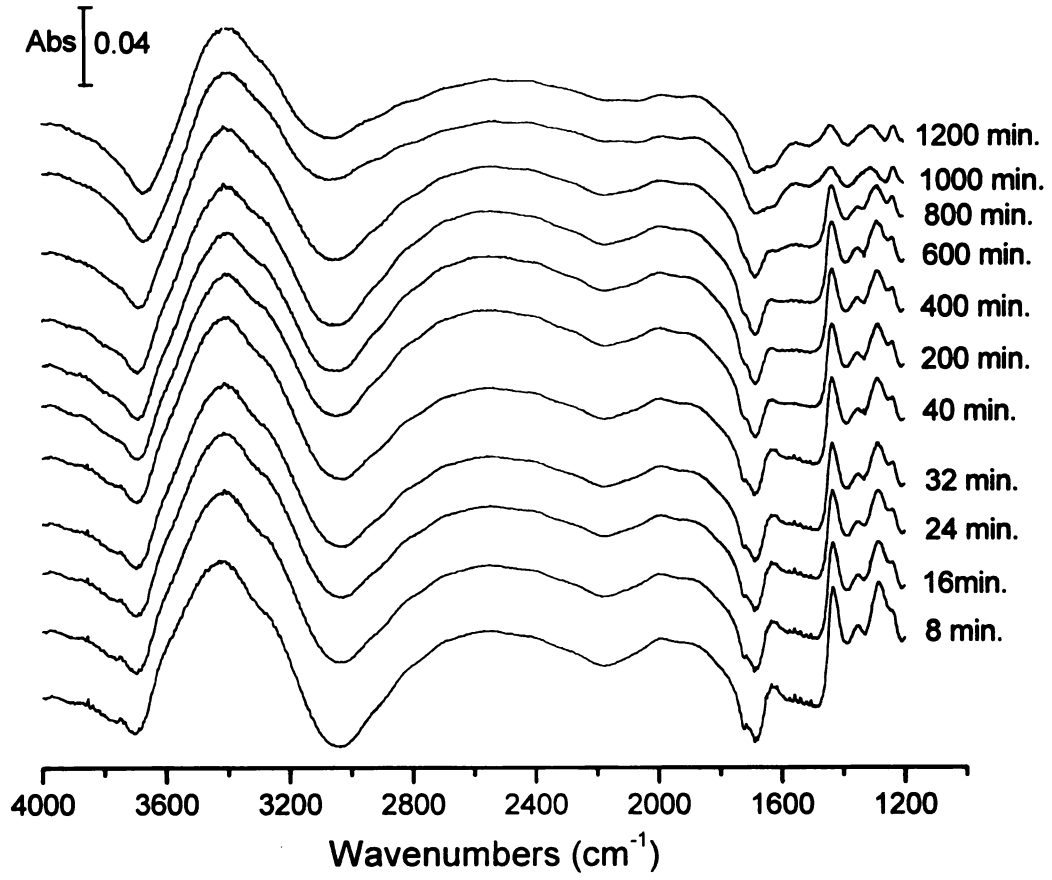

Figure 6.11: Real time ATR-IR spectra of the ECH of lactic acid in 0.01 M $HClO_4$ (T=30°C, E= -400 mV) using the spectrum of 0.01 M $HClO_4$ taken under identical conditions as the reference

6.5 Conclusions

The ECH of lactic acid on a Ru electrode surface has been studied in real time using ATR-FTIR spectroscopy. The conditions used for the FTIR studies were close to the ones used for bulk ECH studies, so the spectra can be correlated with changes occurring on or near the electrode surface during the course of the experiment. The optimum

concentration of lactic acid was calculated to obtain maximum surface selectivity. From the spectra, the ATR technique was found to be very sensitive to species adsorbed on the surface or present within the electrical double layer. The *in-situ* infrared spectra of lactic acid were obtained in three electrolytes- H_2SO_4, HCl and $HClO_4$. Background subtraction and analysis of the spectra allowed us to detect an electrode surface poisoning effect, probably due to species derived from sulfate and perchlorate anions associated with the electrolyte, which blocks lactic acid adsorption. The difference in the rate of ECH observed in the three electrolytes can be correlated with the extent of surface poisoning by the electrolyte anions or species derived from them. It was also found that lactic acid adsorbs on Ru through the chelating bidentate mode without involving the α-OH group. Therefore, the α-hydroxy group does not facilitate the hydrogenation of lactic acid (and other α-hydroxy acids) by forming a more stable adsorbed intermediate or by influencing the initial adsorption of lactic acid, but it may indirectly increase the hydrogenation rate by facilitating the adsorption of water on the metal surface through the formation of hydrogen bonds.

It was also determined that chloride does not block adsorption of lactic acid, and the enhancement of the ECH rate in HCl may be due to partial desorption of chloride from the electrode surface at longer times and subsequent adsorption of water molecules, which play an important role in ECH.

CHAPTER 7

CONCLUSIONS AND FUTURE WORK

7.1 Conclusions

Electrocatalytic hydrogenation provides a greener, milder and more convenient alternative to the chemical catalytic hydrogenation of lactic acid, which requires 150°C and 1200 psi H_2 gas, mainly due to the poor solubility of hydrogen gas in water. In ECH, the hydrogen required for hydrogenation is produced close to the reaction site on the catalyst surface, thus eliminating the kinetic barrier to the dissolution and splitting of H_2. As a practical matter, ECH eliminates the requirement for external supply of hydrogen, thus improving safety. The milder conditions and easy controllability of the ECH method may also improve stereoselectivity of the reduction. Finally, it is amenable to *in-situ* vibrational spectroscopic studies, which give structural information about adsorbed intermediates and enable us to probe into mechanistic details.

In this study, the ECH of various α-functionalized carboxylic acids has been attempted and optimized. To the best of our knowledge, this is the first study of the ECH of carboxylic acids. Initial studies using the model compound benzoyl formic acid showed that the ECH reaction is dependent more on the availability of surface sites, rather than the rate of mass transport, consistent with the results obtained with the chemical catalytic hydrogenation of lactic acid. ECH of lactic acid using electrodeposited Ru on carbon felt, though giving a poor yield of product, enabled the determination of kinetic parameters, such as order of reaction, fractional surface coverages of lactic acid and hydrogen, rate constants, adsorption constants and activation energy using the Langmuir-Hinshelwood

model. The apparent activation energy determined to be 76.0 $kJmol^{-1}$ is approximately half the value of 138 $kJmol^{-1}$, determined for the batch hydrogenation of lactic acid. ECH of lactic acid using 5% Ru/C agglomerated in RVC resulted in much higher conversion. The effects of various parameters such as temperature, ECH current and nature of electrolyte on the yields and distribution of products were studied. In all cases, lactaldehyde was obtained as a major product with small quantities of propylene glycol obtained only with 5% Ru/C/RVC. This unexpected result is attributed to the existence of lactaldehyde mostly in the hydrated form under the mild conditions used. Dehydration of the hydrated lactaldehyde and subsequent hydrogenation to propylene glycol is presumably slower than desorption into solution. The formation of propylene glycol is also favored by higher surface concentration of H. In the chemical catalytic hydrogenation of lactic acid, lactaldehyde was proposed to be an intermediate, but was never isolated. The formation of lactaldehyde as the major product of ECH supports its proposed intermediacy en route to propylene glycol. Although this project was begun as a way to carry out lactic acid to propylene glycol reduction under mild conditions, the discovery of a pathway that directly reduces an aqueous carboxylic acid to an aldehyde and then stops is substantially more interesting, in terms of both fundamental chemistry and practical process. This unexpected process can provide a clean, convenient and efficient method to prepare lactaldehyde, a compound that is not commercially available and that is difficult to obtain in pure form.

ECH of lactic acid is also influenced by the nature of the electrolyte used, indicating significant anion adsorption and modification of the electrode surface under the conditions used. The most intriguing finding is the much higher enhancement of the rate

of ECH in HCl, as compared to H_2SO_4 and $HClO_4$, especially during the later stages of the reaction. From control experiments in the absence of electrolyte and from the *in situ* ATR-IR studies, this has been attributed to the desorption of Cl from the electrode surface at longer times due to Cl_2 evolution at the anode, thus leaving sites for the adsorption of relevant species such as water molecules, which are required for hydrogenation. The chloride ions partially covering the Ru surface may also have an electronic effect that favors adsorption of lactic acid and hydrogen. The fact that the product ratio of ECH depends on the electrolyte used is also intriguing and can be exploited in future applications to control the selectivity of the reaction towards specific products by using specific electrolytes or a combination of different electrolytes.

Using *in-situ* FTIR, the initial mode of adsorption of lactic acid on the electrode surface was determined to be chelating bidentate, without involving the α-OH group. Therefore, the α-hydroxy group does not facilitate the hydrogenation of lactic acid (and other α-hydroxy acids) by forming a more stable adsorbed intermediate or by influencing the initial adsorption of lactic acid, but it may indirectly increase the hydrogenation rate by facilitating the adsorption of water on the metal surface through the formation of hydrogen bonds. The study of the ECH of lactic acid using RVC cathode and Ru dispersed on non-carbon supports shows that the chemical nature and porosity of the support and the characteristics of the Ru particles deposited on the support play an important role in determining the rate and product distribution in ECH.

This work is a step towards ultimately using electrocatalytic hydrogenation as a convenient laboratory process and possibly a commercial process for the conversion of lactic acid to value added chemicals. It demonstrates the feasibility of the process at the

laboratory scale and the feasibility of using *in-situ* spectroelectrochemical studies for understanding the mechanism. This will lead to the development of more efficient catalysts in the future. Lactic acid is an important feedstock due to its ready availability from the fermentation of biomass and therefore, its conversion to value-added chemicals using various catalytic processes is being extensively studied. Though electrocatalytic reactions are not widely used in commercial processes due to the difficulty involved in scaling up, it is a viable alternative that may be used in medium scale conversions, where a high product selectivity is desired.

7.2 Suggestions for future work

In this work, the ECH of lactic acid has been achieved under mild conditions of temperature and pressure compared to the chemical catalytic method. However, much more work needs to be carried out in order to improve the process both with respect to application and fundamental understanding. From the calculations reported in chapter 4, it was seen that the current efficiency of the process is too low for practical applications, and this can be attributed to the slow kinetics of the ECH reaction. In the 5% Ru/C RVC system, the amount of active electrocatalyst at any given time is very low as the technique relies on efficient agglomeration of the catalyst, which is affected by various factors such as particle size, fluid dynamics, etc. The kinetics can be improved by developing better electrode materials based on Ru and C, which will consist of well-dispersed Ru nanoparticles on a solid phase carbon of similar porosity.

The process needs to be improved to achieve higher yields of propylene glycol, which is the desired product. The exact conditions which favor the formation of propylene glycol,

both in terms of reaction conditions and electrode microenvironment need to be determined. Toward this aim, in-situ Raman spectroelectrochemistry using single crystal Ru electrodes appears to be the technique of choice. From initial studies on Raman spectroscopy, it was found that lactic acid does give reasonably strong Raman signals in aqueous solution, which are slightly attenuated on Ru. Raman spectroscopy is desirable for the study of electrode reactions in aqueous phase for several reasons. Water, being a poor Raman scatterer does not give strong signals and hence offers minimum interference. Also Raman spectroscopy is very useful for obtaining information in the lower frequency region (400-900cm^{-1}), which could not be studied with infrared spectroscopy, due to strong absorption by the Si window in this region. The bands in this region will provide more detailed information about the modes of adsorption of electrolyte anions and the presence of M-O or M-C bonds, giving further insight into the manner in which anion adsorption affects lactic acid and hydrogen adsorption and the ECH reaction. Spectroelectrochemistry experiments with single crystal Ru electrodes should afford more information about the specific sites on which the various reactants (lactic acid, hydrogen and water) and intermediates adsorb and would enable us finally to propose a reaction mechanism for lactic acid hydrogenation involving surface bound intermediates. The use of single crystal electrodes is expected to simplify the spectra considerably, compared to polycrystalline electrodes, thus making spectral interpretation easier.

Though this study deals mainly with the ECH of lactic acid, the process has been extended to other α-functionalized carboxylic acids, which are essentially analogs of lactic acid, namely, glycolic acid, glyceric acid and alanine. Since this process was found

to give the aldehyde as the major product, it would be interesting and useful to extend the ECH method to other water soluble unsubstituted organic acids such as propanoic acid and isobutyric acid to produce the corresponding aldehydes, which have commercial value and are more difficult to obtain from other sources. However, attempts at ECH of these substrates have been unsuccessful with no conversion achieved to date. One reason for this may be that the adsorption of electrolyte anions makes the electrode surface hydrophilic, thus inhibiting the adsorption of the organic acid, which are rendered hydrophobic by the hydrocarbon chain. This problem may be overcome by including a non-micelle forming cationic surfactant such as didodecyl dimethyl ammonium bromide (DDAB) in the reaction mixture, which would bind to the electrode surface through electrostatic interactions by displacing the anions, and its long hydrocarbon tail would provide a hydrophobic surface which would enhance the adsorption of the organic acid, as shown in figure 7.1. A similar method of enhancing the rate of ECH of hydrophobic substrates such as alkyl phenols using cationic surfactants has been reported by Thomalla.[38,39]

However, in spite of the absence of electrolytes and harsher conditions, the hydrogenation of these acids was found to be slow in the batch process, compared to lactic acid and amino acids. This finding has been attributed to a kinetic effect of the α-hydroxy or amino group, which facilitates adsorption of water molecules essential for hydrogenation. Therefore, even if the substrate adsorption is enhanced, other challenges may have to be overcome to achieve hydrogenation of these substrates.

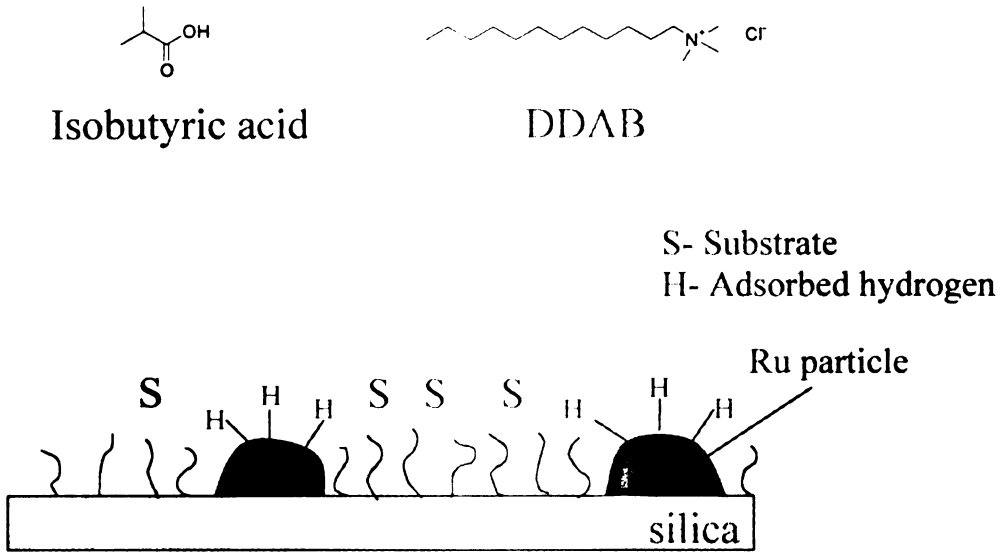

Figure 7.1: Use of a cationic surfactant to modify the electrode surface

APPENDIX

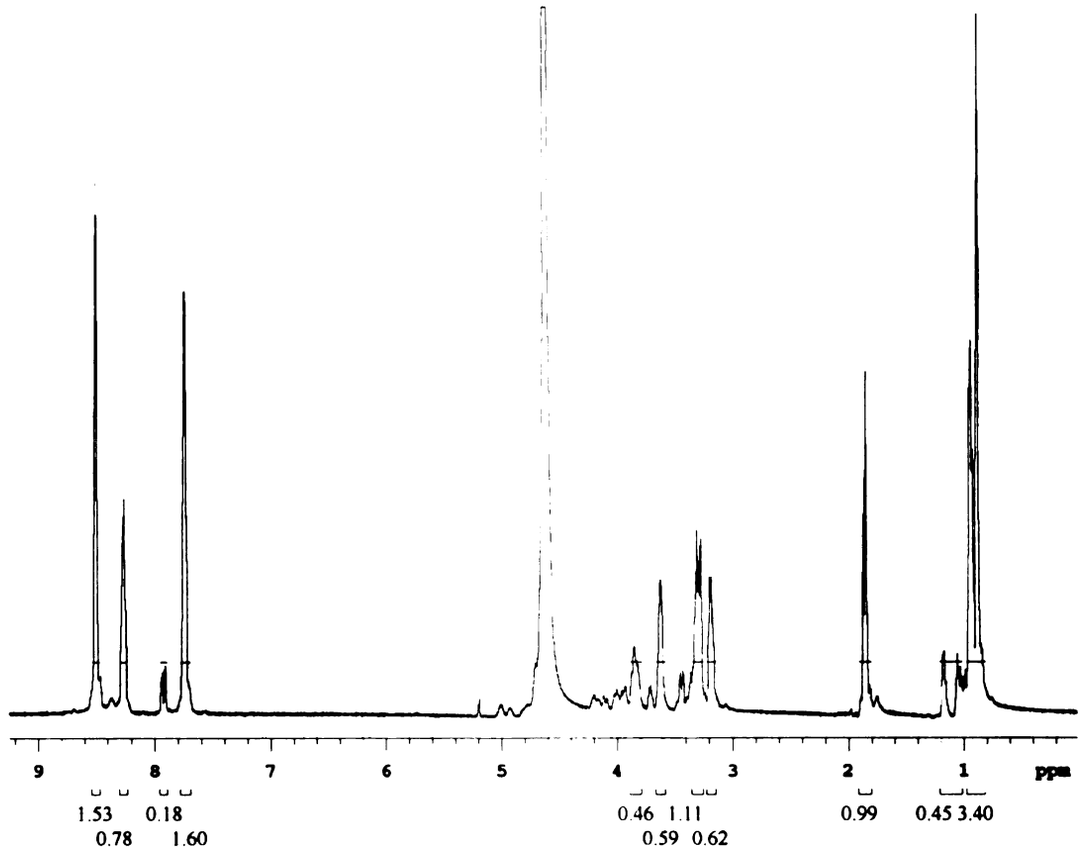

Figure A1: NMR spectrum of the D_2O extract obtained from PCC oxidation of 1,2-propanediol (^1H, D_2O).

Lactaldehyde, pyruvaldehyde and 1,2-propanediol are present in the mixture; δ 0.9 ppm [d, -CH_3 (1,2-propanediol)], δ 1.1 ppm (d, -CH_3 (lactaldehyde)], δ 1.9 ppm [s, -CH_3 (pyruvaldehyde)], δ 3.3 ppm [m, -CHOH (1,2-propanediol)], δ 3.6 ppm [d, -CH_2OH (1,2-propanediol)], δ 3.8 ppm [m, -CHOH (lactaldehyde)], δ 8.0 ppm [d, -CHO (lactaldehyde)], δ 8.3 ppm [s, -CHO, (pyruvaldehyde)], δ 7.7 and 8.5 ppm [d, C_6H_5N-(pyridine)]. Peak splitting is obscured in some cases due to the presence of chromate from PCC.

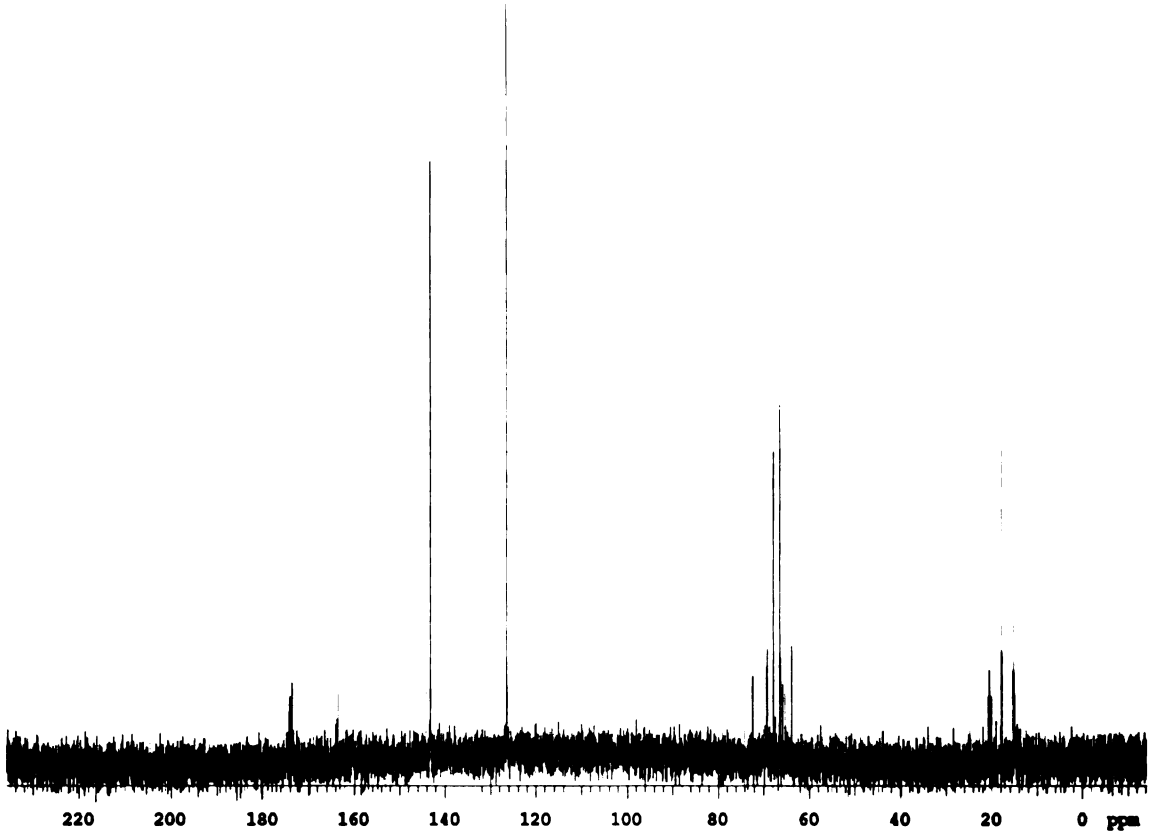

Figure A2: NMR spectrum of the D_2O extract obtained from PCC oxidation of 1,2-propanediol (^{13}C, D_2O).

Lactaldehyde, pyruvaldehyde and 1,2-propanediol are present; δ 19 ppm [-CH_3 (1,2-propanediol)], δ 20 ppm [-CH_3 (lactaldehyde)], δ 66 ppm [-CHOH (1,2-propanediol)], δ 67 ppm [-CH_2OH (1,2-propanediol)], δ 69 ppm [-CH_3 (pyruvaldehyde)], δ 72 ppm [-CHOH (lactaldehyde)], δ 126, 143 and 144 ppm [C_6H_5N- (pyridine)], δ 164 ppm (unknown peak), δ 174 ppm [-CHO (pyruvaldehyde)], δ 175 ppm [-CHO (lactaldehyde)],

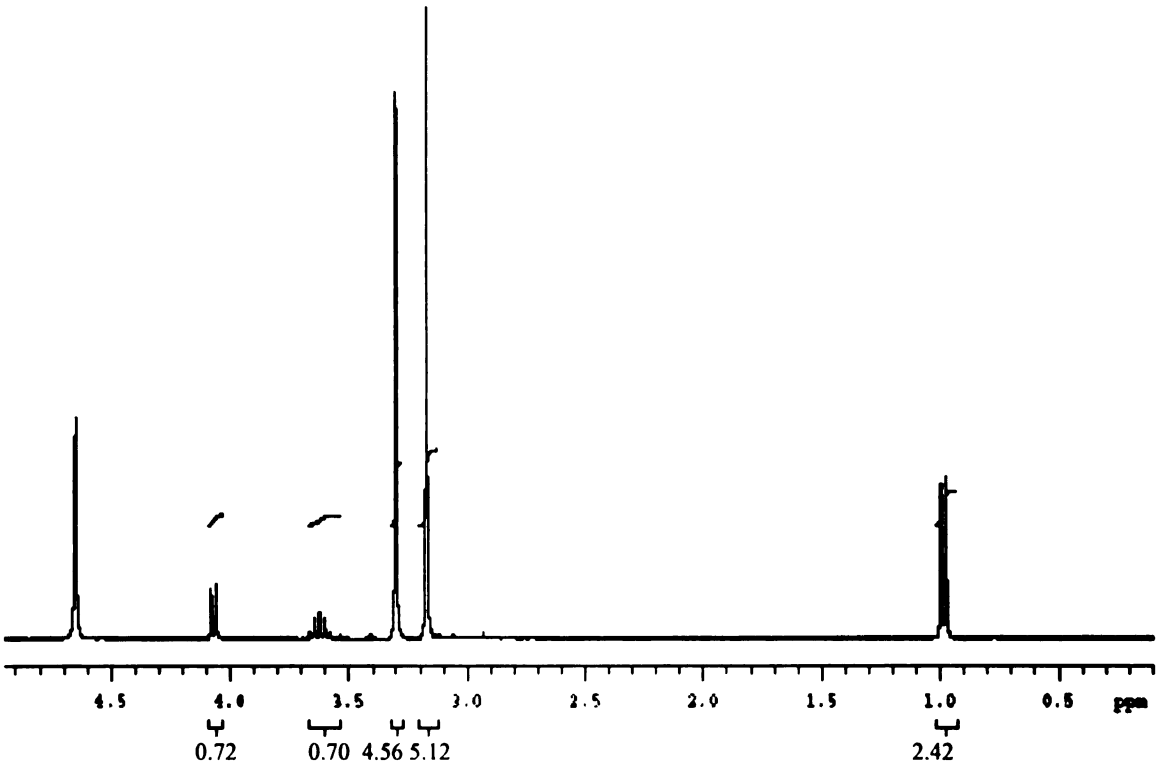

Figure A3: NMR spectrum of lactaldehyde dimethyl acetal (^1H, D_2O)

Peak assignments: δ 1.0 ppm (d, 3H, $-CH_3$), δ 3.2 ppm (s, 3H, $-OCH_3$), δ 3.3 ppm (s, 3H, $-OCH_3$), δ 3.6 ppm (m, 1H, -CHOH), δ 4.1 ppm [d, 1H, $-CH(OCH_3)_2$]

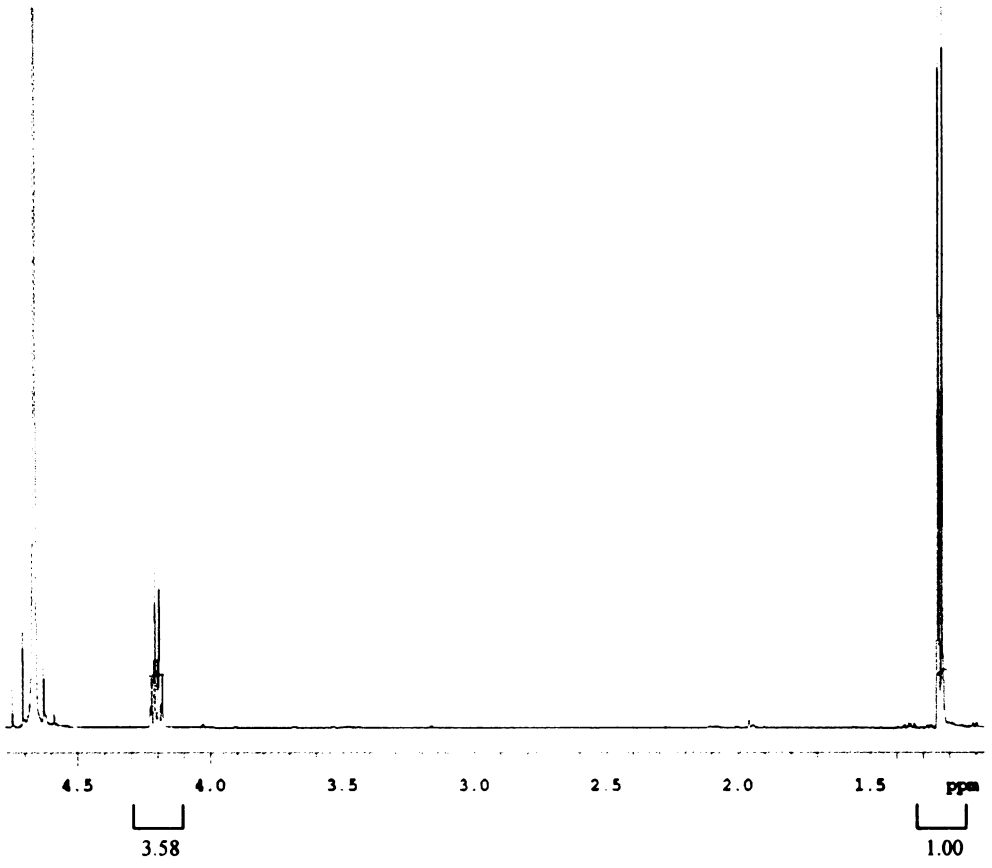

Figure A4: NMR spectrum of lactaldehyde obtained by the hydrolysis of lactaldehyde dimethyl acetal in 0.05 M H_2SO_4 for 2 h (^1H, D_2O)

Peak assignments: δ 1.3 ppm (d, 3H, $-CH_3$), δ 4.25 ppm (q, 1H, -CHOH) (aldehyde peak not visible)

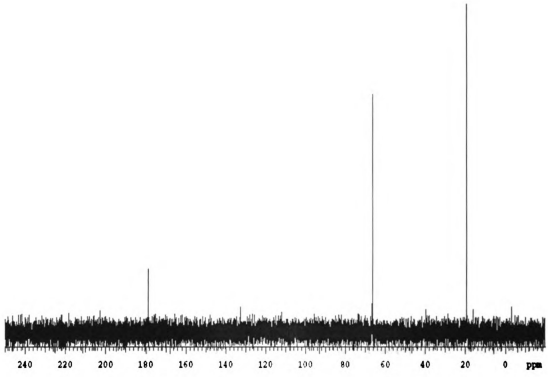

Figure A5: NMR spectrum of lactaldehyde obtained by hydrolysis of lactaldehyde dimethyl acetal in 0.05 M H_2SO_4 for 2 h (^{13}C, D_2O)

Peak assignments: δ 20ppm (-CH_3), δ 66 ppm (-CHOH), δ 179 ppm (-CHO hydrated)

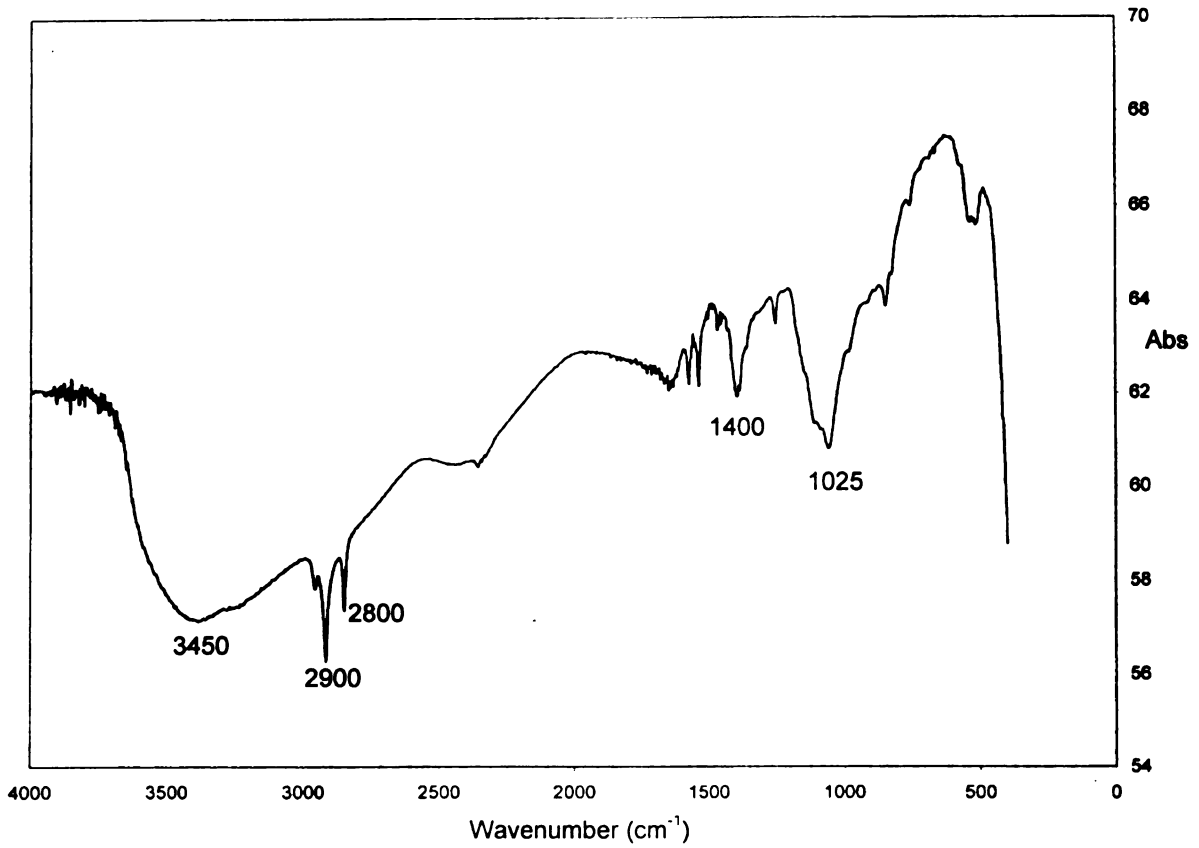

Figure A6: FTIR spectrum of lactaldehyde obtained by hydrolysis of lactaldehyde dimethyl acetal in 0.05 M H_2SO_4 for 2 h (NaCl plate)

Peak assignments: 1025 cm^{-1}: υC-O (alcohol), 1400 cm^{-1}: υC-O (hydrated aldehyde), 2800 and 2900 cm^{-1}: υC-H (sp^3), 3450 cm^{-1}: υO-H

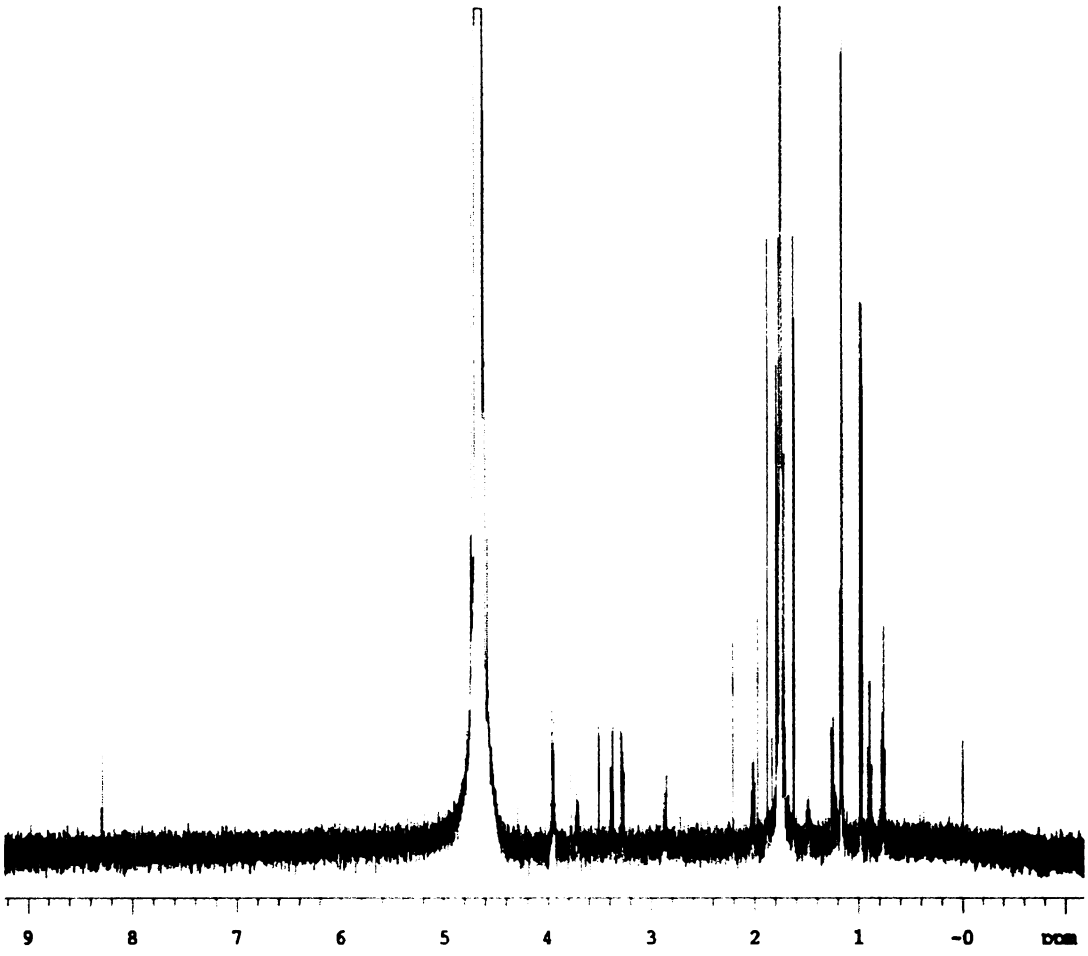

Figure A7: NMR spectrum of product mixture obtained after electrocatalytic hydrogenation of lactic acid in 0.01 M $HClO_4$ for 21 h (^1H, D_2O)

Both lactaldehyde and 1,2-propanediol are present in the mixture; δ 1.0 ppm [d, -CH_3 (1,2-propanediol)], δ 1.2 ppm (d, -CH_3 (lactaldehyde)], δ 1.75 ppm (unknown peak, visible in all electrohydrogenation product mixtures, probably associated with mineral acid used as electrolyte), δ 3.3 ppm [m, -CHOH (1,2-propanediol)], δ 3.7 ppm [d, -CH_2OH (1,2-propanediol)], δ 4.0 ppm [q, -CHOH (lactaldehyde)], δ 8.3 ppm [d, -CHO (lactaldehyde)]

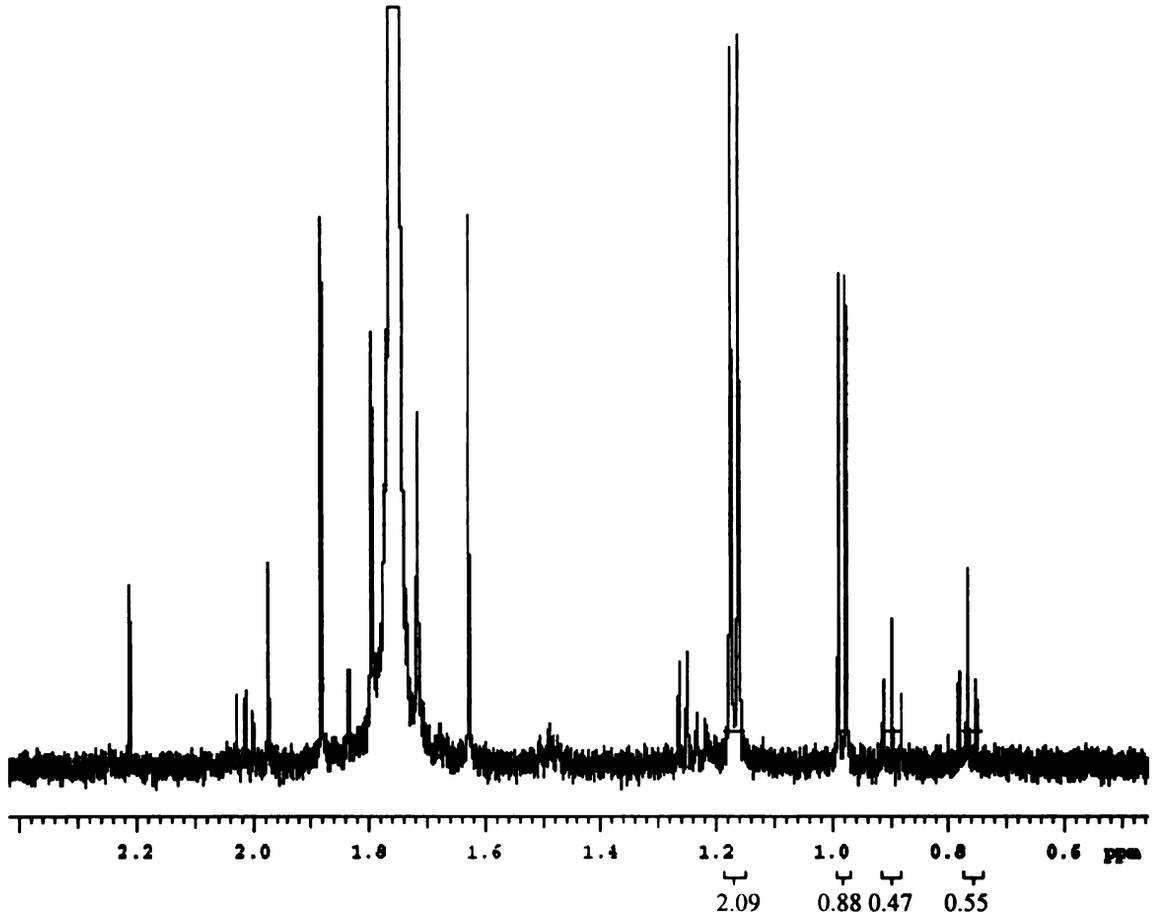

Figure A8.1: Expansion of the peaks in figure A7 (δ 0.5-3.0 ppm).

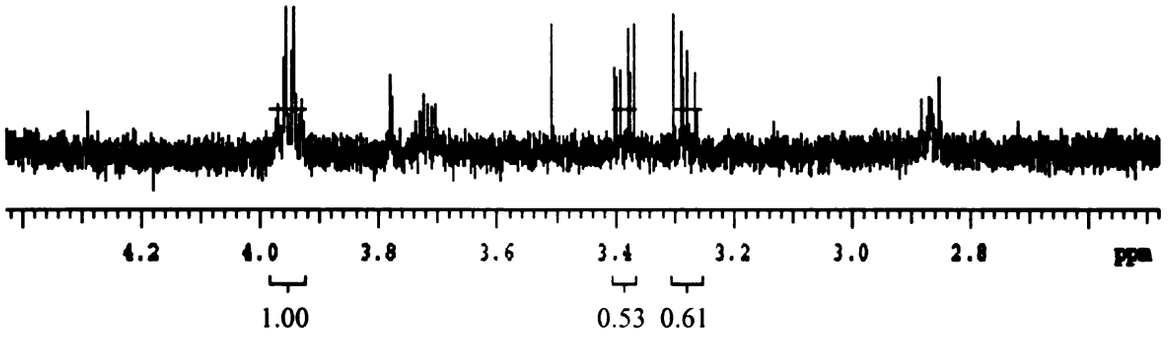

Figure A8.2: Expansion of the peaks in figure A7 (δ 2.6-4.4 ppm)

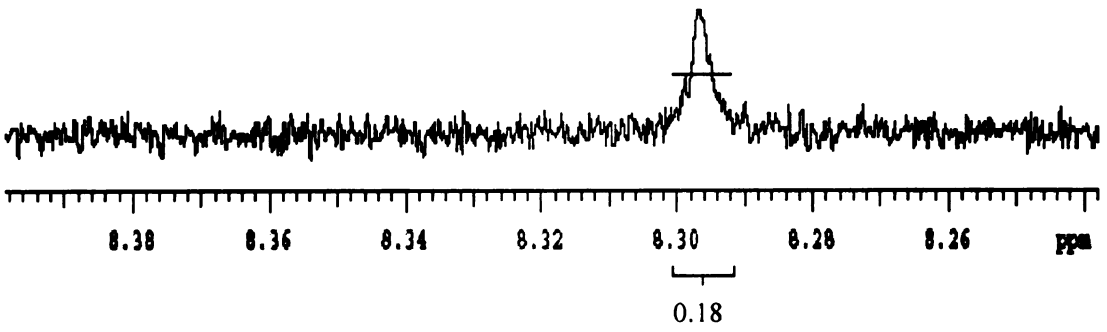

Figure A8.3: Expansion of the peaks in figure A7 (δ 8.24-8.40 ppm)

Splitting of the –CHO peak into a doublet is not very clear and may be obscured by the presence of residual acid or ClO_4^- ions from the electrolyte. The –CHOH peak is a quartet instead of a multiplet in both the chemically synthesized and the electrocatalytically synthesized lactaldehyde. This may be a result of the acidic environment and the lability of the aldehyde proton.

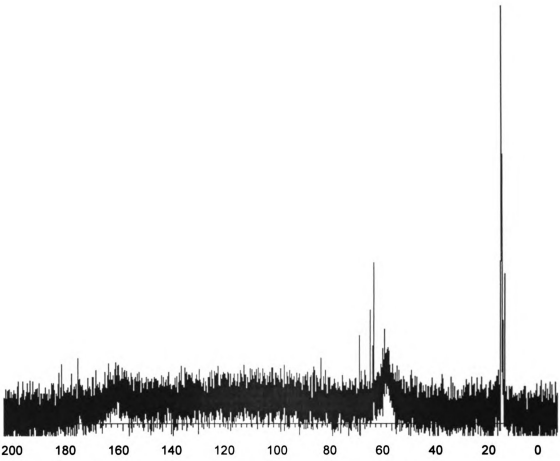

Figure A9: NMR spectrum of product mixture obtained after electrohydrogenation of lactic acid in 0.01 M $HClO_4$ for 21 h (^{13}C, D_2O)

Both lactaldehyde and 1,2-propanediol are present; δ 19 ppm [-CH_3 (1,2-propanediol)], δ 20 ppm [-CH_3 (lactaldehyde)], δ 66 ppm [-CHOH (1,2-propanediol)], δ 67 ppm [-CH_2OH (1,2-propanediol)], δ 72 ppm [-CHOH (lactaldehyde)], δ 178 ppm [-CHO (lactaldehyde)]

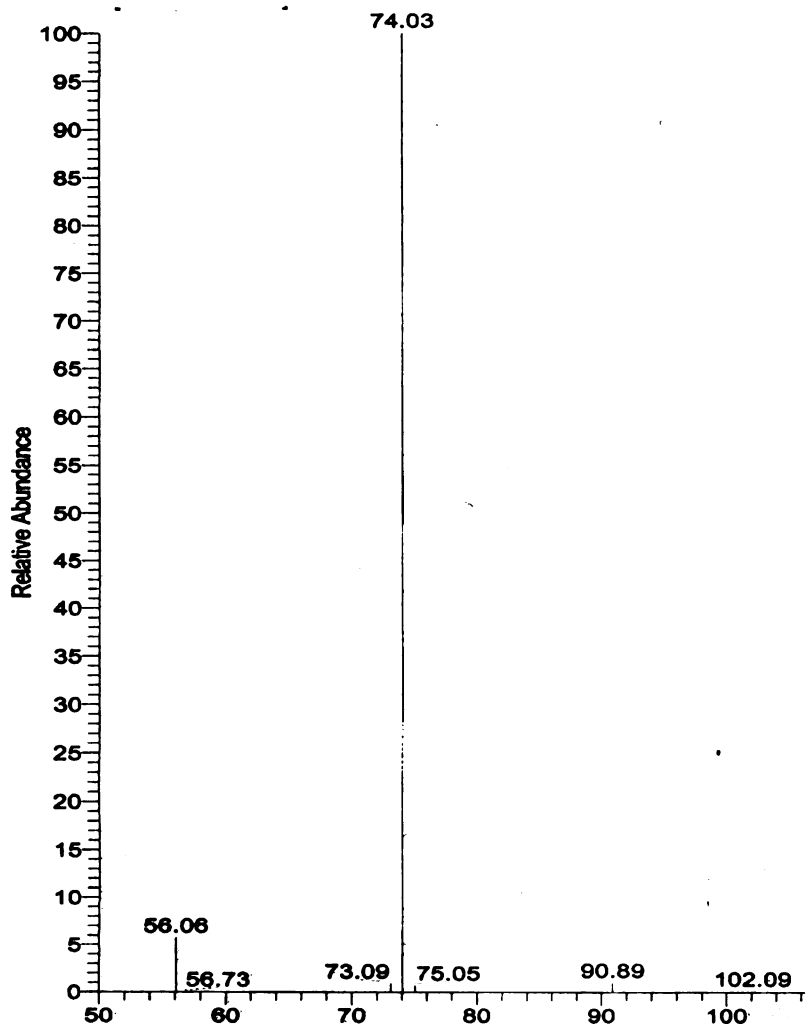

Figure A10: ESI-MS of chemically synthesized lactaldehyde

Peak assignments: m/z 74.03 (M^+ ion peak), m/z 56.06 $(M-H_2O)^+$

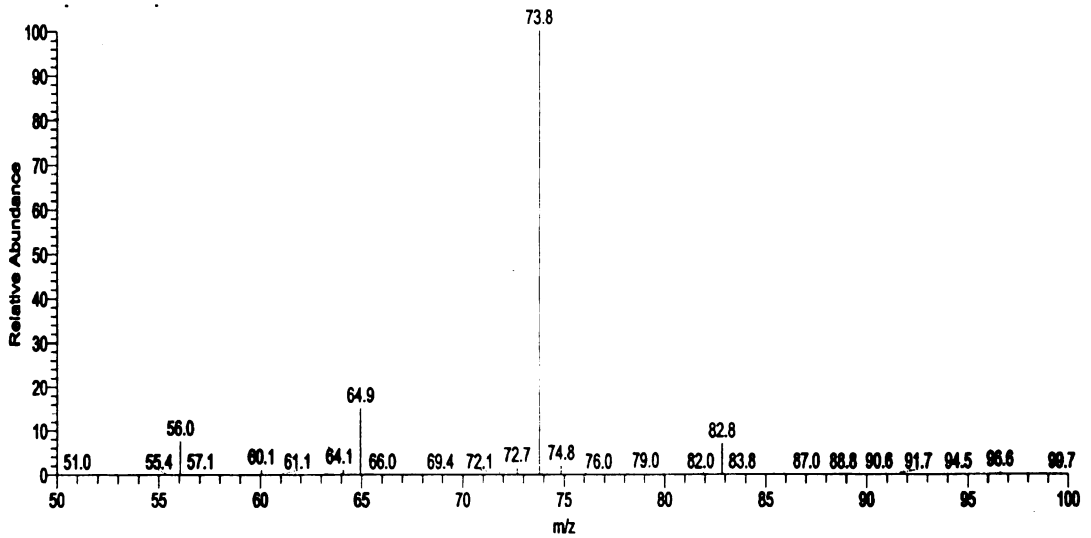

Figure A11: ESI-MS of lactaldehyde obtained after electrohydrogenation of lactic acid in 0.01 M $HClO_4$

Peak assignments: m/z 82.8 (unknown peak), m/z 73.8 (M^+ ion peak), m/z 64.0 (formed by loss of 2O from $HClO_4$), m/z 56.0 $(M\text{-}H_2O)^+$

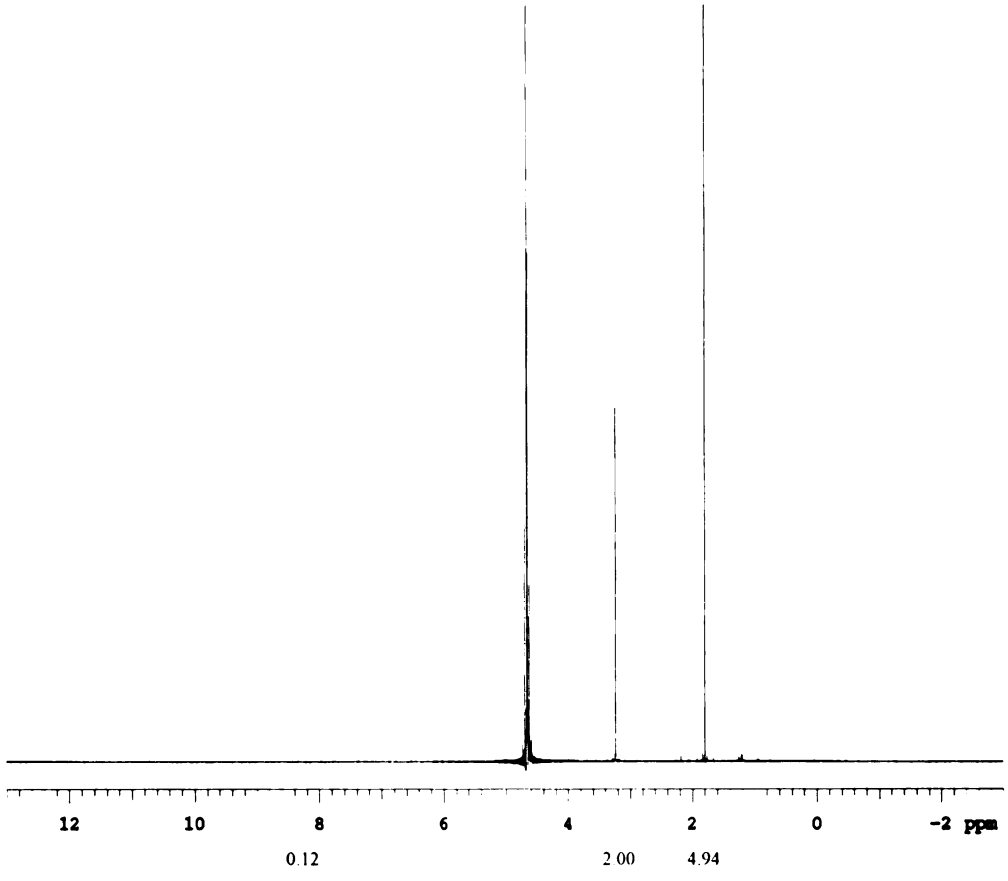

Figure A12: NMR spectrum of product mixture obtained after electrocatalytic hydrogenation of glycolic acid in 0.01 M HCl for 21 h (^{1}H, D_2O)

Only glycolic aldehyde was detected in the mixture; δ 3.2 ppm [d, -CH_2- (glycolic aldehyde)], δ 1.75 ppm (unknown peak, visible in all electrohydrogenation product mixtures, probably associated with mineral acid used as electrolyte), δ 8.3 ppm [d, -CHO (glycolic aldehyde)]

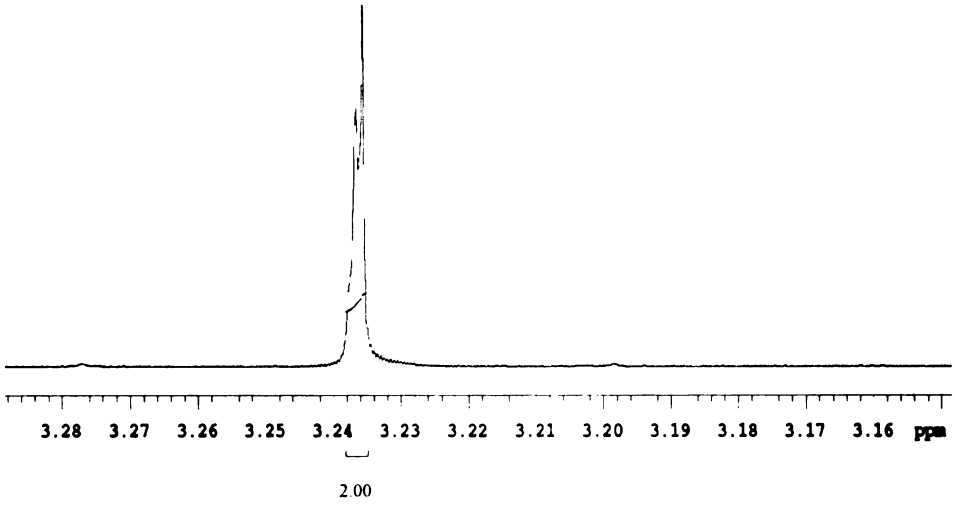

Figure A13.1: Expansion of the peaks in figure A12 (δ 3.16-3.28 ppm)

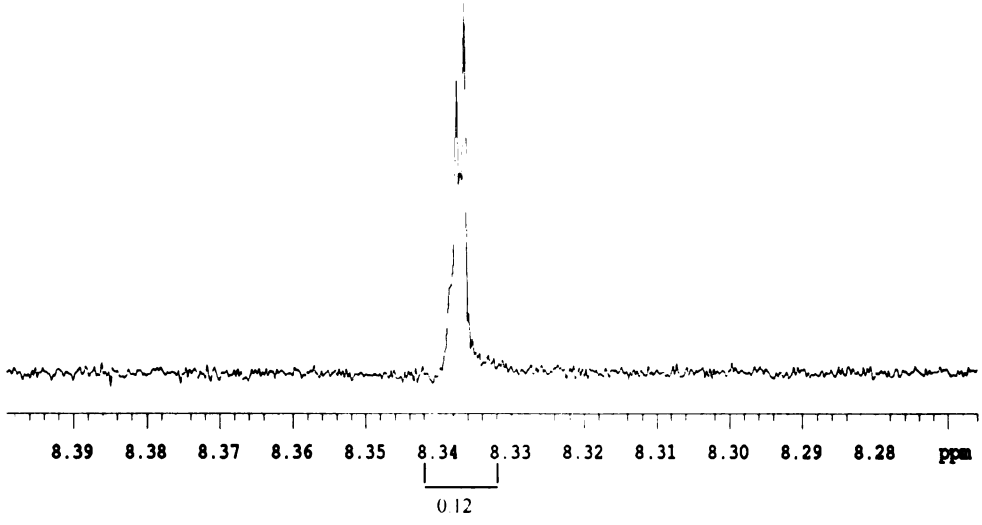

Figure A13.2: Expansion of the peaks in figure A12 (δ 8.28-8.39 ppm)

Splitting of the –CHO peak into a triplet is not very clear and may be obscured by the presence of residual acid or Cl^- ions from the electrolyte.

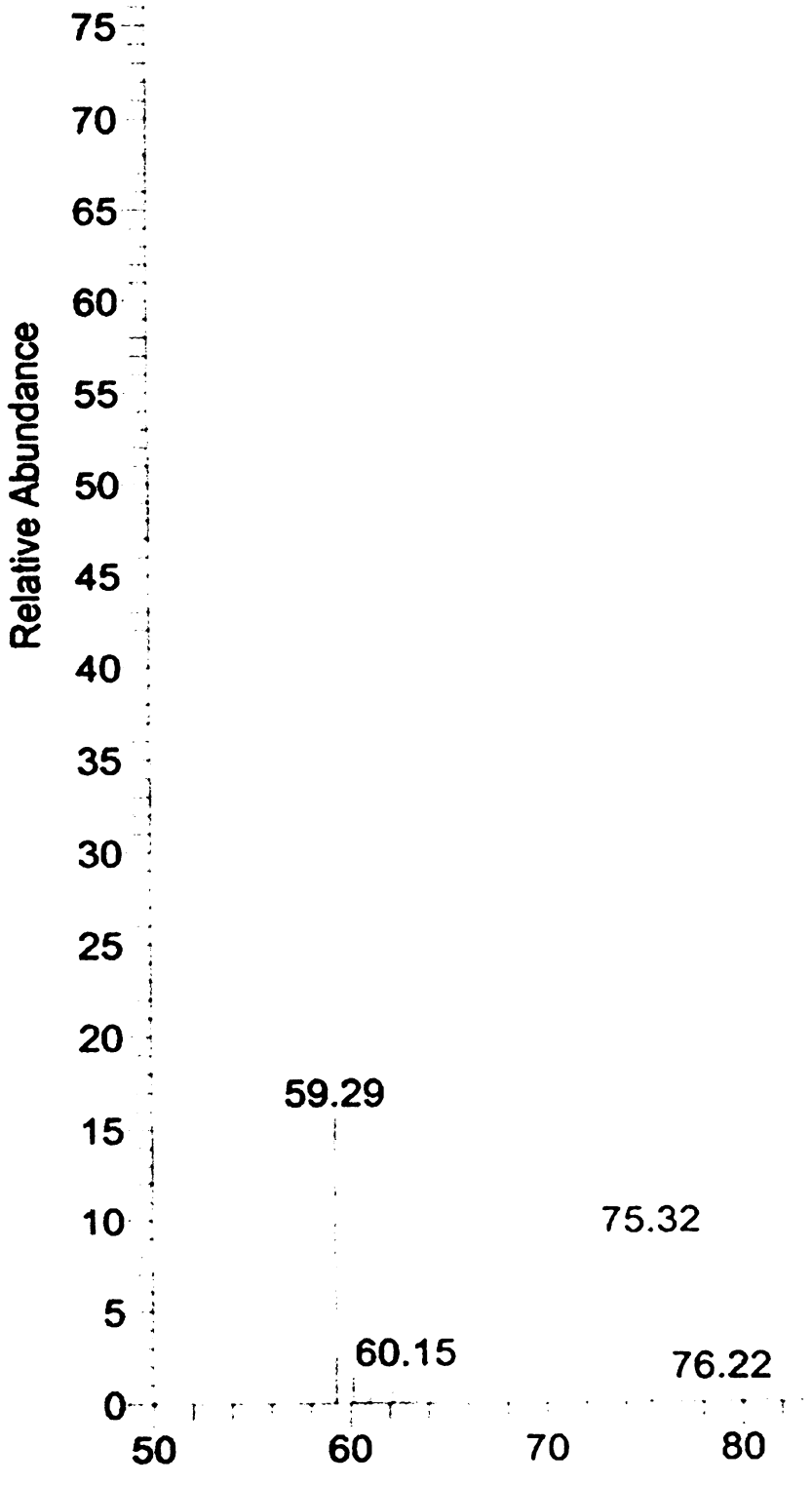

Figure A14: ESI-MS of sample obtained after electrohydrogenation of glycolic acid in 0.01 M HCl

Peak assignments: m/z 76.22 (M^+ ion peak, glycolic acid), m/z 75.32 [$(M-H)^+$, glycolic acid], m/z 60.15 (M^+ ion peak, glycolic aldehyde), m/z 59.29 [$(M-H)^+$, glycolic aldehyde]

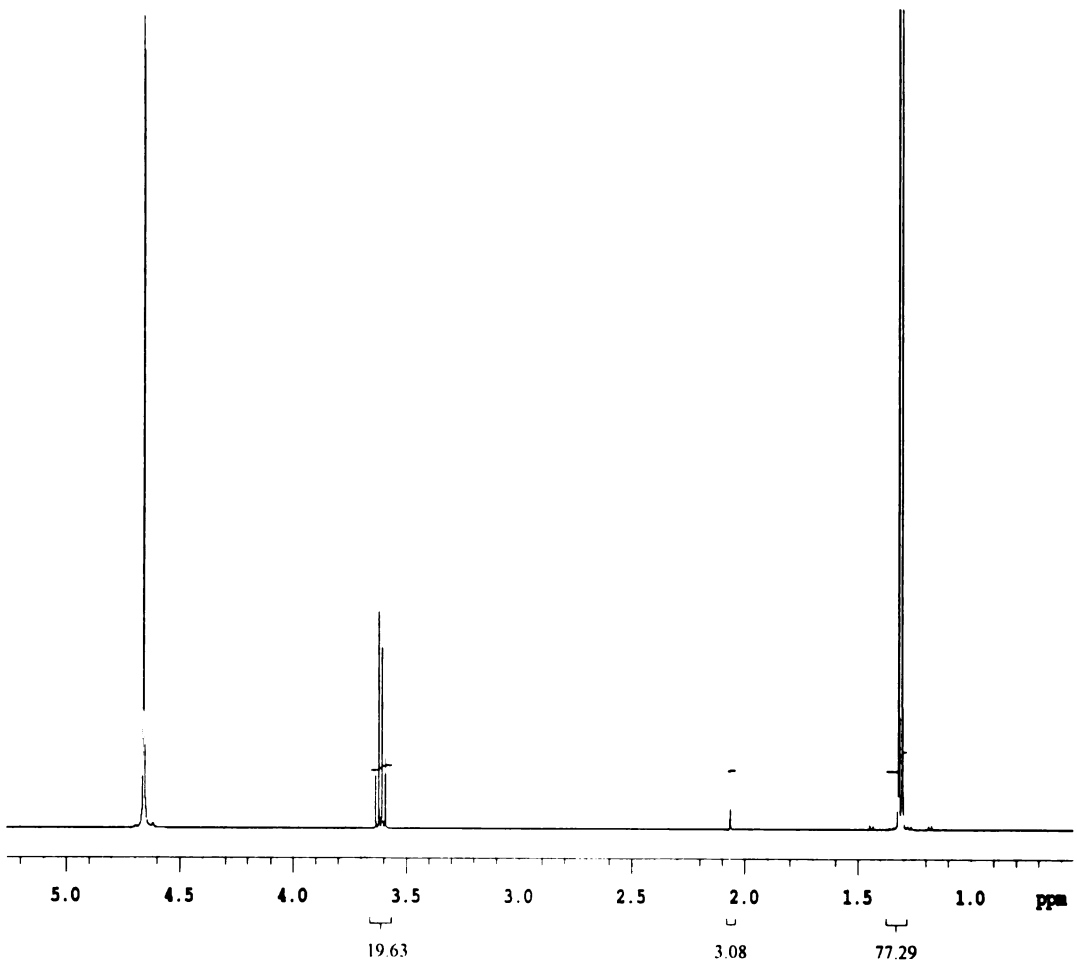

Figure A15: NMR spectrum of alanine (^1H, D_2O)

Peak assignments: δ 1.3 ppm (d, 3H, $-CH_3$), δ 2.1 ppm (d, 2H, $-NH_2$), δ 3.6 ppm (q, 1H, -CHOH)

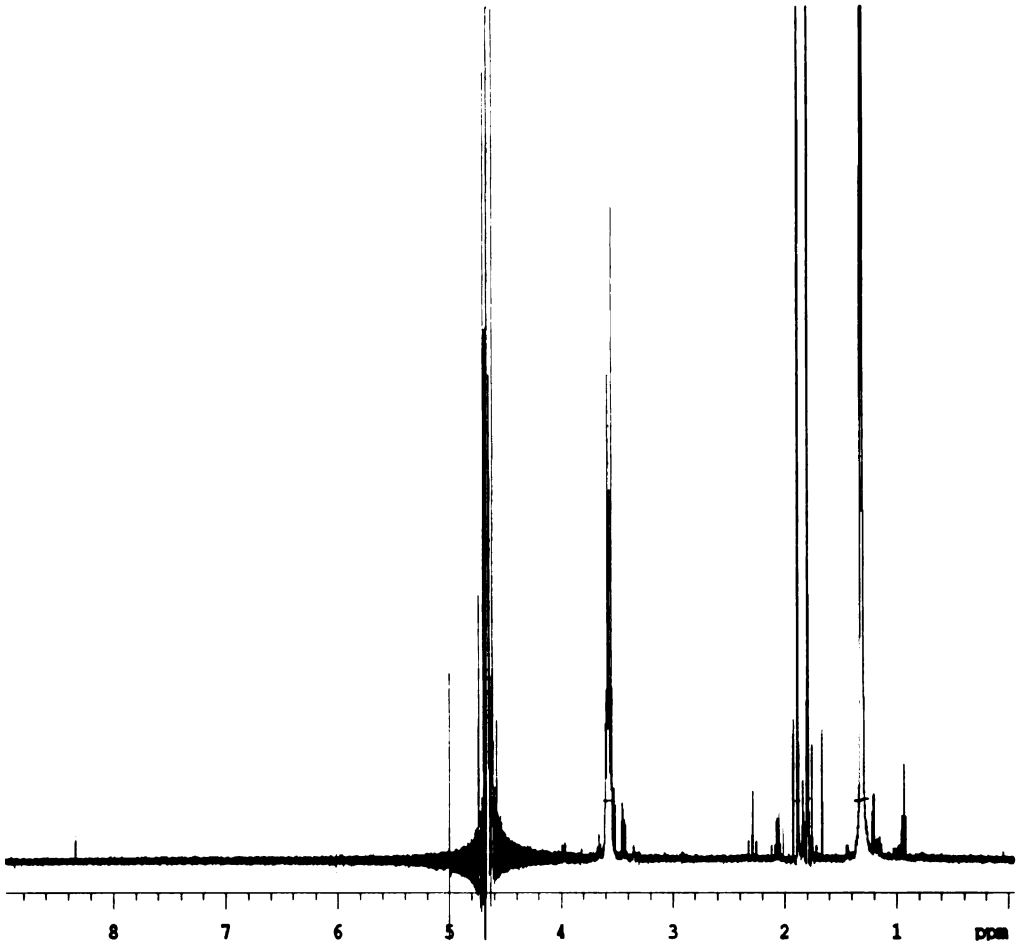

Figure A16: NMR spectrum of product mixture obtained after electrocatalytic hydrogenation of alanine in 0.01 M HCl for 21 h (^1H, D_2O)

The product was identified as 2-amino propanal; δ 1.2 ppm (d, 2H, $-CH_3$), δ 1.75 ppm (unknown peak, visible in all electrohydrogenation product mixtures, probably associated with mineral acid used as electrolyte), δ 3.6 ppm (q, 1H, -CHOH), δ 8.3 ppm (d, 1H, -CHO).

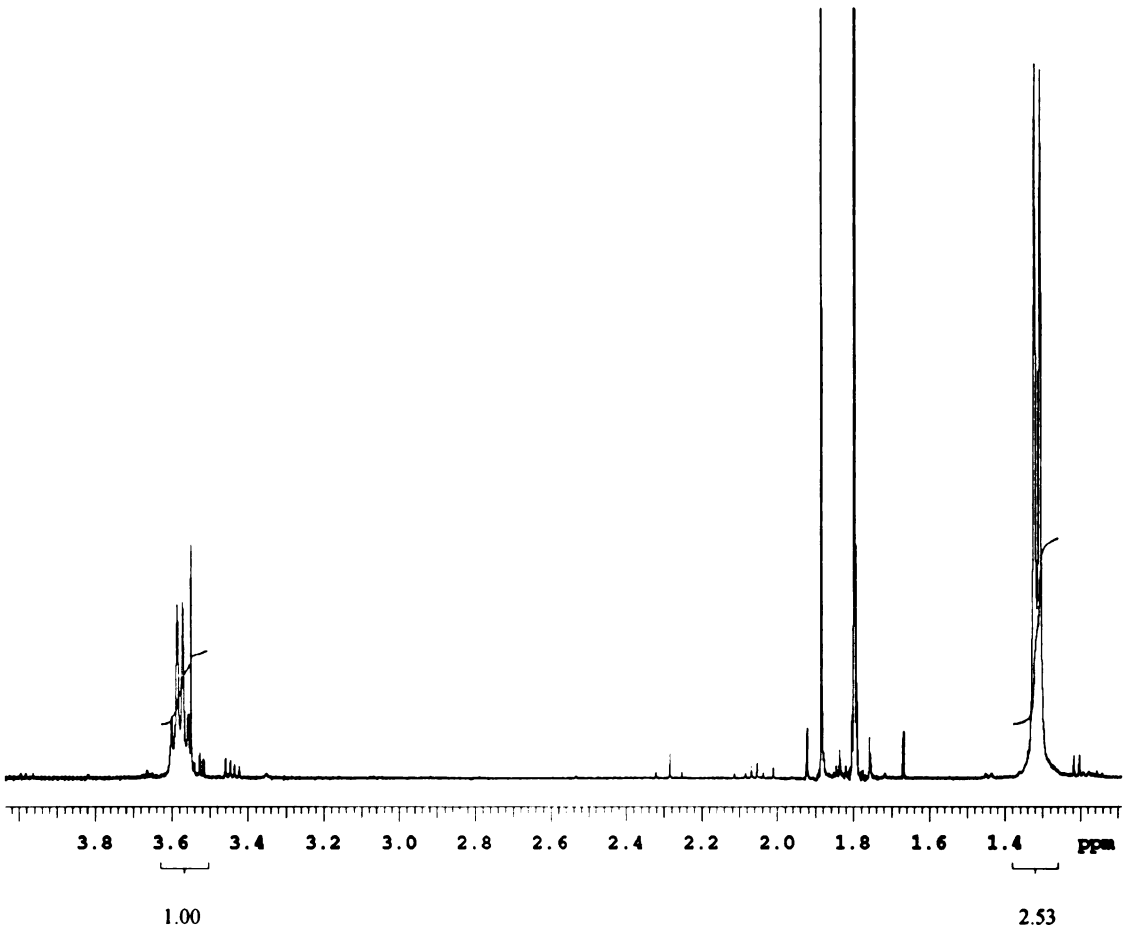

Figure A17.1: Expansion of the peaks in figure A16 (δ 1.2-3.8 ppm)

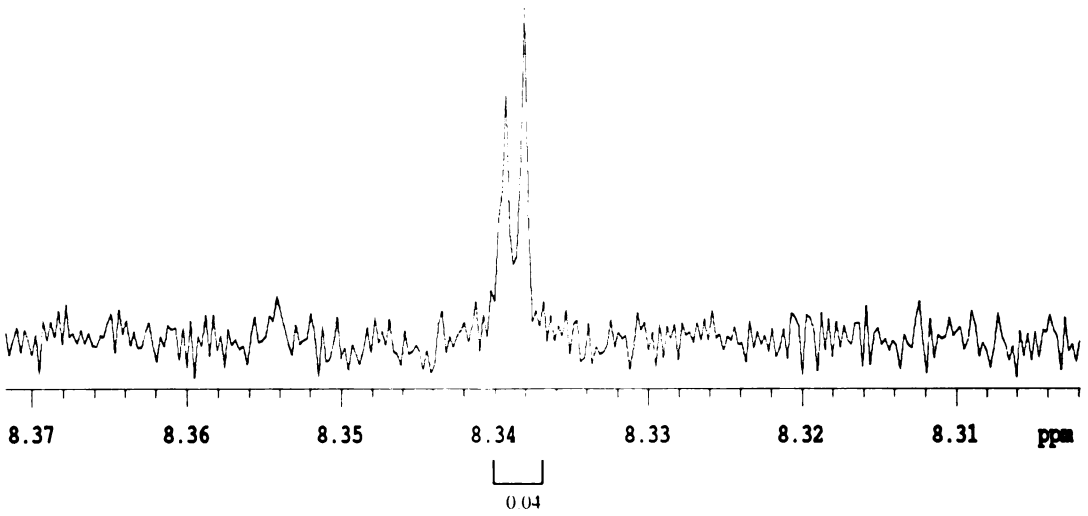

Figure A17.2: Expansion of the peaks in figure A16 (δ 8.30-8.37 ppm)

Splitting of the –CHO peak into a doublet is quite clear in this case. The –CHOH peak is a quartet instead of a multiplet. This may be a result of the acidic environment and the lability of the aldehyde proton.

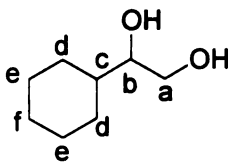

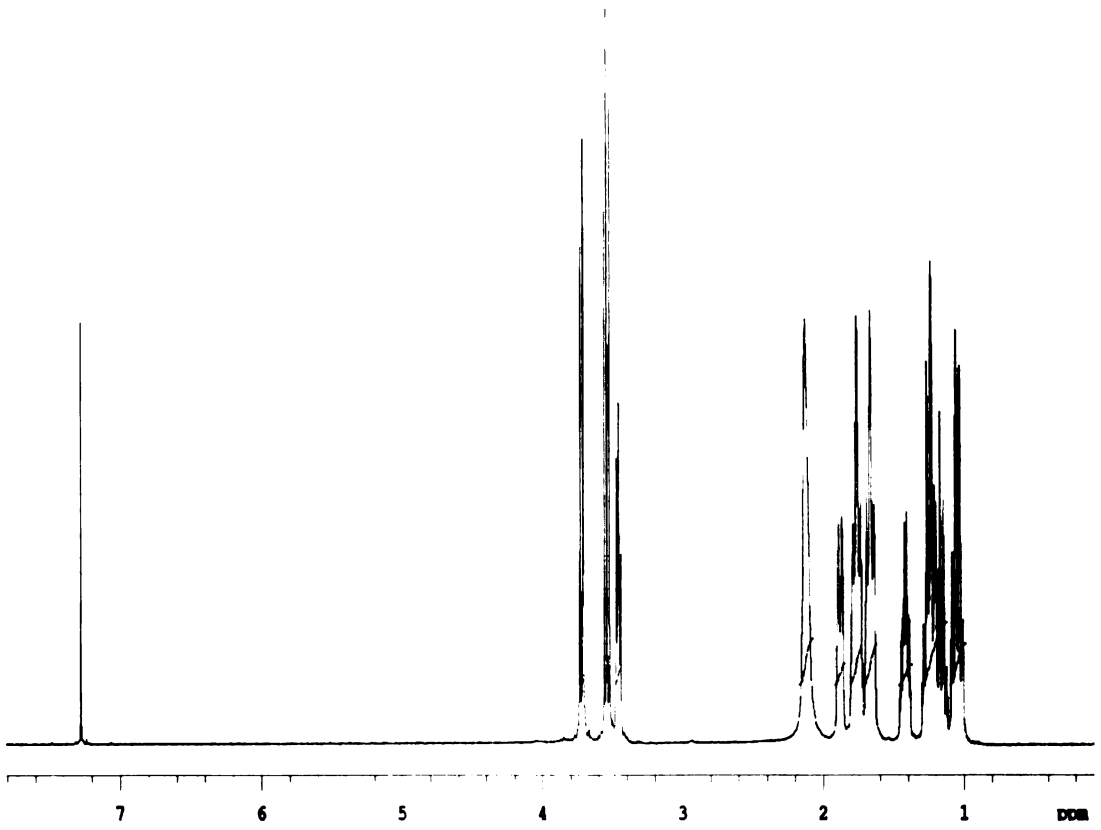

Figure A18: NMR spectrum of the product of batch reduction of 1-phenyl 1,2-ethanediol (PED) (^1H, $CDCl_3$).

Cyclohexyl ethylene glycol (CEG) (structure shown above) was the major product with small amount of 2-cyclohexyl ethanol (CE) (from GC analysis); (C atoms are labeled as shown in the structure) δ 1.04 ppm [q, -Cf-H (cyclohexyl)], δ 1.20 ppm [m, Ce-H and Cd-H (cyclohexyl)], δ 1.42 ppm [m, Cc-H (cyclohexyl)], δ 1.66 ppm [t, C2-H (CE)], 1.76

ppm [t, Ca-OH (CEG)], δ 1.88 ppm [d, Cb-OH (CEG)], δ 2.12 ppm [s (broad), O-H (water)], δ 3.46 ppm [dt, Cb-H (CEG)], δ 3.54 ppm [t, C1-H (CE)], δ 3.72 ppm [dd, Ca-H (CEG)]

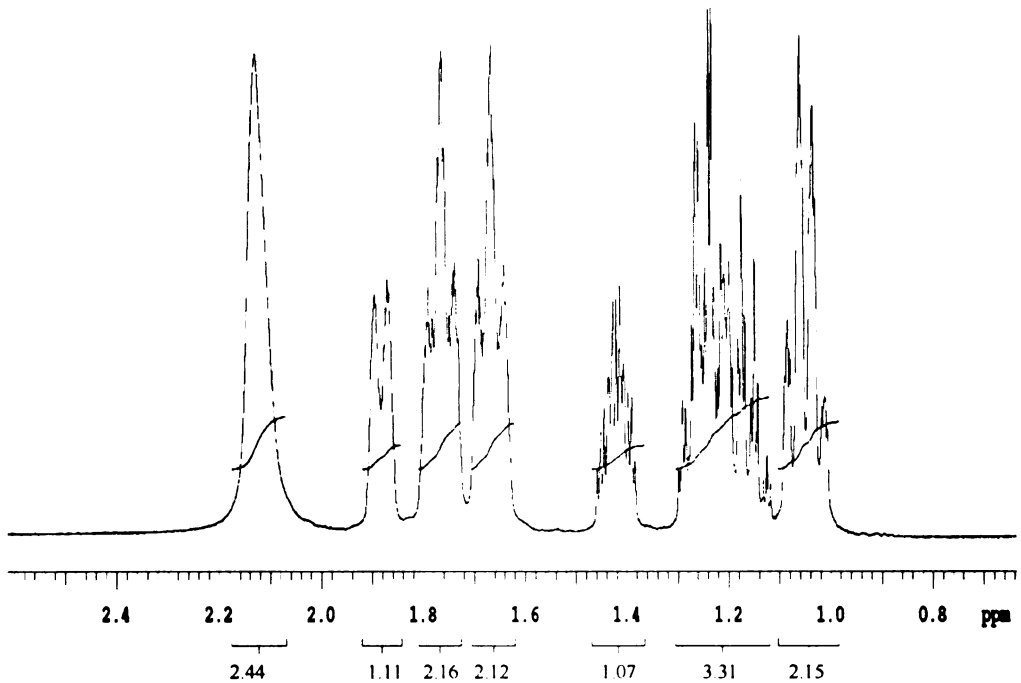

Figure A19.1: Expansion of the peaks in figure A18 (δ 0.6-2.6 ppm)

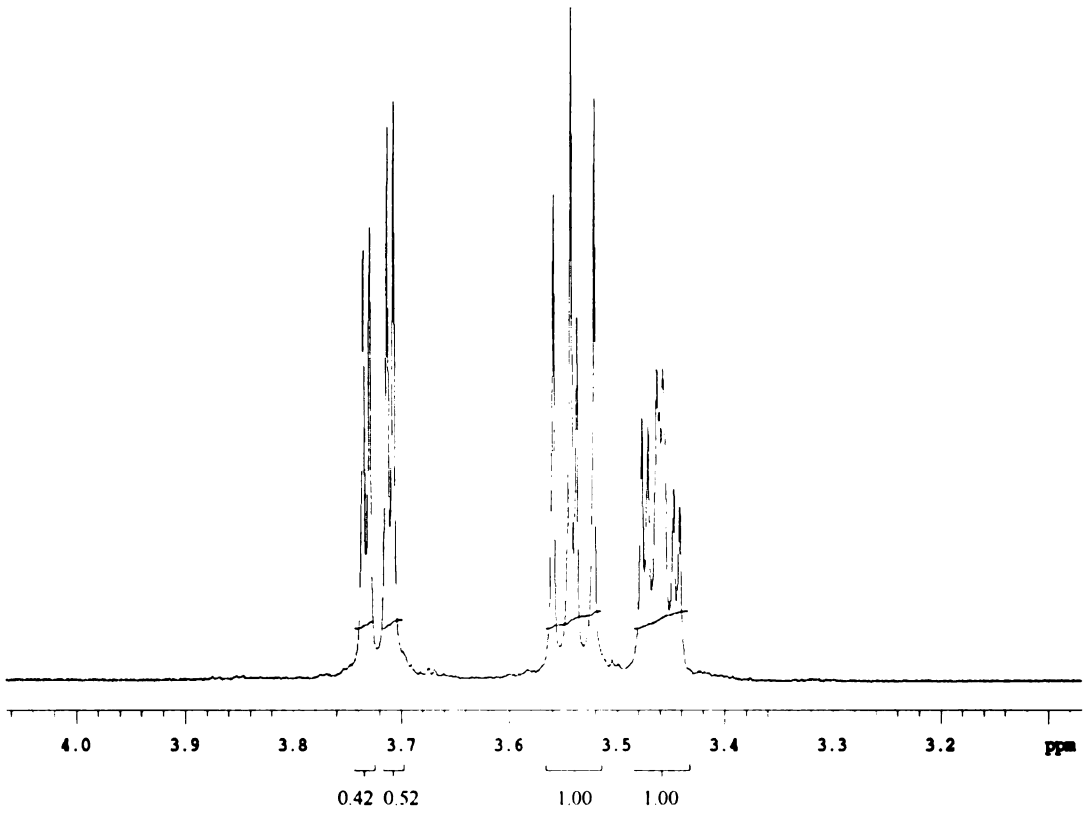

Figure A19.2: Expansion of the peaks in figure A18 (δ 3.1-4.0 ppm)

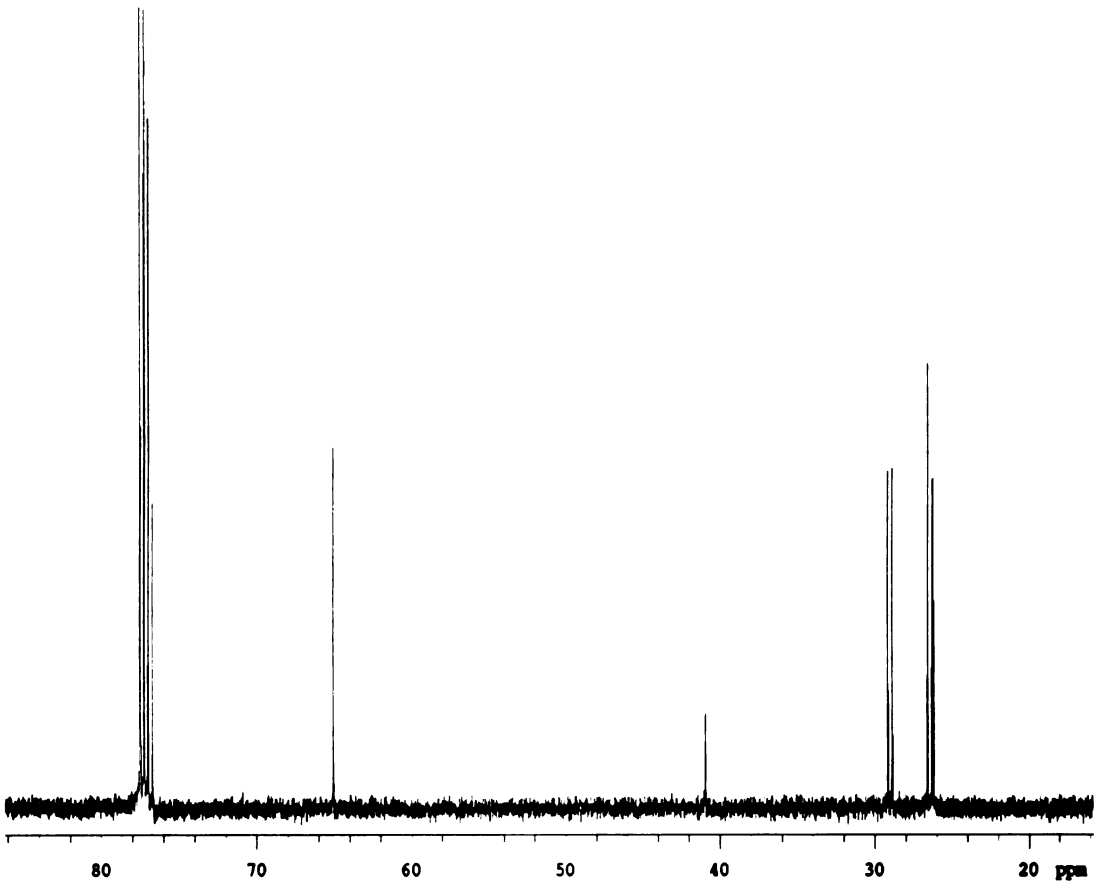

Figure A20: NMR spectrum of the product of batch reduction of 1-phenyl 1,2-ethanediol (PED) (^{13}C, $CDCl_3$)

Cyclohexyl ethylene glycol (CEG) was the major product with small amount of 2-cyclohexyl ethanol (CE); (C atoms are labeled as shown in the structure) δ 26.2 ppm [Cf (cyclohexyl), δ 26.3 ppm [Ce (cyclohexyl)], δ 26.6 ppm [Cd (cyclohexyl)], δ 28.9 ppm [Cc (cyclohexyl) (CE)], δ 29.2 ppm [Cc (cyclohexyl) (CEG)], δ 41.0 ppm [C2 (CE)], δ 65.0 ppm [C1 (CE)], δ 77.3 ppm [Cb (CEG)], δ 77.5 ppm [Ca (CEG)]

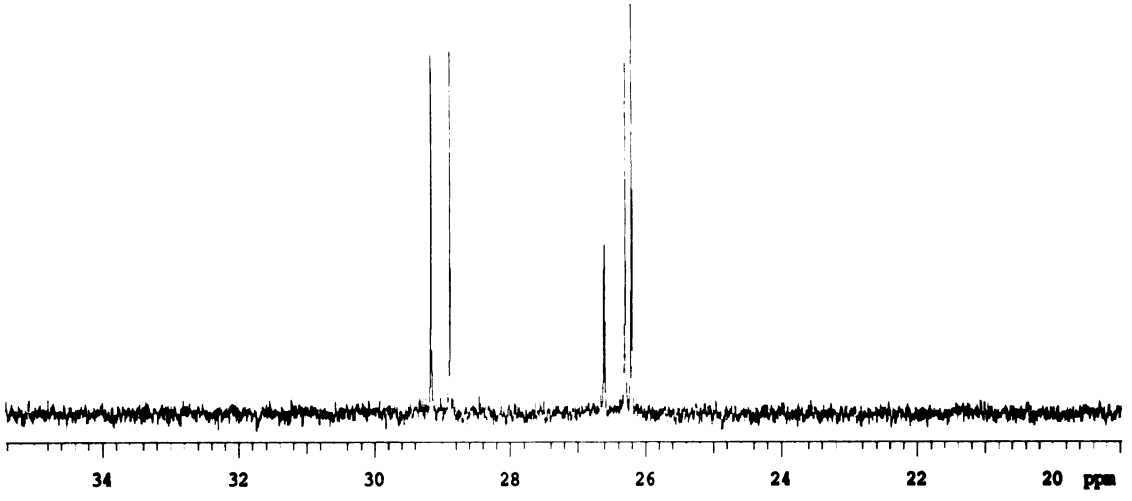

Figure A21.1: Expansion of the peaks in figure A20 (δ 20-34 ppm)

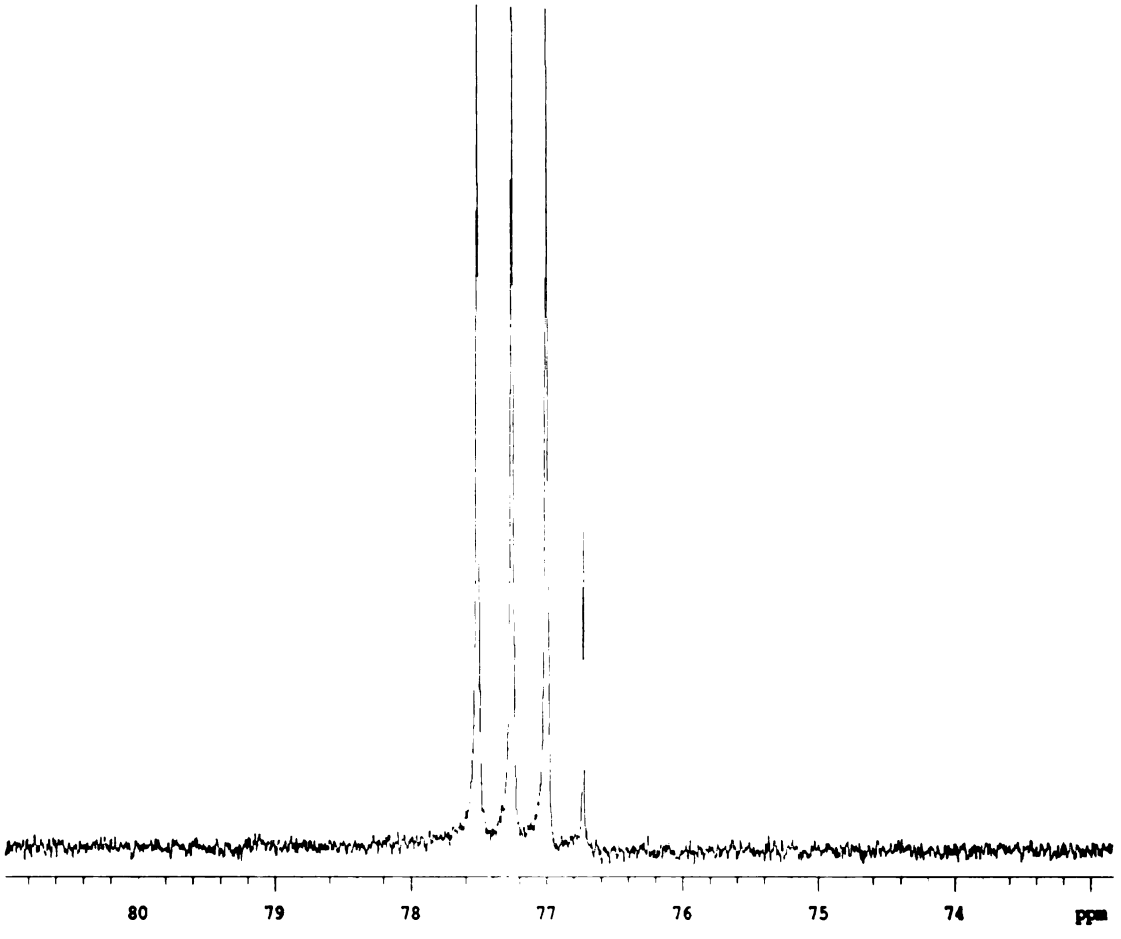

Figure A21.2: Expansion of the peaks in figure A20 (δ 73-81 ppm)

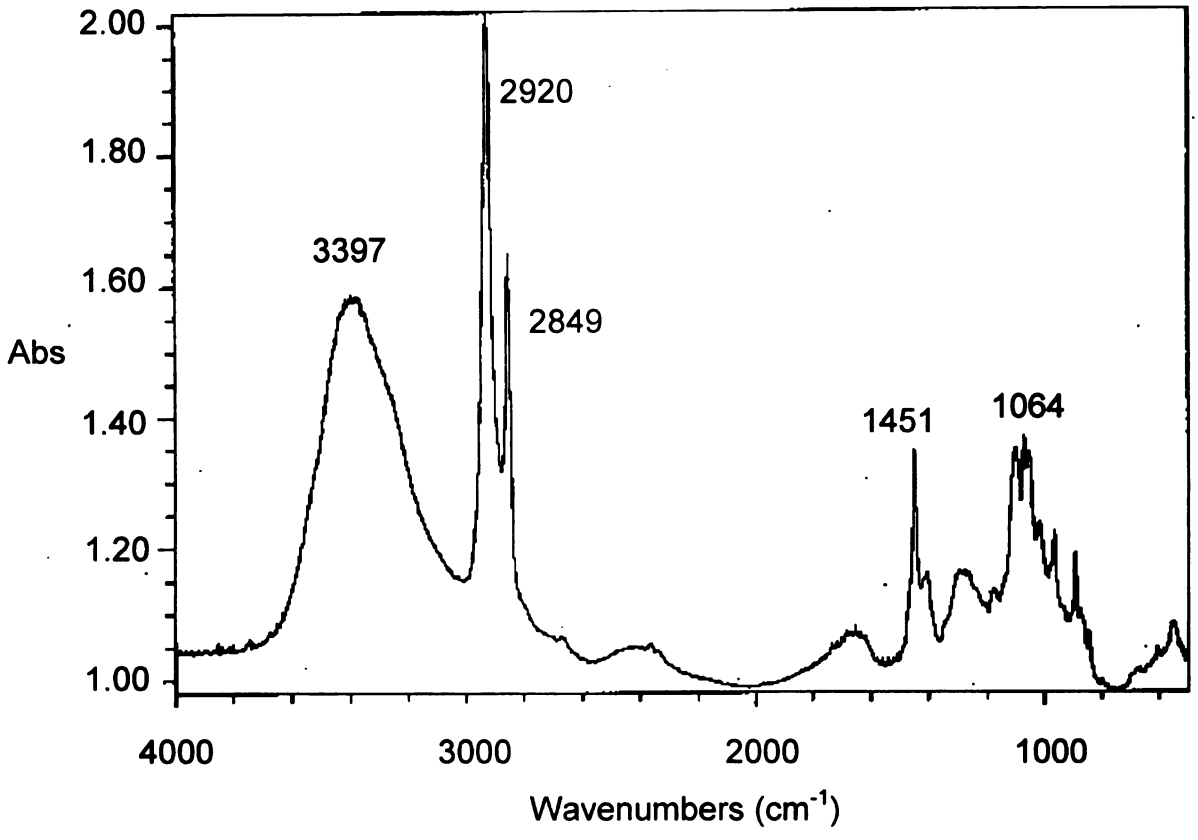

Figure A22: FTIR spectrum of cyclohexyl ethylene glycol (CEG) synthesized by batch reduction of phenyl ethanediol (PED) (KBr pellet)

Peak assignments: 1064 cm^{-1}: υC-O (alcohol), 1451 cm^{-1}: δCH_2-C, 2849 and 2920 cm^{-1}: υC-H (sp^3), 3397 cm^{-1}: υO-H

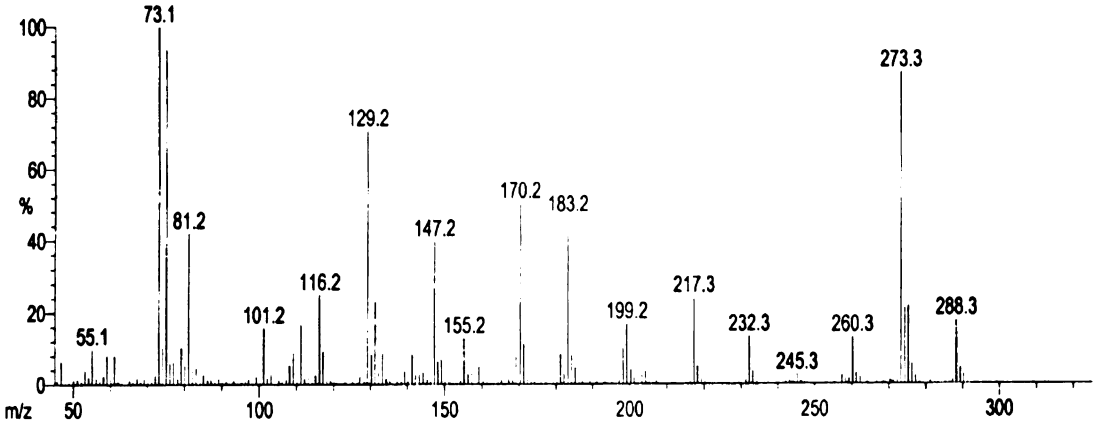

Figure A23: Electron ionization mass spectrum (EI-MS) of trimethyl silyl (TMS) derivative of cyclohexyl ethylene glycol (CEG) synthesized by batch reduction of phenyl ethanediol (PED) derivatized using BSTFA and separated by GC (DB1 column)

Peak assignments: m/z 288.3 (M^+ ion peak of disilylated CEG); m/z 273.3 (M-15 peak of disilylated CEG); m/z 147.2 (2TMS); m/z 101.2 (CH_2OTMS); m/z 73.1 (TMS)

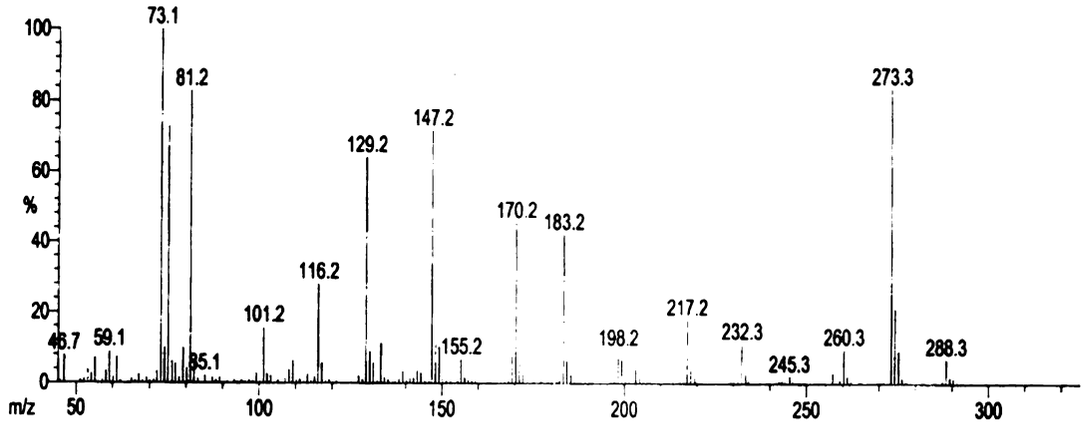

Figure A24: Electron ionization mass spectrum (EI-MS) of CEG obtained by ECH of mandelic acid, after precipitation of sulfate, evaporation of water, derivatization using BSTFA and separation by GC (DB1 column)

Peak assignments: m/z 288.3 (M^+ ion peak of disilylated CEG); m/z 273.3 (M-15 peak of disilylated CEG); m/z 147.2 (2TMS); m/z 101.2 (CH_2OTMS); m/z 73.1 (TMS)

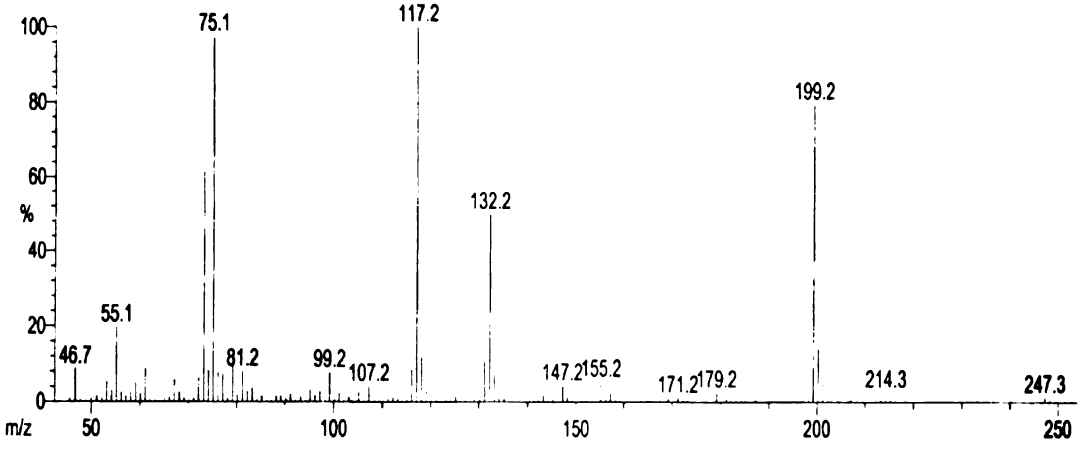

Figure A25: Electron ionization mass spectrum (EI-MS) of 2-cyclohexyl 2-hydroxy acetaldehyde (CHA) obtained by ECH of mandelic acid, after precipitation of sulfate, evaporation of water, derivatization using BSTFA and separation by GC (DB1 column)

Peak assignments: m/z 214.3 (M^+ ion peak of monosilylated CHA); m/z 199.2 (M-15 peak of monosilylated CHA); m/z 147.2 (2TMS); m/z 73.1 (TMS)

REFERENCES

1. (a) Adkins, H.; Wojcik, B.; Covert, L.W., *J. Am. Chem. Soc.* **1932**, *54*, 1145-1154
   (b) Adkins, H.; Wojcik, B.; Covert, L.W., *J. Am. Chem. Soc.* **1933**, *55*, 1669-1676

2. Bowden, E.; Adkins, H., *J. Am. Chem. Soc.* **1934**, *56*, 689-691

3. Um, S.; Han, S.; Jung, K.; Baek, J. Repub. Korea, Patent no. KR 9601911, 1996

4. Roesky, R.; Borchert, H.; Dingerdissen, U. PCT Int. Appl., 1998, 16, Patent no. WO 9841492

5. Luo, G.; Yan, S.; Qiao, M.; Zhuang, J.; Fan, K., *Appl. Catal. A: General*, **2004**, *275*, 95-102

6. Schurch, M.; Heinz, T.; Aeschimann, R.; Mallat, T.; Pfaltz, A.; Baiker, A., *J. Catal.*, **1998**, *173*, 187-195

7. Orito, Y.; Imai, S.; Niwa, S., *J. Chem. Soc. Jpn.*, **1979**, *8*, 1118

8. Adkins, H.; Billica, H.R., *J. Am. Chem. Soc.*, **1948**, *70*, 3121-3125

9. Carnahan, B.; Ford, T.; Gresham, W.; Grisby, W.; Hager, G., *J. Am. Chem. Soc.*, **1955**, *77*, 3766

10. Broadbent, H.; Campbell, G.; Bartley, W.; Johnson, J., *J. Org. Chem.*, **1959**, *24*, 1847

11. Mendes, M.J.; Santos, O.A.A.; Jordao, E., *Appl. Catal. A: General*, **2001**, *217(1-2)*, 253-262

12. Toba, M.; Tanaka, S.; Niwa, S., *Appl. Catal. A: General*, **1999**, *189(2)*, 243-250

13. Rachmady, W. Vannice, M.A., *J. Catal.*, **2000**, *192*, 322-334

14. Zhang, Z.; Jackson, J.E.; Miller, D.J., *Appl. Catal. A: General*, **2001**, *219*, 89-98

15. Zhang, Z.; Jackson, J.E.; Miller, D.J., *Ind. Eng. Chem. Res.* **2002**, *41*, 691

16. Jere, F.T.; Miller, D.J.; Jackson, J.E., *Org. Lett.*, **2003**, *5(4)*, 527-530

17. Sorum, P.A.; Onsager, O.T., *Proceedings- 8th International Congress on Catalysis*, Berlin, **1984**, *8*, 11-23

18. Monti, D.M.; Cant, N.W.; Trimm, D.L.; Wainwright, M.S., *J. Catal.*, **1986**, *100*, 17-27

19. Kohler, M.A.; Cant, N.W.; Wainwright, M.S.; Trimm, D.L., *Proceedings, 9th International Congress on Catalysis*, **1988**, *9*, 1043-1050

20. Natal-Santiago, M.A.; Sanchez-Castillo, M.A.; Cortright, R.D.; Dumesic, J.A., *J. Catal.*, **2000**, *193*, 16-28

21. Pallassana, V.; Neurock, M., *J. Catal.*, **2002**, *209*, 289-305

22. Luo, G.; Yan, S.; Qiao, M.; Fan, K., *J. Mol. Catal. A: Chemical*, **2005**, *230*, 69-77

23. Deshpande, V.M.; Ramnarayan, K.; Narasimhan, C.S., *J. Catal.*, **1990**, *121*, 174

24. Pouilloux, Y. Autin, F.; Guimon, C.; Barrault, J., *J. Catal.*, **1998**, *176*, 215-224

25. Kovacs, D.G.; Peereboom, L.; Jackson, J.E.; Miller, D.J., *Unpublished results*

26. Varga, N., MS thesis

27. Farrugia, J.; Jackson, J.E.; Miller, D.J., *Unpublished results*

28. Dabo, P.; Mahdavi, B.; Menard, H.; Lessard, J., *Electrochim. Acta*, **1997**, *42(9)*, 1457-1459

29. Quiroz, M.A.; Cordova, F.; Lamy-Pitara, E.; Barbier, J., *Electrochim. Acta*, **2000**, *45*, 4291-4298

30. Mahdavi, B.; Chambrion, P.; Binette, J.; Martel, E. Lessard, J., *Can. J. Chem.*, **1995**, *73*, 846-852

31. Bryan, J.; Grimshaw, J., *Electrochim. Acta*, **1997**, *42(13-14)*, 2101-2107

32. Senda, Y.; Tateoka, M.; Itoh, H.; Ishiyama, J., *Bull. Chem. Soc. Jpn.*, **1991**, *64(11)*, 3302-3305

33. DaSilva, J.G.; Goulart, M.O.F.; Navarro, M., *Tetrahedron*, **1999**, *55*, 7405-7410

34. Cheong, A.K.; Bolduc, Y.; Lessard, J., *Can. J. Chem.*, **1993**, *71*, 1850-1856

35. Romulus, A.M.; Savall, A., *J. Appl. Electrochem.*, **2000**, *30*, 967-972

36. Hu, X.E.; Yang, H.W.; Wang, X.J.; Bai, R.S., *J. Appl. Electrochem.*, **2002**, *32*, 321-328

37. Polcaro, A.M.; Palmas, S.; Dernini, S., *Ind. Eng. Chem. Res.*, **1993**, *32*, 1315-1322

38. Ilikti, H.; Rekik, N.; Thomalla, M., *J. Appl. Electrochem.*, **2002**, *32*, 603

39. Ilikti, H.; Rekik, N.; Thomalla, M., *J. Appl. Electrochem.*, **2004**, *34*, 127-136

40. Beraud, V.; Lessard, J.; Thomalla, M., *Can. J. Chem.*, **1997**, *75*, 1529-1535

41. Roessler, A.; Dossenbach, O.; Rys, P., *J. Electrochem. Soc.*, **2003**, *150(1)*, D1-D5

42. (a) Amouzegar, K.; Savadogo, O., *J. Appl. Electrochem.*, **1997**, *27*, 539-542 (b) Amouzegar, K.; Savadogo, O., *Electrochim. Acta*, **1994**, *39(4)*. 557-559

43. Lofrano, R.C.Z.; Madurro, J.M.; Abrantes, L.M.; Romero, J.R., *J. Mol. Catal. A: Chemical*, **2004**, *218*, 73-79

44. Takano, N.; Nakade, A.; Takeno, N., *Bull. Chem. Soc. Jpn.*, **1997**, *70*, 837-840

45. Takano, N.; Seki, C.; Shimono, I., *Bull. Chem. Soc. Jpn.*, **2000**, *73(3)*, 745-746

46. Santana, D.S.; Lima, M.V.F.; Daniel, J.R.R.; Navaro, M., *Tet. Lett.*, **2003**, *44*, 4725-4727

47. Roessler, A.; Dossenbach, O.; Marte, W.; Rys, P., *Dyes and Pigments*, **2002**, *54*, 141-146

48. Raju, R.R.; Mohan, S.K.; Reddy, S.J., *J. Sci. Ind. Res.*, **2003**, *62(4)*, 334-338

49. Wang, J.; Swain, G.M.; Tachibana, T.; Kobashi, K. *Electrochemical and Solid State Letters*, **2000**, *3(6)*, 286-289

50. Wang, J.; Swain, G.M. *J. Electrochem. Soc.*, **2003**, *150(1)*, E24-E32

51. Wang, J.; Swain, G.M.; Tachibana, T.; Kobashi, K. *Proceedings- Electrochemical Society*, **2000**, *99-32* (Diamond Materials), 428-439

52. Dube, P.; Kerdouss, F.; Laplante, F.; Proulx, P.; Brossard, L.; Menard, H. *J. Appl. Electrochem.*, **2003**, *33*, 541-547

53. Polcaro, A.M.; Dernini, S.; Palmas, S. *Electrochim. Acta*, **1992**, *37*, 365-367

54. Inoue, H.; Yoshida, Y.; Ogata, S.; Shimamune, T.; Iwakura, C., *J. Electrochem. Soc.*, **1998**, *145(1)*, 138-141

55. Iwakura, C., *J. Mater. Res.*, **1998**, *13(4)*, 821-824

56. Amouzegar, K.; Savadogo, O., *Electrochim. Acta*, **1998**, *43(5-6)*, 503-508

57. Amouzegar, K.; Savadogo, O., *J. Appl. Electrochem.*, **1997**, *27(5)*, 539-542

58. Vedenyapin, A.A.; Baturova, M.D.; Ioseliani, G.I.; Areshidze, G.K., *Russ. Chem. Bull.*, **1997**, *46(1)*, 76-80

59. George, G., *J. Chem. Edu.*, **1978**, *55(6)*, 410

60. Nambiar, K.P.; Stauffer, D.M.; Kolodziej, P.A.; Benner, S.A., *J. Am. Chem. Soc.*, **1983**, *105*, 5886

61. Wang, J.; Fabrication, characterization and electrocatalytic activity of metal/diamond composite electrodes, Ph.D. Thesis

62. Cyr, A.; Chiltz, F.; Jeanson, P.; Martel, A.; Brossard, L.; Lessard, J.; Menard, H. *Can. J. Chem.*, **2000**, *78*, 307.

63. Dabo, P.; Cyr, A.; Lessard, J.; Brossard, L.; Menard, H., *Can. J. Chem. 1999*, **77**, 1225

64. Giles, R.D.; Harrison, J.A.; Thirsk, H.R., *J. Electroanal. Chem.*, **1969**, *20*, 47-60

65. Breiter, M.W., *J. Electroanal. Chem.*, **1984**, *178*, 53-59

66. Fleischmann, M.; Grenness, M., *J. Chem. Soc.- Faraday Trans. 1*, **1972**, *68(12)*, 2305

67. Laplante, F.; Brossard, L.; Menard, H., *Can. J. Chem.*, **2003**, *81(3)*, 258-264

68. Cyr, A.; Chiltz, F.; Jeanson, P.; Martel, A.; Brossard, L.; Lessard, J.; Menard, H., *Can. J.Chem.*, **2000**, *78*, 307-315.

69. Dabo, P.; Cyr, A.; Lessard, J.; Brossard, L.; Menard, H., *Can. J. Chem.*, **1999**, *77*, 1225-1229

70. Ruest, L.; Menard, H.; Moreau, V.; Laplante, F., *Can. J. Chem.* **2002**, *80*, 1662-1667

71. Dube, P.; Kerdouss, F.; Proulx, P.; Brossard, L.; Menard, H., *J. Appl. Electrochem.* **2003**, *33*, 541-547

72. Robin, D.; Comtois, M.; Martel, A.; Lemieux, R.; Cheong, A.K.; Belot, G.; Lessard, J., *Can J. Chem.*, **1990**, *68*, 1218.

73. Lamy-Pitara, E.; El Mouahid, S.; Barbier, J., *Electrochim. Acta.* **2000**, *43*, 4299

74. Polcaro, A.M.; Palmas, S.; Dernini, S., *Electrochim. Acta*, **1993**, *38(2-3)*, 199-203

75. Horanyi, G., *Electrochim. Acta*, **1991**, *36*, 1453

76. Hadzi-Jordanov, S.; Angerstein-Koziowska, H.; Yukovic, M.; Conway, B.E., *J. Phys. Chem.* **1977**, *81(24)*, 2271

77. Sawatari, Y; Inukai, J.; Ito, M., *J. Electron Spec. and Related Phenomena*, **1993**, *64/65*, 515

78. Hoshi, N.; Kuroda, M.; Ogawa, T.; Koga, O.; Hori, Y., *Langmuir*, **2004**, *20*, 5066

79. Shingaya, Y.; Ito, M., *Electrochim. Acta*, **1992**, *37*, 365

80. Colom, F.; Gonzalez-Tejera, M.J., *J. Electroanal. Chem.*, **1985**, *190*, 243-255

81. Marinkovic, N.S.; Wang, J.X.; Zajonz, H.; Adzic, R.R., *J. Electroanal. Chem.* **2001**, *500 (1-2)*, 388-394

82. Shingaya, Y.; Ito, M., *J. Electroanal. Chem.*, **1999**, *467*, 299

83. Ahmadi, A.; Evans, R.W.; Attard, G., *J. Electroanal. Chem.*, **1993**, *350*, 279-295

84. Horanyi, G.; Rizmayer, E.M., *J. Electroanal. Chem.*, **1984**, *181*, 199-208

85. Wendt, H., 'Electrochemical Hydrogen Technologies', (Elsevier, Amsterdam, 1990), p.8

86. Wiekowski, A., 'Interfacial Electrochemistry: Theory, Experiment and Applications', Marcel Dekker, Inc., 1999, p. 133

87. Gerischer, H., *Bull. Chem. Soc. Belg.*, **1958**, *67*, 506-512.

88. Conway, B.E.; MacDougall, B.R.; Kozlowska, H.A., *J. Chem. Soc.- Faraday Trans. I*, **1972**, *68*, 1566-1574

89. Yokoyama, T.; Yamagata, N., *Applied Catalysis A: General*, **2001**, *221*, 227-239

90. Peereboom, L.; Miller, D.J.; Jackson, J.E., *Unpublished results*

91. Cortright, R.D.; Sanchez-Castillo, M.; Dumesic, J.A., *Appl. Catal. B*, **2002**, *39*, 353

92. Cortright, R.D.; Dumesic, J.A., *Adv. Catal.*, **2001**, *46*, 161

93. Falorni, M.; Giacomelli, G.; Porcheddu, A.; Taddei, M., *J. Org. Chem.*, **1999**, *64*, 8962

94. Kim, Y.G.; Soto, J.E.; Chen, X.; Park, Y.S.; Soriaga, M.P., *J. Electroanal. Chem.*, **2003**, *554-555*, 167-174

95. Kim, Y.G.; Baricuatro, J.H.; Soriaga, M.P.; Wayne, S.D., *J. Electroanal. Chem.*,

2001, *236(1)*, 197-198

96. Soto, J.E.; Kim, Y.G.; Soriaga, M.P., *Electrochemistry Communications*, **1999**, *1(3,4)*, 135-138

97. Pang, K.P.; Benziger, J.B.; Soriaga, M.P.; Hubbard, A.T., *J. Phys. Chem.*, **1984**, *88(20)*, 4583-4586

98. Mebrahtu, T.; Berry, G.M.; Soriaga, M.P., *J. Electroanal. Chem.*, **1988**, *239(1-2)*, 375-386

99. Chia, V.K.F.; White, J.H.; Soriaga, M.P., Hubbard, A.T., *J. Electroanal. Chem.*, **1987**, *217(1)*, 121-128

100. Chia, V.K.F.; Soriaga, M.P.; Hubbard, A.T., *J. Phys. Chem.*, **1987**, *91(1)*, 78-82

101. Song, D.; Soriaga, M.P.; Hubbard, A.T., *J. Electroanal. Chem.*, **1985**, *193(1-2)*, 255-264

102. Song, D.; Soriaga, M.P.; Vjeira, K.L.; Zapien, D.C.; Hubbard, A.T., *J. Phys. Chem.*, **1985**, *89(19)*, 3999-4002

103. Soriaga, M.P.; Song, D.; Hubbard, A.T., *J. Phys. Chem.*, **1985**, *89(2)*, 285-289

104. Soriaga, M.P.; Song, D.; Zapien, D.C.; Hubbard, A.T., *Langmuir*, **1985**, *1(1)*, 123-127

105. White, J.E.; Soriaga, M.P.; Hubbard, A.T., *J. Electroanal. Chem.*, **1984**, *177(1-2)*, 89-96

106. Soriaga, M.P.; White, J.E.; Song, D.; Hubbard, A.T., *J. Electroanal. Chem.*, **1984**, *171(1-2)*, 359-363

107. Chia, V.K.F.; Soriaga, M.P.; Hubbard, A.T., *J. Electroanal. Chem.*, **1984**, *167(1-2)*, 97-106

108. Chia, V.K.F.; Stickney, J.L.; Soriaga, M.P.; Rosasco, S.D.; Salaita, G.N.; Hubbard, A.T.; Benziger, J.B.; Pang, K.W.P., *J. Electroanal. Chem.*, **1984**, *163(1-2)*, 407-413

109. Stern, D.A.; Laguren-Davidson, L.; Frank, D.G.; Gui, J.Y.; Lin, C.H.; Lu, F.; Salaita, G.N.; Walton, N.; Zapien, D.C.; Hubbard, A.T. *J. Am. Chem. Soc.*, **1989**, *111*, 877-891

110. Gui, J.Y.; Stern, D.A.; Lin, C.H.; Gao, P.; Hubbard, A.T. *Langmuir*, **1991**, *7*, 3183-3189

111. Sungho, P.; Tong, Y.Y.; Wieckowski, A.; Weaver, M.J., *Langmuir*, **2002**, *18*, 3233-3240

112. Kardash, D.; Huang, J.; Korzeniewski, C., *Langmuir*, **2000**, *16(4)*, 2019-2023

113. Kim, K.S.; Korzeniewski, C.; Tornquist, W.J., *J. Chem. Phys.*, **1994**, *100(1)*, 628-630

114. Lin, W.F.; Christiansen, P.A., *Faraday Discussions*, **2002**, *121*, 267-284

115. Lin, W.F.; Christiansen, P.A.; Hamnett, A., *Phys. Chem. Chem. Phys.*, **2001**, *3*, 3312-3319

116. Arenz, M.; Stamenkovic, V.; Schmidt, T.J.; Wandelt, K.; Ross, P.N.; Markovic, N.M., *Phys. Chem. Chem. Phys.*, **2003**, *5*, 4242-4251

117. Iwasita, T.; Xia, X.H.; Liess, H.D.; Vielstich, W., *J. Phys. Chem. B*, **1997**, *101*, 7542-7547

118. Iwasita, T.; Xia, X.; Herrero, E.; Liess, H.D., *Langmuir*, **1996**, *12*, 4260-4265

119. Kardash, D.; Korzeniewski, C., *Langmuir*, **2000**, *16*, 8419-8425

120. Sungho, P.; Xie, Y.; Weaver, M.J., *Langmuir*, **2002**, *18*, 5792-5798

121. Iwasita, T.; Hoster, H.; John-Anacker, A.; Lin, W.F.; Vielstich, W., *Langmuir*, **2000**, *16*, 522-529

122. Gomez, R.; Weaver, M.J., *J. Electroanal. Chem.*, **1997**, *435*, 205-215

123. Caram, J.A.; Gutierrez, C., *J. Electroanal. Chem.*, **1992**, *336*, 309

124. Gootzen, J.F.E.; Visscher, W.; Van Veen, J.A.R., *Langmuir*, **1996**, *12*, 5076-5082

125. Xia, X.H.; Liess, H.D.; Iwasita, T., *J. Electroanal. Chem.*, **1997**, *437*, 233-240

126. Morin, S.; Conway, B.E.; Edens, G.J.; Weaver, M.J., J. *Electroanal. Chem.*, **1997**, *421*, 213-220

127. Chang, S.C.; Ho, Y.; Weaver, M.J., *J. Am. Chem. Soc.*, **1991**, *113*, 9506-9513

128. Rodriguez, J.L.; Pastor, E.; Xia, X.H.; Iwasita, T., *Langmuir*, **2000**, *16*, 5479-5486

129. Huerta, F.; Morallon, E.; Perez, J.M.; Vazquez, J.L.; Aldaz, A., *J. Electroanal. Chem.*, **1999**, *469*, 159-169

130. Camara, G.A.; De Lima, R.B.; Iwasita, T., *J. Electroanal. Chem.*, **2005**, *585(1)*, 128-131

131. Kunimatsu, K.; Bewick, A., *Indian. J. Technol.*, **1986**, *24*, 407

132. Parry, D.B.; Samant, M.G.; Seki, H.; Philpott, M.R.; Ashley, K., ***Langmuir*, 1993**, *9*, 1878

133. Osawa, M.; Ataka, K.; Yoshii, K.; Yotsuyanigi, T., *J. Electron Spectrosc. Relat. Phenom.*, **1993**, *64/65*, 371

134. Osawa, M.; Ataka, K.; Yoshii, K.; Yotsuyanigi, T., *Langmuir*, **1994**, *10*, 640

135. Nicholas, R.J.; Burgess, I.; Young, K.L.; Zamlynny, V.; Lipkowski, J., *J. Electroanal. Chem.*, **2004**, *563(1)*, 33-39

136. Hong-Qiang, L.; Roscoe, S.G.; Lipkowski, J., *J. Electroanal. Chem.*, **1999**, *478(1,2)*, 67-75

137. Hong-Qiang, L.; Chen, A.; Roscoe, S.G.; Lipkowski, J., *Proc. Electrochem. Soc.*, **2000**, *15*, 145-148

138. Hoon-Khosla, M.; Fawcett, W.R.; Goddard, J.D.; Lian, W.Q.; Lipkowski, J., *Langmuir*, **2000**, *16(5)*, 2356-2362

139. Hoon-Khosla, M.; Fawcett, W.R.; Chen, A.; Lipkowski, J.; Pettinger, B., *Electrochim. Acta*, **1999**, *45(4-5)*, 611-621

140. Osawa, M., *Bull. Chem. Soc. Jpn.*, **1997**, *70*, 2861-2880

141. Itoh, T.; McCreery, R.L. *J. Am. Chem. Soc.*, **2002**, *124*, 10894-10902

142. Hind, A.R.; Bhargava, S.K.; McKinnon, A. *Advances in Colloid and Interface Science*, **2001**, *93*, 91-114

143. Aroca, R.F.; Ross, D.J., *Appl. Spec.*, **2004**, *58(11)*, 324A-338A

144. Chew, H.; Kerker, M., *J. Opt. Soc. Am.*, **1985**, *B2*, 1025

145. Osawa, M.; Ikeda, M., *J. Phys. Chem.*, **1991**, *95*, 9914-9919

146. Dumas, P.; Tobin, R.G.; Richards, P.L., *Surf. Sci.*, **1986**, *171*, 555

147. Merkin, G.T.; Griffiths, P.R, *Langmuir*, **1997**, 13(23), 6159-6163

148. Devlin, P.J., Consani, K., *J. Phys. Chem.*, **1981**, *85*, 2597

149. Pons, S.; Khoo, S.B.; Bewick, A.; Datta, M.; Smith, J.J.; Hinman, A.S.; Zachmann, G., *J. Phys. Chem.*, **1984**, *88*, 3575

150. Wadayama, T.; Sakurai, T.; Ichikawa, S.; Suetaka, W., Surf, Sci., **1988**, *198*, L359

151. Hahn, F.; Melendres, C.A., *Electrochim. Acta*, **2001**, *46*, 3525-3534

152. Zhu, Y.; Uchida, H.; Yajima, T.; Watanabe, M., *Langmuir*, **2001**, *17*, 146-154

153. Chen, Y.X.; Miki, A.; Ye, S.; Sakai, H.; Osawa, M., *J. Am. Chem. Soc.*, **2003**, *125(13)*, 3680-3681

154. Yajima, T.; Uchida, H.; Watanabe, M., J. Phys. Chem. B, **2004**, *108*, 2654-2659

155. Shiroishi, H.; Ayato, Y.; Kunimatsu, K.; Okada, T., *J. Electroanal. Chem.*, **2005**, *581(1)*, 132-138

156. Shao, M.H.; Adzic, R.R., *Electrochim. Acta*, **2005**, *50(12)*, 2415-2422

157. Futamata, M.; *J. Electroanal. Chem.*, **2003**, *550-551*, 93-103

158. Watanabe, M.; Zhu, Y.; Uchida, H., *J. Phys. Chem. B*, **2000**, *104*, 1762-1768

159. Samjeske, G.; Miki, A.; Ye, S.; Yamakata, A.; Mukouyama, Y.; Okamoto, H.; Osawa, M., *J. Phys. Chem. B*, **2005**, *109*, 23509-23516

160. Samjeske, G.; Osawa, M., *Angew. Chem. Int. Ed.*, **2005**, *44*, 5694-5698

161. Miki, A.; Ye, S.; Senzaki, T.; Osawa, M., *J. Electroanal. Chem.*, **2004**, *563(1)*, 23-31

162. Noda, H.; Ataka, K.; Wan, L.J.; Osawa, M., *Surf. Sci.*, **1999**, *427-428*, 190-194

163. Kunimatsu, K.; Uchida, H.; Osawa, M.; Watanabe, M., *J. Electroanal. Chem.*, **2006**, *587*, 299-307

164. Kunimatsu, K.; Senzaki, T.; Tsushima, M.; Osawa, M., *Chem. Phys. Lett.*, **2005**, *401*, 451-454

165. Miyake, H.; Ye, S.; Osawa, M., *Electrochemistry Communications*, **2002**, *4*, 973-977

166. Thiel, P.A.; Madey, T.E., *Surf. Sci. Rep.*, **1987**, *7*, 211

167. Thiel, P.A.; DePaola, R.A.; Hoffmann, F.M., *J. Chem. Phys.*, **1984**, *80*, 5326

168. Ataka, K.; Yotsuyanigi, T.; Osawa, M., *J. Phys. Chem.*, **1996**, *100*, 10664-10672

169. Brink, G.; Falk, M., *Can. J. Chem.*, **1970**, *48*, 2096

170. (a) Walrafen, G.E., *J. Chem. Phys.*, **1962**, *36*, 1035; (b) Walrafen, G.E., *J. Chem. Phys.*, **1971**, *55*, 768

171. Jonsson, B.; *Chem. Phys. Lett.*, **1981**, *82*, 520

172. Parsonage, N.G.; Nicholson, D., *J. Chem. Soc., Faraday Trans. 2*, **1987**, *83*, 663

173. Lee, C.Y.; McCammon, J.A.; Rossky, P.J., *J. Chem. Phys.*, **1984**, *80*, 4448

174. (a) Nagy, G.; Heinzinger, K., *J. Electroanal. Chem.*, **1990**, *296*, 549; (b) Nagy, G.; Heinzinger, K., *J. Electroanal. Chem.*, **1992**, *327*, 25

175. Nagy, G.; Heinzinger, K.; Spohr, E., *J. Chem. Soc. Faraday Discuss.*, **1992**, *94*, 307

176. Glosli, J.N.; Philpott, M.R., *J. Chem. Phys.*, **1992**, *96*, 6962

177. Xia, X.; Perera, L.; Essemann, E.; Berkowitz, M.L., *Surf. Sci.*, **1995**, *335*, 401

178. Doering, D.; Madey, T.E., *Surf. Sci.*, **1982**, *123*, 305

179. Russell, A.E., Lin, A.S.; O'Grady, W.E., J. Chem. Soc. Faraday Trans, 1993, 89, 195

180. Nakamoto, K., 'Infrared and Raman spectra of Inorganic and Co-ordination Compounds', 4th ed., Wiley, New York, 1986

181. Wagner, F.T.; Moylan, T.E., *Surf. Sci.*, **1987**, *182*, 125

182. Wagner, F.T.; Moylan, T.E., *Surf. Sci.*, **1989**, *216*, 361

183. Ataka, K.; Osawa, M., *Langmuir*, **1998**, *14*, 951-959

184. Pretsch, E.; Seibl, J.; Clerc, D.; Simon, W., 'Tables of Spectral Data for Structure Determination of Organic Compounds (2nd ed.)', Springer-Verlag, 1985, pp I85

185. Cassanas, G.; Morssli, M.; Fabregue, E.; Bardet, L., *Journal of Raman Spectroscopy*, **1991**, *22*, 409-413

186. Vassilev, P.; Van Santen, R.A.; Koper, M.T.M., *J. Chem. Phys.*, **2005**, *122*, 054701

187. Akiyama, R.; Hirata, F., *J. Chem. Phys.*, **1998**, *108(12)*, 4904-4911

188. Kitamura, F.; Nanbu, N.; Ohsaka, T.; Tokuda, K., *J. Electroanal. Chem.*, **1998**, *452*, 241-249

189. Zheng, W.; Tadjeddine, A., *J. Chem. Phys.*, **2003**, *119(24)*, 13096-13099

190. Wandlowski, T.; Ataka, K.; Pronkin, S.; Diesing, D., *Electrochim. Acta*, **2004**, *49(8)*, 1233-1247

191. Futamata, M.; Luo, L.; Nishihara, C., *Surf. Sci.*, **2005**, *590*, 196-211

192. Zhang, Z. 'Aqueous-phase hydrogenation of biomass derived lactic acid to propylene glycol', Ph.D. Thesis

193. Yan, Y.G.; Li, Q.X.; Huo, S.J.; Ma, M.; Cai, W.B.; Osawa, M., *J. Phys. Chem. B*, **2005**, *109*, 7900-7906